
CARSTEN MAYER

WAVELET MODELLING OF IONOSPHERIC
CURRENTS AND INDUCED MAGNETIC
FIELDS FROM SATELLITE DATA

Wavelet Modelling of Ionospheric Currents and Induced Magnetic Fields from Satellite Data

Carsten Mayer
Geomathematics Group
Department of Mathematics
University of Kaiserslautern, Germany

Vom Fachbereich Mathematik
der Universität Kaiserslautern
zur Erlangung des akademischen Grades
Doktor der Naturwissenschaften
(Doctor rerum naturalium, Dr. rer. nat.)
genehmigte Dissertation

1. Gutachter: Prof. Dr. Willi Freeden
2. Gutachter: Prof. Dr. Hermann Lühr

Vollzug der Promotion: 28. August 2003
D 386

Acknowledgements

First of all, I thank Prof. Dr. Willi Freeden for giving me the opportunity to work on this topic and for his support concerning all the problems that have come up during my work.

Moreover, I thank Prof. Dr. H. Lühr for being my second tutor and for giving me helpful advices concerning the geomagnetic background of my work. Furthermore, I want to thank Prof. Dr. N. Olsen and the GFZ Potsdam for providing me with satellite data and numerous software for processing these data.

I am grateful to all the former and present colleagues at the Geomathematics Group, especially Dr. T. Maier, who read the manuscript and gave a lot of valuable comments.

I wish to thank Petra and my parents, Marianne and Richard Mayer, for their encouragement, their patience and their continuous support.

Finally, the financial support of the Graduiertenkolleg, "Mathematics and Practice", University of Kaiserslautern, is gratefully acknowledged.

Table of Contents

Introduction	1
1 Preliminaries	9
1.1 Notation	9
1.2 Scalar Spherical Harmonics	13
1.3 Two Sets of Vector Spherical Harmonics	18
1.4 The Mie Representation	27
2 Multiresolution Analysis of Operator Equations	33
2.1 The Scalar Case	34
2.2 The Vectorial Case	38
2.3 The Tensorial Approach	44
2.4 Regularization by Multiresolution	48
2.4.1 The Scalar Case	50
2.4.2 The Vectorial Case	53
3 Separation of Vectorial Fields With Respect to Sources	59
3.1 Representation by Vector Spherical Harmonic Expansion	62
3.2 Representation by Vector Scaling Functions and Wavelets	67
3.2.1 Scaling Functions and Wavelets	68
3.2.2 Scale and Detail Spaces	76
3.2.3 Examples of Scaling Functions and Wavelets	78
3.2.4 Computational Aspects	82

3.3	A Spectral Scheme for the System $\{u_{n,k}^{(i)}\}$	84
3.3.1	An Application to a Multi-Satellite Constellation	90
3.4	An Application to CHAMP Magnetic Field Data	92
3.5	Improved Crustal Field Modelling	96
4	Determination of Ionospheric Current Systems	101
4.1	The Modelling of the Problem	102
4.2	The Biot-Savart Operator	104
4.3	A Singular System of the Biot-Savart Operator	108
4.4	Simulations and Numerical Applications	117
4.4.1	A Simulation of a Ring Current System	117
4.4.2	A Simulation of a Local Current System (Cowling Channel)	120
4.4.3	An Application to MAGSAT Magnetic Field Data	126
4.4.4	An Application to CHAMP Magnetic Field Data	130
4.4.5	An Application to SWARM Magnetic Field Data	135
	Summary and Outlook	141
	A CHAMP Magnetic Data Preprocessing	145
	B M-Estimation for Outlier Detection	149
	Bibliography	153

Introduction

The major task of this thesis, starting as a topic of the Graduiertenkolleg "Mathematics and Practice", University of Kaiserslautern, was multiscale modelling of ionospheric current systems and the corresponding magnetic field with application to satellite data. The contents of this topic, if analyzed in more detail, spans a wide frame within geophysical as well as mathematical science. First of all, the problem of describing ionospheric current systems and the corresponding magnetic fields is a problem of electromagnetism. Thus, the full set of Maxwell's equations hold (see e.g. [6]). Today's knowledge of the Earth's ionosphere and the geomagnetic field together with the availability of magnetic field measurements do not put us in a position of being able to solve the complete system of Maxwell's equations. Thus, we discuss an approximation by dropping terms from the full system that are suspected of being small. Suppose we are interested in fields whose typical length scale is L and whose typical time scale is T . Since high density spatial coverage of magnetic field data is much easier to obtain than coverage in time with high resolution, it is valid to assume that L/T is much smaller than the velocity of light. Some well known considerations (see e.g. [6]) show that in this case some terms can be dropped in the full system of Maxwell's equations. This simplification causes a decoupling of the system into an electromagnetic and a magnetostatic part, called quasi static approach. The resulting system is called the system of pre-Maxwell equations. Since we are interested in connecting the current systems and the magnetic field we are mainly concerned with the system of magnetostatic equations, i.e.

$$\begin{aligned}\nabla \wedge b(x) &= \mu_0 j(x), \\ \nabla \cdot b(x) &= 0\end{aligned}$$

where x is lying in the area of interest, b denotes the magnetic field, and j the electric current density. μ_0 is the permeability of vacuum with $c^2 = 1/(\mu_0 \varepsilon_0)$, where ε_0 is the capacitivity of vacuum.

In consequence, the pre-Maxwell equations are the leading system of equations in this thesis. They form a system of partial differential equations and if we assume the area of interest to fulfill certain properties, the inhomogeneity j to be given everywhere and boundary values for b to be available, then the theory of partial differential equations gives the unique solvability of the above system. However, there is a critical point in the previous considerations. Neither the current system j nor the magnetic field b are given everywhere in the ionosphere. Thus, the system of pre-Maxwell equations is not solvable at all under the above assumptions.

The only data which are available are magnetic field measurements on an approximately spherical regular surface in the ionosphere, from which as much information concerning ionospheric current systems should be derived as possible. These data are provided by low-flying satellites with nearly circular, near-polar orbits as the German geoscientific satellite CHAMP. In order to obtain as much information as possible the problem demands another modelling step. At this point, a commonly (in geophysics) used simplification can be applied to the model, the height integrated ionosphere. It is assumed that all the horizontal currents of the ionosphere are present at just one altitude, which can be interpreted as a height integrated current system. This simplification turns the problem of deriving the current system from given magnetic field measurements to be uniquely solvable. But it should be noted that the current system calculated in this way will never be present in this form in reality. The system is an equivalent current system which induces the same magnetic field as the real ionospheric current system. This approach has already been used in the geomagnetic literature for modelling the connection between current systems and the corresponding magnetic fields (see e.g. [2], [4] and [37] and the reference about ionospheric current systems therein).

As regards the subject of global and dense coverage of geomagnetic field data, satellites orbiting the Earth in low, near-polar orbits provide a firm basis for acquiring the necessary spatially high resolution observations. MAGSAT (1979-1980) was the first, and for a long time only, geomagnetic field mission with appropriate vector instruments. Despite its comparatively short duration (6 months), the MAGSAT mission built the foundation for a huge amount of scientific geomagnetic results (for results concerning topics of this thesis see [9], [11], [39], [43], [51] or [58]). The Danish satellite Ørsted, which is also equipped with highly accurate scalar as well as vector instruments, orbits the Earth since 1999 and has great impact on main field as well as external field modelling. The German CHAMP mission which started in the summer of 2000 and which is operated by the GFZ Potsdam, is, besides other scientific tasks, designed for highly accurate geomagnetic field mappings. Due to its low orbit compared to Ørsted and MAGSAT and due to its advanced instrumentation CHAMP provides the scientific community with scalar as well as vector magnetic field data enabling an improvement in main, crustal, ionospheric and external field modelling (for recent results concerning the CHAMP mission the reader is referred to [55]). A further step forward concerning the geomagnetic data situation may be achieved by SWARM, a constellation of 4 – 6 low orbiting satellites of the CHAMP type which are designed to measure the magnetic field in different layers of the ionosphere (see e.g. [40]). For more information about flying, upcoming and proposed geomagnetic satellite missions the reader is referred to the internet page http://denali.gsfc.nasa.gov/research/mag_field/purucker/mag_missions.html.

In addition to the availability of adequate data sets, ionospheric current and geomagnetic field modelling need appropriate mathematical tools which allow modelling of the fields adapted to the present data situation and which give the possibility of geophysical interpretation. If looking for first results concerning a mathematical

treatment of ionospheric current systems and the corresponding magnetic fields it is inevitable to have a look at the considerations in [37]. It tells us, that the induced magnetic field above the sphere of the equivalent current system is harmonic and can be developed into a series of outer harmonics. The corresponding Fourier coefficients can be connected to the coefficients of the current function of the spherical current system which is a scalar function on the sphere of the equivalent current system. This gives a first functional connection of the ionospheric current system and the corresponding magnetic field. A major drawback of this ansatz is the global support of the spherical harmonics which does not give rise to the regional shape of the current system. Quiet ionospheric current systems are driven by solar effects and so they mainly appear on the day-side of the Earth. There are also currents present at the night-side of the Earth (see, for example, [41] for a recent result concerning nighttime F region ionospheric currents observed in CHAMP data) but compared to the magnitude of the daytime currents the ones on the night-side of the Earth can be neglected. Scalar spherical harmonics are not appropriate to resolve this discrepancy between the two sides of the sphere. They have to be substituted by basis functions which account to the regional structure of the effects to be modelled. Furthermore, the approach as presented in [37] connects the scalar current function of the current system to the scalar magnetic potential of the induced magnetic field which is not really satisfactory when concerned with vectorial problems. Nevertheless the approach gives the possibility to get a first impression of the shape of the ionospheric current system of the Earth which can be seen in Figure 1.

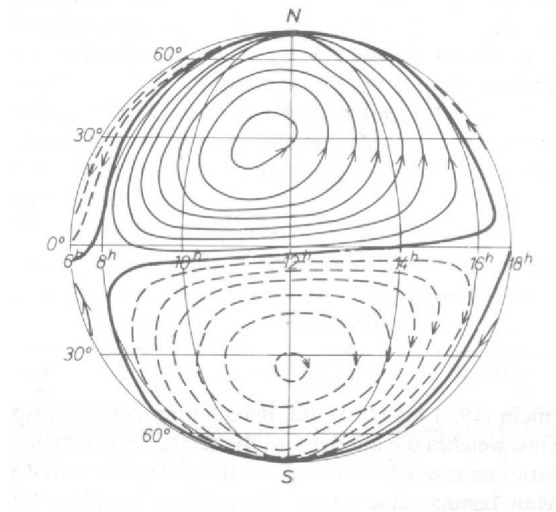


Figure 1: Current function of the ionospheric mid-latitude solar quiet current system. The coordinates are magnetic latitude and local time. ([37], page 303)

The next step in developing a connection between the current system and the induced magnetic field is the transfer of the previously mentioned scalar theory to a vector approach since both magnetic field and current system are vector fields. The system of trial functions which is commonly used in geomathematical applications

for modelling vectorial problems is the system of vector spherical harmonics denoted by $\{y_{n,k}^{(i)}\}$ as, for example, presented in [20]. It is based on the decomposition of spherical vector fields into a radial part and two tangential parts and represents the components of a spherical vector field with respect to the spherical Helmholtz decomposition theorem (see e.g. [42]). This system of vector spherical harmonics has already been used in geomagnetic applications in [7], [9] and [43]. For further theoretical considerations concerning the system $\{y_{n,k}^{(i)}\}$ of vector spherical harmonics, as for example the addition theorem connecting the system to vector Legendre polynomials, the reader is referred to [20]. Observing the applicability of the system to pre-Maxwell problems it becomes soon clear that another system of vector spherical harmonics, denoted by $\{u_{n,k}^{(i)}\}$, is much more advantageous for dealing with these kind of problems. This system has, for example, been introduced in [16] for quantum-mechanical applications, but also in the geomagnetic literature (see e.g. [6]) and in the mathematical literature (see e.g. [20]) it has already been used. The main advantage of the system is the decomposition property. For $i = 1$ the Fourier series with respect to $u_{n,k}^{(1)}$ represents that part of the spherical vector field which is induced by sources lying inside the sphere, where the magnetic field measurements are taken. For $i = 2$ the expansion in terms of the system $u_{n,k}^{(2)}$ represents the part of the field which is created by sources outside the sphere and the series in $u_{n,k}^{(3)}$ gives the part of the field which is due to the radial projection of sources crossing the sphere itself. This major advantage of the system $\{u_{n,k}^{(i)}\}$ of vector spherical harmonics has already been observed in [6]. The system yields the possibility of describing the pre-Maxwell problem in a comprehensive vectorial nomenclature.

Although we have found a way of modelling the problem of combining ionospheric current systems and the corresponding magnetic field in a vectorial way, it is not a satisfactory result, since vector spherical harmonics retain the property of having a polynomial structure and a global support. On the one hand they do not show any space localization which is needed for modelling ionospheric current systems, on the other hand the functions show an ideal spectral or momentum localization which is very advantageous for an interpretation in terms of multipoles. Uncertainty principles describe this discrepancy between ideal space and frequency localization (see e.g. [18] for the scalar case and [10] for a first approach to the vectorial case). The essential result states that simultaneous ideal localization in space and frequency is mutually exclusive. The extreme trial functions in the sense of the uncertainty principle are given by scalar/vector spherical harmonics for ideal frequency localization on the one hand and Dirac functionals for ideal space localization on the other hand. Thus, it becomes clear that Fourier methods, which are based on spherical harmonics are well suited to resolve frequency phenomena, but their application to model and obtain high resolution regional or local phenomena is critical. A trade-off between space and frequency localization has to be found. A compromise can be obtained by special kernel functions which are constructed as weighted sums over the corresponding orthonormal systems (scalar/vector spherical harmonics) of certain frequency bands. According to the uncertainty principle, the reduction of

frequency localization leads to an enhancement of space localization such that the kernel functions show only small spatial extension. This is the reason why these kernel functions can be constructed in all intermediate stages of space localization. The construction principle is illustrated in Table 1.

Ideal frequency localization No space localization	No frequency localization Ideal space localization
← spherical harmonics	scalar / vector kernel functions
	→ Dirac functional

Table 1: A graphical illustration of the construction principle of kernel functions following the uncertainty principle.

Using kernels at different scales to detect and approximate spatial as well as certain frequency features in given data is called multiscale modelling. The special type of kernel functions we use in this thesis are vectorial radial basis functions, called vector scaling functions and vector wavelets. An essential characteristic of wavelets techniques is that they are able to establish a multiresolution analysis, i.e. the function space containing the data is decomposed into a nested sequence of approximating subspaces. It is possible to break up complicated functions, like the geomagnetic field, electric current densities, or geopotentials into different 'pieces' and to study these pieces separately. This procedure called multiresolution analysis can be explained as follows. Starting from a sequence of scaling functions, the multiresolution analysis of the function space under consideration is obtained in terms of the corresponding scale spaces. In each of these scale spaces an approximation of the function at a certain scale is constructed. For increasing scale the approximation improves and the information contained on coarse level is contained in all scale spaces above. The difference between two approximations is called the detail information contained in the so-called detail space. In spectral nomenclature, scaling functions act as a nested sequence of low-pass filters while wavelets establish the corresponding subsequent band-pass filters. An extensive discussion concerning scaling functions and wavelets can be found in [19] and [20], while in [7], [9], [42] and, especially, in [43] applications of the vectorial wavelet approach to geomagnetic field modelling can be found. A construction principle for scaling functions and wavelets for operator equations in a general Hilbert space concept can be found in [21]. A multiscale technique for regularization of inverse problems has been developed in [25] and for a construction principle of scaling functions and wavelets in a general Hilbert space approach the reader is referred to [49].

These special vector kernel functions now give us the possibility to model the pre-Maxwell problem described above in a vectorial nomenclature as well as with space localizing trial functions. This will be done in this thesis in a comprehensive theoretical framework and the application of multiscale methods in this field will be

demonstrated. A first step during the course of this thesis is the construction of scaling functions and wavelets based on the system of vector spherical harmonics $\{u_{n,k}^{(i)}\}$, which retain the property of decomposing a given spherical vector field with respect to its sources. It will give the possibility to decompose a spherical vector field into parts induced by sources inside, outside, or on the sphere just by having only regional data.

Furthermore, a second application of kernel functions is the reconstruction of the source fields, i.e. the ionospheric current distribution corresponding to given magnetic field data. Since this problem is of ill-posed nature it demands more than the simple approximation property of scaling functions and wavelets. Therefore, we develop a method for multiscale regularization of ill-posed vectorial problems and apply it to the problem of determining ionospheric current systems. Numerical applications illustrate the introduced approaches and demonstrate the applicability and practicality of the proposed wavelet techniques. It should be noted that the numerical examples presented here are not intended to be detailed physical case studies but ought to be seen as testing examples and as the starting point for such research.

The outline of the thesis is as follows.

Chapter 1 introduces some basic notations and relations which we are going to use throughout the thesis. Additionally, a couple of well-known results which are useful for an easy understanding of the following discussions are briefly recapitulated. Topics include scalar and vector spherical harmonics, inner and outer harmonics as well as the Helmholtz and the Mie representation.

In Chapter 2 a general approach to the theory of multiscale techniques in separable Hilbert spaces is presented. Section 2.1 starts with the introduction of a scalar multiscale approach in order to deal with scalar operator equations with known singular system. In Section 2.2 the theory is generalized to the vectorial case, i.e. a multiscale decomposition of operator equations between separable Hilbert spaces of vector functions, so called tensor-operator equations, is discussed. The formulation of both, the scalar as well as the vectorial multiscale techniques, is based on the Fourier theory in the respective Hilbert spaces such that the results can easily be interpreted in terms of conventional methods. In Section 2.3 we compare the vector multiresolution technique to the canonical tensorial approach for tensor-operator equations and the equivalence of both approaches is proved. At the end of this chapter in Section 2.4 the theory of multiscale regularization for vectorial inverse problems is embedded in the multiresolution theory for tensor-operator equations. We briefly introduce the theory of ill-posed problems in a general Hilbert space approach and define regularization vector scaling functions and wavelets which are used for the multiscale regularization of vectorial inverse problems in a bilinear approach.

As for the discussion of ionospheric currents and the corresponding magnetic fields, multiscale techniques are of great importance. Magnetic field signatures, either be-

ing of crustal nature or being induced by interior or exterior current systems are of comparably small spatial extend. Therefore, it is reasonable to avoid global trial functions and choose a modelling technique that can cope with the regional features. To fulfill this property spherical vector scaling functions and wavelets are introduced in Chapter 3. First of all the pre-Maxwell problem is discussed and an approach based on the Mie representation is presented to solve the problem in the area of interest (outer space of the Earth). Adapted to the availability of magnetic field data on an (approximately) spherical surface, a decomposition of the magnetic field with respect to a special system of vector spherical harmonics, denoted by $\{u_{n,k}^{(i)}\}$, is presented based on Fourier techniques. The special property of the representation of a spherical vector field in this orthonormal system is the decomposition into parts with respect to the area, where the respective parts are produced. In Section 3.2 the decomposition is transferred to multiscale techniques. Based on the theory of Chapter 2 a multiscale decomposition of the identity operator on the Hilbert space $l^2(\Omega)$ of measurable vector valued functions on the unit sphere Ω is presented. The defined vector scaling functions and wavelets retain the property of decomposing a spherical vector field with respect to its sources. Moreover, they allow a regional decomposition and reconstruction of a vector field, i.e. a spherical vector field can be decomposed into parts induced by sources lying inside, outside or on the sphere referring to the availability of only regional information. At the end of the chapter this approach is applied to CHAMP magnetic field data and it is shown, how crustal field determination, as discussed in a multiscale framework in [43], can be improved by previously applying the technique presented here.

Apart from the challenge of separating magnetic field data with respect to its sources, the task is to reconstruct these sources, i.e. to reconstruct ionospheric current systems corresponding to given magnetic field data, called 'inverse source problem' (see e.g. [5]). This is the main topic of Chapter 4. First of all the problem is formulated and certain modelling steps are applied, as for example the introduction of the height integrated ionosphere, in order to turn the problem to be adequate for satellite data and to be solvable (see e.g. [1], [3] or [37] and the reference therein for a geophysical justification of the height integrated ionosphere). In this context the spherical Biot-Savart operator is introduced which is used to solve the 'direct source problem' as well as the 'inverse source problem' in spherical geometries. The operator is based on Biot-Savart's law of electrodynamics (see e.g. [35]). A major result of this chapter is the calculation of the singular system of this operator, where the system of vector spherical harmonics $\{u_{n,k}^{(i)}\}$ is again involved. Based on the multiresolution regularization technique developed in Section 2.4 and using the calculated singular system, regularization vector scaling functions and wavelets are defined. In order to demonstrate the applicability and the efficiency of our method, we apply the multiscale technique to two simulated current systems. The corresponding magnetic field data are calculated using explicit representations or approximate integration rules. Then the current systems is reconstructed from these data using the multiscale regularization techniques. To emphasise the advantages of regularization scaling functions and wavelets in contrast to vector spherical harmonics, a space localizing current

system (Cowling channel) is simulated.

Since an essential task of this thesis is the application to satellite data we test our approach with magnetic field data of three different satellite missions. At first, we reconstruct current systems from given MAGSAT magnetic field data. With the occurring results, we were able to calculate the course of the equatorial electrojet over the Earth during a day. In a second satellite application we reconstruct a ionospheric current system corresponding to given CHAMP magnetic field data. For a realistic image of the ionosphere an Earth fixed reference frame is the wrong coordinate system. Thus, we transform CHAMP magnetic field data to a Sun fixed reference frame given by the magnetic local time (MLT) and the quasi dipole latitude (QD-lat). In order to apply the multiscale regularization techniques to a global data set in magnetic local time and quasi dipole latitude we use the simulated measurements of the proposed SWARM satellite mission in a third application to satellite magnetic field data.

Chapter 1

Preliminaries

In this chapter the reader is provided with the essential tools used in the course of this thesis. We start with introducing some basic notation and the nomenclature which is used in our considerations. Then we will discuss scalar spherical harmonics which are the basic functions when dealing with problems in spherical geometries. Based on the scalar spherical harmonics we will develop two sets of vector spherical harmonics. At the end we will give two different representations for vector fields, the Helmholtz decomposition which is restricted to regular surfaces and the Mie representation which is true under certain circumstances for a subset of the three-dimensional Euclidean space.

1.1 Notation

During the course of this thesis we will permanently be confronted with scalar, vector and tensor fields. For the notation of these fields we will use the following symbols: Scalar fields will be denoted by capital letters (F, G , etc), vector fields are symbolized by lower-case letters (f, g , etc), and tensor fields are represented by boldface letters ($\mathbf{f}, \mathbf{g}, \mathbf{F}, \mathbf{G}$, etc).

Let $x, y \in \mathbb{R}^3$, then $x \cdot y$ denotes the standard Euclidean inner product of x and y , $x \wedge y$ symbolizes the vector (cross) product and $x \otimes y = xy^T$ is the tensor product of x and y .

Any point $x \in \mathbb{R}^3$ with $x \neq 0$ may be written in the form $x = r\xi$, where $r = |x|$ is the distance of x to the origin 0 and $\xi \in \mathbb{R}^3$, $\xi = (\xi_1, \xi_2, \xi_3)^T$, is the uniquely determined directional unit vector of x .

A sphere of radius R centered around the origin is denoted by $\Omega_R = \{x \in \mathbb{R}^3 \mid |x| = R\}$. In particular, $\Omega = \Omega_1$ is the *unit sphere* in \mathbb{R}^3 . We set Ω_R^{int} for the 'inner space' of Ω_R , $\Omega_R^{int} = \{x \in \mathbb{R}^3 \mid |x| < R\}$ while $\Omega_R^{ext} = \mathbb{R}^3 \setminus \overline{\Omega_R^{int}}$ is the 'outer space' of Ω_R . Clearly, $\Omega_R^{ext} = \{x \in \mathbb{R}^3 \mid |x| > R\}$. By $\Omega_{(R_1, R_1)}$ we denote the open spherical shell

with inner radius R_1 and outer radius R_2 given by

$$\Omega_{(R_1, R_2)} = \{x \in \mathbb{R}^3 \mid R_1 < |x| < R_2\}.$$

Any point $\xi \in \Omega$ can be represented in *polar coordinates* as follows:

$$\begin{aligned} \xi &= \sqrt{1-t^2}(\varepsilon^1 \cos \varphi + \varepsilon^2 \sin \varphi) + \varepsilon^3 t, \\ -1 \leq t \leq 1, \quad 0 \leq \varphi < 2\pi, \quad t &= \cos \vartheta, \end{aligned} \quad (1.1)$$

(ϑ : latitude, φ : longitude, t : polar distance) or equivalently

$$\xi = \varepsilon^1 \sin \vartheta \cos \varphi + \varepsilon^2 \sin \vartheta \sin \varphi + \varepsilon^3 \cos \vartheta,$$

where $\varepsilon^1, \varepsilon^2, \varepsilon^3$ denotes the standard Euclidean basis in \mathbb{R}^3 . The unit vectors corresponding to the spherical polar coordinates are denoted by ε^r , ε^φ and $\varepsilon^t (= -\varepsilon^\vartheta)$ and form the so-called moving local orthonormal triad. The relation of the local system to the standard Euclidean system is given via

$$\begin{aligned} \varepsilon^r(\varphi, t) &= \varepsilon^1 \sqrt{1-t^2} \cos \varphi + \varepsilon^2 \sqrt{1-t^2} \sin \varphi + \varepsilon^3 t, \\ \varepsilon^\varphi(\varphi, t) &= -\varepsilon^1 \sin \varphi + \varepsilon^2 \cos \varphi, \\ \varepsilon^t(\varphi, t) &= -\varepsilon^1 t \cos \varphi - \varepsilon^2 t \sin \varphi + \varepsilon^3 \sqrt{1-t^2}, \end{aligned}$$

and vice versa

$$\begin{aligned} \varepsilon^1 &= \varepsilon^r(\varphi, t) \sqrt{1-t^2} \cos \varphi - \varepsilon^\varphi(\varphi, t) \sin \varphi - \varepsilon^t(\varphi, t) t \cos \varphi, \\ \varepsilon^2 &= \varepsilon^r(\varphi, t) \sqrt{1-t^2} \sin \varphi + \varepsilon^\varphi(\varphi, t) \cos \varphi - \varepsilon^t(\varphi, t) t \sin \varphi, \\ \varepsilon^3 &= \varepsilon^r(\varphi, t) t + \varepsilon^t(\varphi, t) \sqrt{1-t^2}. \end{aligned}$$

In what follows we need a number of differential operators which we introduce next. $\nabla_x = (\partial/\partial x_1, \partial/\partial x_2, \partial/\partial x_3)^T$ denotes the *gradient* in \mathbb{R}^3 and ∇^* represents its tangential part, called *surface gradient*. The *Laplace operator* is symbolized by $\Delta = \nabla \cdot \nabla$ and the corresponding tangential operator, called *Beltrami operator*, is given by $\Delta^* = \nabla^* \cdot \nabla^*$. The *curl gradient* L_x is given by $L_x = x \wedge \nabla_x$ with tangential counterpart given by L^* which is called *surface curl gradient*.

We want to remark, that all these operators are used free of coordinates throughout this thesis. Nevertheless, for the convenience of the reader we give a list of local representations. The operators can be expressed as follows.

$$\nabla_x = \xi \frac{\partial}{\partial r} + \frac{1}{r} \nabla_\xi^*, \quad x = r\xi \in \mathbb{R}^3 \setminus \{0\} \quad (1.2)$$

$$\nabla_\xi^* = \frac{1}{\sqrt{1-t^2}} (-\sin \varphi \varepsilon^1 + \cos \varphi \varepsilon^2) \frac{\partial}{\partial \varphi} \quad (1.3)$$

$$+ \sqrt{1-t^2} \left(-t \cos \varphi \varepsilon^1 - t \sin \varphi \varepsilon^2 + \sqrt{1-t^2} \varepsilon^3 \right) \frac{\partial}{\partial t}, \quad (1.4)$$

$$L_\xi^* = \xi \wedge \nabla_\xi^*, \quad \xi \in \Omega, \quad (1.5)$$

$$= \sqrt{1-t^2} (\sin \varphi \varepsilon^1 - \cos \varphi \varepsilon^2) \frac{\partial}{\partial t} \quad (1.6)$$

$$+ \frac{1}{\sqrt{1-t^2}} \left(-t \cos \varphi \varepsilon^1 - t \sin \varphi \varepsilon^2 + \sqrt{1-t^2} \varepsilon^3 \right) \frac{\partial}{\partial \varphi}, \quad (1.7)$$

$$\Delta_x = \left(\frac{\partial}{\partial r} \right)^2 + \frac{2}{r} \frac{\partial}{\partial r} + \frac{1}{r^2} \Delta_\xi^*, \quad x = r\xi \in \mathbb{R}^3 \setminus \{0\} \quad (1.8)$$

$$\Delta_\xi^* = \frac{\partial}{\partial t} (1-t^2) \frac{\partial}{\partial t} + \frac{1}{1-t^2} \left(\frac{\partial}{\partial t} \right)^2. \quad (1.9)$$

A variety of function spaces will be needed in this thesis. Let $\mathcal{C}(U)$ be the set of all continuous, real functions defined on the set $U \subset \mathbb{R}^3$, equipped with the norm

$$\|F\|_{\mathcal{C}(U)} = \sup_{x \in U} |F(x)|.$$

A function is said to be of class $\mathcal{C}^{(k)}(U)$, $0 \leq k \leq \infty$, if it is k -times continuously differentiable on U . If $U \subset \mathbb{R}^3$ is a measurable subset of \mathbb{R}^3 , the set of scalar functions $F : U \rightarrow \mathbb{R}$ which are measurable and for which

$$\|F\|_{\mathcal{L}^p(U)} = \left(\int_U |F(x)|^p dx \right)^{\frac{1}{p}} < \infty$$

is denoted by $\mathcal{L}^p(U)$, where dx denotes the volume element in U .

In analogy to the scalar case we define function spaces of vector valued functions. These spaces will normally be symbolized by lower-case letters. Let $c(U)$ be the set of all vector valued, continuous functions $f : U \rightarrow \mathbb{R}^n$ defined on the set $U \subset \mathbb{R}^3$, equipped with the norm

$$\|f\|_{c(U)} = \sup_{x \in U} |f(x)|.$$

A vector field f is said to be of class $c^{(k)}(U)$, $0 \leq k \leq \infty$, if every component function $f \cdot \varepsilon^i$, $i = 1, \dots, n$, of f is k -times continuously differentiable on U . If $U \subset \mathbb{R}^3$ is a measurable subset of \mathbb{R}^3 , the set of vector fields $f : U \rightarrow \mathbb{R}^n$ which are measurable and for which

$$\|f\|_{l^p(U)} = \left(\int_U |f(x)|^p dx \right)^{\frac{1}{p}} < \infty$$

is denoted by $l^p(U)$.

The space of rank-2 tensors with continuous coordinate functions defined on the set U is denoted by $\mathbf{c}(U)$. Endowed with the norm

$$\|\mathbf{f}\|_{\mathbf{c}(U)} = \sup_{x \in U} |\mathbf{f}(x)|$$

the space $\mathbf{c}(U)$ is a Banach space. Similarly, the space of all p times continuously differentiable tensor fields is denoted by $\mathbf{c}^{(p)}(U)$, ($0 \leq p \leq \infty$). We define by $\mathbf{l}^2(U)$

the space of all square-integrable tensor fields on the measurable region U . Equipped with the inner product

$$(\mathbf{f}, \mathbf{g})_{l^2(U)} = \int_U \mathbf{f}(x) \cdot \mathbf{g}(x) dx, \quad \mathbf{f}, \mathbf{g} \in l^2(U),$$

the space is a Hilbert space, where the dot product of two rank-2 tensors \mathbf{f}, \mathbf{g} is defined by

$$\mathbf{f} \cdot \mathbf{g} = \sum_{i,j=1}^3 \mathbf{f}_{ij} \mathbf{g}_{ij}.$$

For most of our calculations the set U is given by a regular surface which will be defined next.

Definition 1.1

A surface $\Sigma \subset \mathbb{R}^3$ is called *regular surface*, if it satisfies the following properties:

1. Σ divides the three-dimensional Euclidian space \mathbb{R}^3 into the bounded inner region Σ_{int} and the unbounded outer region $\Sigma_{ext} = \mathbb{R}^3 \setminus \overline{\Sigma_{int}}$, $\overline{\Sigma_{int}} = \Sigma_{int} \cup \Sigma$,
2. Σ_{int} contains the origin,
3. Σ is closed and compact, free of double points,
4. Σ is locally of class $\mathcal{C}^{(2)}$.

By the last point of the above definition, we can conclude that there exists a continuous unit normal field ν on Σ , which can be assumed to be directed into the outer space Σ_{ext} .

In order to separate vector fields into their tangential and normal parts with respect to a regular surface we introduce the projection operators p_{nor} and p_{tan} by

$$\begin{aligned} p_{nor}f(x) &= (f(x) \cdot \nu(x))\nu(x), \quad x \in \Sigma, f \in c(\Sigma), \\ p_{tan}f(x) &= f(x) - p_{nor}f(x), \quad x \in \Sigma, f \in c(\Sigma). \end{aligned}$$

The corresponding subspaces of $c(\Sigma)$ are given by

$$\begin{aligned} c_{nor}(\Sigma) &= \{f \in c(\Sigma) | f = p_{nor}f\}, \\ c_{tan}(\Sigma) &= \{f \in c(\Sigma) | f = p_{tan}f\}. \end{aligned}$$

The spaces $c_{nor}^{(p)}(\Sigma)$ and $c_{tan}^{(p)}(\Sigma)$, $0 \leq p \leq \infty$ are defined in the same fashion.

The set of vector fields $f : \Sigma \rightarrow \mathbb{R}$ which are measurable and for which

$$\|f\|_{l^p(\Sigma)} = \left(\int_{\Sigma} |f(x)|^p d\omega_{\Sigma}(x) \right)^{\frac{1}{p}} < \infty$$

is denoted by $l^p(\Sigma)$, where $d\omega_{\Sigma}(x)$ symbolizes the surface element on Σ . Note that in the case of $\Sigma = \Omega_R$ with radius $R > 0$ we just write $d\omega_R(x)$ instead of $d\omega_{\Omega_R}(x)$

and $d\omega$ instead of $d\omega_1$.

The definition of the normal and the tangential operator is extended in canonical way to vector fields in $l^2(\Sigma)$. Hence,

$$\begin{aligned} l_{nor}^2(\Sigma) &= \{f \in l^2(\Sigma) | f = p_{nor}f\}, \\ l_{tan}^2(\Sigma) &= \{f \in l^2(\Sigma) | f = p_{tan}f\}. \end{aligned}$$

Clearly, we have the orthogonal decomposition

$$l^2(\Sigma) = l_{nor}^2(\Sigma) \oplus l_{tan}^2(\Sigma).$$

Definition 1.2

Let f be a tangential vector field with respect to the regular surface Σ , i.e. $f \in c_{tan}^{(1)}(\Sigma)$. Furthermore, let f possess the component functions F_i , i.e. $f(x) = \sum_{i=1}^3 F_i(x) \varepsilon^i$, $x \in \Sigma$. Then the *surface gradient* $\nabla^* \cdot$ and the *surface curl* $L^* \cdot$ are defined by

$$\begin{aligned} \nabla^* \cdot f &= \sum_{i=1}^3 (\nabla^* F_i) \cdot \varepsilon^i, \\ L^* \cdot f &= \sum_{i=1}^3 (L^* F_i) \cdot \varepsilon^i. \end{aligned}$$

1.2 Scalar Spherical Harmonics

In this section some important results concerning homogeneous harmonic polynomials in \mathbb{R}^3 restricted to the unit sphere Ω will be presented. At first the Legendre polynomials have to be introduced.

Definition 1.3

Let $P_n : [-1, 1] \rightarrow \mathbb{R}$, $n \in \mathbb{N}_0$, be a function satisfying

1. P_n is a polynomial of degree n ,
2. $\int_{-1}^1 P_n(t) P_l(t) dt = 0$, $n \neq l$,
3. $P_n(1) = 1$, for all $n \in \mathbb{N}_0$.

Then the function P_n , $n \in \mathbb{N}_0$, is called the *Legendre polynomial of degree n* .

By the above properties the Legendre polynomial of degree n is uniquely defined. An explicit representation of the Legendre polynomial of degree n is given by

$$P_n(t) = \frac{1}{2^n} \sum_{s=0}^{[n/2]} (-1)^s \frac{(2n-2s)!}{(n-2s)! (n-s)! s!} t^{n-2s}, \quad t \in [-1, 1],$$

where $[\cdot]$ denotes the well known Gauss bracket (see e.g. [20]). The second property of Definition 1.3 demands the orthogonality of two Legendre polynomials of different degree. The $\mathcal{L}^2[-1, 1]$ -norm of a Legendre polynomial of degree n can be calculated using the explicit representation and is given by

$$\int_{-1}^1 P_n(t)P_m(t) dt = \frac{2}{2n+1}\delta_{n,m}, \quad n, m \in \mathbb{N}_0,$$

where $\delta_{n,m}$ is the Kronecker symbol given by $\delta_{n,m} = 1$ if $n = m$ and $\delta_{n,m} = 0$ else.

Due to results of potential theory the relation between the expression $1/|x - y|$ and the Legendre polynomials can be deduced explicitly by

$$\frac{1}{|x - y|} = \frac{1}{|y|} \sum_{n=0}^{\infty} \left(\frac{|x|}{|y|} \right)^n P_n(\xi \cdot \eta). \quad (1.10)$$

provided that $x = |x|\xi, y = |y|\eta, \xi, \eta \in \Omega, |x| < |y|$. For the proof of this formula the reader is referred, for example, to [20].

Finally we mention the notation of a Legendre transform.

Definition 1.4

Suppose that $F \in \mathcal{L}^1[-1, 1]$ is given. Let P_n be the Legendre polynomial of degree n , then the *Legendre transform* is defined by

$$\begin{aligned} LT : \mathcal{L}^1[-1, 1] &\rightarrow \{\{F^\wedge(n)\} | n \in \mathbb{N}_0\} \\ LT(F)(n) &= F^\wedge(n) = \int_{-1}^1 F(t)P_n(t) dt. \end{aligned}$$

The numbers $F^\wedge(n), n \in \mathbb{N}_0$, are called *Legendre coefficients* of the function F .

The Legendre functions are members of a special class of spherical functions introduced by the following remark.

Remark 1.5

Any function of the form

$$\begin{aligned} G_\xi : \Omega &\rightarrow \mathbb{R}, \quad \xi \in \Omega \text{ fixed}, \\ \eta &\mapsto G_\xi(\eta) = G(\xi \cdot \eta), \quad \eta \in \Omega, \end{aligned}$$

is called a *zonal* or *radial basis function* with respect to the axis $\xi \in \Omega$. The set of all zonal functions is isomorphic to the set of all functions of type $G : [-1, 1] \rightarrow \mathbb{R}$, hence, we can regard $\mathcal{C}^{(k)}[-1, 1], 0 \leq k \leq \infty$, and $\mathcal{L}^p[-1, 1]$ equipped with the corresponding norms as subspaces of $\mathcal{C}^{(k)}(\Omega)$ and $\mathcal{L}^p(\Omega)$. Any zonal function $G_\xi(\cdot)$ depends only on the spherical distance between ξ and η .

In what follows scalar spherical harmonics are introduced. The approach presented here is based on [20]. Scalar spherical harmonics are restrictions of homogeneous harmonic polynomials in \mathbb{R}^3 to the unit sphere. More explicitly, let $H_n : \mathbb{R}^3 \rightarrow \mathbb{R}$ be a homogeneous harmonic polynomial of degree n , i.e.

1. H_n is polynomial of degree n in \mathbb{R}^3 ,
2. $H_n(\lambda x) = \lambda^n H_n(x)$ for all $\lambda \in \mathbb{R}$ and $x \in \mathbb{R}^3$ (homogeneity),
3. $\Delta_x H_n(x) = 0$ for all $x \in \mathbb{R}^3$ (harmonicity),

then the restriction $Y_n = H_n|_\Omega$ is called a *scalar spherical harmonic of degree n* . The space of all spherical harmonics of degree n is denoted by $Harm_n(\Omega)$. Its dimension is known to be $d(Harm_n(\Omega)) = 2n + 1$. Spherical harmonics of different degrees are orthogonal in the sense of the $\mathcal{L}^2(\Omega)$ -inner product, i.e.

$$(Y_n, Y_m)_{\mathcal{L}^2(\Omega)} = \int_{\Omega} Y_n(\xi) Y_m(\xi) d\omega(\xi) = 0, \quad n \neq m.$$

An essential result of the theory of scalar spherical harmonics is the fact that any spherical harmonic $Y_n, n \in \mathbb{N}_0$, is an infinitely often differentiable eigenfunction of the Beltrami operator Δ^* corresponding to the eigenvalue $-n(n+1), n \in \mathbb{N}_0$, i.e.

$$\Delta_\xi^* Y_n(\xi) = -n(n+1)Y_n(\xi), \quad \xi \in \Omega, \quad Y_n \in Harm_n(\Omega), \quad n \in \mathbb{N}_0.$$

Throughout the remainder of this work, we denote by $\{Y_{n,k}\}_{k=1,\dots,2n+1}$ a complete orthonormal system in the space $Harm_n(\Omega)$ with respect to the inner product $(\cdot, \cdot)_{\mathcal{L}^2(\Omega)}$.

The following theorem, which is known as the addition theorem of spherical harmonics, relates this orthonormal systems in $Harm_n(\Omega)$ to the aforementioned Legendre polynomials P_n on $[-1, 1]$.

Theorem 1.6

Let $\{Y_{n,k}\}_{k=1,\dots,2n+1}$ be an orthonormal system of spherical harmonics with respect to $(\cdot, \cdot)_{\mathcal{L}^2(\Omega)}$. Then

$$\sum_{k=1}^{2n+1} Y_{n,k}(\xi) Y_{n,k}(\eta) = \frac{2n+1}{4\pi} P_n(\xi \cdot \eta), \quad \xi, \eta \in \Omega.$$

As an immediate consequence of the addition theorem we obtain by letting $\eta = \xi$

$$\sum_{k=1}^{2n+1} |Y_{n,k}(\xi)|^2 = \frac{2n+1}{4\pi}, \quad \xi \in \Omega.$$

The addition theorem also shows us that the Legendre polynomial of degree n (seen as a zonal function, $P_n(\xi \cdot \cdot)$, on the sphere) is the only spherical harmonic of degree

n that is invariant with respect to orthogonal transformations which leave $\xi \in \Omega$ fixed.

The series

$$\sum_{n=0}^{\infty} \sum_{k=1}^{2n+1} F^{\wedge}(n, k) Y_{n,k}$$

is called the *Fourier expansion* or (*spherical harmonic expansion*) of F with *Fourier* or (*spherical harmonic*) *coefficients* given by

$$F^{\wedge}(n, k) = \int_{\Omega} F(\xi) Y_{n,k}(\xi) d\omega(\xi),$$

$n = 0, 1, \dots; k = 1, \dots, 2n + 1$.

The system of spherical harmonics is closed in $\mathcal{L}^2(\Omega)$, i.e. we have, for all $F \in \mathcal{L}^2(\Omega)$,

$$\lim_{N \rightarrow \infty} \left\| F - \sum_{n=0}^N \sum_{k=1}^{2n+1} F^{\wedge}(n, k) Y_{n,k} \right\|_{\mathcal{L}^2(\Omega)} = 0.$$

Furthermore, the system of spherical harmonics is complete in $\mathcal{L}^2(\Omega)$, i.e. $F \in \mathcal{L}^2(\Omega)$ and $F^{\wedge}(n, k) = (F, Y_{n,k})_{\mathcal{L}^2(\Omega)} = 0$ for all $n = 0, 1, \dots; k = 1, \dots, 2n + 1$, implies $F = 0$. For a general definition of closure and completeness and relations between the two terms in Hilbert spaces the reader is referred to [13].

By $Harm_{p,\dots,q}(\Omega)$, $q \geq p \geq 0$, we denote the space of all spherical harmonics of degree n with $p \leq n \leq q$. The orthogonality of the spherical harmonics of different degree yields

$$Harm_{p,\dots,q}(\Omega) = \bigoplus_{n=p}^q Harm_n(\Omega).$$

The dimensions of this spaces are given by

$$\begin{aligned} d(Harm_{p,\dots,q}(\Omega)) &= \sum_{n=p}^q (2n + 1), \\ d(Harm_{0,\dots,q}(\Omega)) &= (q + 1)^2. \end{aligned}$$

If $Y_n \in Harm_n(\Omega)$, then

$$\frac{2n + 1}{4\pi} \int_{\Omega} P_n(\xi \cdot \eta) Y_n(\eta) d\omega(\eta) = Y_n(\xi), \quad \xi \in \Omega.$$

In other words, the kernel function $K_{Harm_n(\Omega)} : \Omega \times \Omega \rightarrow \mathbb{R}$ defined by

$$K_{Harm_n(\Omega)}(\xi, \eta) = \frac{2n + 1}{4\pi} P_n(\xi \cdot \eta), \quad (\xi, \eta) \in \Omega \times \Omega,$$

represents the unique reproducing kernel in the Hilbert space $Harm_n(\Omega)$ with respect to the $\mathcal{L}^2(\Omega)$ -inner product. Moreover, $K_{Harm_{p,\dots,q}(\Omega)} = \sum_{n=p}^q K_{Harm_n(\Omega)}$ is

the reproducing kernel in $Harm_{p,\dots,q}(\Omega)$. For the definition of a reproducing kernel and the corresponding reproducing kernel Hilbert space the reader is referred to [13].

The formula of Funk and Hecke,

$$\int_{\Omega} G(\xi \cdot \eta) Y_n(\eta) d\omega(\eta) = G^\wedge(n) Y_n(\xi), \quad \xi \in \Omega, G \in \mathcal{L}^1[-1, 1], \quad (1.11)$$

establishes a connection between spherical harmonics and radial basis functions. It should be noted that this formula, together with the reproducing scalar kernel $K_{Harm_{p,\dots,q}(\Omega)}$, constitutes the basis for the introduction of spherical singular integrals and spherical wavelets (see e.g. [20] and [26]).

For later use we introduce the inner (outer) harmonics as the solution of the exterior (interior) Dirichlet problem in Ω_R^{int} (Ω_R^{ext}) corresponding to boundary values $Y_{n,k}$ on Ω_R .

Definition 1.7

The system of *inner (outer) harmonics* $\{H_{n,k}^{int}(R; \cdot)\}$ ($\{H_{n,k}^{ext}(R; \cdot)\}$), $n = 0, 1, \dots; k = 1, \dots, 2n + 1$, of degree n is defined by

$$\begin{aligned} H_{n,k}^{int}(R; x) &= \frac{1}{R} \left(\frac{|x|}{R} \right)^n Y_{n,k} \left(\frac{x}{|x|} \right), \quad x \in \overline{\Omega_R^{int}}, \\ H_{n,k}^{ext}(R; x) &= \frac{1}{R} \left(\frac{R}{|x|} \right)^{n+1} Y_{n,k} \left(\frac{x}{|x|} \right), \quad x \in \overline{\Omega_R^{ext}}. \end{aligned}$$

The systems of inner and outer harmonics satisfy the following properties

1. $H_{n,k}^{ext}(R; \cdot)$ is of class $\mathcal{C}^{(\infty)}(\Omega_R^{ext})$, $H_{n,k}^{int}(R; \cdot)$ is of class $\mathcal{C}^{(\infty)}(\Omega_R^{int})$.
2. $\Delta_x H_{n,k}^{ext}(R; x) = 0$ for all $x \in \Omega_R^{ext}$, $\Delta_x H_{n,k}^{int}(R; x) = 0$ for all $x \in \Omega_R^{int}$.
3. $H_{n,k}^{ext}(R; \cdot)$ is regular at infinity, i.e. $|H_{n,k}^{ext}(R; x)| = \mathcal{O}(1/|x|)$ and $|\nabla_x H_{n,k}^{ext}(R; x)| = \mathcal{O}(1/|x|^2)$ as $|x| \rightarrow \infty$.
4. $(H_{n,k}^i(R; \cdot), H_{m,l}^j(R; \cdot))_{\mathcal{L}^2(\Omega_R)} = \delta_{n,m} \delta_{k,l}$ for $i, j \in \{int, ext\}$.

More information about these systems of functions and proofs of the above relations can be found in [20]. According to our construction, it is clear that in the case of $\Omega_R = \Omega$ we have $H_{n,k}^{int}(R; \cdot)|_{R=1} = H_{n,k}^{ext}(R; \cdot)|_{R=1} = Y_{n,k}$ for all $n = 0, 1, \dots; k = 1, \dots, 2n + 1$.

It is obvious that the system $\{Y_{n,k}^R\} = \{H_{n,k}^{int}(R; \cdot)|_{\Omega_R}\} = \{H_{n,k}^{ext}(R; \cdot)|_{\Omega_R}\}$ forms an orthonormal system in $\mathcal{L}^2(\Omega_R)$. Furthermore, the system $\{Y_{n,k}^R\}$ is closed and complete in $\mathcal{L}^2(\Omega_R)$.

1.3 Two Sets of Vector Spherical Harmonics

Definition 1.8

For $\xi \in \Omega$ and $F \in \mathcal{C}^{(0_i)}(\Omega)$ the operators $o^{(i)} : \mathcal{C}^{(0_i)}(\Omega) \rightarrow c(\Omega)$, $i \in \{1, 2, 3\}$, are defined via the spherical operators

$$\begin{aligned} o_\xi^{(1)} F(\xi) &= \xi F(\xi), \\ o_\xi^{(2)} F(\xi) &= \nabla_\xi^* F(\xi), \\ o_\xi^{(3)} F(\xi) &= L_\xi^* F(\xi). \end{aligned}$$

where we have used the abbreviation

$$0_i = \begin{cases} 0 & \text{if } i = 1 \\ 1 & \text{if } i = 2, 3. \end{cases}$$

The reader should note that the definition domain of the operator $o^{(1)}$ is the space of all continuous functions, while the operators $o^{(2)}$ and $o^{(3)}$ are defined for continuously differentiable scalar fields. It is clear that $o^{(1)}F$ is a radial vector field, while $o^{(2)}F$ and $o^{(3)}F$ are purely tangential. Furthermore, the operators $o^{(i)}$ can be extended in a canonical way to the space $l^2(\Omega)$.

The adjoint operators $O^{(i)} : c^{(0_i)}(\Omega) \rightarrow \mathcal{C}(\Omega)$ of $o^{(i)}$ with respect to the $l^2(\Omega)$ –inner product are defined by

$$(o^{(i)}G, f)_{l^2(\Omega)} = (G, O^{(i)}f)_{\mathcal{L}^2(\Omega)}, \quad i \in \{1, 2, 3\},$$

for all $f \in c^{(0_i)}(\Omega)$ and $G \in \mathcal{C}^{(0_i)}(\Omega)$. An easy calculation shows the following explicit representations of $O^{(i)}$ for $\xi \in \Omega$ and $f \in c^{(0_i)}(\Omega)$

$$\begin{aligned} O_\xi^{(1)} f(\xi) &= \xi \cdot p_{nor} f(\xi), \\ O_\xi^{(2)} f(\xi) &= -\nabla_\xi^* \cdot p_{tan} f(\xi), \\ O_\xi^{(3)} f(\xi) &= -L_\xi^* \cdot p_{tan} f(\xi) \end{aligned}$$

where p_{nor} is the normal projection and p_{tan} is the tangential projection of a continuous vector field $f \in c(\Omega)$ with respect to the unit sphere.

Some useful relations concerning the application of the operators $o^{(i)}$, $i \in \{1, 2, 3\}$, to a radial basis function defined in Remark 1.5 can be given (cf. [20]). More detailed, if $F \in \mathcal{C}^{(0_i)}[-1, 1]$, then

$$o_\xi^{(1)} F(\xi \cdot \eta) = F(\xi \cdot \eta) \xi, \tag{1.12}$$

$$o_\xi^{(2)} F(\xi \cdot \eta) = F'(\xi \cdot \eta)(\eta - (\xi \cdot \eta)\xi), \tag{1.13}$$

$$o_\xi^{(3)} F(\xi \cdot \eta) = F'(\xi \cdot \eta)(\xi \wedge \eta). \tag{1.14}$$

Motivated by the operators $o^{(i)}$ we will now introduce vector spherical harmonics.

Definition 1.9

For any $Y_n \in Harm_n(\Omega)$ the vector field

$$y_n^{(i)} = o^{(i)}Y_n, \quad n \geq 0, \quad i \in \{1, 2, 3\},$$

is called a *vector spherical harmonic of degree n and type i* .

According to our construction we get

$$\xi \wedge y_n^{(1)}(\xi) = 0, \quad \xi \cdot y_n^{(2)}(\xi) = 0, \quad \xi \cdot y_n^{(3)}(\xi) = 0,$$

and

$$L_\xi^* \cdot y_n^{(2)}(\xi) = 0, \quad \nabla_\xi^* \cdot y_n^{(3)}(\xi) = 0,$$

i.e. $y_n^{(1)}$ is a purely radial field while $y_n^{(2)}$ and $y_n^{(3)}$ are tangential vector fields. The set $harm_n^{(i)}$ denotes the set of all vector spherical harmonics of order n and type i . By definition, we let

$$\begin{aligned} harm_0 &= harm_0^{(1)}, \\ harm_n &= \bigoplus_{i=1}^3 harm_n^{(i)}, \quad n \geq 1. \end{aligned}$$

If $\{Y_{n,k}\}_{n=0,1,\dots; k=1,\dots,2n+1}$ is an $\mathcal{L}^2(\Omega)$ –orthonormal set of scalar spherical harmonics it easily follows by the properties of the $o^{(i)}$ –operators (see [20]) that

$$y_{n,k}^{(i)} = (\mu_n^{(i)})^{-1/2} o^{(i)}Y_{n,k},$$

$i \in \{1, 2, 3\}, n \geq 0; k = 1, \dots, 2n+1$, forms an $l^2(\Omega)$ –orthonormal system of vector spherical harmonics, where the normalization values $\mu_n^{(i)}$ are given by

$$\mu_n^{(i)} = \begin{cases} 1 & \text{if } i = 1 \\ n(n+1) & \text{if } i = 2, 3. \end{cases} \quad (1.15)$$

It is known that the system $\{y_{n,k}^{(i)}\}$ is a complete and closed orthonormal system in $l^2(\Omega)$. To explain this we need some further notation and preparation which follows mainly the course of [20].

Definition 1.10

A vector field $h_n : \mathbb{R}^3 \rightarrow \mathbb{R}^3, n \in \mathbb{N}_0$, is called a *homogeneous harmonic vector polynomial of degree n* if $h_n \cdot \varepsilon^i$ is a homogenous harmonic polynomial of degree n for every $i \in \{1, 2, 3\}$.

Using the abbreviation

$$Harm_n(\mathbb{R}^3)\varepsilon^i = \{H_n \varepsilon^i \mid H_n \in Harm_n(\mathbb{R}^3)\},$$

the space of all homogeneous vector polynomials of degree n is characterized by

$$\bigoplus_{i=1}^3 \text{Harm}_n(\mathbb{R}^3) \varepsilon^i.$$

Suppose that H_n is of class $\text{Harm}_n(\mathbb{R}^3)$, then it is immediately clear, that ∇H_n is a homogeneous harmonic vector polynomial of degree $n-1$. A simple calculation shows that $x \mapsto x \wedge \nabla_x H_n(x)$, $x \in \mathbb{R}^3$, yields a homogeneous harmonic vector polynomial of degree n and it easily follows that $x \mapsto ((2n+1)x - |x|^2 \nabla_x) H_n(x)$, $x \in \mathbb{R}^3$, is a homogeneous vector polynomial of degree $n+1$ (see e.g. [20]).

This motivates the following definition.

Definition 1.11

For $F : \mathbb{R}^3 \rightarrow \mathbb{R}$ being sufficiently smooth the operators $k_n^{(i)}$, $i \in \{1, 2, 3\}$, are, for $x \in \mathbb{R}^3$, defined by

$$\begin{aligned} k_n^{(1)} F(x) &= ((2n+1)x - |x|^2 \nabla_x) F(x), \\ k_n^{(2)} F(x) &= \nabla_x F(x), \\ k_n^{(3)} F(x) &= x \wedge \nabla_x F(x). \end{aligned}$$

For later use we need the curl in \mathbb{R}^3 of the above vector fields $k_n^{(i)} F$, $i \in \{1, 2, 3\}$, which will be given here.

Lemma 1.12

Let the function $F \in \mathcal{C}^{(2)}(\mathbb{R}^3)$ be given. Then we have

$$\nabla_x \wedge (k_n^{(1)} F(x)) = -(2n+3) k_n^{(3)} F(x), \quad (1.16)$$

$$\nabla_x \wedge (k_n^{(2)} F(x)) = 0, \quad (1.17)$$

$$\nabla_x \wedge (k_n^{(3)} F(x)) = x(\Delta_x F(x)) - 2k_n^{(2)} F(x) - (x \cdot \nabla_x) k_n^{(2)} F(x) \quad (1.18)$$

for $x \in \mathbb{R}^3$.

Proof:

An easy calculation shows that

$$\begin{aligned} \nabla_x \wedge k_n^{(1)} F(x) &= \nabla_x \wedge ((2n+1)x - |x|^2 \nabla_x) F(x) \\ &= (2n+1) \nabla_x F(x) \wedge x + F(x) (\nabla_x \wedge x) \\ &\quad - \nabla_x |x|^2 \wedge \nabla_x F(x) - |x|^2 (\nabla_x \wedge \nabla_x F(x)). \end{aligned} \quad (1.19)$$

Observing that the second and the fourth term in (1.19) vanish we obtain

$$\begin{aligned} \nabla_x \wedge k_n^{(1)} F(x) &= -(2n+1)(x \wedge \nabla_x) F(x) - 2(x \wedge \nabla_x) F(x) \\ &= -(2n+3) k_n^{(3)} F(x). \end{aligned}$$

This yields (1.16). Equation (1.17) is obvious and by some similar calculations as performed in (1.16) we get

$$\begin{aligned}
 \nabla_x \wedge k_n^{(3)} F(x) &= \nabla_x \wedge (x \wedge \nabla_x F(x)) \\
 &= x(\Delta F(x)) - \nabla_x F(x)(\nabla_x \cdot x) \\
 &\quad + (\nabla_x F(x) \cdot \nabla_x)x - (x \cdot \nabla_x)\nabla_x F(x) \\
 &= x(\Delta_x F(x)) - 2k_n^{(2)} F(x) - (x \cdot \nabla_x)k_n^{(2)} F(x).
 \end{aligned}$$

This finally gives the desired result. \square

An important consequence of (1.18) can be achieved by using the decomposition of the gradient into a normal and a tangential part with respect to the unit sphere Ω , $\nabla_x = \xi \partial_r + (1/r)\nabla_\xi^*$, and the representation of the Laplace operator in spherical coordinates, $\Delta_x = \partial_r^2 + (2/r)\partial_r + (1/r^2)\Delta_\xi^*$. For $x = r\xi$, $r = |x| > 0$, we obtain

$$\begin{aligned}
 \nabla_x \wedge k_n^{(3)} F(x) &= x(\Delta_x F(x)) - 2\nabla_x F(x) - (x \cdot \nabla_x)\nabla_x F(x) \\
 &= x(\Delta_x F(x)) - 2\nabla_x F(x) - (r\partial_r) \left(\xi \partial_r F(x) + \frac{1}{r}\nabla_\xi^* F(x) \right) \\
 &= x(\Delta_x F(x)) - 2\xi \partial_r F(x) + \frac{2}{r}\nabla_\xi^* F(x) \\
 &\quad - x\partial_r^2 F(x) + \frac{1}{r}\nabla_\xi^* F(x) - \partial_r \nabla_\xi^* F(x) \\
 &= x \left(\Delta_x F(x) - \partial_r^2 F(x) - \frac{2}{r}\partial_r F(x) \right) + \nabla_\xi^* \left(-\frac{1}{r}\partial_r(rF(x)) \right) \\
 &= \xi \left(\frac{1}{r}\Delta_\xi^* F(x) \right) + \nabla_\xi^* \left(-\frac{1}{r}\partial_r(rF(x)) \right)
 \end{aligned}$$

where we have used the abbreviation $\partial_r = \partial/\partial r$. Thus we find, for $x = r\xi \in \mathbb{R}^3 \setminus \{0\}$,

$$\nabla_x \wedge k_n^{(3)} F(x) = o_\xi^{(1)} \left(\frac{1}{r}\Delta_\xi^* F(r\xi) \right) + o_\xi^{(2)} \left(-\frac{1}{r}\partial_r(rF(x)) \right), \quad (1.20)$$

where the operators $o^{(1)}$ and $o^{(2)}$ are given as formulated in Definition 1.8.

Let us now return to the operators $k_n^{(i)}$ and their connection to homogeneous harmonic vector polynomials. Observing the aforementioned properties of the operators $k_n^{(i)}$, we can summarize our results as follows.

Lemma 1.13

Let H_n be of class $\text{Harm}_n(\mathbb{R}^3)$, $n \in \mathbb{N}_0$. Then $k_n^{(i)} H_n$ is a homogeneous harmonic vector polynomial of degree $\deg^{(i)}(n)$, where we have used the abbreviation

$$\deg^{(i)}(n) = \begin{cases} n+1 & \text{if } i = 1 \\ n-1 & \text{if } i = 2 \\ n & \text{if } i = 3. \end{cases}$$

From the representation of the gradient in spherical coordinates (1.2) it follows that

$$\begin{aligned} k_n^{(1)}(r^n Y_n(\xi)) &= (n+1)r^{n+1}Y_n(\xi)\xi - r^{n+1}\nabla_\xi^* Y_n(\xi), \\ k_n^{(2)}(r^n Y_n(\xi)) &= nr^{n-1}Y_n(\xi)\xi + r^{n-1}\nabla_\xi^* Y_n(\xi), \\ k_n^{(3)}(r^n Y_n(\xi)) &= r^n L_\xi^* Y_n(\xi) \end{aligned} \quad (1.21)$$

for $Y_n \in \text{Harm}_n(\Omega)$ and $x = r\xi, r = |x| > 0$. Thus, we get by virtue of the Definition of the $o^{(i)}$ -operators (see Definition 1.8),

$$\begin{aligned} k_n^{(1)}Y_n(\xi) &= (n+1)o^{(1)}Y_n(\xi) - o^{(2)}Y_n(\xi), \\ k_n^{(2)}Y_n(\xi) &= no^{(1)}Y_n(\xi) + o^{(2)}Y_n(\xi), \\ k_n^{(3)}Y_n(\xi) &= o^{(3)}Y_n(\xi). \end{aligned}$$

for $Y_n \in \text{Harm}_n(\Omega)$ and $\xi \in \Omega$. Note that the operators $k_n^{(i)}$ act on the variable ξ , as does $o^{(i)}$, but this will not be indicated in our notation unless it does not lead to confusion.

By a simple rearrangement of the above equations it can be verified that every type 1 or type 2 vector spherical harmonic of degree n can be expressed as linear combinations of homogeneous vector polynomials of degree $n-1$ and $n+1$, restricted to the unit sphere, whereas a spherical harmonic of order n and type 3 is a linear combination of scalar spherical harmonics of order n , i.e.

$$\begin{aligned} o^{(1)}Y_n(\xi) &= \frac{1}{2n+1} (k_n^{(1)}r^n Y_n(\xi))_{r=1} + \frac{1}{2n+1} (k_n^{(2)}r^n Y_n(\xi))_{r=1}, \\ o^{(2)}Y_n(\xi) &= \frac{-n}{2n+1} (k_n^{(1)}r^n Y_n(\xi))_{r=1} + \frac{n+1}{2n+1} (k_n^{(2)}r^n Y_n(\xi))_{r=1}, \\ o^{(3)}Y_n(\xi) &= (k_n^{(3)}r^n Y_n(\xi))_{r=1}, \end{aligned}$$

In conclusion, we get

$$\text{harm}_n^{(i)} \subset \bigoplus_{j=1}^3 \text{Harm}_{n-1}(\Omega)\varepsilon^j \oplus \bigoplus_{j=1}^3 \text{Harm}_{n+1}(\Omega)\varepsilon^j, \quad i = 1, 2, \quad (1.22)$$

$$\text{harm}_n^{(3)} \subset \bigoplus_{j=1}^3 \text{Harm}_{n-1}(\Omega)\varepsilon^j. \quad (1.23)$$

From (1.22) and (1.23) we can easily deduce the following orthogonality relations.

Lemma 1.14

Let $y_n^{(i)} \in \text{harm}_n^{(i)}$ and $Y_m \in \text{Harm}_m$. Then

$$\int_{\Omega} y_n^{(i)}(\xi) Y_m(\xi) d\omega(\xi) = 0,$$

whenever $i \in \{1, 2\}$ and $m \notin \{n-1, n+1\}$ or $i = 3$ and $m \neq n$.

At this point we give a result of the theory of vector spherical harmonics which will be of use later on but fits into the concept at this point, namely a generalization of the Funk–Hecke formula (see (1.11)) to the vectorial case. We give the theorem without any proof. The motivation, the development and the proof can be found in [20].

Theorem 1.15

Let $G \in \mathcal{L}^1[-1, +1]$ and assume Y_n to be of class $Harm_n$. Then, for all $\eta \in \Omega$, we have

$$\begin{aligned} \int_{\Omega} G(\xi \cdot \eta) o_{\xi}^{(1)} Y_n(\xi) d\omega(\xi) &= G_{(1,1)}^{\wedge}(n) o_{\eta}^{(1)} Y_n(\eta) + G_{(1,2)}^{\wedge}(n) o_{\eta}^{(2)} Y_n(\eta), \\ \int_{\Omega} G(\xi \cdot \eta) o_{\xi}^{(2)} Y_n(\xi) d\omega(\xi) &= G_{(2,1)}^{\wedge}(n) o_{\eta}^{(1)} Y_n(\eta) + G_{(2,2)}^{\wedge}(n) o_{\eta}^{(2)} Y_n(\eta), \\ \int_{\Omega} G(\xi \cdot \eta) o_{\xi}^{(3)} Y_n(\xi) d\omega(\xi) &= G_{(3,3)}^{\wedge}(n) o_{\eta}^{(3)} Y_n(\eta), \end{aligned}$$

where the numbers $G_{(i,j)}^{\wedge}(n)$ are given by

$$\begin{aligned} G_{(1,1)}^{\wedge}(n) &= \frac{1}{2n+1} ((n+1)G^{\wedge}(n+1) + nG^{\wedge}(n-1)), \\ G_{(1,2)}^{\wedge}(n) &= \frac{1}{2n+1} (G^{\wedge}(n-1) - G^{\wedge}(n+1)), \\ G_{(2,1)}^{\wedge}(n) &= \frac{n(n+1)}{2n+1} (G^{\wedge}(n-1) - G^{\wedge}(n+1)), \\ G_{(2,2)}^{\wedge}(n) &= \frac{1}{2n+1} (nG^{\wedge}(n+1) + (n+1)G^{\wedge}(n-1)), \\ G_{(3,3)}^{\wedge}(n) &= G^{\wedge}(n). \end{aligned}$$

Another property which is deducible from (1.22) and (1.23) is the fact, that

$$harm_n \subset \bigoplus_{m=n-1}^{n+1} \bigoplus_{i=1}^3 Harm_m(\Omega) \varepsilon^i.$$

On the other hand it is obvious from the corresponding results of the theory of scalar spherical harmonics that $\bigoplus_{m=0}^{\infty} \bigoplus_{i=1}^3 Harm_m(\Omega) \varepsilon^i$ is dense in $c(\Omega)$ with respect to $\|\cdot\|_{c(\Omega)}$ and dense in $l^2(\Omega)$ with respect to $(\cdot, \cdot)_{l^2(\Omega)}$.

Summarizing the result we obtain the following theorem.

Theorem 1.16

Let the system of vector spherical harmonics $\{y_{n,k}^{(i)}\}_{\substack{n=0,\dots; \\ k=1,\dots,2n+1}}, i \in \{1, 2, 3\}$, be defined as in (1.15). Then the following statements are valid:

1. The system of vector spherical harmonics is closed in $c(\Omega)$ with respect to $\|\cdot\|_{c(\Omega)}$ and $\|\cdot\|_{l^2(\Omega)}$.

2. The system is complete in $l^2(\Omega)$ with respect to $(\cdot, \cdot)_{l^2(\Omega)}$.

Note that the system of vector spherical harmonics given by

$$y_{n,k}^{(i),R} = \frac{1}{R} y_{n,k}^{(i)}, \quad i \in \{1, 2, 3\}; n = 0, \dots; k = 1, \dots, 2n+1, \quad (1.24)$$

establishes a closed and complete orthonormal system in the Hilbert space $l^2(\Omega_R)$.

Part (1) of this theorem states, that every continuous vector field $f \in c(\Omega)$ can be approximated with arbitrary accuracy by a finite linear combination of vector spherical harmonics. Part (2) is equivalent to the fact that every vector field in $l^2(\Omega)$ can be expressed by its Fourier series in terms of the system $\{y_{n,k}^{(i)}\}$, i.e.

$$\lim_{N \rightarrow \infty} \left\| f - \sum_{i=1}^3 \sum_{n=0}^N \sum_{k=1}^{2n+1} (f_{\mathcal{Y}}^{(i)})^\wedge(n, k) y_{n,k}^{(i)} \right\|_{l^2(\Omega)} = 0, \quad (1.25)$$

with the Fourier coefficients

$$(f_{\mathcal{Y}}^{(i)})^\wedge(n, k) = \left(f, y_{n,k}^{(i)} \right)_{l^2(\Omega)} = \int_{\Omega} f(\xi) \cdot y_{n,k}^{(i)}(\xi) d\omega(\xi).$$

The subscript \mathcal{Y} thereby denotes that the Fourier coefficients are taken with respect to the orthonormal system of vector spherical harmonics $\mathcal{Y} = \{y_{n,k}^{(i)}\}_{\substack{n=0, \dots; \\ k=1, \dots, 2n+1}}, i \in \{1, 2, 3\}$.

In terms of subspaces of $l^2(\Omega)$ we may, of course, write

$$f = \sum_{i=1}^3 f_{\mathcal{Y}}^{(i)}$$

with the vector fields $f_{\mathcal{Y}}^{(i)}$, $i \in \{1, 2, 3\}$, given by

$$f_{\mathcal{Y}}^{(i)} = \sum_{(n,k) \in \mathcal{N}^{(i)}} (f_{\mathcal{Y}}^{(i)})^\wedge(n, k) y_{n,k}^{(i)}$$

in the sense of the $l^2(\Omega)$ -norm, where we have used the abbreviation

$$\mathcal{N}^{(i)} = \{n = 0, \dots; k = 1, \dots, 2n+1\}. \quad (1.26)$$

Consequently, we are able to write

$$l^2(\Omega) = l_{\mathcal{Y}}^{2,(1)}(\Omega) \oplus l_{\mathcal{Y}}^{2,(2)}(\Omega) \oplus l_{\mathcal{Y}}^{2,(3)}(\Omega), \quad (1.27)$$

with

$$l_{\mathcal{Y}}^{2,(1)}(\Omega) = \overline{\bigoplus_{n=0}^{\infty} \text{span}\{y_{n,k}^{(1)} | k = 1, \dots, 2n+1\}}}_{\|\cdot\|_{l^2(\Omega)}}, \quad (1.28)$$

$$l_{\mathcal{Y}}^{2,(2)}(\Omega) = \overline{\bigoplus_{n=1}^{\infty} \text{span}\{y_{n,k}^{(2)} | k = 1, \dots, 2n+1\}}}_{\|\cdot\|_{l^2(\Omega)}}, \quad (1.29)$$

$$l_{\mathcal{Y}}^{2,(3)}(\Omega) = \overline{\bigoplus_{n=1}^{\infty} \text{span}\{y_{n,k}^{(3)} | k = 1, \dots, 2n+1\}}}_{\|\cdot\|_{l^2(\Omega)}}. \quad (1.30)$$

The decomposition of $l^2(\Omega)$ into the subspaces $l_{\mathcal{Y}}^{2,(i)}(\Omega)$ separates between purely radial and tangential vector fields. It consists of the space $l_{\mathcal{Y}}^{2,(1)}(\Omega)$ which contains purely radial fields and the two tangential field spaces $l_{\mathcal{Y}}^{2,(2)}(\Omega)$ and $l_{\mathcal{Y}}^{2,(3)}(\Omega)$, the first of which contains surface curl free vector fields and the second contains surface divergence free fields.

To construct a second set of vector spherical harmonics we use the restriction of homogeneous harmonic vector polynomials to the sphere. Thus, we return to (1.21) where we have applied the operators $k_n^{(i)}$ defined in Definition 1.11 to the harmonic function $r^n Y_n$. If we restrict the resulting functions to the unit sphere we get another system of vector spherical harmonics. This system is known from theoretical physics and developed, for example, in [5] or [16]. The introduction of the system given in this thesis follows mainly the course of [20] and [50]. In our nomenclature a system of vector spherical harmonics is described by the following lemma.

Lemma 1.17

Let $\{Y_{n,k}\}_{\substack{n=0,1,\dots; \\ k=1,\dots,2n+1}}$ be an $\mathcal{L}^2(\Omega)$ – orthonormal system of scalar spherical harmonics. Then the vector fields

$$\begin{aligned} u_{n,k}^{(1)} &= (\nu_n^{(1)})^{-1/2} ((n+1)o^{(1)}Y_{n,k} - o^{(2)}Y_{n,k}), \\ &= \sqrt{\frac{n+1}{2n+1}}y_{n,k}^{(1)} - \sqrt{\frac{n}{2n+1}}y_{n,k}^{(2)}, \end{aligned}$$

$$n = 0, 1, \dots; k = 1, \dots, 2n+1,$$

$$\begin{aligned} u_{n,k}^{(2)} &= (\nu_n^{(2)})^{-1/2} (no^{(1)}Y_{n,k} + o^{(2)}Y_{n,k}), \\ &= \sqrt{\frac{n}{2n+1}}y_{n,k}^{(1)} + \sqrt{\frac{n+1}{2n+1}}y_{n,k}^{(2)}, \end{aligned}$$

$$n = 1, 2, \dots; k = 1, \dots, 2n+1,$$

$$u_{n,k}^{(3)} = (\nu_n^{(3)})^{-1/2} o^{(3)}Y_{n,k} = y_{n,k}^{(3)},$$

$$n = 1, 2, \dots; k = 1, \dots, 2n+1,$$

form an $l^2(\Omega)$ –orthonormal set of vector spherical harmonics with the normalization coefficients given by

$$\begin{aligned} \nu_n^{(1)} &= (n+1)(2n+1), \quad n \in \mathbb{N}_0, \\ \nu_n^{(2)} &= n(2n+1), \quad n \in \mathbb{N}, \\ \nu_n^{(3)} &= n(n+1), \quad n \in \mathbb{N}. \end{aligned}$$

The proof of this lemma easily follows from computations involving the orthonormality of the system $\{y_{n,k}^{(i)}\}$. The reader should note, that the system $\{u_{n,k}^{(i)}\}$ does not separate between radial and tangential fields. However, as we will see later, this system has other advantageous properties in electro- and magnetostatic modelling.

A direct consequence of Theorem 1.16 is the following result.

Corollary 1.18

Let the system of vector spherical harmonics $\{u_{n,k}^{(i)}\}_{\substack{n=0_i,\dots; \\ k=1,\dots,2n+1}}, i \in \{1, 2, 3\}$, be defined as in Lemma 1.17. Then the following statements are valid:

1. The system of vector spherical harmonics is closed in $c(\Omega)$ with respect to $\|\cdot\|_{c(\Omega)}$ and $\|\cdot\|_{l^2(\Omega)}$.
2. The system is complete in $l^2(\Omega)$ with respect to $(\cdot, \cdot)_{l^2(\Omega)}$.

Note that the system of vector spherical harmonics given by

$$u_{n,k}^{(i),R} = \frac{1}{R} u_{n,k}^{(i)}, \quad i \in \{1, 2, 3\}; n = 0_i, \dots; k = 1, \dots, 2n + 1, \quad (1.31)$$

establishes a closed and complete orthonormal system in the Hilbert space $l^2(\Omega_R)$.

Part (2) of Corollary 1.18 enables us to represent every $l^2(\Omega)$ -vector field f by its Fourier series in terms of the system $\{u_{n,k}^{(i)}\}_{\substack{n=0_i,\dots; \\ k=1,\dots,2n+1}}, i \in \{1, 2, 3\}$, i.e. we have

$$\lim_{N \rightarrow \infty} \left\| f - \sum_{i=1}^3 \sum_{n=0_i}^N \sum_{k=1}^{2n+1} (f_{\mathcal{U}}^{(i)})^\wedge(n, k) u_{n,k}^{(i)} \right\|_{l^2(\Omega)} = 0,$$

with Fourier coefficients

$$(f_{\mathcal{U}}^{(i)})^\wedge(n, k) = \left(f, u_{n,k}^{(i)} \right)_{l^2(\Omega)} = \int_{\Omega} f(\xi) \cdot u_{n,k}^{(i)}(\xi) d\omega(\xi).$$

Note that, as before, the subscript \mathcal{U} denotes that the Fourier coefficients are taken with respect to the orthonormal system of vector spherical harmonics $\mathcal{U} = \{u_{n,k}^{(i)}\}_{\substack{n=0_i,\dots; \\ k=1,\dots,2n+1}}, i \in \{1, 2, 3\}$.

Alternatively to the above representation, we can write

$$f = \sum_{i=1}^3 f_{\mathcal{U}}^{(i)}$$

with the vector fields $f_{\mathcal{U}}^{(i)}, i \in \{1, 2, 3\}$, given by

$$f_{\mathcal{U}}^{(i)} = \sum_{(n,k) \in \mathcal{N}^{(i)}} (f_{\mathcal{U}}^{(i)})^\wedge(n, k) u_{n,k}^{(i)}$$

in the sense of the $l^2(\Omega)$ –norm. In the sense of subspaces of the Hilbert space $l^2(\Omega)$ the above results may be written as follows.

$$l^2(\Omega) = l_{\mathcal{U}}^{2,(1)}(\Omega) \oplus l_{\mathcal{U}}^{2,(2)}(\Omega) \oplus l_{\mathcal{U}}^{2,(3)}(\Omega), \quad (1.32)$$

with

$$l_{\mathcal{U}}^{2,(1)}(\Omega) = \overline{\bigoplus_{n=0}^{\infty} \text{span}\{u_{n,k}^{(1)} | k = 1, \dots, 2n+1\}}^{\|\cdot\|_{l^2(\Omega)}}, \quad (1.33)$$

$$l_{\mathcal{U}}^{2,(2)}(\Omega) = \overline{\bigoplus_{n=1}^{\infty} \text{span}\{u_{n,k}^{(2)} | k = 1, \dots, 2n+1\}}^{\|\cdot\|_{l^2(\Omega)}}, \quad (1.34)$$

$$l_{\mathcal{U}}^{2,(3)}(\Omega) = \overline{\bigoplus_{n=1}^{\infty} \text{span}\{u_{n,k}^{(3)} | k = 1, \dots, 2n+1\}}^{\|\cdot\|_{l^2(\Omega)}}. \quad (1.35)$$

For both orthonormal systems there are certain vectorial addition theorems available as for the case of scalar spherical harmonics (see Theorem 1.6). For the formulation of the vectorial addition theorems tensorial Legendre functions have to be introduced. Since these functions are not further needed during the course of this thesis they are not given here. The interested reader is referred to [50], where systems of vector spherical harmonics are introduced in a very complete manner.

Finally, it should be mentioned that both system of spherical harmonics of degree n are infinitely often differentiable eigenfunctions of the vectorial Beltrami operator Δ^* , defined by

$$\Delta^* = p_{\text{norm}}(\Delta^* + 2)p_{\text{norm}} + p_{\text{tan}}\Delta^*p_{\text{tan}},$$

to the eigenvalue $-n(n+1)$, i.e. we have for all $n = 0, \dots; k = 1, \dots, 2n+1$ and $i \in \{1, 2, 3\}$,

$$\begin{aligned} \Delta^* y_{n,k}^{(i)} &= -n(n+1)y_{n,k}^{(i)}, \\ \Delta^* u_{n,k}^{(i)} &= -n(n+1)u_{n,k}^{(i)}. \end{aligned}$$

For more information concerning the definition and the properties of the vectorial Beltrami operator the reader is again referred to [50].

1.4 The Mie Representation

The following section is concerned with the introduction of two different kinds of representing vector fields. First of all we will formulate the Helmholtz decomposition for vector fields on a regular surface and specify the decomposition for spherical vector fields. We will see that this decomposition is strongly related to the operators $o^{(i)}$ introduced in the last section. The Helmholtz representation theorem for regular surfaces is just a special case of the general Helmholtz decomposition theorem for

vector fields defined on the Euclidean space \mathbb{R}^3 .

In addition to the Helmholtz representation we will present another decomposition, called Mie representation, which can be formulated for solenoidal vector fields defined in a subset of \mathbb{R}^3 . The Mie representation is well known especially in the geomagnetic literature (see [5], [6]) but also used in mathematics (see [29], [59]). We will just recapitulate some important facts of the Mie representation which are useful for further considerations.

In the nomenclature introduced in the previous sections the Helmholtz decomposition theorem for vector fields on regular surfaces reads as follows.

Theorem 1.19

Let Σ be a regular surface. Furthermore, let $f : \Sigma \rightarrow \mathbb{R}^3$ be a continuously differentiable vector field on Σ . Then there exist uniquely determined scalar fields $F_1 \in \mathcal{C}^{(1)}(\Sigma)$ and $F_2, F_3 \in \mathcal{C}^{(2)}(\Sigma)$ satisfying

$$\int_{\Sigma} F_i(x) d\omega_{\Sigma}(x) = 0, \quad i = 2, 3,$$

such that

$$f = \nu F_1 + \nabla^* F_2 + L^* F_3. \quad (1.36)$$

Equation (1.36) is called Helmholtz decomposition of f with respect to the regular surface Σ .

For a proof of this theorem the reader is referred, for example, to [45] and for a development of this result from the more practical point of view with application to geomagnetism see, for example, [6].

Observing that the sphere Ω is just a special regular surface in \mathbb{R}^3 we get the following result.

Corollary 1.20

Let $f : \Omega \rightarrow \mathbb{R}^3$ be a continuously differentiable vector field. Then there exist uniquely determined scalar functions $F_1 \in \mathcal{C}^{(1)}(\Omega)$ and $F_2, F_3 \in \mathcal{C}^{(2)}(\Omega)$ satisfying

$$\int_{\Omega} F_i(\xi) d\omega(\xi) = 0, \quad i = 2, 3,$$

such that

$$\begin{aligned} f(\xi) &= \xi F_1(\xi) + \nabla_{\xi}^* F_2(\xi) + L_{\xi}^* F_3(\xi) \\ &= o^{(1)} F_1(\xi) + o^{(2)} F_2(\xi) + o^{(3)} F_3(\xi), \quad \xi \in \Omega \end{aligned} \quad (1.37)$$

where the operators $o^{(i)}, i \in \{1, 2, 3\}$, are given in Definition 1.8.

Because of (1.37) the operators $o^{(i)}, i \in \{1, 2, 3\}$, are sometimes called Helmholtz operators.

It should be mentioned that F_1 is just the radial projection of f and that for the Helmholtz scalars F_2 and F_3 explicit representations are available in terms of the Green function with respect to the Beltrami operator (see [20]). Note that the Helmholtz theorem for the sphere is also valid for vector fields on Ω_R , $R > 0$, since a vector field defined on Ω_R can be mapped isomorphically to a vector field defined on Ω .

If the vector field f is defined on a spherical shell $\Omega_{(a,b)} \subset \mathbb{R}^3$ the spherical Helmholtz decomposition can be applied on every sphere Ω_r with $r \in (a, b)$. This procedure results in sufficiently smooth scalar fields $F_1, F_2, F_3 : \Omega_{(a,b)} \rightarrow \mathbb{R}$ with

$$f(r\xi) = \xi F_1(r\xi) + \nabla_\xi^* F_2(r\xi) + L_\xi^* F_3(r\xi) \quad r \in (a, b), \xi \in \Omega. \quad (1.38)$$

Using representation (1.38) we can apply the curl operator to a vector field f in Helmholtz representation.

Lemma 1.21

Let the vector field $f : \Omega_{(a,b)} \rightarrow \mathbb{R}^3$ be decomposed as in (1.38). Then we have

$$(\nabla \wedge f)(r\xi) = \xi \left[\frac{\Delta_\xi^* F_3(r\xi)}{r} \right] + \nabla_\xi^* \left[-\frac{\partial_r(r F_3(r, \xi))}{r} \right] + L_\xi^* \left[\frac{\partial_r(r F_2(r\xi))}{r} - \frac{F_1(r\xi)}{r} \right],$$

for $r \in (a, b)$ and $\xi \in \Omega$.

A proof of this result can be found, for example, in [6].

For a scalar field F the abbreviation $\partial_r F$ is in a mathematically correct notation given by

$$\partial_r F(r\xi) = \left(\frac{\partial}{\partial r'} F(r'\xi) \right) |_{r'=r}.$$

As we can see in the above version of the spherical Helmholtz theorem, the decomposition of a vector field into Helmholtz scalars is restricted to spheres or to regular surfaces. If the radius of the sphere changes the Helmholtz scalars change and they may even mix. Thus, the Helmholtz decomposition does not seem to be the best method to cope with given three-dimensional vector fields. To overcome this drawback we introduce another decomposition of a vector field, called Mie representation. This method is just applicable for certain so-called solenoidal vector fields, which turns out to be not a severe restriction in most geomathematical applications. The Mie representation is a decomposition of a solenoidal vector field into a poloidal and a toroidal part, which are special types of vector fields.

Most of the definitions and proofs in this paragraph can be found in [6] and the references therein.

Definition 1.22

Let f be a vector field defined on a non-empty region $U \subset \mathbb{R}^3$. f is called *solenoidal* in U if, for every closed surface S lying entirely in U ,

$$\int_S f(y) \cdot d\omega_S(y) = 0.$$

By Gauss' theorem it is clear that every vector field being solenoidal in U is divergence free in U . The converse is false as the reader can verify with the vector field $f(x) = x/|x|^2$, $x \in \Omega_{(a,b)}$ with $0 < a < b$.

After this preparation we are able to formulate the Mie representation, which is the fundamental theorem for our further considerations concerning geomathematical vector fields.

Theorem 1.23

Let $\Omega_{(a,b)}$ be a spherical shell with $0 \leq a < b < \infty$. Furthermore, let f be a solenoidal vector field in $\Omega_{(a,b)}$. Then there exist unique scalar fields P, Q in $\Omega_{(a,b)}$ such that

$$\int_{\Omega_r} P(x) d\omega_r(x) = \int_{\Omega_r} Q(x) d\omega_r(x) = 0, \quad r \in (a, b),$$

and

$$f = p + q = \nabla \wedge LP + LQ \quad \text{in } \Omega_{(a,b)}.$$

The vector field $p = \nabla \wedge LP$ is called the poloidal part of f and the field $q = LQ$ is called the toroidal part of f .

This nomenclature is put in concrete terms in the following definitions.

Definition 1.24

Let $\Omega_{(a,b)}$ be defined as above, then a vector field q is called *toroidal* in $\Omega_{(a,b)}$ if there exists a scalar field Q in $\Omega_{(a,b)}$ such that

$$q = LQ \quad \text{in } \Omega_{(a,b)}.$$

Q is called the toroidal scalar of q in $\Omega_{(a,b)}$.

Furthermore, a vector field p is called *poloidal* in $\Omega_{(a,b)}$ if there exists a scalar field P in $\Omega_{(a,b)}$ such that

$$p = \nabla \wedge LP \quad \text{in } \Omega_{(a,b)}.$$

P is called the poloidal scalar of p in $\Omega_{(a,b)}$.

If we have a look at the definition of the curl gradient as $L_x = x \wedge \nabla_x$ and use the representation of the gradient in polar coordinates $\nabla_x = \xi \frac{\partial}{\partial r} + \frac{1}{r} \nabla_\xi^*$ with $x = r\xi \in \mathbb{R}^3 \setminus \{0\}$, then we see that

$$L_x = r\xi \wedge \left(\xi \frac{\partial}{\partial r} + \frac{1}{r} \nabla_\xi^* \right) = \xi \wedge \nabla_\xi^* = L_\xi^*.$$

But this shows us that toroidal vector fields are purely tangential fields if restricted to a sphere Ω_r with $r \in (a, b)$.

Next, we recapitulate a theorem which gives a possibility to test whether a vector field is poloidal or toroidal in a spherical shell $\Omega_{(a,b)}$.

Theorem 1.25

1. A vector field p in $\Omega_{(a,b)}$ is poloidal if and only if it is solenoidal and its curl is tangential, i.e. $(x/|x|) \cdot (\nabla_x \wedge p(x)) = 0$ for all $x \in \Omega_{(a,b)}$.
2. A vector field q in $\Omega_{(a,b)}$ is toroidal if and only if it is solenoidal and tangential, i.e. $(x/|x|) \cdot q(x) = 0$ for all $x \in \Omega_{(a,b)}$.

A proof of this theorem can be found, for example, in [6].

At the end, we connect the two fundamental representations of this section, the Mie representation given in Theorem 1.23 and the Helmholtz representation given in Corollary 1.20.

Theorem 1.26

Let f be solenoidal in $\Omega_{(a,b)}$. Let, furthermore, the Mie representation of f be given by

$$f = \nabla \wedge LP + LQ \quad \text{in } \Omega_{(a,b)}.$$

Then the Helmholtz representation of f restricted to a sphere Ω_r with $r \in (a, b)$ is given by

$$f(x) = \xi \left(\frac{\Delta_\xi^* P(x)}{r} \right) + \nabla_\xi^* \left(-\frac{1}{r} \frac{\partial}{\partial r} (rP(x)) \right) + L_\xi^* Q(x), \quad x \in \Omega_r.$$

A proof of this theorem can be found in [6].

In this case the application of the (spherical) operators ∇^* and L^* to the three-dimensional scalar fields P and Q , must be seen as the application to the restrictions of the scalar fields P and Q to the corresponding sphere Ω_r .

Chapter 2

Multiresolution Analysis of Operator Equations

In this chapter we introduce a multiresolution analysis for operator equations between two separable Hilbert spaces of scalar or vector valued functions, based on the knowledge of the singular system of the operator. The theory as presented here, is based on [21] and [25].

At first we will formulate the multiscale approach for operators between two Hilbert spaces of scalar valued functions. This concise introduction should give the reader a feeling how scaling functions and wavelets for evaluating operator equations can be built and how a multiresolution decomposition of the evaluation of an operator equation can be established. Then we will go over to operator equations between two vector valued function spaces and formulate a vectorial multiresolution analysis by means of vector scaling functions and wavelets. The canonical approach for dealing with operator equations between vector valued function spaces would be by means of tensorial kernel functions which will briefly be introduced and which will be shown to be equivalent to the vectorial ansatz.

At the end of the chapter we include the method of regularization of inverse problems by a multiresolution analysis using scaling functions and wavelets. The approach presented here is (for the scalar case) mainly due to [25]. First our purpose is to give some general properties concerning inverse problems. Then we will formulate the multiscale regularization approach for scalar valued problems and after this generalize the ansatz to vectorial problems. The bilinear vectorial multiscale approach was the leading task for the formulation of this chapter since our main interest is a regularization of vectorial inverse problems in terms of a multiresolution analysis.

For more information about multiresolution of operator equations the reader is referred to [49] and the reference therein, who has developed a multiresolution approach within a general Hilbert space concept. Similar formulations of multiscale evaluation of operator equations and regularization by multiresolution can be found in [21] and [30] for the scalar case and in [43] for the vectorial case with application to geomagnetism. As already done in these thesis, we restrict ourselves in this

chapter to the scale discrete case, because it is the important one for numerical applications. But it should be noted that the theory can also be formulated for the scale continuous case.

Furthermore the major task of this chapter is the development of vector scaling functions and wavelets in a general Hilbert space context which can only be done in a bilinear approach. Thus, we will restrict ourselves in the scalar as well as in the tensorial ansatz to the bilinear case but it should be noted that these two approaches can also be formulated in a linear sense (cf. [49].)

2.1 The Scalar Case

Consider two separable Hilbert spaces $(\mathcal{H}, (\cdot, \cdot)_{\mathcal{H}})$ and $(\mathcal{K}, (\cdot, \cdot)_{\mathcal{K}})$ of scalar valued functions defined on domains $D_{\mathcal{H}} \subset \mathbb{R}^n$ and $D_{\mathcal{K}} \subset \mathbb{R}^n$, respectively. Additionally, let the operator $\Lambda : \mathcal{H} \rightarrow \mathcal{K}$, defined by

$$\Lambda F = G, \quad F \in \mathcal{H}, G \in \mathcal{K},$$

be injective, bounded, linear and compact. Any compact operator $\Lambda : \mathcal{H} \rightarrow \mathcal{K}$ can be represented by its singular system (σ_n, H_n, K_n) , where $\{\sigma_n^2\}$ are the non-zero eigenvalues of the selfadjoint operator $\Lambda^* \Lambda$ which are assumed to be numbered in descending order. $\{H_n\}$ is a complete orthonormal system in $\overline{\mathcal{R}(\Lambda^*)}^{\|\cdot\|_{\mathcal{H}}}$ (of corresponding eigenfunctions of $\Lambda^* \Lambda$), while $\{K_n\}$ denotes a complete orthonormal system in $\overline{\mathcal{R}(\Lambda)}^{\|\cdot\|_{\mathcal{K}}}$ (of corresponding eigenfunctions of $\Lambda \Lambda^*$). A diagonalized version of the operator equation is then obtained by the following equations:

$$\begin{aligned} \Lambda H_n &= \sigma_n K_n, & \Lambda F &= \sum_{n=0}^{\infty} \sigma_n (F, H_n)_{\mathcal{H}} K_n, & F &\in \mathcal{H}, \\ \Lambda^* K_n &= \sigma_n H_n, & \Lambda^* G &= \sum_{n=0}^{\infty} \sigma_n (G, K_n)_{\mathcal{K}} H_n, & G &\in \mathcal{K}. \end{aligned}$$

The development of the multiresolution analysis will be based on so-called product kernels which are defined in the following definition, which is due to [25].

Definition 2.1

A function $\Gamma(\cdot, \cdot) : D_{\mathcal{H}} \times D_{\mathcal{K}} \rightarrow \mathbb{R}$ of the form

$$\Gamma(x, y) = \sum_{n=0}^{\infty} \Gamma^{\wedge}(n) H_n(x) K_n(y), \quad x \in D_{\mathcal{H}}, y \in D_{\mathcal{K}}$$

is called $(\mathcal{H}, \mathcal{K})$ -product kernel. The sequence $\{\Gamma^{\wedge}(n)\}_{n=0,1,\dots}$ is called the *symbol of the product kernel*. If

$$\begin{aligned} \sum_{n=0}^{\infty} ((\Phi_J)^{\wedge}(n) H_n(x))^2 &< \infty \quad \text{for all } x \in D_{\mathcal{H}}, \\ \sum_{n=0}^{\infty} ((\Phi_J)^{\wedge}(n) K_n(y))^2 &< \infty \quad \text{for all } y \in D_{\mathcal{K}}. \end{aligned}$$

then the product kernel is called *admissible*.

The \mathcal{H} -convolution of a product kernel Γ against a function $F \in \mathcal{H}$ is defined by

$$(\Gamma *_{\mathcal{H}} F)(y) = (\Gamma(\cdot, y), F)_{\mathcal{H}}, \quad y \in D_{\mathcal{K}},$$

while the \mathcal{K} -convolution of a product kernel Γ against a function $G \in \mathcal{K}$ is defined by

$$(\Gamma *_{\mathcal{K}} F)(x) = (\Gamma(x, \cdot), G)_{\mathcal{K}}, \quad x \in D_{\mathcal{H}}.$$

It is clear by definition that, for an admissible product kernel, $\Gamma(x, \cdot)$ is of class \mathcal{K} for every fixed $x \in D_{\mathcal{H}}$ and $\Gamma(\cdot, y) \in \mathcal{H}$ for every fixed $y \in D_{\mathcal{K}}$.

We are now interested in introducing countable families $\{\Phi_J\}, J \in \mathbb{Z}$, of kernel functions which may be understood as scaling functions in our wavelet concept for scalar operator equations under consideration.

Definition 2.2

Let $\{(\Phi_J)^\wedge(n)\}_{n=0,1,\dots}, J \in \mathbb{Z}$, be a family of admissible symbols satisfying the following properties:

1. $\lim_{J \rightarrow \infty} ((\Phi_J)^\wedge(n))^2 = \sigma_n, \quad n \in \mathbb{N}_0,$
2. $((\Phi_{J-1})^\wedge(n))^2 \leq ((\Phi_J)^\wedge(n))^2, \quad J \in \mathbb{Z}, n \in \mathbb{N}_0,$
3. $\lim_{J \rightarrow -\infty} ((\Phi_J)^\wedge(n))^2 = 0, \quad n \in \mathbb{N}_0.$

Then $\{(\Phi_J)^\wedge(n)\}_{n=0,1,\dots}, J \in \mathbb{Z}$, is called the *generating symbol of a scaling function*. The family of kernels $\{^d\Phi_J\}, J \in \mathbb{Z}$, given by

$$^d\Phi_J(x, y) = \sum_{n=0}^{\infty} (\Phi_J)^\wedge(n) H_n(x) K_n(y), \quad x \in D_{\mathcal{H}}, y \in D_{\mathcal{K}}$$

is called *decomposition scaling function* and the family of kernels $\{^r\Phi_J\}, J \in \mathbb{Z}$, given by

$$^r\Phi_J(x, y) = \sum_{n=0}^{\infty} (\Phi_J)^\wedge(n) K_n(x) K_n(y), \quad x, y \in D_{\mathcal{K}}$$

is called *reconstruction scaling function*.

By the admissibility of the generating symbol $\{(\Phi_J)^\wedge(n)\}$ it follows that for fixed $y \in D_{\mathcal{K}}, ^d\Phi_J(\cdot, y) \in \mathcal{H}, ^r\Phi_J(\cdot, y) \in \mathcal{K}$ for all $J \in \mathbb{Z}$. This enables us to verify a reconstruction formula. More explicitly, the scaling functions establish a "discrete approximate identity".

Theorem 2.3

Let $\{(\Phi_J)^\wedge(n)\}_{n=0,1,\dots}$, $J \in \mathbb{Z}$, be the generating symbol of the scaling functions ${}^d\Phi_J$ and ${}^r\Phi_J$. Furthermore, let, for $F \in \mathcal{H}$, the function G_J be given by

$$G_J = {}^r\Phi_J *_{\mathcal{K}} ({}^d\Phi_J *_{\mathcal{H}} F). \quad (2.1)$$

Then

$$\lim_{J \rightarrow \infty} \|G_J - G\|_{\mathcal{K}} = 0$$

holds for all $G \in \mathcal{K}$ with $\Lambda F = G$.

The proof of this theorem can simply be deduced by the properties of the generating symbol $\{(\Phi_J)^\wedge(n)\}$ in Definition 2.2 and can in detail be found, for example, in [21] or [30].

According to our construction, for any $F \in \mathcal{H}$, each convolution operator $T_J F$ defined by $T_J : \mathcal{H} \rightarrow \mathcal{K}$, $T_J F = G_J = {}^r\Phi_J *_{\mathcal{K}} ({}^d\Phi_J *_{\mathcal{H}} F)$, $J \in \mathbb{Z}$, provides an approximation of $G = \Lambda F$ at scale J . In terms of filtering T_J may be interpreted as *low-pass projection filter*. Accordingly, we understand the *scale space* \mathcal{V}_J to be the image of \mathcal{H} under the operator T_J :

$$\mathcal{V}_J = T_J(\mathcal{H}) = \{ {}^r\Phi_J *_{\mathcal{K}} ({}^d\Phi_J *_{\mathcal{H}} F) \mid F \in \mathcal{H} \}.$$

The following result is an immediate consequence of the previous ones.

Theorem 2.4

The scale spaces $\{\mathcal{V}_J\}_{J \in \mathbb{Z}}$ satisfy the following properties:

$$1. \mathcal{V}_J \subset \mathcal{V}_{J'} \subset \mathcal{K}, \quad J \leq J',$$

$$2. \overline{\bigcup_{J=-\infty}^{\infty} \mathcal{V}_J}^{\|\cdot\|_{\mathcal{K}}} = \mathcal{K},$$

Proof:

The properties follow directly from Definition 2.2 (2.) and Theorem 2.3. \square

If a sequence of subspaces of a Hilbert space \mathcal{K} satisfies the conditions of Theorem 2.4, then we call them a *multiresolution analysis* (MRA).

The definition of the scaling function now allows us to introduce wavelets. Wavelets are defined via their symbol by aid of a "refinement (scaling) equation".

Definition 2.5

Let $\{(\Phi_J)^\wedge(n)\}_{n=0,1,\dots}$, $J \in \mathbb{Z}$, be the generating symbol of scaling functions according to Definition 2.2. Then the generating symbol $\{(\Psi_J)^\wedge(n)\}_{n=0,1,\dots}$, $J \in \mathbb{Z}$, of the associated wavelets is defined via the "refinement equation"

$$(\Psi_J)^\wedge(n) = ((\Phi_{J+1})^\wedge(n)^2 - (\Phi_J)^\wedge(n)^2)^{1/2}, \quad n \in \mathbb{N}_0. \quad (2.2)$$

The family $\{^d\Psi_J\}$, $J \in \mathbb{Z}$, of kernels given by

$$^d\Psi_J(x, y) = \sum_{n=0}^{\infty} (\Psi_J)^\wedge(n) H_n(x) K_n(y), \quad x \in D_{\mathcal{H}}, y \in D_{\mathcal{K}},$$

is called *decomposition wavelet* associated to the family of decomposition scaling functions $\{^d\Phi_J\}$, $J \in \mathbb{Z}$, whereas the family $\{^r\Psi_J\}$, $J \in \mathbb{Z}$, of kernels given by

$$^r\Psi_J(x, y) = \sum_{n=0}^{\infty} (\Psi_J)^\wedge(n) K_n(x) K_n(y), \quad x, y \in D_{\mathcal{K}},$$

is called *reconstruction wavelet* associated to the family of reconstruction scaling functions $\{^r\Phi_J\}$, $J \in \mathbb{Z}$.

The corresponding mother wavelets are denoted by $^d\Psi_0$ and $^r\Psi_0$, respectively.

We can easily derive from the refinement equation (2.2) that, for $n \in \mathbb{N}_0$,

$$((\Phi_{J+1})^\wedge(n))^2 = \sum_{j=-\infty}^J ((\Psi_j)^\wedge(n))^2 = ((\Phi_0)^\wedge(n))^2 + \sum_{j=0}^J ((\Psi_j)^\wedge(n))^2. \quad (2.3)$$

Thus, we can deduce from (2.3) that

$$^r\Phi_{J+1} *_{\mathcal{K}} ^d\Phi_{J+1} = \sum_{j=-\infty}^J (^r\Psi_j *_{\mathcal{K}} ^d\Psi_j) = ^r\Phi_0 *_{\mathcal{K}} ^d\Phi_0 + \sum_{j=0}^J (^r\Psi_j *_{\mathcal{K}} ^d\Psi_j) \quad (2.4)$$

holds pointwise in $D_{\mathcal{H}} \times D_{\mathcal{K}}$. Similar to the definition of the operator T_J we are now led to convolution operators $R_J : \mathcal{H} \rightarrow \mathcal{K}$, $J \in \mathbb{Z}$, defined by

$$R_J F = ^r\Psi_J *_{\mathcal{K}} (^d\Psi_J *_{\mathcal{H}} F), \quad F \in \mathcal{H}.$$

Thus, Equation (2.4) can be rewritten in operator notation as

$$T_{J+1} = \sum_{j=-\infty}^J R_j = T_0 + \sum_{j=0}^J R_j.$$

The convolution operator R_J describes the detail information of F at scale J . In terms of filtering, $R_J = ^r\Psi_J *_{\mathcal{K}} ^d\Psi_J *_{\mathcal{H}}$, $J \in \mathbb{Z}$, may be interpreted as a *band-pass filter*. This fact immediately gives rise to introduce the *detail spaces* \mathcal{W}_J as follows:

$$\mathcal{W}_J = R_J(\mathcal{H}) = \{^r\Psi_J *_{\mathcal{K}} (^d\Psi_J *_{\mathcal{H}} F) | F \in \mathcal{H}\}.$$

For example, \mathcal{W}_J contains the detail information needed to go from an approximation G_J at level J to an approximation G_{J+1} at level $J+1$. Hence, we get

$$\mathcal{V}_J + \mathcal{W}_J = \mathcal{V}_{J+1}, \quad J \in \mathbb{Z}.$$

It should be noted that, in general, the sum in the last equation is neither direct nor orthogonal.

The main result of our wavelet approach now can be formulated in the following theorem.

Theorem 2.6

Let $\{(\Phi_J)^\wedge(n)\}_{n=0,1,\dots}$, $J \in \mathbb{Z}$, be the generating symbol of a scaling function. Suppose that $\{(\Psi_J)^\wedge(n)\}_{n=0,1,\dots}$, $J \in \mathbb{Z}$, is the generating symbol of the associated wavelet. Furthermore, let F be of class \mathcal{H} . Then

$$G_J = {}^r\Phi_0 *_{\mathcal{K}} ({}^d\Phi_0 *_{\mathcal{H}} F) + \sum_{j=0}^{J-1} {}^r\Psi_j *_{\mathcal{K}} ({}^d\Psi_j *_{\mathcal{H}} F)$$

is the J -level approximation of G satisfying

$$\lim_{J \rightarrow \infty} \|G_J - G\|_{\mathcal{K}} = 0.$$

for all $G \in \mathcal{K}$ with $\Lambda F = G$.

The last equations show the main characteristics of the multiresolution analysis by wavelets. The approximated solution $G_J \in \mathcal{V}_J$ is improved to $G_{J+1} \in \mathcal{V}_{J+1}$ by adding the so-called detail information of level J contained in \mathcal{W}_J . An even more important property of the multiresolution analysis by wavelets is that we are able to guarantee $\lim_{J \rightarrow \infty} G_J = G$ in the sense of the $\|\cdot\|_{\mathcal{K}}$ -norm.

2.2 The Vectorial Case

In the following section we generalize the previously presented concept for a multi-scale analysis of a scalar operator equation to the vectorial case. Similar considerations can be found in [43] in a general Hilbert space concept and for the special case of spherical functions in [8].

Let us now consider two separable Hilbert spaces $(\mathfrak{h}, (\cdot, \cdot)_{\mathfrak{h}})$ and $(\mathfrak{k}, (\cdot, \cdot)_{\mathfrak{k}})$ of vector valued functions (with values in \mathbb{R}^3) defined on domains $D_{\mathfrak{h}} \subset \mathbb{R}^m$ and $D_{\mathfrak{k}} \subset \mathbb{R}^m$, respectively, where \mathbb{R}^m is in most of our applications the space \mathbb{R}^3 . Furthermore, let the operator $\Lambda : \mathfrak{h} \rightarrow \mathfrak{k}$, defined by

$$\Lambda f = g, \quad g \in \mathfrak{k}, f \in \mathfrak{h},$$

be injective, bounded, linear and compact. Such an operator will from now on be called briefly *tensor-operator*, because it maps vector fields to vector fields. Any compact operator $\Lambda : \mathfrak{h} \rightarrow \mathfrak{k}$ between two separable Hilbert spaces can be represented by its singular system (σ_n, h_n, k_n) where $\{\sigma_n^2\}$ are the non-zero eigenvalues of the selfadjoint operator $\Lambda^* \Lambda$ which are assumed to be numbered in descending order. $\{h_n\}$ is a complete orthonormal system in $\overline{\mathcal{R}(\Lambda^*)}^{\|\cdot\|_{\mathfrak{h}}}$, while $\{k_n\}$ denotes a complete orthonormal system in $\overline{\mathcal{R}(\Lambda)}^{\|\cdot\|_{\mathfrak{k}}}$. A diagonalized version of the operator equation is then obtained by the following equations:

$$\begin{aligned} \Lambda h_n &= \sigma_n k_n, & \Lambda f &= \sum_{n=0}^{\infty} \sigma_n (f, h_n)_{\mathfrak{h}} k_n, & f &\in \mathfrak{h}, \\ \Lambda^* k_n &= \sigma_n h_n, & \Lambda^* g &= \sum_{n=0}^{\infty} \sigma_n (g, k_n)_{\mathfrak{k}} h_n, & g &\in \mathfrak{k}. \end{aligned}$$

In what follows, the development of the multiresolution analysis will be based on so-called vector product kernels which are defined next. For the definition we need another separable Hilbert space of scalar valued functions defined over the domain $D_{\mathcal{H}}$ which will be given by $(\mathcal{H}, (\cdot, \cdot)_{\mathcal{H}})$.

Definition 2.7

Let $(\mathfrak{h}, (\cdot, \cdot)_{\mathfrak{h}})$ and $(\mathcal{H}, (\cdot, \cdot)_{\mathcal{H}})$ be real separable Hilbert spaces of vector, respectively, scalar valued functions over the domain $D_{\mathfrak{h}} \subset \mathbb{R}^m$, respectively, $D_{\mathcal{H}} \subset \mathbb{R}^m$. Let, furthermore, $\{h_n\}_{n \in \mathbb{N}}$ and $\{H_n\}_{n \in \mathbb{N}}$ be corresponding countable, orthonormal and complete systems in \mathfrak{h} and \mathcal{H} , respectively. Then, a function $\gamma(\cdot, \cdot) : D_{\mathfrak{h}} \times D_{\mathcal{H}} \rightarrow \mathbb{R}^3$ of the form

$$\gamma(x, y) = \sum_{n=0}^{\infty} \gamma^{\wedge}(n) h_n(x) H_n(y), \quad x \in D_{\mathfrak{h}}, y \in D_{\mathcal{H}},$$

is called $(\mathfrak{h}, \mathcal{H})$ -vector product kernel. The sequence $\{\gamma^{\wedge}(n)\}_{n=0,1,\dots}$ is the symbol of the vector product kernel.

As in the scalar case, the symbol $\{\gamma^{\wedge}(n)\}$ is called *admissible* if

$$\begin{aligned} \sum_{n=0}^{\infty} (\gamma^{\wedge}(n) h_n(x))^2 &< \infty \quad \text{for all } x \in D_{\mathfrak{h}}, \\ \sum_{n=0}^{\infty} (\gamma^{\wedge}(n) H_n(y))^2 &< \infty \quad \text{for all } y \in D_{\mathcal{H}}. \end{aligned}$$

By the admissibility of the symbol we can conclude that $\varepsilon^i \cdot \gamma(x, \cdot) \in \mathcal{H}$ for every fixed $x \in D_{\mathfrak{h}}$ and $i = 1, 2, 3$, and $\gamma(\cdot, y) \in \mathfrak{h}$ for every fixed $y \in D_{\mathcal{H}}$.

In contrast to the scalar case, we now have to introduce two different convolutions, i.e. a decomposition convolution, called the \mathfrak{h} -convolution, which results in a scalar function and a reconstruction convolution, called the \star -convolution, which maps the scalar field back to a vector valued function.

Definition 2.8

Let $\gamma : D_{\mathfrak{h}} \times D_{\mathcal{H}} \rightarrow \mathbb{R}^3$ be a vector product kernel with admissible symbol. The \mathfrak{h} -convolution of γ against a vector valued function $f \in \mathfrak{h}$ is defined by

$$(\gamma *_{\mathfrak{h}} f)(y) = (\gamma(\cdot, y), f)_{\mathfrak{h}}, \quad y \in D_{\mathcal{H}},$$

while the \star -convolution of a product kernel γ against a scalar valued function $G \in \mathcal{H}$ is defined by

$$(\gamma \star G)(x) = \sum_{i=1}^3 (\varepsilon^i \cdot \gamma(x, \cdot), G)_{\mathcal{H}}, \quad x \in D_{\mathfrak{h}}.$$

By the admissibility of the product kernel γ it is clear that

$$\begin{aligned} (\gamma *_{\mathfrak{h}} f) &\in \mathcal{H} \quad \text{for all } f \in \mathfrak{h}, \\ (\gamma \star G) &\in \mathfrak{h} \quad \text{for all } G \in \mathcal{H}. \end{aligned}$$

Using the orthonormality of the system $\{h_n\}$ in the Hilbert space \mathfrak{h} we easily get for $f \in \mathfrak{h}$

$$\gamma *_{\mathfrak{h}} f = \sum_{n=0}^{\infty} \gamma^{\wedge}(n) f^{\wedge}(n) H_n \quad (2.5)$$

in the sense of the \mathcal{H} –norm, where $\{f^{\wedge}(n)\}$ are the Fourier coefficients of f with respect to the system $\{h_n\} \subset \mathfrak{h}$. With the same argument we find for $G \in \mathcal{H}$

$$\gamma \star G = \sum_{n=0}^{\infty} \gamma^{\wedge}(n) G^{\wedge}(n) h_n \quad (2.6)$$

in the sense of the \mathfrak{h} –norm where $\{G^{\wedge}(n)\}$ are the Fourier coefficients of G with respect to the system $\{H_n\} \subset \mathcal{H}$.

The following theorem leads us to the construction of decomposition and reconstruction vector kernel functions which will be called vector scaling functions.

Theorem 2.9

Let \mathfrak{h} , \mathfrak{k} and \mathcal{H} be Hilbert spaces as given in the course of this section. Furthermore, let γ_1 be a $(\mathfrak{h}, \mathcal{H})$ –vector product kernel with admissible symbol $\{\gamma_1^{\wedge}(n)\}$ and γ_2 be a $(\mathfrak{k}, \mathcal{H})$ –vector product kernel with admissible symbol $\{\gamma_2^{\wedge}(n)\}$. Then, for each $f \in \mathfrak{h}$, we obtain

$$\gamma_2 \star \gamma_1 *_{\mathfrak{h}} f = \sum_{n=0}^{\infty} \gamma_1^{\wedge}(n) \gamma_2^{\wedge}(n) f^{\wedge}(n) k_n$$

in the sense of the \mathfrak{k} –norm where $\{f^{\wedge}(n)\}$ are the Fourier coefficients of f with respect to the orthonormal system $\{h_n\} \subset \mathfrak{h}$.

Proof:

Observing that for $f \in \mathfrak{h}$, $\gamma_1 *_{\mathfrak{h}} f$ is an element of \mathcal{H} , the proof is just a combination of Equation (2.5) and Equation (2.6). \square

Remark 2.10

The reader should note that the Hilbert space \mathcal{H} of scalar valued functions over the domain $D_{\mathcal{H}}$ is just a "park" Hilbert space in our bilinear multiscale theory for tensor-operator equations. The only prerequisite imposed on \mathcal{H} is the separability, i.e. the existence of a countable orthonormal system $\{H_n\}_{n=0,1,\dots}$ in \mathcal{H} . No other conditions on \mathcal{H} or $D_{\mathcal{H}}$ have to be assumed. If either \mathfrak{h} or \mathfrak{k} are Hilbert spaces of vector valued functions over a regular surface which have emerged from a Hilbert space of scalar valued functions over the same regular surface (as for example by the Helmholtz theorem), then it is obvious to choose \mathcal{H} to be this special Hilbert space of scalar valued functions. For example if $\mathfrak{h} = l^2(\Sigma)$ and $\mathfrak{k} = l^2(\Sigma')$, where Σ and Σ' are both regular surfaces, then \mathcal{H} is either chosen to be $\mathcal{L}^2(\Sigma)$ or $\mathcal{L}^2(\Sigma')$.

We are now interested in developing countable families $\{\varphi_J\}, J \in \mathbb{Z}$, of vector kernel functions as in the scalar case which are called vector scaling functions in our multiscale concept for tensor-operator equations.

Definition 2.11

Let \mathfrak{h} , \mathfrak{k} and \mathcal{H} be Hilbert spaces as given in the course of this section and let $\{h_n\}$, $\{k_n\}$ and $\{H_n\}$ be the respective orthonormal systems. Furthermore, let $\{(\varphi_J)^\wedge(n)\}_{n=0,1,\dots}, J \in \mathbb{Z}$, be a family of admissible sequences satisfying the following properties;

1. $\lim_{J \rightarrow \infty} ((\varphi_J)^\wedge(n))^2 = \sigma_n, \quad n \in \mathbb{N}_0,$
2. $((\varphi_{J-1})^\wedge(n))^2 \leq ((\varphi_J)^\wedge(n))^2, \quad J \in \mathbb{Z}, n \in \mathbb{N}_0,$
3. $\lim_{J \rightarrow -\infty} ((\varphi_J)^\wedge(n))^2 = 0, \quad n \in \mathbb{N}_0,$

where σ_n are the singular values of the operator $\Lambda : \mathfrak{h} \rightarrow \mathfrak{k}$. Then $\{(\varphi_J)^\wedge(n)\}_{n=0,1,\dots}, J \in \mathbb{Z}$, is called the *generating symbol* of a vector scaling function. The family of kernels $\{{}^d\varphi_J\}, J \in \mathbb{Z}$, given by

$${}^d\varphi_J(x, y) = \sum_{n=0}^{\infty} (\varphi_J)^\wedge(n) h_n(x) H_n(y), \quad x \in D_{\mathfrak{h}}, y \in D_{\mathcal{H}}$$

is called *decomposition vector scaling function* and the family of kernels $\{{}^r\varphi_J\}, J \in \mathbb{Z}$, given by

$${}^r\varphi_J(x, y) = \sum_{n=0}^{\infty} (\varphi_J)^\wedge(n) k_n(x) H_n(y), \quad x \in D_{\mathfrak{k}}, y \in D_{\mathcal{H}}$$

is called *reconstruction vector scaling function*.

By the admissibility of the generating symbol $\{(\varphi_J)^\wedge(n)\}$ it follows that, for fixed $y \in D_{\mathcal{H}}$,

$${}^d\varphi_J(\cdot, y) \in \mathfrak{h}, \quad J \in \mathbb{Z}, \quad {}^r\varphi_J(\cdot, y) \in \mathfrak{k}, \quad J \in \mathbb{Z}.$$

This enables us to verify that the scaling functions establish a "discrete approximate identity".

Theorem 2.12

Let $\{(\varphi_J)^\wedge(n)\}_{n=0,1,\dots}, J \in \mathbb{Z}$, be the generating symbol of the vector scaling functions ${}^d\varphi_J$ and ${}^r\varphi_J$. Furthermore let, for $f \in \mathfrak{h}$, the function g_J be given by

$$g_J = {}^r\varphi_J \star ({}^d\varphi_J \star_{\mathfrak{h}} f). \quad (2.7)$$

Then

$$\lim_{J \rightarrow \infty} \|g_J - g\|_{\mathfrak{k}} = 0$$

holds for all $g \in \mathfrak{k}$ with $\Lambda f = g$.

Proof:

Let the operator $T_J : \mathfrak{h} \rightarrow \mathfrak{k}$, $J \in \mathbb{Z}$, be given by

$$T_J f = {}^r\varphi_J \star ({}^d\varphi_J *_{\mathfrak{h}} f).$$

Then we can easily deduce by Theorem 2.9 that

$$T_J f = \sum_{n=0}^{\infty} ((\varphi_J)^{\wedge}(n))^2 f^{\wedge}(n) k_n$$

holds in the sense of the \mathfrak{k} -norm where $\{f^{\wedge}(n)\}_{n=0,1,\dots}$ are the Fourier coefficients of f with respect to the system $\{h_n\} \subset \mathfrak{h}$. Furthermore, we are able to deduce that

$$\begin{aligned} \|T_J\| &= \sup_{f \in \mathfrak{h}} \frac{\|T_J f\|_{\mathfrak{k}}}{\|f\|_{\mathfrak{h}}} = \sup_{f \in \mathfrak{h}, \|f\|_{\mathfrak{h}}=1} \|T_J f\|_{\mathfrak{k}} \\ &= \sup_{f \in \mathfrak{h}, \|f\|_{\mathfrak{h}}=1} \left(\sum_{n=0}^{\infty} ((\varphi_J)^{\wedge}(n))^4 (f^{\wedge}(n))^2 \right)^{1/2} \\ &\leq \sup_{n \in \mathbb{N}_0} ((\varphi_J)^{\wedge}(n))^2 \left(\sum_{n=0}^{\infty} (f^{\wedge}(n))^2 \right)^{1/2} \\ &= \sup_{n \in \mathbb{N}_0} ((\varphi_J)^{\wedge}(n))^2 < \infty \end{aligned}$$

for every $J \in \mathbb{Z}$, since $\{((\varphi_J)^{\wedge}(n))^2\}_{n \in \mathbb{N}_0}$ is an admissible symbol. Now we obtain from Parseval's identity (see e.g. [13]) that

$$\lim_{J \rightarrow \infty} \|\Lambda f - T_J f\|_{\mathfrak{k}}^2 = \lim_{J \rightarrow \infty} \sum_{n=0}^{\infty} \left(\sigma_n - ((\varphi_J)^{\wedge}(n))^2 \right)^2 (f^{\wedge}(n))^2. \quad (2.8)$$

Finally, Definition 2.11 yields

$$0 \leq \left(\sigma_n - ((\varphi_J)^{\wedge}(n))^2 \right)^2 = \sigma_n^2 - 2\sigma_n((\varphi_J)^{\wedge}(n))^2 + ((\varphi_J)^{\wedge}(n))^4 \leq 4\sigma_n^2,$$

which allows us to interchange the limit and the sum in (2.8), since $(\sigma_n)_{n \in \mathbb{N}_0}$ is bounded. Using Definition 2.11 we deduce the desired result. \square

According to our construction, for any $f \in \mathfrak{h}$, each operator T_J defined by

$$\begin{aligned} T_J : \mathfrak{h} &\rightarrow \mathfrak{k}, \\ f &\mapsto T_J f = g_J = {}^r\varphi_J \star ({}^d\varphi_J *_{\mathfrak{h}} f), \quad J \in \mathbb{Z}, \end{aligned}$$

provides an approximation of $g = \Lambda f$ at scale J . In terms of filtering T_J may be interpreted as *vectorial low-pass projection filter*. Accordingly, we understand the *vector valued scale space* v_J to be the image of \mathfrak{h} under the operator T_J :

$$v_J = T_J(\mathfrak{h}) = \{ {}^r\varphi_J \star ({}^d\varphi_J *_{\mathfrak{h}} f) \mid f \in \mathfrak{h} \}.$$

The following result is an immediate consequence of the previous ones.

Theorem 2.13

The scale spaces $\{v_J\}_{J \in \mathbb{Z}}$ satisfy the following properties:

1. $v_J \subset v_{J'} \subset \mathfrak{k}, \quad J \leq J',$

2. $\overline{\bigcup_{J=-\infty}^{\infty} v_J}^{\|\cdot\|_{\mathfrak{k}}} = \mathfrak{k}.$

Proof:

The properties follow directly by Definition 2.11 (2.) and by Theorem 2.12. \square

If a sequence of subspaces of a Hilbert space of vector valued functions \mathfrak{k} satisfies the conditions of Theorem 2.13, then we call them a *vector multiresolution analysis* (VMRA).

The definition of the vector scaling function now allows us to introduce vector wavelets. They are introduced via their symbol by aid of a "refinement (scaling) equation" which is an equivalent definition as in the scalar case (see Definition 2.5).

Definition 2.14

Let $\{(\varphi_J)^\wedge(n)\}_{n=0,1,\dots}, J \in \mathbb{Z}$, be the generating symbol of vector scaling functions according to Definition 2.11. Then the generating symbol $\{(\psi_J)^\wedge(n)\}_{n=0,1,\dots}, J \in \mathbb{Z}$, of the associated vector wavelets is defined via the "refinement equation"

$$(\psi_J)^\wedge(n) = ((\varphi_{J+1})^\wedge(n)^2 - (\varphi_J)^\wedge(n)^2)^{1/2}, \quad n \in \mathbb{N}_0. \quad (2.9)$$

The family $\{{}^d\psi_J\}, J \in \mathbb{Z}$, of kernels given by

$${}^d\psi_J(x, y) = \sum_{n=0}^{\infty} (\psi_J)^\wedge(n) h_n(x) H_n(y), \quad x \in D_{\mathfrak{h}}, y \in D_{\mathcal{H}},$$

is called *decomposition vector wavelet* associated to the family of decomposition vector scaling functions, whereas the family $\{{}^r\psi_J\}, J \in \mathbb{Z}$, of kernels given by

$${}^r\psi_J(x, y) = \sum_{n=0}^{\infty} (\psi_J)^\wedge(n) k_n(x) H_n(y), \quad x \in D_{\mathfrak{k}}, y \in D_{\mathcal{H}},$$

is called *reconstruction vector wavelet* associated to the family of reconstruction vector scaling functions

Similar to the definition of the operator T_J we are now led to convolution operators $R_J : \mathfrak{h} \rightarrow \mathfrak{k}, J \in \mathbb{Z}$, defined by

$$R_J f = {}^r\psi_J \star ({}^d\psi_J \star_{\mathfrak{h}} f), \quad f \in \mathfrak{h}.$$

The convolution operators R_J describe the detail information of f at scale J . In terms of filtering, $R_J = {}^r\psi_J \star {}^d\psi_J \star_{\mathfrak{h}}$, $J \in \mathbb{Z}$, may be interpreted as a *vectorial band-pass filter*. This fact immediately gives rise to introduce the *vector valued detail spaces* w_J as follows:

$$w_J = R_J(\mathfrak{h}) = \{ {}^r\psi_J \star ({}^d\psi_J \star_{\mathfrak{h}} f) | f \in \mathfrak{h} \} .$$

The main result of our vector wavelet approach for tensor-operator equations can be formulated in the following theorem.

Theorem 2.15

Let $\{(\varphi_J)^\wedge(n)\}_{n=0,1,\dots}$, $J \in \mathbb{Z}$, be the generating symbol of a vector scaling function. Suppose that $\{(\psi_J)^\wedge(n)\}_{n=0,1,\dots}$, $J \in \mathbb{Z}$, is the generating symbol of the associated vector wavelet. Furthermore, let f be of class \mathfrak{h} . Then

$$g_J = {}^r\varphi_0 \star ({}^d\varphi_0 \star_{\mathfrak{h}} f) + \sum_{j=0}^{J-1} {}^r\psi_j \star ({}^d\psi_j \star_{\mathfrak{h}} f)$$

is the J -level approximation of g satisfying

$$\lim_{J \rightarrow \infty} \|g_J - g\|_{\mathfrak{k}} = 0 ,$$

for all $g \in \mathfrak{k}$ with $\Lambda f = g$.

Remark 2.16

It should be noted that the wavelet concept for operator equations in the scalar case presented in Section 2.1 is just a special case of the previously discussed multiscale theory for tensor-operator equations. Even the case if one of both Hilbert spaces of vector valued functions \mathfrak{h} or \mathfrak{k} consists of scalar valued functions is included in the vectorial theory. It is obvious that in this case the "park" Hilbert space \mathcal{H} is chosen to be that very Hilbert space of scalar valued functions which is just to prevent any confusion. If both Hilbert spaces consist of scalar valued functions, the choice of \mathcal{H} is arbitrary. In this case the \star -convolution becomes the \mathcal{K} -convolution of Section 2.1.

2.3 The Tensorial Approach

The last section on vector wavelets provides us with a multiscale technique for dealing with tensor-operator equations. From the theoretical point of view this is not the canonical way to handle vectorial problems. The natural way of dealing with vector fields in a multiscale framework is given by tensor kernel functions and tensor convolutions (see e.g. [8], [20], [49], or [50]). We will now present a brief introduction of the tensorial theory for tensor-operator equations in Hilbert spaces which will be based on [49]. At the end we will show that both multiscale theories, the tensorial one and the vectorial ansatz presented in Section 2.2 are equivalent.

Thus, as at the beginning of Section 2.2, let us consider two separable Hilbert spaces $(\mathfrak{h}, (\cdot, \cdot)_{\mathfrak{h}})$ and $(\mathfrak{k}, (\cdot, \cdot)_{\mathfrak{k}})$ of vector valued functions defined on domains $D_{\mathfrak{h}} \subset \mathbb{R}^m$ and $D_{\mathfrak{k}} \subset \mathbb{R}^m$, respectively. Furthermore, let the tensor-operator $\Lambda : \mathfrak{h} \rightarrow \mathfrak{k}$, defined by

$$\Lambda f = g, \quad f \in \mathfrak{h}, g \in \mathfrak{k},$$

be injective, bounded, linear and compact with singular system (σ_n, h_n, k_n) .

Definition 2.17

Any function $\Gamma : D_{\mathfrak{h}} \times D_{\mathfrak{k}} \rightarrow \mathbb{R}^{3 \times 3}$ of the form

$$\Gamma(x, y) = \sum_{i=1}^{\infty} \Gamma^{\wedge}(n) k_n(x) \otimes h_n(y), \quad x \in D_{\mathfrak{k}}, y \in D_{\mathfrak{h}}$$

is called $(\mathfrak{h}, \mathfrak{k})$ -tensor kernel function if its symbol $\{\Gamma^{\wedge}(n)\}_{n \in \mathbb{N}_0} \subset \mathbb{R}$ is admissible, i.e.

$$\begin{aligned} \sum_{n=0}^{\infty} (\Gamma^{\wedge}(n) k_n(x))^2 &< \infty \quad \text{for all } x \in D_{\mathfrak{k}}, \\ \sum_{n=0}^{\infty} (\Gamma^{\wedge}(n) h_n(y))^2 &< \infty \quad \text{for all } y \in D_{\mathfrak{h}}. \end{aligned}$$

The convolution of a $(\mathfrak{h}, \mathfrak{k})$ -tensor kernel function against a vector field f of class \mathfrak{h} is defined by

$$(\Gamma * f)(x) = \int_{D_{\mathfrak{h}}} \Gamma(x, y) f(y) d\omega_{D_{\mathfrak{h}}}(y), \quad x \in D_{\mathfrak{k}}.$$

For the convolution of a $(\mathfrak{h}, \mathfrak{k})$ -tensor kernel function against a vector field we easily get, for $f \in \mathfrak{h}$,

$$\Gamma * f = \sum_{n=0}^{\infty} \Gamma^{\wedge}(n) f^{\wedge}(n) k_n$$

in the sense of the \mathfrak{k} -norm where $\{f^{\wedge}(n)\}_{n \in \mathbb{N}_0}$ are the Fourier coefficients of f with respect to the orthonormal system $\{h_n\} \subset \mathfrak{h}$. By applying this result twice we can formulate, for two tensor kernel functions, the following theorem.

Theorem 2.18

Let Γ_1 be a $(\mathfrak{h}, \mathfrak{k})$ -tensor product kernel with admissible symbol $\{\Gamma_1^{\wedge}(n)\}$ and Γ_2 be a $(\mathfrak{k}, \mathfrak{k})$ -tensor product kernel with admissible symbol $\{\Gamma_2^{\wedge}(n)\}$. Then for each $f \in \mathfrak{h}$ we have that

$$\Gamma_2 * \Gamma_1 * f = \sum_{n=0}^{\infty} \Gamma_1^{\wedge}(n) \Gamma_2^{\wedge}(n) f^{\wedge}(n) k_n$$

in the sense of the \mathfrak{k} -norm where $\{f^{\wedge}(n)\}$ are the Fourier coefficients of f with respect to the orthonormal system $\{h_n\} \subset \mathfrak{h}$.

This leads us as in the scalar case (see Section 2.1) to the definition of tensor scaling functions and tensor wavelets as reproducing tensor kernel functions.

Definition 2.19

Let $\{(\Phi_J)^\wedge(n)\}_{n=0,1,\dots}$, $J \in \mathbb{Z}$ be a family of admissible symbols satisfying the following properties:

1. $\lim_{J \rightarrow \infty} ((\Phi_J)^\wedge(n))^2 = \sigma_n$, $n \in \mathbb{N}_0$,
2. $((\Phi_{J-1})^\wedge(n))^2 \leq ((\Phi_J)^\wedge(n))^2$, $J \in \mathbb{Z}, n \in \mathbb{N}_0$,
3. $\lim_{J \rightarrow -\infty} ((\Phi_J)^\wedge(n))^2 = 0$, $n \in \mathbb{N}_0$,

where σ_n are the singular values of the operator $\Lambda : \mathfrak{h} \rightarrow \mathfrak{k}$. Then $\{(\Phi_J)^\wedge(n)\}_{n=0,1,\dots}$, $J \in \mathbb{Z}$, is called the *generating symbol* of a tensor scaling function. The family of kernels $\{^d\Phi_J\}$, $J \in \mathbb{Z}$, given by

$$^d\Phi_J(x, y) = \sum_{n=0}^{\infty} (\Phi_J)^\wedge(n) k_n(x) \otimes h_n(y), \quad x \in D_{\mathfrak{k}}, y \in D_{\mathfrak{h}},$$

is called *decomposition tensor scaling function* and the family of kernels $\{^r\Phi_J\}$, $J \in \mathbb{Z}$, given by

$$^r\Phi_J(x, y) = \sum_{n=0}^{\infty} (\Phi_J)^\wedge(n) k_n(x) \otimes k_n(y), \quad x, y \in D_{\mathfrak{k}},$$

is called *reconstruction tensor scaling function*. Furthermore, let as in the scalar case the symbol $\{(\Psi_J)^\wedge(n)\}_{n=0,1,\dots}$, $J \in \mathbb{Z}$, of the associated tensor wavelets be defined via the scaling equation

$$(\Psi_J)^\wedge(n) = ((\Phi_{J+1})^\wedge(n)^2 - (\Phi_J)^\wedge(n)^2)^{1/2}, \quad n \in \mathbb{N}_0.$$

Then the family $\{^d\Psi_J\}$, $J \in \mathbb{Z}$, of kernels given by

$$^d\Psi_J(x, y) = \sum_{n=0}^{\infty} (\Psi_J)^\wedge(n) k_n(x) \otimes h_n(y), \quad x \in D_{\mathfrak{k}}, y \in D_{\mathfrak{h}},$$

is called *decomposition tensor wavelet* associated to the family of decomposition tensor scaling functions, whereas the family $\{^r\Psi_J\}$, $J \in \mathbb{Z}$, of kernels given by

$$^r\Psi_J(x, y) = \sum_{n=0}^{\infty} (\Psi_J)^\wedge(n) k_n(x) \otimes k_n(y), \quad x, y \in D_{\mathfrak{k}},$$

is called *reconstruction tensor wavelet* associated to the family of reconstruction tensor scaling functions.

This definition together with Theorem 2.18 enables us to formulate the following statement (reconstruction formula).

Theorem 2.20

Let f be of class \mathfrak{h} . Suppose $\{^r\Phi_J\}$ and $\{^d\Phi_J\}$ to be decomposition and reconstruction tensor scaling functions and $\{^r\Psi_J\}$ and $\{^d\Psi_J\}$ to be the associated tensor wavelets. Then

$$\lim_{J \rightarrow \infty} \left\| ^r\Phi_J * ^d\Phi_J * f - \Lambda f \right\|_{\mathfrak{k}} = 0$$

as well as

$$\lim_{J \rightarrow \infty} \left\| \left(^r\Phi_0 * ^d\Phi_0 * f + \sum_{j=0}^J ^r\Psi_j * ^d\Psi_j * f \right) - \Lambda f \right\|_{\mathfrak{k}} = 0.$$

This theorem gives us the theoretical foundation for the multiscale treatment of vector fields as given by the canonical approach for tensor-operator equations. Finally, we show that the multiscale ansatz of vector scaling functions and wavelets presented in Section 2.2 is equivalent to the tensorial case presented in this section. Similar results have been formulated in [8], [43] and [50]. In the last reference nearly the approach which we present here has been introduced while the other ones have formulated the equivalence for special cases of operator equations.

Theorem 2.21

Let f be of class \mathfrak{h} . Suppose Γ_1 to be a $(\mathfrak{h}, \mathfrak{k})$ -tensor product kernel with admissible symbol $\{(\Gamma_1)^\wedge(n)\}$ and Γ_2 to be a $(\mathfrak{k}, \mathfrak{k})$ -tensor product kernel with admissible symbol $\{(\Gamma_2)^\wedge(n)\}$. Furthermore, let γ_1 be a $(\mathfrak{h}, \mathcal{H})$ -vector product kernel and γ_2 be a $(\mathfrak{k}, \mathcal{H})$ -vector product kernel with symbols $\{(\gamma_1)^\wedge(n)\}$ and $\{(\gamma_2)^\wedge(n)\}$ as defined in Definition 2.7 satisfying

$$\begin{aligned} (\gamma_1)^\wedge(n) &= (\Gamma_1)^\wedge(n), \\ (\gamma_2)^\wedge(n) &= (\Gamma_2)^\wedge(n) \end{aligned}$$

for all $n \in \mathbb{N}_0$. Then

$$\Gamma_2 * \Gamma_1 * f = \gamma_2 \star \gamma_1 *_\mathfrak{h} f$$

holds in the sense of the \mathfrak{k} -norm.

Proof:

From Theorem 2.18 we know that

$$\Gamma_2 * \Gamma_1 * f = \sum_{n=0}^{\infty} (\Gamma_1)^\wedge(n) (\Gamma_2)^\wedge(n) f^\wedge(n) k_n$$

in the sense of the \mathfrak{k} -norm where $\{f^\wedge(n)\}$ are the Fourier coefficients of f with respect to the orthonormal system $\{h_n\} \subset \mathfrak{h}$. The assumption

$$\begin{aligned} (\gamma_1)^\wedge(n) &= (\Gamma_1)^\wedge(n), \\ (\gamma_2)^\wedge(n) &= (\Gamma_2)^\wedge(n) \end{aligned}$$

for all $n \in \mathbb{N}_0$ leads to

$$\mathbf{\Gamma}_2 * \mathbf{\Gamma}_1 * f = \sum_{n=0}^{\infty} (\gamma_1)^\wedge(n) (\gamma_2)^\wedge(n) f^\wedge(n) k_n$$

in the sense of the \mathfrak{k} -norm. Using Theorem 2.9 yields

$$\mathbf{\Gamma}_2 * \mathbf{\Gamma}_1 * f = \gamma_2 \star \gamma_1 *_h f$$

in the sense of the \mathfrak{k} -norm which is the desired result. \square

2.4 Regularization by Multiresolution

Based on the theory presented in the previous sections we will now give an overview on wavelet regularization techniques in a general Hilbert space framework. The considerations (especially in the scalar case) follow mainly the course of [25]. But at first we recapitulate some facts concerning the solution of inverse problems.

Let $(\mathcal{H}, (\cdot, \cdot)_{\mathcal{H}})$ and $(\mathcal{K}, (\cdot, \cdot)_{\mathcal{K}})$ be two separable Hilbert spaces of either scalar or vector valued functions and let $G \in \mathcal{K}$ be given. Then we are interested in finding the function $F \in \mathcal{H}$ which is related to G via

$$\Lambda : \mathcal{H} \rightarrow \mathcal{K}, \quad \Lambda F = G, \tag{2.10}$$

where the operator Λ is assumed to be bounded and linear. The problem of solving this operator equation is called *well-posed* in the sense of Hadamard, if the following statements hold true:

1. For each $G \in \mathcal{K}$ there exists at least one $F \in \mathcal{H}$ with $\Lambda F = G$.
(Existence of the inverse)
2. For each $G \in \mathcal{K}$ there exists one and only one $F \in \mathcal{H}$ with $\Lambda F = G$.
(Uniqueness of the inverse)
3. The solution $F \in \mathcal{H}$ depends continuously on the right hand side $G \in \mathcal{K}$.
(Continuity of the inverse)

If at least one of this properties is violated, then the problem is said to be *ill-posed*.

In practical applications we are generally not concerned with the ideal situation of a well-posed problem. First of all a solution of $\Lambda F = G$ exists only if G is in $\mathcal{R}(\Lambda)$, the range of Λ . Errors due to unprecise measurements result in noisy data which may cause that $G \notin \mathcal{R}(\Lambda)$. The perturbed right hand side will be denoted by G^δ with a known error level given by

$$\|G^\delta - G\|_{\mathcal{K}} \leq \delta. \tag{2.11}$$

In order to define a solution even in this case we consider an approximate solution, which occupies the least-squares property, i.e. one seeks that element of \mathcal{H} solving $\min_{F \in \mathcal{H}} \|\Lambda F - G^\delta\|_{\mathcal{K}}$. If Λ is injective, the solution of $\min_{F \in \mathcal{H}} \|\Lambda F - G^\delta\|_{\mathcal{K}}$ is uniquely determined as the orthogonal projection of G^δ onto $\overline{\mathcal{R}(\Lambda)}^{\|\cdot\|_{\mathcal{K}}}$, otherwise there exist infinitely many solutions if $G^\delta \in \mathcal{R}(\Lambda)^\perp$. Then we are interested in the least-squares solution which is of minimal norm $\|F\|_{\mathcal{H}}$.

Determining the desired least-squares solution with minimal norm is equivalent to the determination of the (unique) generalized solution F^+ . It is defined via an additional mapping, the so-called *generalized inverse* (or *Moore-Penrose inverse*) $\Lambda^+ : \mathcal{R}(\Lambda) \oplus \mathcal{R}(\Lambda)^\perp \rightarrow \mathcal{H}$. For $G \in \mathcal{R}(\Lambda) \oplus \mathcal{R}(\Lambda)^\perp$ any $F \in \mathcal{H}$ is least-squares solution of $\Lambda F = G$ if and only if F is a solution of the normal equations $\Lambda^* \Lambda F = \Lambda^* G$. It follows that the generalized solution is just that very least-squares solution that minimizes $\|F\|_{\mathcal{H}}$. The space of all least-squares solutions is $(F^+ + \ker(\Lambda))$. However, the described concept of least-squares solution with minimal norm fails, if $G \notin \mathcal{R}(\Lambda) \oplus \mathcal{R}(\Lambda)^\perp$ or the inverse operator Λ^{-1} is not continuous. Then, the lack of continuity needs to be replaced by a regularization of Λ^+ . In other words, in the situation that only a disturbed right hand side is known instead of G , we are interested in an approximation of the generalized solution F^+ which depends continuously on the given data.

At first we have to define exactly what is understood by the above mentioned term of regularization.

Definition 2.22

Let $(\mathcal{H}, (\cdot, \cdot)_{\mathcal{H}})$ and $(\mathcal{K}, (\cdot, \cdot)_{\mathcal{K}})$ be two separable Hilbert spaces and let $\Lambda : \mathcal{H} \rightarrow \mathcal{K}$ be linear and bounded. Then the family of operators $\Lambda_J : \mathcal{K} \rightarrow \mathcal{H}$, $J \in \mathbb{Z}$, is called a *regularization* of the generalized inverse Λ^+ if the following conditions are fulfilled:

1. Λ_J is linear and bounded on \mathcal{K} for all $J \in \mathbb{Z}$.
2. For any $G \in \mathcal{R}(\Lambda) \oplus \mathcal{R}(\Lambda)^\perp$, the limit relation

$$\lim_{J \rightarrow \infty} \|\Lambda_J G - \Lambda^+ G\|_{\mathcal{H}} = 0$$

holds.

The function $F_J = \Lambda_J G$ is called *J-level regularization* of the problem $\Lambda F = G$ and the parameter J is called *regularization parameter*.

If we apply the regularization Λ_J to a disturbed right hand side G^δ we get for the approximation error of F_J with respect to F^+

$$\|F_J - F^+\|_{\mathcal{H}} \leq \|\Lambda_J G^\delta - \Lambda_J G\|_{\mathcal{H}} + \|\Lambda_J G - \Lambda^+ G\|_{\mathcal{H}} \quad (2.12)$$

$$\leq \|\Lambda_J\| \|G^\delta - G\|_{\mathcal{K}} + \|\Lambda_J G - \Lambda^+ G\|_{\mathcal{H}} \quad (2.13)$$

$$\leq \delta \|\Lambda_J\| + \|\Lambda_J G - \Lambda^+ G\|_{\mathcal{H}} \quad (2.14)$$

with $\|\Lambda_J\| = \sup_{\|G\|_{\mathcal{K}}=1} \|\Lambda_J G\|_{\mathcal{H}}$. This decomposition shows that the error consists of two parts: the first term reflects the influence of the incorrect data and the second term is due to the approximation error between Λ_J and Λ^+ . Typically the first term will increase as $J \rightarrow \infty$ because of the ill-posed nature of the problem, whereas the second term will decrease as $J \rightarrow \infty$ according to the definition of a regularization (see Definition 2.22). Every regularization scheme requires a strategy for choosing the parameter J in dependence on the error level δ in order to achieve an acceptable total error for the regularized solution.

2.4.1 The Scalar Case

Let us now at first consider \mathcal{H} and \mathcal{K} to be Hilbert spaces of scalar valued functions. An important tool in this context is the concept of the singular system of the operator Λ . Let $\Lambda : \mathcal{H} \rightarrow \mathcal{K}$ be injective, bounded, linear and compact with countable singular system $\{\sigma_n, H_n, K_n\}_{n=0,1,\dots}$, where $\{\sigma_n^2\}$ are the non-zero eigenvalues of the selfadjoint operator $\Lambda^* \Lambda$ which are assumed to be numbered in descending order. $\{H_n\}$ is a complete orthonormal system in $\overline{\mathcal{R}(\Lambda^*)}^{\|\cdot\|_{\mathcal{H}}}$ such that $\Lambda H_n = \sigma_n K_n$, while $\{K_n\}$ denotes a complete orthonormal system in $\overline{\mathcal{R}(\Lambda)}^{\|\cdot\|_{\mathcal{K}}}$ such that $\Lambda^* K_n = \sigma_n H_n$. The generalized inverse of the operator Λ can be given in terms of the singular system by

$$F^+ = \Lambda^+ G = \sum_{n=0}^{\infty} \sigma_n^{-1} (G, K_n)_{\mathcal{K}} H_n, \quad G \in \mathcal{R}(\Lambda) \oplus \mathcal{R}(\Lambda)^{\perp}. \quad (2.15)$$

It is well known, that the sequence $\{\sigma_n\}_{n \in \mathbb{N}_0}$ has a unique cluster point 0, i.e. $\lim_{n \rightarrow \infty} \sigma_n = 0$, but this does not guarantee the convergence of the sum in (2.15). Another problem may be, that the generalized solution does not depend continuously on the data G . To overcome these problems our purpose is to construct a regularization in terms of a multiresolution analysis.

We now define regularization scaling functions via their symbol as we have done for scaling functions for the solution of operator equations.

Definition 2.23

Let $\{(\Phi_J)^{\wedge}(n)\}_{n=0,1,\dots}$, $J \in \mathbb{Z}$, define a family of admissible product kernels in the sense of Definition 2.1 satisfying additionally the following properties:

1. $\lim_{J \rightarrow \infty} ((\Phi_J)^{\wedge}(n))^2 = \sigma_n^{-1}, \quad n \in \mathbb{N}_0,$
2. $((\Phi_J)^{\wedge}(n))^2 \geq ((\Phi_{J-1})^{\wedge}(n))^2, \quad J \in \mathbb{Z}, n \in \mathbb{N}_0,$
3. $\lim_{J \rightarrow -\infty} ((\Phi_J)^{\wedge}(n))^2 = 0, \quad n \in \mathbb{N}_0.$

Then $\{(\Phi_J)^\wedge(n)\}_{n=0,1,\dots}$ is called the *generating symbol of a regularization scaling function* $\{\Phi_J\}$, $J \in \mathbb{Z}$. The family of kernels $\{^d\Phi_J\}$, $J \in \mathbb{Z}$, given by

$$^d\Phi_J(x, y) = \sum_{n=0}^{\infty} (\Phi_J)^\wedge(n) H_n(x) K_n(y), \quad x \in D_{\mathcal{H}}, y \in D_{\mathcal{K}},$$

is called *decomposition regularization scaling function* and the family of kernels $\{^r\Phi_J\}$, $J \in \mathbb{Z}$, given by

$$^r\Phi_J(x, y) = \sum_{n=0}^{\infty} (\Phi_J)^\wedge(n) H_n(x) H_n(y), \quad x, y \in D_{\mathcal{H}},$$

is called *reconstruction regularization scaling function*.

In analogy to Theorem 2.3 we establish the following result.

Theorem 2.24

Let $\{(\Phi_J)^\wedge(n)\}_{n=0,1,\dots}$, $J \in \mathbb{Z}$, be the generating symbol of the regularization scaling functions $^d\Phi_J$ and $^r\Phi_J$, respectively, as defined in Definition 2.23. Then

$$\lim_{J \rightarrow \infty} \|F_J - \Lambda^+ G\|_{\mathcal{H}} = 0$$

holds for all $G \in \mathcal{R}(\Lambda) \oplus \mathcal{R}(\Lambda)^\perp$ with $\Lambda F = G$, where F_J , given by

$$F_J = \Lambda_J G = ^r\Phi_J *_{\mathcal{H}} (^d\Phi_J *_{\mathcal{K}} G), \quad (2.16)$$

is said to be the J -level approximation of $\Lambda^+ G$.

Proof:

The proof follows analogously to the one of Theorem 2.3. □

It is clear, that the sequence of operators Λ_J , $J \in \mathbb{Z}$, defined in (2.16) is a regularization in the sense of Definition 2.22.

From now on the complete theory of multiresolution for operator equations can be transferred to the case of multiscale regularization. We can define decomposition and reconstruction regularization wavelets (as in Definition 2.5) and give a wavelet regularization theorem (compared to Theorem 2.6). We will just repeat some important facts of regularizing wavelet theory and regularizing multiresolution at this point.

Definition 2.25

Let $\{(\Phi_J)^\wedge(n)\}_{n=0,1,\dots}$, $J \in \mathbb{Z}$, be the generating symbol of a regularization scaling function. Then the generating symbol $\{(\Psi_J)^\wedge(n)\}_{n=0,1,\dots}$, $J \in \mathbb{Z}$, of the associated regularization wavelets is defined via the refinement equation

$$(\Psi_J)^\wedge(n) = ((\Phi_{J+1})^\wedge(n)^2 - (\Phi_J)^\wedge(n)^2)^{1/2}, \quad n \in \mathbb{N}_0. \quad (2.17)$$

The family $\{^d\Psi_J\}$, $J \in \mathbb{Z}$, of kernels given by

$$^d\Psi_J(x, y) = \sum_{n=0}^{\infty} (\Psi_J)^\wedge(n) K_n(x) H_n(y), \quad x \in D_{\mathcal{H}}, y \in D_{\mathcal{K}},$$

is called *decomposition regularization wavelet*, whereas the family $\{^r\Psi_J\}$, $J \in \mathbb{Z}$, of kernels given by

$$^r\Psi_J(x, y) = \sum_{n=0}^{\infty} (\Psi_J)^\wedge(n) H_n(x) H_n(y), \quad x, y \in D_{\mathcal{H}},$$

is called *reconstruction regularization wavelet*.

Next, we will give the analogue to Theorem 2.6 for the case of regularization in terms of multiresolution.

Theorem 2.26

Let $\{(\Phi_J)^\wedge(n)\}_{n=0,1,\dots}$, $J \in \mathbb{Z}$, be the generating symbol of a regularization scaling function. Suppose that $\{(\Psi_J)^\wedge(n)\}_{n=0,1,\dots}$, $J \in \mathbb{Z}$, is the generating symbol of the associated regularization wavelet. Then

$$F_J = {}^r\Phi_0 *_{\mathcal{H}} ({}^d\Phi_0 *_{\mathcal{K}} G) + \sum_{j=0}^{J-1} {}^r\Psi_j *_{\mathcal{H}} ({}^d\Psi_j *_{\mathcal{K}} G)$$

is the J -level approximation of Λ^+G satisfying

$$\lim_{J \rightarrow \infty} \|F_J - \Lambda^+G\|_{\mathcal{H}} = 0,$$

for all G of class $\mathcal{R}(\Lambda) \oplus \mathcal{R}(\Lambda)^\perp$ with $\Lambda F = G$.

The proof of this theorem immediately follows from Definition 2.25 of regularization wavelets.

At last, we give the important fact of multiresolution for the regularization case.

Theorem 2.27

The scale spaces V_J defined by $V_J = \Lambda_J (\mathcal{R}(\Lambda) \oplus \mathcal{R}(\Lambda)^\perp)$ satisfy the following properties:

1. $V_J \subset V_{J'} \subset \mathcal{H}$, $J < J'$,
2. $\overline{\bigcup_{J=-\infty}^{\infty} V_J}^{\|\cdot\|_{\mathcal{H}}} = \mathcal{H}$.

Proof:

The assertions follow immediately by Definition 2.23 and Theorem 2.24. \square

2.4.2 The Vectorial Case

Next, we consider the vectorial case. Thus, let $(\mathfrak{h}, (\cdot, \cdot)_{\mathfrak{h}})$ and $(\mathfrak{k}, (\cdot, \cdot)_{\mathfrak{k}})$ be two separable Hilbert spaces of both vector valued functions (with values in \mathbb{R}^3) and let $g \in \mathfrak{k}$ be given. Then we search the function $f \in \mathfrak{h}$, which is related to g via

$$\Lambda : \mathfrak{h} \rightarrow \mathfrak{k}, \quad \Lambda f = g, \quad (2.18)$$

where the tensor-operator Λ is assumed to be bounded, linear, injective, and compact with singular system $\{\sigma_n, h_n, k_n\}_{n=0,1,\dots}$. $\{\sigma_n^2\}$ are the non-zero eigenvalues of the selfadjoint operator $\Lambda^* \Lambda$ which are assumed to be numbered in descending order. $\{h_n\}$ is a complete orthonormal system in $\overline{\mathcal{R}(\Lambda^*)}^{\|\cdot\|_{\mathfrak{h}}}$ such that $\Lambda h_n = \sigma_n k_n$, while $\{k_n\}$ denotes a complete orthonormal system in $\overline{\mathcal{R}(\Lambda)}^{\|\cdot\|_{\mathfrak{k}}}$ such that $\Lambda^* k_n = \sigma_n h_n$. The generalized inverse for this problem can as in the scalar case be given in terms of the singular system by

$$f^+ = \Lambda^+ g = \sum_{n=0}^{\infty} \sigma_n^{-1} (g, k_n)_{\mathfrak{k}} h_n, \quad g \in \mathcal{R}(\Lambda) \oplus \mathcal{R}(\Lambda)^{\perp}. \quad (2.19)$$

As for the case of operator equations the standard approach of regularizing this vector valued inverse problem would be a multiresolution by means of regularizing tensor scaling functions and wavelets (see e.g. [49]). We do not introduce this canonical approach here because it can easily be derived from the tensorial approach for operator equations presented in Section 2.3, but it will not be used any more in this thesis.

To regularize this vectorial problem we construct a regularization in terms of a vector multiresolution analysis. We define regularization vector scaling functions via their symbol as we have done for vector scaling functions for the evaluation of operator equations.

Definition 2.28

Let the Hilbert spaces \mathfrak{h} , \mathfrak{k} and \mathcal{H} be spaces of vector and scalar valued functions, respectively, as given in Section 2.2 and let $\{h_n\}$, $\{k_n\}$ and $\{H_n\}$ be the corresponding orthonormal systems in \mathfrak{h} , \mathfrak{k} and \mathcal{H} , respectively. Furthermore, let $\{(\varphi_J)^{\wedge}(n)\}_{n=0,1,\dots}$, $J \in \mathbb{Z}$, define a family of admissible product kernels satisfying additionally the following properties:

1. $\lim_{J \rightarrow \infty} ((\varphi_J)^{\wedge}(n))^2 = \sigma_n^{-1}, \quad n \in \mathbb{N}_0,$
2. $((\varphi_J)^{\wedge}(n))^2 \geq ((\varphi_{J-1})^{\wedge}(n))^2, \quad J \in \mathbb{Z}, n \in \mathbb{N}_0,$
3. $\lim_{J \rightarrow -\infty} ((\varphi_J)^{\wedge}(n))^2 = 0, \quad n \in \mathbb{N}_0.$

Then $\{(\varphi_J)^{\wedge}(n)\}_{n=0,1,\dots}$ is called the *generating symbol of a regularization vector scaling function*. The family of kernels $\{^d \varphi_J\}$, $J \in \mathbb{Z}$, given by

$$^d \varphi_J(x, y) = \sum_{n=0}^{\infty} (\varphi_J)^{\wedge}(n) k_n(x) H_n(y), \quad x \in D_{\mathfrak{k}}, y \in D_{\mathcal{H}},$$

is called *decomposition regularization vector scaling function* and the family of kernels $\{^r\varphi_J\}$, $J \in \mathbb{Z}$, given by

$$^r\varphi_J(x, y) = \sum_{n=0}^{\infty} (\varphi_J)^\wedge(n) h_n(x) H_n(y), \quad x \in D_{\mathfrak{k}}, y \in D_{\mathcal{H}},$$

is called *reconstruction regularization vector scaling function*.

In analogy to Theorem 2.12 we are led to the following result.

Theorem 2.29

Let $\{(\varphi_J)^\wedge(n)\}_{n=0,1,\dots}$, $J \in \mathbb{Z}$, be the generating symbol of the regularization vector scaling functions $^d\varphi_J$ and $^r\varphi_J$, respectively, as given in Definition 2.28. Then

$$\lim_{J \rightarrow \infty} \|f_J - \Lambda^+ g\|_{\mathfrak{h}} = 0$$

holds for all $g \in \mathcal{R}(\Lambda) \oplus \mathcal{R}(\Lambda)^\perp$ with $\Lambda f = g$, where f_J , given by

$$f_J = \Lambda_J g = ^r\varphi_J \star (^d\varphi_J *_{\mathfrak{k}} g), \quad (2.20)$$

is said to be the J -level approximation of $\Lambda^+ g$.

Proof:

The proof follows analogously to that of Theorem 2.12. □

It is clear, that the sequence of operators Λ_J , $J \in \mathbb{Z}$, defined in (2.20) is a vectorial regularization in the sense of Definition 2.22.

From now on the complete theory of multiresolution for tensor-operator equations can be transferred to the case of regularization. We can define decomposition and reconstruction regularization vector wavelets (as in Definition 2.14) and give a wavelet regularization theorem (compared to Theorem 2.15). Some important facts of regularizing vector wavelet theory and regularizing vector multiresolution analysis will be repeated at this point.

Definition 2.30

Let $\{(\varphi_J)^\wedge(n)\}_{n=0,1,\dots}$, $J \in \mathbb{Z}$, be the generating symbol of a regularization scaling function. Then the generating symbol $\{(\psi_J)^\wedge(n)\}_{n=0,1,\dots}$, $J \in \mathbb{Z}$, of the associated regularization wavelets is defined via the refinement equation

$$(\psi_J)^\wedge(n) = ((\varphi_{J+1})^\wedge(n)^2 - (\varphi_J)^\wedge(n)^2)^{1/2}, \quad n \in \mathbb{N}_0. \quad (2.21)$$

The family $\{^d\psi_J\}$, $J \in \mathbb{Z}$, of kernels given by

$$^d\psi_J(x, y) = \sum_{n=0}^{\infty} (\psi_J)^\wedge(n) k_n(x) H_n(y), \quad x \in D_{\mathfrak{k}}, y \in D_{\mathcal{H}},$$

is called *decomposition regularization vector wavelet*, whereas the family $\{{}^r\psi_J\}$, $J \in \mathbb{Z}$, of kernels given by

$${}^r\psi_J(x, y) = \sum_{n=0}^{\infty} (\psi_J)^\wedge(n) h_n(x) H_n(y), \quad x \in D_{\mathfrak{h}}, y \in D_{\mathcal{H}},$$

is called *reconstruction regularization vector wavelet*.

Next, we will give analogue to Theorem 2.15 for the case of multiscale regularization.

Theorem 2.31

Let $\{(\varphi_J)^\wedge(n)\}_{n=0,1,\dots}$, $J \in \mathbb{Z}$, be the generating symbol of a regularization vector scaling function. Suppose that $\{(\psi_J)^\wedge(n)\}_{n=0,1,\dots}$, $J \in \mathbb{Z}$, is the generating symbol of the associated regularization vector wavelet. Furthermore, let g be of class $\mathcal{R}(\Lambda) \oplus \mathcal{R}(\Lambda)^\perp$ with $\Lambda f = g$. Then

$$f_J = {}^r\varphi_0 \star ({}^d\varphi_0 *_{\mathfrak{k}} g) + \sum_{j=0}^{J-1} {}^r\psi_j \star ({}^d\psi_j *_{\mathfrak{k}} g)$$

is the J -level approximation of $\Lambda^+ g$ satisfying

$$\lim_{J \rightarrow \infty} \|f_J - \Lambda^+ g\|_{\mathfrak{h}} = 0.$$

The proof of this theorem immediately follows by Definition 2.30 of a regularization wavelet. At last, we give the important fact of a vectorial multiresolution for the regularization case.

Theorem 2.32

The scale spaces v_J defined by $v_J = \Lambda_J (\mathcal{R}(\Lambda) \oplus \mathcal{R}(\Lambda)^\perp)$ satisfy the following properties:

1. $v_J \subset v_{J'} \subset \mathfrak{h}, \quad J < J',$
2. $\overline{\bigcup_{J=-\infty}^{\infty} v_J}^{\|\cdot\|_{\mathfrak{h}}} = \mathfrak{h}.$

Proof:

The assertions follow immediately by Definition 2.28 and Theorem 2.29. \square

Finally we present four possible choices for the generating symbol $\{(\varphi_J)^\wedge(n)\}$ of a regularization vector scaling function.

1. Truncated Singular Value Regularization (TSVR)

$$(\varphi_J)^\wedge(n) = \begin{cases} \sqrt{\sigma_n^{-1}} & n = 0, \dots, N_J \\ 0 & n \geq N_J + 1 \end{cases}. \quad (2.22)$$

This is the simplest method of regularization. The singular values are taken up to a certain threshold N_J , while the others are discarded. A possible choice for N_J could be

$$N_J = \begin{cases} 0 & J \in \mathbb{Z}, J < 0 \\ 2^J - 1 & J \in \mathbb{Z}, J \geq 0 \end{cases}.$$

For a graphical illustration of the symbols for truncated singular value decomposition see Figure 2.1.

2. smoothed Truncated Singular Value Regularization

$$(\varphi_J)^\wedge(n) = \begin{cases} \sqrt{\sigma_n^{-1}} & n = 0, \dots, M_J \\ \sqrt{\sigma_n^{-1}} \tau_J(n) & n = M_J + 1, \dots, N_J \\ 0 & n \geq N_J + 1 \end{cases} \quad (2.23)$$

where $\tau_J(n)$ is monotonically decreasing in $[M_J, N_J]$ from $\tau_J(M_J) = 1$ to $\tau_J(N_J) = 0$. A possible choice for M_J, N_J could be

$$M_J = \begin{cases} 0 & J \in \mathbb{Z}, J < 0 \\ 2^J - 1 & J \in \mathbb{Z}, J \geq 0 \end{cases}, \quad N_J = \begin{cases} 0 & J \in \mathbb{Z}, J < 0 \\ 2^{J+1} - 1 & J \in \mathbb{Z}, J \geq 0 \end{cases}.$$

3. CP, Cubic Polynomial regularization

$$(\varphi_J)^\wedge(n) = \begin{cases} \sqrt{\sigma_n^{-1}} \left(1 - \frac{n}{N_J}\right)^2 \left(1 + 2\frac{n}{N_J}\right) & n = 0, \dots, N_J \\ 0 & \text{else} \end{cases}.$$

As for TSVR, a possible choice for N_J could be

$$N_J = \begin{cases} 0 & J \in \mathbb{Z}, J < 0 \\ 2^J - 1 & J \in \mathbb{Z}, J \geq 0 \end{cases}.$$

For a graphical illustration of the symbols for CP regularization see Figure 2.2.

4. Tikhonov (TH) regularization

$$(\varphi_J)^\wedge(n) = \sqrt{\frac{\sigma_n}{\sigma_n^2 + \gamma_J}}, \quad n = 0, 1, \dots; J \in \mathbb{Z}, \quad (2.24)$$

with $\{\gamma_J\}_{J \in \mathbb{Z}}$ being a sequence satisfying $\lim_{J \rightarrow \infty} \gamma_J = 0$ and $\lim_{J \rightarrow -\infty} \gamma_J = \infty$. For singular values that are large compared to γ_J , we obtain $(\varphi_J)^\wedge(n) \simeq \sqrt{\sigma_n^{-1}}$, i.e. there is almost no regularization. If the singular values are small compared to γ_J , we end up with $(\varphi_J)^\wedge(n) \simeq 0$. For a discussion of choosing the regularization parameter γ_J in practical applications see [30].

For a graphical illustration of the symbols for Tikhonov regularization see Figure 2.3.

At the end we give a concrete example of the truncated singular value (TSVR), the cubic polynomial (CP) and the Tikhonov (TH) regularization. The singular values which we use appear in the relation between spherical current fields and their respective magnetic field which will be used later on and which is one of the essential applications of this thesis. The singular values are given by

$$\sigma_n = \sqrt{\frac{n}{2n+1}} \left(\frac{R_1}{R_2} \right)^{n+1}, \quad n \in \mathbb{N}_0, \quad (2.25)$$

where R_1 is the height of the current system, typically $R_1 = 100 \text{ km}$ above the Earth's surface, and R_2 is the height, where the magnetic field is evaluated, resp. where the magnetic field measurements are taken, typically $R_2 = 400 \text{ km}$ above the Earth's surface. The exponentially ill-posed nature of the inverse problem is obvious and can be seen very well in the semilogarithmic illustration of the singular values (see Figure 2.2 and Figure 2.3).

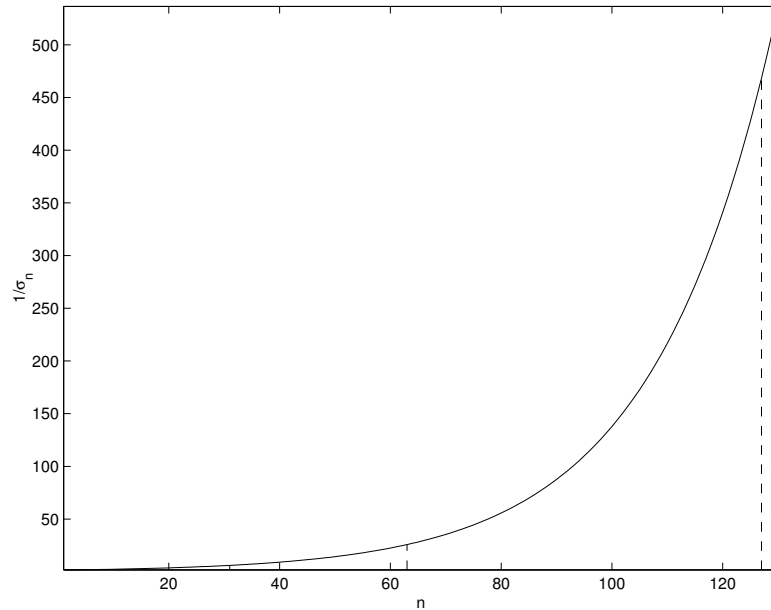


Figure 2.1: Symbols $(\varphi_J)^\wedge(n)$ for truncated singular value regularization (TSVR) for different values of N_J given by $N_J = 2^5 - 1 = 31$, $N_J = 2^6 - 1 = 63$, and $N_J = 2^7 - 1 = 127$. The singular value is thereby given by (2.25).

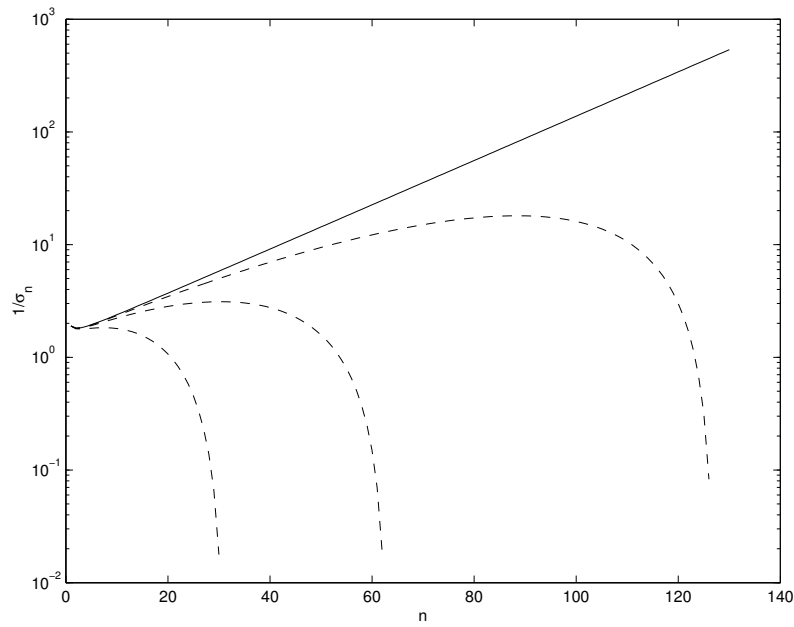


Figure 2.2: Symbols $(\varphi_J)^\wedge(n)$ for cubic polynomial (CP) regularization for different values of N_J given by $N_J = 2^5 - 1$, $N_J = 2^6 - 1$, and $N_J = 2^7 - 1$. Note the semilogarithmic scaling of the axis for the singular values.

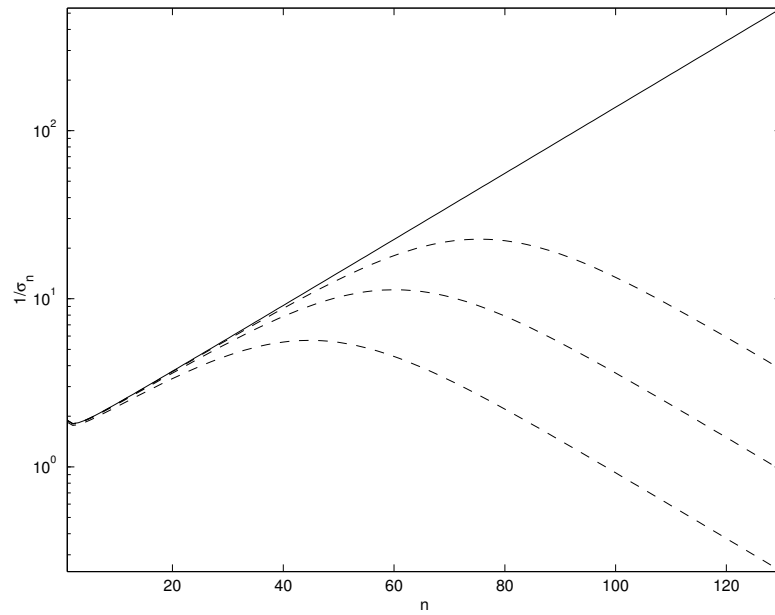


Figure 2.3: Symbols $(\varphi_J)^\wedge(n)$ for Tikhonov regularization for values $\gamma_J = 2^{-7}$, $\gamma_J = 2^{-9}$, and $\gamma_J = 2^{-11}$. Observe the semilogarithmic scaling of the axis for the singular values.

Chapter 3

Separation of Vectorial Fields With Respect to Sources

This chapter is concerned with the first major result of this thesis, the separation of vector fields with respect to their sources. First of all, we will define what is meant by a source and resulting field, respectively, and how they are coupled. The dominating differential equations in this context are the system of pre-Maxwell equations. We will see that the Mie representation presented in Section 1.4 is the appropriate representation to handle this system of differential equations. In the second section of this chapter we will present a method of separating vector fields on a sphere with respect to their sources, which is mainly due to [6]. It is based on a special Fourier decomposition of a spherical vector field and in this context the orthonormal system $\{u_{n,k}^{(i)}\}$ of vector spherical harmonics plays an essential role. After that we are concerned with an approach of decomposing a vector field by scale dependent, space localizing radial basis functions, called scaling functions and wavelets. This approach is developed in the context of Chapter 2 by establishing a multiscale decomposition of the identity operator on $l^2(\Omega)$. In contrast to the Fourier approach involving the orthonormal system $\{u_{n,k}^{(i)}\}$ this ansatz provides us with the possibility to separate a vector field locally with respect to its sources. This fact results in the advantageous property that we do not need a global coverage of data to decide whether the vector field is induced by sources inside or outside the sphere where the measurements are taken. This decision can be made only based on local information of the field.

Definition 3.1

Let $\Omega_{(a,b)}$ be a spherical shell with $0 \leq a < b < \infty$. The vector field g is called a *vectorial source* and the scalar field G is called a *scalar source* of the vector field $f \in c^{(1)}(\Omega_{(a,b)})$ if the three fields are coupled in $\Omega_{(a,b)}$ via the pre-Maxwell equations

$$\begin{aligned}\nabla \wedge f &= g, \\ \nabla \cdot f &= G.\end{aligned}$$

Note that for given g and G in $\Omega_{(a,b)}$ the problem of finding f fulfilling the above equations is not uniquely solvable. The problem can be made unique by imposing

certain boundary conditions for f on Ω_a and Ω_b .

Physically interpreted the equations state that f is induced by the vectorial current density g and the scalar charge density G . Since we are mainly interested in vectorial source fields we assume G to vanish in $\Omega_{(a,b)}$. The resulting equations, called *pre-Maxwell equations*, are given by

$$\nabla \wedge f = g, \quad (3.1a)$$

$$\nabla \cdot f = 0. \quad (3.1b)$$

in $\Omega_{(a,b)}$. Applying the divergence to (3.1a) results in a third equation given by

$$\nabla \cdot g = 0 \quad \text{in } \Omega_{(a,b)}. \quad (3.2)$$

An appropriate approach of handling the system of differential equations (3.1) is given by the Mie representation. If we assume f to be solenoidal in $\Omega_{(a,b)}$ (see Definition 1.22), we can conclude by Gauss' Theorem, that f is divergence free. Thus, every vector field f , solenoidal in $\Omega_{(a,b)}$, fulfills equation (3.1b) and has a Mie representation given by

$$f = p_f + q_f = \nabla \wedge LP_f + LQ_f \quad \text{in } \Omega_{(a,b)}$$

with P_f, Q_f being the Mie scalars of f . Because of (3.2) the same arguments and the same approach for the source field g can be used. Thus, g yields a Mie representation, too, given by

$$g = p_g + q_g = \nabla \wedge LP_g + LQ_g \quad \text{in } \Omega_{(a,b)} \quad (3.3)$$

with P_g, Q_g being the Mie scalars of g . Taking the curl of the Mie representation of f we deduce by Equation (3.1a)

$$g = \nabla \wedge LQ_f + L(-\Delta P_f) \quad \text{in } \Omega_{(a,b)}. \quad (3.4)$$

Since the Mie representation of a solenoidal vector field is unique (see Theorem 1.23), comparing (3.3) and (3.4) results in the following system of fundamental equations

$$Q_f = P_g, \quad (3.5a)$$

$$\Delta P_f = -Q_g, \quad (3.5b)$$

in $\Omega_{(a,b)}$. These equations state that poloidal sources produce toroidal fields, and toroidal sources produce poloidal fields. Furthermore, the toroidal scalar of the resulting field f is just the poloidal scalar of the source field g , and the poloidal scalar of f and the toroidal scalar of the source g are connected via the Poisson equation in $\Omega_{(a,b)}$. This shows that the problem of solving (3.1) on $\Omega_{(a,b)}$ is reduced to the problem of solving a scalar Poisson problem, which is an elliptic partial differential problem. The equations are solvable if the inhomogeneity g and by this Q_g is given and boundary values for f are given on Ω_a and Ω_b .

It is well known from classical Gauss theory (see [6]) that, if the spherical shell $\Omega_{(a,b)}$ is free of source fields, the resulting vector field f restricted to a sphere Ω_c with $c \in (a, b)$ can be decomposed into two parts

$$f = f^{I(c)} + f^{E(c)} \quad (3.6)$$

where $f^{I(c)}$ is the field produced by sources inside Ω_a and $f^{E(c)}$ by sources outside Ω_b .

The main questions concerning this formulation are now:

Is such a separation of the resulting field also possible if we use the Mie representation and, furthermore, can it be applied to the case, where $\Omega_{(a,b)}$ contains a source field g ? This question will be answered in the following paragraph.

Suppose g to be a source field in $\Omega_{(a,b)}$. Assume that the Mie representation of g is given by

$$g = p_g + q_g = \nabla \wedge LP_g + LQ_g \quad \text{in } \Omega_{(a,b)}.$$

Furthermore, let Ω_c be a sphere with radius $c \in (a, b)$.

Following Biot-Savart's law (see [35]) the definition of a field induced by sources g inside Ω_c is known to be

$$f^{I(c)}(x) = \nabla \wedge a^{I(c)}(x), \quad x \in \mathbb{R}^3, \quad (3.7)$$

with

$$a^{I(c)}(x) = \frac{1}{4\pi} \int_{\Omega_c^{int}} \frac{g(y)}{|x-y|} dy, \quad x \in \mathbb{R}^3, \quad (3.8)$$

Is by this definition the field g the only source field of $f^{I(c)}$ or are there other sources? Following Definition 3.1 we have to calculate $\nabla \wedge f^{I(c)}$ to get the source fields of $f^{I(c)}$. It is given by

$$\nabla \wedge f^{I(c)} = \nabla (\nabla \cdot a^{I(c)}) - \Delta a^{I(c)}. \quad (3.9)$$

Because of the well known relation between the Coulomb integral and the Poisson equation, the expression (3.8) implies

$$\begin{aligned} \Delta a^{I(c)} &= -g \quad \text{in } \Omega_{(a,c)}, \\ &= 0 \quad \text{in } \Omega_{(c,b)}. \end{aligned}$$

Thus, Equation (3.9) becomes

$$\begin{aligned} \nabla \wedge f^{I(c)} &= g + \nabla (\nabla \cdot a^{I(c)}) \quad \text{in } \Omega_{(a,c)}, \\ &= \nabla (\nabla \cdot a^{I(c)}) \quad \text{in } \Omega_{(c,b)}. \end{aligned}$$

This equation shows us that g certainly is a source field of $f^{I(c)}$, but we have to compute $\nabla \cdot a^{I(c)}$ to get all source terms of $f^{I(c)}$. Using $\nabla \cdot g = 0$ and Gauss' theorem yields

$$\nabla \cdot a^{I(c)}(x) = -\frac{1}{4\pi} \int_{\Omega_c} \frac{\nu(y) \cdot g(y)}{|x-y|} d\omega_c(y), \quad x \in \mathbb{R}^3, \quad (3.10)$$

where ν is the unit normal field on Ω_c pointing into the outer space Ω_c^{ext} . Consequently, we see that, in general, g is not the only source field of $f^{I(c)}$. There is also a source part coming from $\nabla(\nabla \cdot a^{I(c)})$ which might be different from zero. The integral in (3.10) only vanishes if $\nu \cdot g = 0$ on Ω_c , i.e. if g is a tangential field on Ω_c .

Although the above considerations seem to be a complication, they are not. From the fundamental equations (3.5) we know that toroidal sources, which are purely tangential, produce poloidal fields, and vice versa. If we now just take the poloidal part p_f of f and separate this vector field into an internally induced part $p_f^{I(c)}$ and an externally produced part $p_f^{E(c)}$, as we have done in (3.6), we can conclude from the considerations of (3.7), (3.8) and (3.9) that

$$\begin{aligned} \nabla \wedge p_f^{I(c)} &= q_g && \text{in } \Omega_{(a,c)}, \\ &= 0 && \text{in } \Omega_{(c,b)}, \end{aligned} \quad (3.11)$$

$$\begin{aligned} \nabla \wedge p_f^{E(c)} &= 0 && \text{in } \Omega_{(a,c)}, \\ &= q_g && \text{in } \Omega_{(c,b)}. \end{aligned} \quad (3.12)$$

The terms $\nabla(\nabla \cdot a^{I(c)})$ and $\nabla(\nabla \cdot a^{E(c)})$ vanish, since q_g as a toroidal field is purely tangential. By using the fundamental equations (3.5) we can easily deduce that

$$\begin{aligned} \Delta P_f^{I(c)} &= -Q_g && \text{in } \Omega_{(a,c)}, \\ &= 0 && \text{in } \Omega_{(c,b)}, \end{aligned} \quad (3.13)$$

$$\begin{aligned} \Delta P_f^{E(c)} &= 0 && \text{in } \Omega_{(a,c)}, \\ &= -Q_g && \text{in } \Omega_{(c,b)}. \end{aligned} \quad (3.14)$$

So at least we have succeeded in meaningfully defining what is meant by the part of the poloidal field produced by sources inside Ω_c and the part produced by sources outside it, i.e. we are able to separate the resulting field in the Mie representation. For a presentation of the above considerations from the point of view of geophysical applications the reader is referred to [6].

3.1 Representation by Vector Spherical Harmonic Expansion

The following section is concerned with the separation of a resulting vector field in terms of an internally and an externally induced part. First of all we present the classical ansatz by decomposition into a Fourier series of vector spherical harmonics. This approach follows mainly [6], but we will put it into a more mathematical framework at this point.

Let the inner and outer harmonics $\{H_{n,k}^{int}\}$, $\{H_{n,k}^{ext}\}$, respectively, be given as in Definition 1.7. According to Equation (3.11), $p_f^{I(c)}$ can be represented by a scalar

potential $U_f^{I(c)}$ with $p_f^{I(c)} = -\nabla U_f^{I(c)}$ in Ω_c^{ext} and $U_f^{I(c)}$ being harmonic in Ω_c^{ext} , i.e. there exist coefficients $(p_f^{I(c)})^\wedge(c; n, k)$ such that

$$U_f^{I(c)}(x) = \sum_{n=0}^{\infty} \sum_{k=1}^{2n+1} (p_f^{I(c)})^\wedge(c; n, k) H_{n,k}^{ext}(c; x), \quad x \in \Omega_c^{ext}. \quad (3.15)$$

Similarly, by Equation (3.12), $p_f^{E(c)}$ can be written as $p_f^{E(c)} = \nabla U_f^{E(c)}$ in Ω_c^{int} , where the scalar potential $U_f^{E(c)}$ is harmonic in Ω_c^{int} . Thus, there exist coefficients $(p_f^{E(c)})^\wedge(c; n, k)$ such that

$$U_f^{E(c)}(x) = \sum_{n=0}^{\infty} \sum_{k=1}^{2n+1} (p_f^{E(c)})^\wedge(c; n, k) H_{n,k}^{int}(c; x), \quad x \in \Omega_c^{int}. \quad (3.16)$$

Finally, we can expand the toroidal scalar Q_f of f on Ω_c into a Fourier series of spherical harmonics, i.e. there are coefficients $(q_f)^\wedge(c; n, k)$ such that

$$Q_f(x) = \sum_{n=0}^{\infty} \sum_{k=1}^{2n+1} (q_f)^\wedge(c; n, k) Y_{n,k}^c(x), \quad x \in \Omega_c. \quad (3.17)$$

In order to present the separation of the resulting field in a more comprehensive manner we introduce the following nomenclature.

Definition 3.2

Let $\{H_{n,k}^{ext}(c; x)\}, \{H_{n,k}^{int}(c; x)\}$ be the system of outer, respectively, inner harmonics defined in Definition 1.7.

The system $\{h_{n,k}^{(1)}(c; \cdot)\}_{\substack{n=0,1,\dots; \\ k=1,\dots,2n+1}}$ is, for $x \in \overline{\Omega_c^{ext}}$, defined by

$$\begin{aligned} h_{n,k}^{(1)}(c; x) &= -\nabla_x H_{n,k}^{ext}(c, x) \\ &= \frac{1}{c^2} \left(\frac{c}{r}\right)^{n+2} ((n+1)\xi Y_{n,k}(\xi) - \nabla_\xi^* Y_{n,k}(\xi)), \quad x = r\xi, r = |x|, r \geq c, \\ &\quad n = 0, 1, \dots; k = 1, \dots, 2n+1. \end{aligned}$$

The system $\{h_{n,k}^{(2)}(c; \cdot)\}_{\substack{n=1,2,\dots; \\ k=1,\dots,2n+1}}$ is, for $x \in \overline{\Omega_c^{int}}$, defined by

$$\begin{aligned} h_{n,k}^{(2)}(c; x) &= \nabla_x H_{n,k}^{int}(c, x) \\ &= \frac{1}{c^2} \left(\frac{r}{c}\right)^{n-1} (n\xi Y_{n,k}(\xi) + \nabla_\xi^* Y_{n,k}(\xi)), \quad x = r\xi, r = |x|, r \leq c, \\ &\quad n = 1, 2, \dots; k = 1, \dots, 2n+1. \end{aligned}$$

Finally, the system $\{h_{n,k}^{(3)}(c; \cdot)\}_{\substack{n=1,2,\dots; \\ k=1,\dots,2n+1}}$ is, for $x \in \Omega_c$, defined by

$$\begin{aligned} h_{n,k}^{(3)}(c; x) &= L_x Y_{n,k}^c(x) = \frac{1}{c} L_\xi^* Y_{n,k}(\xi), \quad x = c\xi, \xi \in \Omega, \\ &\quad n = 1, 2, \dots; k = 1, \dots, 2n+1. \end{aligned}$$

By the harmonicity of the inner and outer harmonics, respectively, we immediately see that the vector fields $h_{n,k}^{(1)}$ are divergence free in $\overline{\Omega_c^{ext}}$, the system $h_{n,k}^{(2)}$ is divergence free in $\overline{\Omega_c^{int}}$, and the fields $h_{n,k}^{(3)}$ are surface divergence free on Ω_c . The vector fields $h_{n,k}^{(1)}$ and $h_{n,k}^{(2)}$, respectively, may be called divergence free vector outer and inner harmonics with respect to the sphere Ω_c .

In the following lemma we connect the system of vector outer resp. inner harmonics $\{h_{n,k}^{(i)}\}$ to the system $\{u_{n,k}^{(i)}\}$ of vector spherical harmonics defined in Lemma 1.17.

Lemma 3.3

Let $\{u_{n,k}^{(i)}\}$ be the system of vector spherical harmonics defined in Lemma 1.17. For $x = r\xi$, $r = |x|$, $\xi \in \Omega$, and $n = 0, \dots; k = 1, \dots, 2n+1$ we have

$$h_{n,k}^{(1)}(c; x) = \frac{\sqrt{(n+1)(2n+1)}}{c^2} \left(\frac{c}{r}\right)^{n+2} u_{n,k}^{(1)}(\xi), \quad x \in \overline{\Omega_c^{ext}}, \quad (3.18)$$

$$h_{n,k}^{(2)}(c; x) = \frac{\sqrt{n(2n+1)}}{c^2} \left(\frac{r}{c}\right)^{n-1} u_{n,k}^{(2)}(\xi), \quad x \in \overline{\Omega_c^{int}}, \quad (3.19)$$

$$h_{n,k}^{(3)}(c; x) = \frac{\sqrt{n(n+1)}}{c} u_{n,k}^{(3)}(\xi), \quad x \in \Omega_c. \quad (3.20)$$

Restricting the system $\{h_{n,k}^{(i)}\}$ to a sphere Ω_c and reordering the statements of the above lemma yields

$$\begin{aligned} u_{n,k}^{(1)}(\xi) &= \frac{c^2}{\sqrt{(n+1)(2n+1)}} h_{n,k}^{(1)}(c; c\xi), \\ u_{n,k}^{(2)}(\xi) &= \frac{c^2}{\sqrt{n(2n+1)}} h_{n,k}^{(2)}(c; c\xi), \\ u_{n,k}^{(3)}(\xi) &= \frac{c}{\sqrt{n(n+1)}} h_{n,k}^{(3)}(c; c\xi) \end{aligned}$$

for $\xi \in \Omega$ and $c > 0$. Restricting the system $\{h_{n,k}^{(i)}\}$ especially to the unit sphere $\Omega = \Omega_1$ results in

$$u_{n,k}^{(i)} = (\nu_n^{(i)})^{-1/2} h_{n,k}^{(i)}(1; \xi),$$

for $n = 0, \dots; k = 1, \dots, 2n+1$, $i \in \{1, 2, 3\}$, where the normalization coefficients $\nu_n^{(i)}$ are given in Lemma 1.17.

The above lemma shows that the system $\{u_{n,k}^{(i)}\}$ of vector spherical harmonics has its profound background in another physical context than it seems to be in Lemma 1.17, where the system was just introduced as a linear combination of the system $\{y_{n,k}^{(i)}\}$. The system $\{u_{n,k}^{(1)}\}$ is the restriction of a vector field being divergence free in Ω^{ext} to the unit sphere Ω . Furthermore, the system $\{u_{n,k}^{(2)}\}$ is the restriction of a vector field being divergence free in Ω^{int} to the unit sphere Ω . Finally, the vector fields $\{u_{n,k}^{(3)}\}$

are toroidal vector spherical harmonics on Ω , which are surface divergence free.

Using the relations of Lemma 3.3 we immediately obtain the following orthogonality relations for the system $\{h_{n,k}^{(i)}\}$ if restricted to the sphere Ω_c .

Corollary 3.4

Let $\{h_{n,k}^{(i)}\}$ be the system of vector fields defined in Definition 3.2. Then, for all $n, m = 0, \dots; k, l = 1, \dots, 2n+1$, we have

1. $\left(h_{n,k}^{(i)}, h_{m,l}^{(j)}\right)_{l^2(\Omega_c)} = 0, \quad \text{if } i \neq j,$
2. $\left(h_{n,k}^{(1)}, h_{m,l}^{(1)}\right)_{l^2(\Omega_c)} = \delta_{n,m} \delta_{k,l} \frac{\nu_n^{(1)}}{c^2},$
3. $\left(h_{n,k}^{(2)}, h_{m,l}^{(2)}\right)_{l^2(\Omega_c)} = \delta_{n,m} \delta_{k,l} \frac{\nu_n^{(2)}}{c^2},$
4. $\left(h_{n,k}^{(3)}, h_{m,l}^{(3)}\right)_{l^2(\Omega_c)} = \delta_{n,m} \delta_{k,l} \nu_n^{(3)}.$

These considerations help us to represent the vector fields $p_f^{I(c)}$, $p_f^{E(c)}$ and q_f in an orthogonal expansion of the system $\{h_{n,k}^{(i)}\}$ based on (3.15), (3.16) and (3.17) and the notation of Definition 3.2. We arrive at

$$p_f^{I(c)}(x) = -\nabla_x U_f^{I(c)}(x) = \sum_{n=0}^{\infty} \sum_{k=1}^{2n+1} (p_f^{I(c)})^\wedge(c; n, k) h_{n,k}^{(1)}(c; x), \quad x \in \Omega_c^{ext}, \quad (3.21)$$

$$p_f^{E(c)}(x) = \nabla_x U_f^{E(c)}(x) = \sum_{n=1}^{\infty} \sum_{k=1}^{2n+1} (p_f^{E(c)})^\wedge(c; n, k) h_{n,k}^{(2)}(c; x), \quad x \in \Omega_c^{int}, \quad (3.22)$$

$$q_f(x) = L_x Q_f(x) = \sum_{n=1}^{\infty} \sum_{k=1}^{2n+1} (q_f)^\wedge(c; n, k) h_{n,k}^{(3)}(c; x), \quad x \in \Omega_c. \quad (3.23)$$

Following an argument in [6], if the source field g is piecewise continuous, (3.15) and (3.16) and, hence, (3.21) and (3.22) remain true pointwise in the limit $r \rightarrow c$, i.e. they hold in $\overline{\Omega_c^{ext}}$, respectively, $\overline{\Omega_c^{int}}$. Therefore, we can write, for $x \in \Omega_c$,

$$\begin{aligned} f(x) &= p_f^{I(c)}(x) + p_f^{E(c)}(x) + q_f(x) \\ &= \sum_{n=0}^{\infty} \sum_{k=1}^{2n+1} (p_f^{I(c)})^\wedge(c; n, k) h_{n,k}^{(1)}(c; x) \\ &\quad + \sum_{n=1}^{\infty} \sum_{k=1}^{2n+1} \left((p_f^{E(c)})^\wedge(c; n, k) h_{n,k}^{(2)}(c; x) + (q_f)^\wedge(c; n, k) h_{n,k}^{(3)}(c; x) \right). \end{aligned} \quad (3.24)$$

Corollary 3.4 enables us to calculate the coefficients $(p_f^{I(c)})^\wedge(c; n, k)$, $(p_f^{E(c)})^\wedge(c; n, k)$ and $(q_f)^\wedge(c; n, k)$ as follows

$$\begin{aligned} \frac{(n+1)(2n+1)}{c^2} (p_f^{I(c)})^\wedge(c; n, k) &= \left(h_{n,k}^{(1)}(c; \cdot), f \right)_{l^2(\Omega_c)}, \\ \frac{n(2n+1)}{c^2} (p_f^{E(c)})^\wedge(c; n, k) &= \left(h_{n,k}^{(2)}(c; \cdot), f \right)_{l^2(\Omega_c)}, \\ n(n+1) (q_f)^\wedge(c; n, k) &= \left(h_{n,k}^{(3)}(c; \cdot), f \right)_{l^2(\Omega_c)}. \end{aligned}$$

These coefficients can be substituted in (3.24) to give a Fourier representation of the internally produced poloidal field $p_f^{I(c)}$, the externally poloidal field $p_f^{E(c)}$, and the toroidal part q_f of f on Ω_c .

Finally, we can replace the system $\{h_{n,k}^{(i)}\}$ restricted to Ω_c by the system $\{u_{n,k}^{(i)}\}$ in accordance with Lemma 3.3.

Theorem 3.5

Let the system $\{u_{n,k}^{(i)}\}$ of vector spherical harmonics be defined as in Lemma 1.17. Furthermore, let the vector field f be of class $l^2(\Omega_c)$ with $0 < c < \infty$. Then we have

$$\begin{aligned} f(c\xi) &= \sum_{n=0}^{\infty} \sum_{k=1}^{2n+1} (p_f^{I(c)})^\wedge(c; n, k) u_{n,k}^{(1)}(\xi) \\ &+ \sum_{n=1}^{\infty} \sum_{k=1}^{2n+1} \left((p_f^{E(c)})^\wedge(c; n, k) u_{n,k}^{(2)}(\xi) + (q_f)^\wedge(c; n, k) u_{n,k}^{(3)}(\xi) \right), \quad (3.25) \end{aligned}$$

for $\xi \in \Omega$ with the coefficients given by

$$(p_f^{I(c)})^\wedge(c; n, k) = \left(u_{n,k}^{(1)}, f(c\cdot) \right)_{l^2(\Omega)} \quad (3.26a)$$

$$(p_f^{E(c)})^\wedge(c; n, k) = \left(u_{n,k}^{(2)}, f(c\cdot) \right)_{l^2(\Omega)} \quad (3.26b)$$

$$(q_f)^\wedge(c; n, k) = \left(u_{n,k}^{(3)}, f(c\cdot) \right)_{l^2(\Omega)}. \quad (3.26c)$$

The first part represents the field resulting from sources inside Ω_c , the second part is coming from sources outside Ω_c and the third part is the toroidal part of f on Ω_c .

This theorem provides a first step to separate a field vector f on a sphere Ω_c into a poloidal internally generated, a poloidal externally generated and a toroidal part. It should be noted that for numerical implementations, i.e. the evaluation of the integrals appearing in (3.26), a global coverage of observational data all over the sphere is needed. To overcome this difficulty a local concept for the reconstruction of the different parts of the vector field f has to be formulated. This will be done in the following section.

3.2 Representation by Vector Scaling Functions and Wavelets

In contrast to Section 3.1, where we have presented a representation of the internally and externally induced parts of a vector field f in terms of vector spherical harmonics, we now develop a decomposition of a vector field f on the sphere by spherical vector wavelets, i.e. by scale dependent, space localizing radial basis functions.

Referring to the nomenclature of Chapter 2 we present a special multiresolution analysis of the identity operator $Id : l^2(\Omega) \rightarrow l^2(\Omega)$ given by $Id(f) = f$, $f \in l^2(\Omega)$. In Chapter 1 we have introduced two different orthonormal systems for the Hilbert space $l^2(\Omega)$ which both can be used for establishing the singular system of the identity operator. A multiscale analysis of the identity using the system of vector spherical harmonics $\{y_{n,k}^{(i)}\}$ is extensively discussed in [42]. We use in this section the $\{u_{n,k}^{(i)}\}$ system of vector spherical harmonics defined in Lemma 1.17. More explicitly, the singular system $\{\sigma_{n'}, h_{n'}, k_{n'}\}$ of the identity operator $Id : \mathfrak{h} = l^2(\Omega) \rightarrow \mathfrak{k} = l^2(\Omega)$ is given by

$$\begin{aligned} h_{n'} &= u_{n,k}^{(i)}, & (n,k) \in \mathcal{N}_i, i \in \{1,2,3\}, \\ k_{n'} &= u_{n,k}^{(i)}, & (n,k) \in \mathcal{N}_i, i \in \{1,2,3\}, \\ \sigma_{n'} &= 1, & n' \in \mathbb{N}_0. \end{aligned}$$

The theory of multiresolution for operator equations as presented in Chapter 2 can now easily be applied to the case of the identity operator. Basically, this does not give any new information compared to a multiscale decomposition of the identity based on the system $\{y_{n,k}^{(i)}\}$. Nevertheless there is an advantage in the special choice of the singular system. We have already seen in the previous section that the system $\{u_{n,k}^{(i)}\}$ of vector spherical harmonics fulfills the property of separating a given spherical vector field into an internally induced part, an externally induced part, and a part produced by sources on the sphere itself. In the following section this advantageous property will be transferred to the case of a multiscale representation. By this, it can be shown that the decomposition with respect to sources is also possible in a space localizing framework.

We restrict ourselves to vector fields $f \in l^2(\Omega)$ which is no loss of generality since every vector field f of class $l^2(\Omega_c)$, $c \in (0, \infty)$, can be mapped isomorphically to a vector field of class $l^2(\Omega)$.

Because of the importance for the following considerations we recapitulate a combination of Corollary 1.18 and Theorem 3.5.

Corollary 3.6

Let $\{u_{n,k}^{(i)}\}$ be the system of vector spherical harmonics as defined in Lemma 1.17.

Suppose that $f \in l^2(\Omega)$. Then

$$\begin{aligned} f &= f_{\mathcal{U}}^{(1)} + f_{\mathcal{U}}^{(2)} + f_{\mathcal{U}}^{(3)} \\ &= \sum_{i=1}^3 \sum_{n=0_i}^{\infty} \sum_{k=1}^{2n+1} (f_{\mathcal{U}}^{(i)})^{\wedge}(n, k) u_{n,k}^{(i)} \end{aligned} \quad (3.27)$$

holds in the sense of the $l^2(\Omega)$ -norm, where the Fourier coefficients are, for $n = 0_i, \dots; k = 1, \dots, 2n+1$, given by

$$\begin{aligned} (f_{\mathcal{U}}^{(1)})^{\wedge}(n, k) &= \left(u_{n,k}^{(1)}, f \right)_{l^2(\Omega)}, \\ (f_{\mathcal{U}}^{(2)})^{\wedge}(n, k) &= \left(u_{n,k}^{(2)}, f \right)_{l^2(\Omega)}, \\ (f_{\mathcal{U}}^{(3)})^{\wedge}(n, k) &= \left(u_{n,k}^{(3)}, f \right)_{l^2(\Omega)}. \end{aligned}$$

The first part in (3.27), $f_{\mathcal{U}}^{(1)}$, represents the poloidal field resulting from sources inside Ω , the second part, $f_{\mathcal{U}}^{(2)}$, is the field corresponding to sources outside Ω , and the third part, $f_{\mathcal{U}}^{(3)}$, is the toroidal part of the vector field f on Ω .

3.2.1 Scaling Functions and Wavelets

At first we introduce special vector kernel functions, which are the starting point of the multiscale approximation theory of $l^2(\Omega)$ vector fields. This will be done in accordance with the nomenclature presented in Section 2.2 in a general Hilbert space concept.

Definition 3.7

Let $\{(k^{(i)})^{\wedge}(n)\}_{n=0_i, \dots}$, $i \in \{1, 2, 3\}$, be an admissible sequence of real numbers, i.e.

$$\sum_{n=0_i}^{\infty} \frac{2n+1}{4\pi} |(k^{(i)})^{\wedge}(n)|^2 < \infty. \quad (3.28)$$

Then a *vector kernel function* $k^{(i)}$ is defined by

$$k^{(i)} : \Omega \times \Omega \rightarrow \mathbb{R}^3 \quad (3.29)$$

$$k^{(i)}(\xi, \eta) = \sum_{n=0_i}^{\infty} \sum_{k=1}^{2n+1} (k^{(i)})^{\wedge}(n) u_{n,k}^{(i)}(\xi) Y_{n,k}(\eta), \quad \xi, \eta \in \Omega. \quad (3.30)$$

Next, as in Section 2.2, two types of convolutions are introduced which are equivalent to the convolutions defined in Definition 2.8. The first one enables us to calculate scalar coefficients for each vector field f of class $l^2(\Omega)$, a process which will be called decomposition. The second type of convolution will give us the possibility to reconstruct the vector field from its scalar coefficients.

Definition 3.8

Let the vector kernels $k^{(i)}, i \in \{1, 2, 3\}$, be given as in Definition 3.7. Furthermore, let f be a vector field of class $l^2(\Omega)$. Then the (*decomposing*) *convolution* of $k^{(i)}$ against f is defined by

$$(k^{(i)} * f)(\xi) = \int_{\Omega} k^{(i)}(\eta, \xi) \cdot f(\eta) d\omega(\eta), \quad \xi \in \Omega. \quad (3.31)$$

Furthermore, let F be of class $\mathcal{L}^2(\Omega)$. Then the (*reconstructing*) *convolution* of $k^{(i)}$ against F is defined by

$$(k^{(i)} \star F)(\xi) = \int_{\Omega} k^{(i)}(\xi, \eta) F(\eta) d\omega(\eta). \quad (3.32)$$

The two types of convolutions satisfy a substantial property of Fourier analysis, namely that the convolution of two functions in spatial domain is equivalent to multiplication of the Fourier representations of the two functions in the spectral domain. It can easily be shown that

$$(k^{(i)} * f) = \sum_{n=0_i}^{\infty} \sum_{k=1}^{2n+1} (k^{(i)})^{\wedge}(n) (f_{\mathcal{U}}^{(i)})^{\wedge}(n, k) Y_{n,k}, \quad (3.33)$$

$$(k^{(i)} \star F) = \sum_{n=0_i}^{\infty} \sum_{k=1}^{2n+1} (k^{(i)})^{\wedge}(n) F^{\wedge}(n, k) u_{n,k}^{(i)} \quad (3.34)$$

holds in the sense of the $\mathcal{L}^2(\Omega)$ –norm, respectively, the $l^2(\Omega)$ –norm. If we combine the two convolutions of a function $f \in l^2(\Omega)$ against two kernel functions $h^{(i)}$ and $k^{(i)}, i \in \{1, 2, 3\}$ fixed, we get

$$(k^{(i)} \star (h^{(i)} * f)) = \sum_{n=0_i}^{\infty} \sum_{k=1}^{2n+1} (h^{(i)})^{\wedge}(n) (k^{(i)})^{\wedge}(n) (f_{\mathcal{U}}^{(i)})^{\wedge}(n, k) u_{n,k}^{(i)} \quad (3.35)$$

in the sense of the $l^2(\Omega)$ –norm, which is the Fourier representation of the internally produced poloidal (for the case $i = 1$), the externally produced poloidal (if $i = 2$) or the toroidal part (if $i = 3$) of f , where the Fourier coefficients $(f_{\mathcal{U}}^{(i)})^{\wedge}(n, k)$ of $f_{\mathcal{U}}^{(i)}$ are filtered with the symbol $(h^{(i)})^{\wedge}(n) (k^{(i)})^{\wedge}(n)$. It is obvious that we can get an approximation of each part of f just by a suitable choice of the kernel functions, respectively, their symbols. This leads us to scaling functions and wavelets as special reproducing vector kernel functions.

Definition 3.9

Let $\{(\varphi_J^{(i)})^{\wedge}(n)\}_{n=0_i, \dots, J} \in \mathbb{Z}, i \in \{1, 2, 3\}$, be a family of symbols satisfying

1. $\{(\varphi_J^{(i)})^{\wedge}(n)\}$ is admissible for all $J \in \mathbb{Z}$, i.e.

$$\sum_{n=0_i}^{\infty} \frac{2n+1}{4\pi} \left| (\varphi_J^{(i)})^{\wedge}(n) \right|^2 < \infty,$$

2. $\lim_{J \rightarrow \infty} (\varphi_J^{(i)})^\wedge(n) = 1$ and $\lim_{J \rightarrow -\infty} (\varphi_J^{(i)})^\wedge(n) = 0$ for all $n \in \mathbb{N}_{0_i}$,
3. $(\varphi_J^{(i)})^\wedge(n) \leq (\varphi_{J+1}^{(i)})^\wedge(n)$, $J \in \mathbb{Z}, n \in \mathbb{N}_{0_i}$.

Then the vector symbol $(\varphi_J)^\wedge(n) = \left((\varphi_J^{(1)})^\wedge(n), (\varphi_J^{(2)})^\wedge(n), (\varphi_J^{(3)})^\wedge(n) \right)^T$ is called the family of *generating symbols of a scale discrete vector scaling function*.

Definition 3.10

Let $J_1, J_2 \in \mathbb{Z}$ be fixed and let $\{(\varphi_{J_1}^{(i)})^\wedge(n)\}$ be a generating symbol of a vector scaling function as given by Definition 3.9, then the *scale discrete dilation operator* D_{J_2} is defined by

$$(D_{J_2} \varphi_{J_1}^{(i)})^\wedge(n) = (\varphi_{J_1+J_2}^{(i)})^\wedge(n), \quad i \in \{1, 2, 3\}, \quad n \in \mathbb{N}_{0_i}. \quad (3.36)$$

The application of D_{J_2} on the vector symbol $\{(\varphi_{J_1})^\wedge(n)\}$ is given by

$$(D_{J_2} \varphi_{J_1})^\wedge(n) = (\varphi_{J_1+J_2})^\wedge(n) = \left((\varphi_{J_1+J_2}^{(1)})^\wedge(n), (\varphi_{J_1+J_2}^{(2)})^\wedge(n), (\varphi_{J_1+J_2}^{(3)})^\wedge(n) \right)^T.$$

Vector scaling functions are now introduced by choosing an admissible generating symbol as the symbol of a vector kernel function.

Definition 3.11

Let $\{(\varphi_J)^\wedge(n)\}$, $J \in \mathbb{Z}$, be a family of generating symbols of a vector scaling function as defined in Definition 3.9, then the kernel function

$$\varphi_0(\xi, \eta) = \sum_{i=1}^3 \sum_{n=0_i}^{\infty} \sum_{k=1}^{2n+1} (\varphi_0^{(i)})^\wedge(n) u_{n,k}^{(i)}(\xi) Y_{n,k}(\eta), \quad \xi, \eta \in \Omega,$$

is called the *scale discrete mother vector scaling function*. The *dilated scale discrete vector scaling function* (or just dilated vector scaling function if no confusion is likely to arise) is defined via

$$\varphi_J(\xi, \eta) = D_J \varphi_0(\xi, \eta) = \sum_{i=1}^3 \sum_{n=0_i}^{\infty} \sum_{k=1}^{2n+1} (\varphi_J^{(i)})^\wedge(n) u_{n,k}^{(i)}(\xi) Y_{n,k}(\eta), \quad \xi, \eta \in \Omega.$$

Note that

$$\varphi_J(\xi, \eta) = \sum_{i=1}^3 \varphi_J^{(i)}(\xi, \eta), \quad \xi, \eta \in \Omega,$$

with

$$\varphi_J^{(i)}(\xi, \eta) = \sum_{n=0_i}^{\infty} \sum_{k=1}^{2n+1} (\varphi_J^{(i)})^\wedge(n) u_{n,k}^{(i)}(\xi) Y_{n,k}(\eta), \quad \xi, \eta \in \Omega.$$

The functions $\varphi_J^{(i)}(\cdot, \cdot)$ are called *scale discrete vector scaling functions of type i*.

In Chapter 2 we have introduced decomposition vector scaling functions ${}^r\varphi_J$ and decomposition vector scaling functions ${}^d\varphi_J$ in a general Hilbert space concept. Both are in the case of a multiscale decomposition of the identity operator just equal, ${}^r\varphi_J = {}^d\varphi_J$, and given by the above defined vector scaling function.

It is clear by definition that the generating symbol $(\varphi_J)^\wedge(n) = ((\varphi_J^{(1)})^\wedge(n), (\varphi_J^{(2)})^\wedge(n), (\varphi_J^{(3)})^\wedge(n))^T$ tends componentwise to 1 as J tends to infinity. This enables us to approximate an $l^2(\Omega)$ -vector fields using the convolutions introduced in Definition 3.8.

Theorem 3.12

Let $\{(\varphi_J)^\wedge(n)\}$, $J \in \mathbb{Z}$, be the generating symbol of a vector scaling function. Suppose that φ_J is the corresponding vector scaling function. Furthermore, let f be of class $l^2(\Omega)$. Then, for $i \in \{1, 2, 3\}$,

$$\lim_{J \rightarrow \infty} \left\| \varphi_J^{(i)} \star \varphi_J^{(i)} * f - f_{\mathcal{U}}^{(i)} \right\|_{l^2(\Omega)} = 0.$$

Moreover,

$$\lim_{J \rightarrow \infty} \left\| \varphi_J \star \varphi_J * f - f \right\|_{l^2(\Omega)} = 0.$$

Proof:

Using (3.35) and Parseval's identity we obtain, for $J \in \mathbb{N}_0$ and $i \in \{1, 2, 3\}$,

$$\begin{aligned} & \lim_{J \rightarrow \infty} \left\| \varphi_J^{(i)} \star \varphi_J^{(i)} * f - f_{\mathcal{U}}^{(i)} \right\|_{l^2(\Omega)}^2 \\ &= \lim_{J \rightarrow \infty} \int_{\Omega} \left| \sum_{n=0_i}^{\infty} \sum_{k=1}^{2n+1} \left(((\varphi_J^{(i)})^\wedge(n))^2 (f_{\mathcal{U}}^{(i)})^\wedge(n, k) u_{n,k}^{(i)}(\xi) - (f_{\mathcal{U}}^{(i)})^\wedge(n, k) u_{n,k}^{(i)}(\xi) \right) \right|^2 d\omega(\xi) \\ &= \lim_{J \rightarrow \infty} \int_{\Omega} \left| \sum_{n=0_i}^{\infty} \sum_{k=1}^{2n+1} \left(((\varphi_J^{(i)})^\wedge(n))^2 - 1 \right) (f_{\mathcal{U}}^{(i)})^\wedge(n, k) u_{n,k}^{(i)}(\xi) \right|^2 d\omega(\xi) \\ &= \lim_{J \rightarrow \infty} \sum_{n=0_i}^{\infty} \sum_{k=1}^{2n+1} \left(((\varphi_J^{(i)})^\wedge(n))^2 - 1 \right)^2 \left((f_{\mathcal{U}}^{(i)})^\wedge(n, k) \right)^2. \end{aligned}$$

Since the admissible symbol $\{(\varphi_J^{(i)})^\wedge(n)\}$ tends to 1 if J tends to infinity and is monotonically increasing in J , the term $\left(((\varphi_J^{(i)})^\wedge(n))^2 - 1 \right)$ is smaller than 1 for all $n \in \mathbb{N}$ and for J sufficiently large. Thus, we can interchange sum and limit and from $\lim_{J \rightarrow \infty} (\varphi_J^{(i)})^\wedge(n) = 1$ we finally get the desired result. \square

Theorem 3.12 can be interpreted as the wavelet counterpart of Theorem 3.5. It tells us that, if we convolve a spherical vector field f of class $l^2(\Omega)$ twice with the scaling function $\varphi_J^{(i)}$, we obtain an approximation of $f_{\mathcal{U}}^{(i)}$ at scale J . In the case $i = 1$ this is an approximation of that part of f which is induced by sources inside Ω , if $i = 2$ it is the part of f which is induced by sources outside Ω and in the case $i = 3$ it is an approximation of the toroidal part of f which is induced by the radial projection of

source fields crossing Ω .

From the point of view of Fourier theory the reader may argue that the same result has already been achieved in Theorem 3.5 in an easier context and nomenclature. The main advantage of the above theorem results from a substantial property of wavelet theory, the localization property. Scaling functions and special kernel functions called wavelets, which are defined in the next paragraph, are known as very well space localizing functions. This property is due to scaling functions to be clusters of a system of orthonormal functions in the corresponding Hilbert space. The mathematical background for the discrepancy between spatial and spectral localization is given by the uncertainty principle. It is a general result of Fourier analysis and tells us that the product of the variance in space and the variance in frequency of a function is bounded away from zero. In other words, a function cannot possess a good localization behavior in spatial domain and in the Fourier domain at the same time. The extreme trial functions in the sense of the uncertainty principle are given by vector spherical harmonics $\{u_{n,k}^{(i)}\}$ for ideal frequency localization on the one hand and the Dirac functional $\delta_{\Omega}^{(i)}$ on $l_{\mathcal{U}}^{2,(i)}$ given by

$$\delta_{\Omega}^{(i)}(.,.) = \sum_{n=0_i}^{\infty} \sum_{k=1}^{2n+1} u_{n,k}^{(i)}(.) Y_{n,k}(.), \quad i \in \{1, 2, 3\}, \quad (3.37)$$

for ideal space localization on the other hand. A graphical illustration of the uncertainty principle and the construction of vector kernel functions is given in Table 3.1.

Ideal frequency localization No space localization		No frequency localization Ideal space localization
←		→
vector spherical harmonics $u_{n,k}^{(i)}$ Lemma 1.17	vector kernels $k^{(i)}(.,.)$ Definition 3.7	Dirac functional $\delta_{\Omega}^{(i)}(.,.)$ Equation (3.37)

Table 3.1: The uncertainty principle.

For the scalar case on the sphere the uncertainty principle has been established in [18] and [19]. A first approach for a vectorial uncertainty principle has been made in [10] based on the orthonormal system $\{y_{n,k}^{(i)}\}$. There, the author has classified vector kernel functions following the uncertainty principle. For further information about these results the reader is referred to this thesis. From the point of view of functional analysis it is clear that a similar relation as the one presented in [10] can be developed based on the orthonormal system $\{u_{n,k}^{(i)}\}$ defined in Lemma 1.17.

By the space localizing property of scaling functions and wavelets we are now able to separate a given field $f \in l^2(\Omega)$ locally with respect to its sources. In consequence, we do not need a global coverage of data as for the application of Theorem 3.5. With given data only in a regional area of the unit sphere Ω we are able to decide

which part of f results from sources inside, outside or on the sphere.

To complete the theory of a multiscale decomposition of the identity, we introduce the above mentioned scale discrete vector wavelets as special vector kernel functions. Similar to vector scaling functions they are determined via their symbols. The symbols of vector wavelets are related to the symbols of the corresponding vector scaling function via the refinement equation which will be given next.

Definition 3.13

Let $\{(\varphi_J)^\wedge(n)\}_{n=0_i, \dots, J \in \mathbb{Z}}$, be the family of generating symbols of a scale discrete vector scaling function. Furthermore, let $\{(\psi_J^{(i)})^\wedge(n)\}_{n=0_i, \dots, J \in \mathbb{Z}, i \in \{1, 2, 3\}}$, and $\{(\tilde{\psi}_J^{(i)})^\wedge(n)\}_{n=0, 1, \dots, J \in \mathbb{Z}, i \in \{1, 2, 3\}}$, be symbols satisfying

1. $\{(\psi_J^{(i)})^\wedge(n)\}$ and $\{(\tilde{\psi}_J^{(i)})^\wedge(n)\}$ are admissible for all $J \in \mathbb{Z}$, i.e.

$$\sum_{n=0_i}^{\infty} \frac{2n+1}{4\pi} \left| (\psi_J^{(i)})^\wedge(n) \right|^2 < \infty, \quad \sum_{n=0_i}^{\infty} \frac{2n+1}{4\pi} \left| (\tilde{\psi}_J^{(i)})^\wedge(n) \right|^2 < \infty,$$

2. $\{(\psi_J^{(i)})^\wedge(n)\}$ and $\{(\tilde{\psi}_J^{(i)})^\wedge(n)\}$ fulfill the refinement equation, i.e.

$$(\psi_J^{(i)})^\wedge(n) (\tilde{\psi}_J^{(i)})^\wedge(n) = \left((\varphi_{J+1}^{(i)})^\wedge(n) \right)^2 - \left((\varphi_J^{(i)})^\wedge(n) \right)^2, \quad n \in \mathbb{N}_{0_i}, J \in \mathbb{Z}.$$

Then

$$(\psi_J)^\wedge(n) = \left((\psi_J^{(1)})^\wedge(n), (\psi_J^{(2)})^\wedge(n), (\psi_J^{(3)})^\wedge(n) \right)^T$$

and

$$(\tilde{\psi}_J)^\wedge(n) = \left((\tilde{\psi}_J^{(1)})^\wedge(n), (\tilde{\psi}_J^{(2)})^\wedge(n), (\tilde{\psi}_J^{(3)})^\wedge(n) \right)^T$$

are called the family of *generating symbols of a scale discrete vector wavelet* and the family of *generating symbols of a scale discrete dual vector wavelet*, respectively.

In the same manner as in Definition 3.10 we can define the application of the dilation operator $D_{J_2}, J_2 \in \mathbb{Z}$, on the generating symbol of a discrete mother wavelet $\{(\psi_{J_1})^\wedge(n)\}$ and a discrete dual mother wavelet $\{(\tilde{\psi}_{J_1})^\wedge(n)\}$, for $n \in \mathbb{N}_{0_i}$, by

$$\begin{aligned} (D_{J_2} \psi_{J_1})^\wedge(n) &= (\psi_{J_1+J_2})^\wedge(n), \\ (D_{J_2} \tilde{\psi}_{J_1})^\wedge(n) &= (\tilde{\psi}_{J_1+J_2})^\wedge(n). \end{aligned}$$

With the aid of these generating symbols we are now able to introduce vector wavelets as a special class of vector kernel functions.

Definition 3.14

Let $\{(\psi_J)^\wedge(n)\}$, $J \in \mathbb{Z}$, and $\{(\tilde{\psi}_J)^\wedge(n)\}$, $J \in \mathbb{Z}$, be generating symbols of scale discrete wavelets as given in Definition 3.13. Then the scale discrete *mother vector wavelet* and the scale discrete *dual mother vector wavelet* are given by

$$\psi_0(\xi, \eta) = \sum_{i=1}^3 \sum_{n=0_i}^{\infty} \sum_{k=1}^{2n+1} (\psi_0^{(i)})^\wedge(n) u_{n,k}^{(i)}(\xi) Y_{n,k}(\eta), \quad \xi, \eta \in \Omega,$$

and

$$\tilde{\psi}_0(\xi, \eta) = \sum_{i=1}^3 \sum_{n=0_i}^{\infty} \sum_{k=1}^{2n+1} (\tilde{\psi}_0^{(i)})^\wedge(n) u_{n,k}^{(i)}(\xi) Y_{n,k}(\eta), \quad \xi, \eta \in \Omega.$$

The dilated versions of the mother wavelet and the dual mother wavelet are defined by

$$\psi_J(\xi, \eta) = D_J \psi_0(\xi, \eta) = \sum_{i=1}^3 \sum_{n=0_i}^{\infty} \sum_{k=1}^{2n+1} (\psi_J^{(i)})^\wedge(n) u_{n,k}^{(i)}(\xi) Y_{n,k}(\eta), \quad \xi, \eta \in \Omega,$$

and

$$\tilde{\psi}_J(\xi, \eta) = D_J \tilde{\psi}_0(\xi, \eta) = \sum_{i=1}^3 \sum_{n=0_i}^{\infty} \sum_{k=1}^{2n+1} (\tilde{\psi}_J^{(i)})^\wedge(n) u_{n,k}^{(i)}(\xi) Y_{n,k}(\eta), \quad \xi, \eta \in \Omega.$$

As in Definition 3.10 of a vector scaling function we can also write

$$\psi_J(\xi, \eta) = \sum_{i=1}^3 \psi_J^{(i)}(\xi, \eta), \quad \xi, \eta \in \Omega,$$

with

$$\psi_J^{(i)}(\xi, \eta) = \sum_{n=0_i}^{\infty} \sum_{k=1}^{2n+1} (\psi_J^{(i)})^\wedge(n) u_{n,k}^{(i)}(\xi) Y_{n,k}(\eta), \quad \xi, \eta \in \Omega$$

and

$$\tilde{\psi}_J(\xi, \eta) = \sum_{i=1}^3 \tilde{\psi}_J^{(i)}(\xi, \eta), \quad \xi, \eta \in \Omega$$

with

$$\tilde{\psi}_J^{(i)}(\xi, \eta) = \sum_{n=0_i}^{\infty} \sum_{k=1}^{2n+1} (\tilde{\psi}_J^{(i)})^\wedge(n) u_{n,k}^{(i)}(\xi) Y_{n,k}(\eta), \quad \xi, \eta \in \Omega.$$

The functions $\psi_J^{(i)}(\cdot, \cdot)$ and $\tilde{\psi}_J^{(i)}(\cdot, \cdot)$ are called *scale discrete vector wavelets of type i* and *scale discrete dual vector wavelets of type i*, respectively.

Using this definition we are led to a reconstruction of a vector field $f \in l^2(\Omega)$ by means of its wavelet transform which will be introduced in the following.

Definition 3.15

Let φ_J be a scale discrete vector scaling function and ψ_J be the corresponding scale discrete vector wavelet. Then, for $f \in l^2(\Omega)$, the *spherical vector wavelet transform* of type i and the *spherical vector wavelet transform* are defined by

$$(WT)_{\psi_0^{(i)}}(f)(J; \xi) = (\psi_J^{(i)} * f)(\xi) = \int_{\Omega} \psi_J^{(i)}(\xi, \eta) \cdot f(\eta) d\omega(\eta)$$

and

$$(WT)_{\psi_0}(f)(J; \xi) = (\psi_J * f)(\xi) = \int_{\Omega} \psi_J(\xi, \eta) \cdot f(\eta) d\omega(\eta).$$

Now, we are able to give the above mentioned reconstruction of a vector field $f \in l^2(\Omega)$ by means of its wavelet transform.

Theorem 3.16

Let φ_J , $J \in \mathbb{Z}$, be a vector scaling function and let ψ_J , $J \in \mathbb{Z}$, and $\tilde{\psi}_J$, $J \in \mathbb{Z}$, be the corresponding vector wavelet function and its dual. Then, for $f \in l^2(\Omega)$, the following reconstruction formula holds true

$$\begin{aligned} f_U^{(i)} &= \varphi_0^{(i)} \star \varphi_0^{(i)} * f + \sum_{j=0}^{\infty} \tilde{\psi}_j^{(i)} \star \psi_j^{(i)} * f, \\ &= \varphi_0^{(i)} \star \varphi_0^{(i)} * f + \sum_{j=0}^{\infty} \tilde{\psi}_j^{(i)} \star (WT)_{\psi_0^{(i)}}(f)(j; \cdot), \quad i \in \{1, 2, 3\}, \end{aligned}$$

in the sense of the $l^2(\Omega)$ -norm. Moreover,

$$\begin{aligned} f &= \varphi_0 \star \varphi_0 * f + \sum_{j=0}^{\infty} \tilde{\psi}_j \star \psi_j * f, \\ &= \varphi_0 \star \varphi_0 * f + \sum_{j=0}^{\infty} \tilde{\psi}_j \star (WT)_{\psi_0}(f)(j; \cdot), \end{aligned}$$

in the sense of the $l^2(\Omega)$ -norm

Proof:

Observing the definition of the dilates we obtain for the generating symbol of the vector wavelet functions

$$(\psi_J^{(i)})^{\wedge}(n)(\tilde{\psi}_J^{(i)})^{\wedge}(n) = \left((\varphi_{J+1}^{(i)})(n) \right)^2 - \left((\varphi_J^{(i)})(n) \right)^2, \quad n \in \mathbb{N}_{0_i}.$$

Via summation we get

$$\begin{aligned} \sum_{j=0}^J (\psi_j^{(i)})^{\wedge}(n)(\tilde{\psi}_j^{(i)})^{\wedge}(n) &= \sum_{j=0}^J \left[\left((\varphi_{j+1}^{(i)})^{\wedge}(n) \right)^2 - \left((\varphi_j^{(i)})^{\wedge}(n) \right)^2 \right], \\ &= \left((\varphi_{J+1}^{(i)})^{\wedge}(n) \right)^2 - \left((\varphi_0^{(i)})^{\wedge}(n) \right)^2, \quad n \in \mathbb{N}_{0_i}. \end{aligned}$$

Simply rearranged, this yields

$$\left((\varphi_0^{(i)})^\wedge(n)\right)^2 + \sum_{j=0}^J (\psi_j^{(i)})^\wedge(n) (\tilde{\psi}_j^{(i)})^\wedge(n) = \left((\varphi_{J+1}^{(i)})^\wedge(n)\right)^2, \quad n \in \mathbb{N}_{0_i}.$$

By this formula for the generators and the linearity of the convolutions we can deduce that, for $f \in l^2(\Omega)$,

$$\varphi_0^{(i)} \star \varphi_0^{(i)} \star f + \sum_{j=0}^J \tilde{\psi}_0^{(i)} \star \psi_0^{(i)} \star f = \varphi_{J+1}^{(i)} \star \varphi_{J+1}^{(i)} \star f.$$

holds in the sense of the $l^2(\Omega)$ -norm. Letting J tend to infinity, Theorem 3.12 finally gives the desired result. \square

Remark 3.17

Definition 3.13 and 3.14 are quite general construction principles for scale discrete vector wavelets. Many concrete examples for the scalar case can be found in [20] and for the vectorial case in [7]. In this work we will only use so called *P-scale discrete vector wavelets*, which are defined by equaling the two generators of a vector wavelet function and its dual, i.e. $(\psi_J^{(i)})^\wedge(n) = (\tilde{\psi}_J^{(i)})^\wedge(n)$, $n \in \mathbb{N}_{0_i}$. Thus, the refinement equation reads for all $n \in \mathbb{N}_{0_i}$

$$(\psi_J^{(i)})^\wedge(n) = (\tilde{\psi}_J^{(i)})^\wedge(n) = \sqrt{\left((\varphi_{J+1}^{(i)})^\wedge(n)\right)^2 - \left((\varphi_J^{(i)})^\wedge(n)\right)^2}, \quad J \in \mathbb{Z}. \quad (3.38)$$

3.2.2 Scale and Detail Spaces

In this section a main ingredient of a multiscale theory will be formulated, viz. the so called *vector multiresolution analysis*. At first we introduce operators which represent the decomposition and reconstruction of the space $l^2(\Omega)$ in terms of vector scaling functions and wavelets.

Definition 3.18

The operators $P_J^{(i)}, R_J^{(i)}, i \in \{1, 2, 3\}$, and P_J, R_J are defined by

$$\begin{aligned} P_J^{(i)} : l^2(\Omega) &\rightarrow l_{\mathcal{U}}^{2,(i)}(\Omega) & P_J : l^2(\Omega) &\rightarrow l^2(\Omega) \\ P_J^{(i)} f &= \varphi_J^{(i)} \star \varphi_J^{(i)} \star f, \quad J \in \mathbb{Z}, & P_J f &= \varphi_J \star \varphi_J \star f, \quad J \in \mathbb{Z}, \\ R_J^{(i)} : l^2(\Omega) &\rightarrow l_{\mathcal{U}}^{2,(i)}(\Omega) & R_J f : l^2(\Omega) &\rightarrow l^2(\Omega) \\ R_J^{(i)} f &= \tilde{\psi}_J^{(i)} \star \psi_J^{(i)} \star f, \quad J \in \mathbb{Z}, & R_J &= \tilde{\psi}_J \star \psi_J \star f, \quad J \in \mathbb{Z}. \end{aligned}$$

The image spaces of $l^2(\Omega)$ under the above operators are given by

$$\begin{aligned} V_J^{(i)} &= \left\{ P_J^{(i)} f \mid f \in l^2(\Omega) \right\}, \quad i \in \{1, 2, 3\}, \\ V_J &= \left\{ P_J f \mid f \in l^2(\Omega) \right\}, \\ W_J^{(i)} &= \left\{ R_J^{(i)} f \mid f \in l^2(\Omega) \right\}, \quad i \in \{1, 2, 3\}, \\ W_J &= \left\{ R_J f \mid f \in l^2(\Omega) \right\}. \end{aligned}$$

The spaces $V_J, V_J^{(i)}$ are called *scale spaces (of type (i))* and the spaces $W_J, W_J^{(i)}$ are called *detail spaces (of type (i))*.

The operators P_J and $P_J^{(i)}$ may be understood as low pass filters which provide filtered information of the function f , while R_J and $R_J^{(i)}$ may be interpreted as band pass filters which deliver detail information between two consecutive scales. This becomes much clearer if we look at the following statements.

Obviously, due to Theorem 3.12, we know that

$$\overline{\bigcup_{j=0}^{\infty} V_j^{(i)}}^{\|\cdot\|_{l^2(\Omega)}} = l_{\mathcal{U}}^{2,(i)}(\Omega), \quad i \in \{1, 2, 3\}, \quad (3.39)$$

$$\overline{\bigcup_{j=0}^{\infty} V_j}^{\|\cdot\|_{l^2(\Omega)}} = l^2(\Omega). \quad (3.40)$$

We also know, that the generators $\{(\varphi_J)^{\wedge}(n)\}$ and, hence, $\{((\varphi_J)^{\wedge}(n))^2\}$ are monotonically increasing in J for $n \in \mathbb{N}_{0_i}$ fixed, such that, for $i \in \{1, 2, 3\}$, the dilated generators satisfy

$$(\varphi_J^{(i)})^{\wedge}(n) \leq (\varphi_{J+1}^{(i)})^{\wedge}(n), \quad n \in \mathbb{N}_{0_i},$$

and

$$\left((\varphi_J^{(i)})^{\wedge}(n) \right)^2 \leq \left((\varphi_{J+1}^{(i)})^{\wedge}(n) \right)^2, \quad n \in \mathbb{N}_{0_i}.$$

This immediately leads to

$$V_0^{(i)} \subset \cdots \subset V_J^{(i)} \subset V_{J+1}^{(i)} \subset \cdots \subset l_{\mathcal{U}}^{2,(i)}(\Omega), \quad i \in \{1, 2, 3\}, \quad J > 0, \quad (3.41)$$

as well as

$$V_0 \subset \cdots \subset V_J \subset V_{J+1} \subset \cdots \subset l^2(\Omega), \quad J > 0. \quad (3.42)$$

The last two properties form substantial results of scaling function and wavelet theory called the *vector multiresolution analysis* (VMRA). Equation (3.39) and (3.40) tell us that the approximation of a vector field converges to the original vector field when the scale is increased. From (3.41) and (3.42) we can see, that an approximation at some resolution contains all the information of an approximation at lower scale. Hence the operators P_J and $P_J^{(i)}$ can clearly be understood as low pass filters for vector fields in $l^2(\Omega)$.

Observing Theorem 3.16 we easily obtain the following relations

$$\begin{aligned} V_J^{(i)} &= V_0^{(i)} + \sum_{j=0}^{J-1} W_j^{(i)}, \quad i \in \{1, 2, 3\}, \quad J > 0, \\ V_J &= V_0 + \sum_{j=0}^{J-1} W_j, \quad J > 0. \end{aligned}$$

In particular,

$$V_{J+1}^{(i)} = V_J^{(i)} + W_J^{(i)}, \quad i \in \{1, 2, 3\}, \quad J \in \mathbb{Z}, \quad (3.43)$$

$$V_{J+1} = V_J + W_J \quad J \in \mathbb{Z}. \quad (3.44)$$

This may be interpreted as follows. The scale space V_J contains a P_J –filtered version of a vector field of class $l^2(\Omega)$. The lower the scale, the higher the intensity of filtering. By adding R_J –details contained in the space W_J the scale space V_{J+1} is created, which consists of filtered versions at resolution $J+1$. However, it should be remarked that the sum in (3.43) is, in general, neither direct nor orthogonal.

3.2.3 Examples of Scaling Functions and Wavelets

In this section some generators and their corresponding scale discrete scaling functions and wavelets are presented and graphically illustrated. We distinguish between bandlimited and non-bandlimited wavelets.

Bandlimited Wavelets

From the various possibilities of bandlimited wavelets (see, for example, [20]) we present here only two of them, the Shannon wavelets and the Cubic Polynomial (CP) wavelets, because they will be the preferred kernel functions in our applications.

Shannon Wavelet The family of generating symbols of the Shannon scaling function is given by

$$(\varphi_J^{(i)})^\wedge(n) = \begin{cases} 1 & n < 2^J, \\ 0 & \text{else,} \end{cases} \quad n \in \mathbb{N}_{0_i}, \quad J \in \mathbb{Z},$$

for $i \in \{1, 2, 3\}$. Using the refinement equation for P –scale wavelets (3.38) we immediately get

$$(\tilde{\psi}_J^{(i)})^\wedge(n) = (\psi_J^{(i)})^\wedge(n) = \begin{cases} 1 & 2^J \leq n < 2^{J+1}, \\ 0 & \text{else,} \end{cases} \quad n \in \mathbb{N}_{0_i}, \quad J \in \mathbb{Z}.$$

It can be concluded from Equation (3.35) that the reconstruction via the Shannon wavelets is given by

$$\begin{aligned} P_J f &= \sum_{i=1}^3 \sum_{n=0}^{2^J-1} \sum_{k=1}^{2n+1} (f_{\mathcal{U}}^{(i)})^{\wedge}(n, k) u_{n,k}^{(i)}, \quad J \in \mathbb{Z}, \\ R_J f &= \sum_{i=1}^3 \sum_{n=2^J}^{2^{J+1}-1} \sum_{k=1}^{2n+1} (f_{\mathcal{U}}^{(i)})^{\wedge}(n, k) u_{n,k}^{(i)} \quad J \in \mathbb{Z}. \end{aligned}$$

But these equations are just partial sums out of the Fourier expansion of f . This means that we have constructed an orthogonal multiresolution analysis, and the sums in (3.43) are orthogonal and direct in this case.

In Figure 3.1 the Shannon scaling function of different types and at different scales can be seen.

CP-Wavelet Shannon scaling functions and wavelets establish an orthogonal multiresolution analysis, i.e. on the one hand they show advantageous behavior in the Fourier domain but on the other hand they are highly oscillating in the space domain (see Figure 3.1) which is a great disadvantage for local decomposition and reconstruction. These oscillations can be reduced by modifying the symbols $\{(\varphi_J)^{\wedge}(n)\}$. The step at $n = 2^J$ in the frequency domain has to be smoothed to reduce the oscillations in the space domain. A good modification is the *CP-generating symbol*, defined by

$$(\varphi_J^{(i)})^{\wedge}(n) = \begin{cases} \left(1 - \frac{n}{2^J}\right)^2 \left(1 + \frac{n}{2^J}\right) & n < 2^J, \\ 0 & \text{else,} \end{cases} \quad n \in \mathbb{N}_{0_i}, \quad J \in \mathbb{Z}.$$

for $i \in \{1, 2, 3\}$. The corresponding P -scale wavelet generators are, for $n \in \mathbb{N}_{0_i}$, given by

$$\begin{aligned} (\tilde{\psi}_J^{(i)})^{\wedge}(n) &= (\psi_J^{(i)})^{\wedge}(n) = \\ &= \begin{cases} \left(\left(\left(1 - \frac{n}{2^{J+1}}\right)^2 \left(1 + \frac{n}{2^J}\right) \right)^2 - \left(\left(1 - \frac{n}{2^J}\right)^2 \left(1 + \frac{n}{2^{J-1}}\right) \right)^2 \right)^{1/2} & n < 2^J \\ \left(\left(1 - \frac{x}{2^{J+1}}\right)^2 \left(1 + \frac{n}{2^J}\right) \right)^{1/2} & 2^J \leq n < 2^{J+1} \\ 0 & \text{else} \end{cases} \end{aligned}$$

Naturally, the orthogonality of the scale spaces in (3.43) is lost.

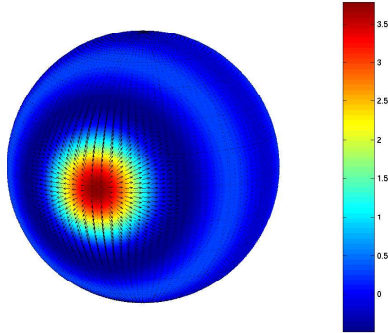
Figure 3.2 shows the cubic polynomial (CP) scaling function of different types and at different scales.

Non-Bandlimited Wavelets

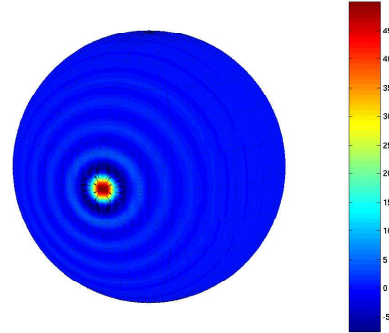
In the non-bandlimited case we have a global support of the generating symbol, i.e.

$$(\varphi_J^{(i)})^{\wedge}(n) \neq 0, \quad \text{for all } n \in \mathbb{N}_{0_i}.$$

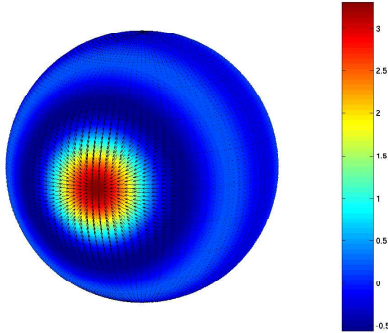
We will again only give some examples of the vast amount of non-bandlimited wavelets. For more examples the interested reader is referred to [20].



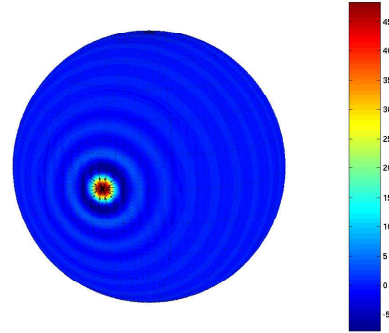
(a) Type 1 scaling function $\varphi_J^{(1)}$ at scale $J = 3$



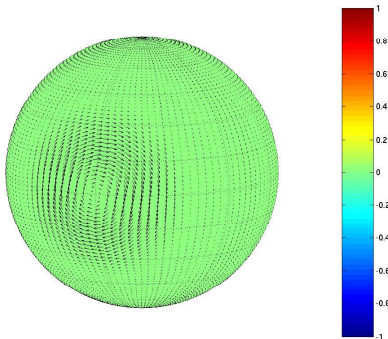
(b) Type 1 scaling function $\varphi_J^{(1)}$ at scale $J = 5$



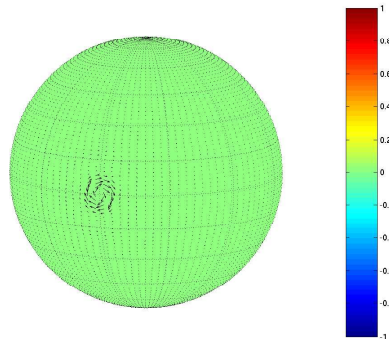
(c) Type 2 scaling function $\varphi_J^{(2)}$ at scale $J = 3$



(d) Type 2 scaling function $\varphi_J^{(2)}$ at scale $J = 5$



(e) Type 3 scaling function $\varphi_J^{(3)}$ at scale $J = 3$



(f) Type 3 scaling function $\varphi_J^{(3)}$ at scale $J = 5$

Figure 3.1: Shannon vector scaling function $\varphi_J^{(i)}$ of different types and at different scales. Colors indicate the radial component and arrows the tangential direction.

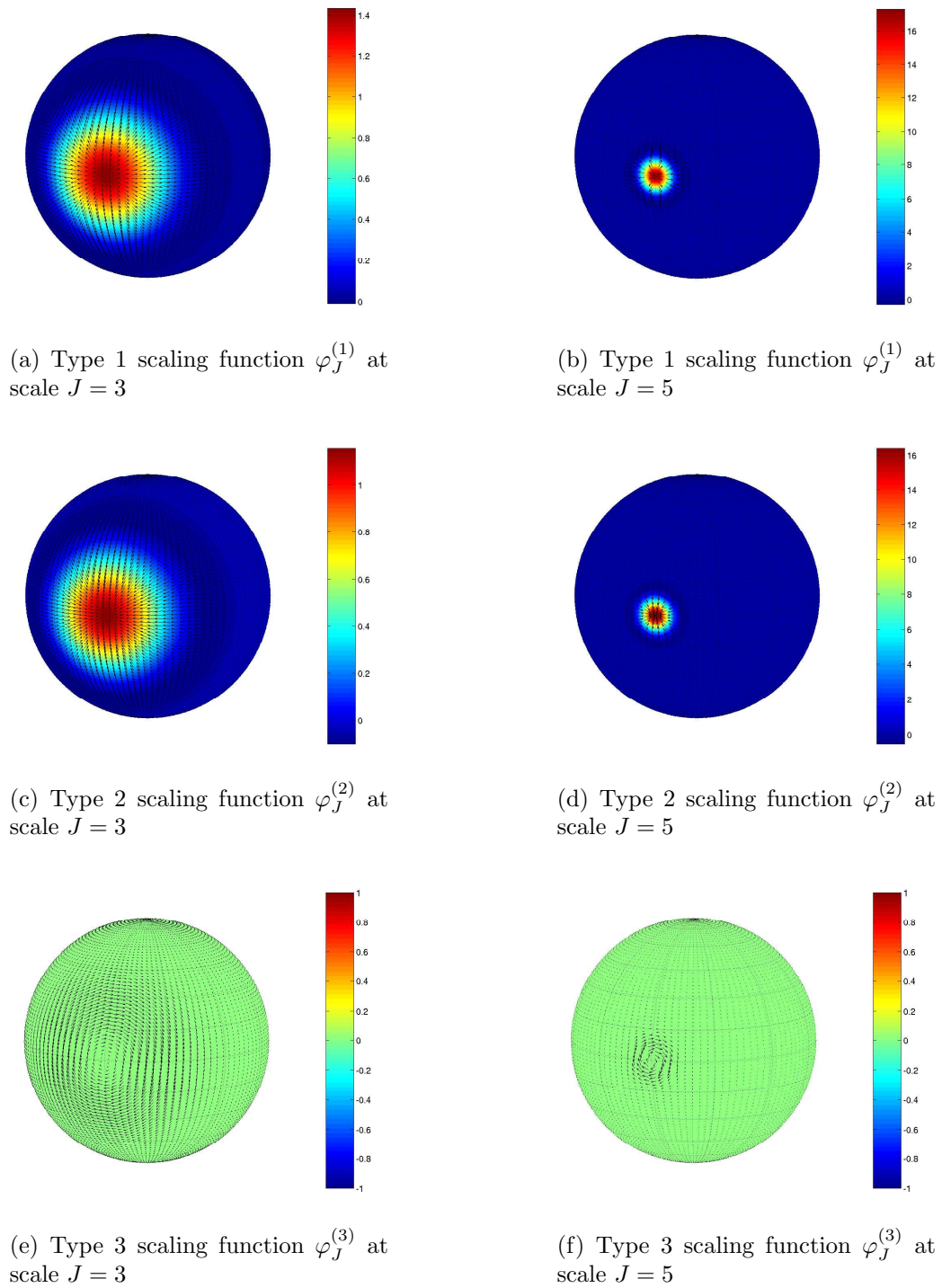


Figure 3.2: Cubic polynomial vector scaling function $\varphi_J^{(i)}$ of different types and at different scales. Colors indicate the radial component and arrows the tangential direction.

Exponential Wavelets The generator of this scaling function is of the form

$$(\varphi_0^{(i)})^\wedge(n) = \exp(-h(n)), \quad n \in \mathbb{N}_{0_i}$$

for $i \in \{1, 2, 3\}$, where the function $h : [0, \infty) \rightarrow \mathbb{R}$ has to satisfy

1. $h(0) = 0$, $h(x) > 0$ for $x > 0$,
2. $h(x)$ is strict monotonically increasing,
3. $\sum_{n=0}^{\infty} \frac{2n+1}{4\pi} \exp(-2h(n)) < \infty$.

Two special cases for this type of scaling functions are well known. The first example is the *Abel-Poisson scaling function* with $h(x) = Rx$ with some $R > 0$. The second one is the *Gauss-Weierstrass scaling function* where $h(x) = Rx(x+1)$ with some $R > 0$. For the Abel-Poisson scaling function we easily get

$$\begin{aligned} (\varphi_J^{(i)})^\wedge(n) &= \exp\left(-R\frac{n}{2^J}\right) \\ (\tilde{\psi}_J^{(i)})^\wedge(n) = (\psi_J^{(i)})^\wedge(n) &= \sqrt{\left(\exp\left(-R\frac{n}{2^{J+1}}\right)\right)^2 - \left(\exp\left(-R\frac{n}{2^J}\right)\right)^2}. \end{aligned}$$

for $i \in \{1, 2, 3\}$, $J \in \mathbb{Z}$ and $n \in \mathbb{N}_{0_i}$.

Rational Wavelets The generating symbol of the *Rational scaling function* is given by

$$(\varphi_J^{(i)})^\wedge(n) = (1 - 2^{-J}n)^s, \quad n \in \mathbb{N}_0, J \in \mathbb{Z}$$

for $i \in \{1, 2, 3\}$ and given $s > 1$.

At the end of this section it should be remarked that a pyramid scheme for the computation of the wavelet coefficients is available. This is a recursive method for the determination of the wavelet coefficients from level to level, starting from an initial approximation of a given field. For more information concerning pyramid schemes see [20] for the scalar case and [7] or [22] for the case of vector scaling functions and wavelets based on the system $\{y_{n,k}^{(i)}\}$ of vector spherical harmonics.

3.2.4 Computational Aspects

As we have already stated in Section 2.3 the canonical approach for multiscale approximation of vectorial problems are tensor scaling functions and wavelets. In the nomenclature of the previous sections these tensor kernels are of the form

$$\mathbf{k}(\xi, \eta) = \sum_{i=1}^3 \sum_{n=0_i}^{\infty} \sum_{k=1}^{2n+1} (\mathbf{k})^\wedge(n) u_{n,k}^{(i)}(\eta) \otimes u_{n,k}^{(i)}(\xi), \quad \xi, \eta \in \Omega. \quad (3.45)$$

Although this statement can be simplified by suitable vectorial addition theorems (see [50]) the main problem of the tensorial approach is the evaluation of the tensorial

terms in (3.45) and the evaluation of the tensor Legendre polynomials appearing in the addition theorems. To overcome these problems we have introduced a vectorial approach for the decomposition and approximation of vector fields in the previous section. But, up to this point, we have not shown that the problem of evaluating the scaling functions and wavelets has been solved. This will be done in this section, i.e. we show how vector kernel functions of the form

$$k^{(i)}(\xi, \eta) = \sum_{n=0_i}^{\infty} \sum_{k=1}^{2n+1} (k^{(i)})^{\wedge}(n) u_{n,k}^{(i)}(\xi) Y_{n,k}(\eta), \quad \xi, \eta \in \Omega, i \in \{1, 2, 3\}$$

can be evaluated in numerical applications.

At first, we give some rearrangements of the kernel functions. Using the relations of Lemma 1.17 and the scalar addition Theorem 1.6 we get, for $\xi, \eta \in \Omega$,

$$\begin{aligned} k^{(1)}(\xi, \eta) &= \sum_{n=0}^{\infty} \frac{2n+1}{4\pi} \frac{(k^{(1)})^{\wedge}(n)}{\sqrt{(n+1)(2n+1)}} \left((n+1) o_{\xi}^{(1)} P_n(\xi \cdot \eta) - o_{\xi}^{(2)} P_n(\xi \cdot \eta) \right), \\ k^{(2)}(\xi, \eta) &= \sum_{n=1}^{\infty} \frac{2n+1}{4\pi} \frac{(k^{(2)})^{\wedge}(n)}{\sqrt{n(2n+1)}} \left(n o_{\xi}^{(1)} P_n(\xi \cdot \eta) + o_{\xi}^{(2)} P_n(\xi \cdot \eta) \right), \\ k^{(3)}(\xi, \eta) &= \sum_{n=1}^{\infty} \frac{2n+1}{4\pi} \frac{(k^{(3)})^{\wedge}(n)}{\sqrt{n(n+1)}} o_{\xi}^{(3)} P_n(\xi \cdot \eta). \end{aligned}$$

Using the rules (1.12–1.14) for the application of the operators $o^{(i)}, i \in \{1, 2, 3\}$, to a zonal function we arrive at

$$\begin{aligned} k^{(1)}(\xi, \eta) &= \xi \sum_{n=0}^{\infty} \frac{2n+1}{4\pi} \sqrt{\frac{n+1}{2n+1}} (k^{(1)})^{\wedge}(n) P_n(\xi \cdot \eta) \\ &\quad - (\eta - (\xi \cdot \eta)\xi) \sum_{n=1}^{\infty} \frac{2n+1}{4\pi} \frac{(k^{(1)})^{\wedge}(n)}{\sqrt{(n+1)(2n+1)}} P'_n(\xi \cdot \eta), \end{aligned} \quad (3.46)$$

$$\begin{aligned} k^{(2)}(\xi, \eta) &= \xi \sum_{n=1}^{\infty} \frac{2n+1}{4\pi} \sqrt{\frac{n}{2n+1}} (k^{(2)})^{\wedge}(n) P_n(\xi \cdot \eta) \\ &\quad + (\eta - (\xi \cdot \eta)\xi) \sum_{n=1}^{\infty} \frac{2n+1}{4\pi} \frac{(k^{(2)})^{\wedge}(n)}{\sqrt{n(2n+1)}} P'_n(\xi \cdot \eta), \end{aligned} \quad (3.47)$$

$$k^{(3)}(\xi, \eta) = (\xi \wedge \eta) \sum_{n=1}^{\infty} \frac{2n+1}{4\pi} \frac{(k^{(3)})^{\wedge}(n)}{\sqrt{n(n+1)}} P'_n(\xi \cdot \eta) \quad (3.48)$$

for $\xi, \eta \in \Omega$. These formulas show that the kernel functions $k^{(1)}$ and $k^{(2)}$ are the sum of two terms, each of them consisting of a directional part times a scalar sum over weighted Legendre polynomials or derivatives of Legendre polynomials. The kernel function $k^{(3)}$ can just be expressed by a directional part times a scalar sum of derivatives of Legendre polynomials. Obviously, the main task is to calculate the weighted sums over Legendre polynomials $P_n(t), t = \xi \cdot \eta$, or their derivatives $P'_n(t)$.

Note that in the case of bandlimited kernels the sums are, of course, finite. In the non-bandlimited case if no explicit representation is available, (which is the matter in the majority of cases), the sums in (3.46), (3.47) and (3.48) need to be suitably truncated.

A naive method of summation would be to use well known recurrence relations for the functions $P_n(t)$ and $P'_n(t)$ to calculate the polynomials and their derivatives of different degrees and then to sum up. This method turns out to be extremely unstable for higher degrees, such that another technique should be used. We use a method due to [14] called *Clenshaw algorithm* which deals with the computation of sums of certain special functions. The method has been applied to sums as they appear in (3.46), (3.47) and (3.48) in the literature about vector kernel functions (see e.g. [7], [8] or [42]) and shown to run perfect. For more details about the application of the Clenshaw algorithm for the evaluation of vector kernel functions the reader is referred to [42].

3.3 A Spectral Scheme for the System $\{u_{n,k}^{(i)}\}$

In the following section we introduce the necessary nomenclature and the functionalanalytic framework for transforming homogeneous harmonic vector fields in spherical geometries. First of all, we have to discuss the operators which transform the fields and then we have to derive the corresponding singular systems in order to apply our multiscale approach for operator equations, respectively for regularization developed in Chapter 2.

Our starting point is the space of all homogeneous harmonic polynomials U defined outside a sphere Ω_R . Following a classical ansatz due to [28] these scalar fields can be characterized as follows. For any given boundary function $F \in \mathcal{L}^2(\Omega_R)$, the corresponding Fourier series in outer harmonics is locally uniformly convergent on each subset of Ω_R^{ext} with positive distance to the boundary (see e.g. [24]). Thus, the following definition is mathematically sound.

Definition 3.19

Let $\{Y_{n,k}^R\}_{\substack{n=0,1,\dots; \\ k=1,\dots,2n+1}}$ be a system of scalar spherical harmonics in $\mathcal{L}^2(\Omega_R)$ and let $\{H_{n,k}^{ext}(R; \cdot)\}_{\substack{n=0,1,\dots; \\ k=1,\dots,2n+1}}$ be the system of outer harmonics with respect to the sphere Ω_R introduced in Definition 1.7. Then the space $Pot(\Omega_R^{ext})$ is defined to be the space of all potentials $U : \overline{\Omega_R^{ext}} \rightarrow \mathbb{R}$ of the form

$$U(x) = \sum_{n=0}^{\infty} \sum_{k=1}^{2n+1} U_R^\wedge(n, k) H_{n,k}^{ext}(R; x), \quad x \in \overline{\Omega_R^{ext}},$$

where the coefficients $U_R^\wedge(n, k)$ are given by

$$U_R^\wedge(n, k) = \int_{\Omega_R} U(x) Y_{n,k}^R(x) d\omega_R(x),$$

for $n = 0, 1, \dots; k = 1, \dots, 2n + 1$, and the coefficients satisfy

$$\sum_{n=0}^{\infty} \sum_{k=1}^n |U_R^\wedge(n, k)|^2 < \infty.$$

Loosely spoken, the space $Pot(\Omega_R^{ext})$ consists of all harmonic functions in Ω_R^{ext} corresponding to square-integrable Dirichlet boundary conditions on Ω_R .

If we assume the vector field f to be source free in Ω_R^{ext} , i.e.

$$\begin{aligned} \nabla \wedge f &= 0, \\ \nabla \cdot f &= 0, \end{aligned}$$

in Ω_R^{ext} , then there exists a potential $U \in Pot(\Omega_R^{ext})$ such that $f = -\nabla U$ in Ω_R^{ext} . The gradient field to the potential U of class $Pot(\Omega_R^{ext})$ can easily be calculated by using the decomposition of the gradient in terms of a normal and a tangential part (see Equation (1.2)). Applying the definition of the $o^{(i)}$ -operators we obtain for $U \in Pot(\Omega_R^{ext})$

$$\begin{aligned} f(x) &= (-\nabla U)(x) \\ &= \sum_{n=0}^{\infty} \sum_{k=1}^{2n+1} U_R^\wedge(n, k) \left(\frac{R}{|x|} \right)^n \left(\frac{n+1}{|x|^2} o^{(1)} Y_{n,k} \left(\frac{x}{|x|} \right) - \frac{1}{|x|^2} o^{(2)} Y_{n,k} \left(\frac{x}{|x|} \right) \right), \\ &= \sum_{n=0}^{\infty} \sum_{k=1}^{2n+1} U_R^\wedge(n, k) \left(\frac{R}{|x|} \right)^n \frac{\sqrt{(n+1)(2n+1)}}{|x|} u_{n,k}^{(1),R}(x), \end{aligned}$$

for all $x \in \overline{\Omega_R^{ext}}$. Especially, for $x \in \Omega_R$, we arrive at

$$f(x) = \sum_{n=0}^{\infty} \sum_{k=1}^{2n+1} U_R^\wedge(n, k) \frac{\sqrt{(n+1)(2n+1)}}{R} u_{n,k}^{(1),R}(x).$$

In order to map a potential U , restricted to a sphere Ω_{R_1} to a second sphere Ω_{R_2} we have to apply the well known Abel-Poisson operator. The operator is a pseudo-differential operator which is defined via its symbol according to [19].

Definition 3.20

Let the operator $\Lambda_{AP} : \mathcal{L}^2(\Omega_{R_1}) \rightarrow C^{(\infty)}(\Omega_{R_2})$ be given via

$$(\Lambda_{AP} F)(x) = \int_{\Omega_{R_1}} K_{\Lambda_{AP}}(x, y) F(y) d\omega_{R_1}(y), \quad F \in \mathcal{L}^2(\Omega_{R_1}), \quad x \in \Omega_{R_2},$$

where the scalar kernel function $K_{\Lambda_{AP}}$ is defined to be

$$K_{\Lambda_{AP}}(x, y) = \sum_{n=0}^{\infty} \sum_{k=1}^{2n+1} (\Lambda_{AP})^\wedge(n) Y_{n,k}^{R_2}(x) Y_{n,k}^{R_1}(y), \quad x \in \Omega_{R_2}, \quad y \in \Omega_{R_1},$$

and the symbol $\{(\Lambda_{AP}(n))\}_{n=0,1,\dots}$ is given by

$$(\Lambda_{AP})(n) = \left(\frac{R_2}{R_1}\right)^n, \quad n = 0, 1, \dots$$

This transformation of a harmonic function from one sphere to another can equivalently be extended to the gradient of the potential, for which we have to introduce a tensorial analogue of the Abel-Poisson operator.

Definition 3.21

Let the operator $\mathbf{\Lambda}_{AP} : l^2(\Omega_{R_1}) \rightarrow c^{(\infty)}(\Omega_{R_2})$ be given via

$$(\mathbf{\Lambda}_{AP}f)(x) = \int_{\Omega_{R_1}} \mathbf{k}_{\mathbf{\Lambda}_{AP}}(x, y) f(y) d\omega_{R_1}(y), \quad f \in l^2(\Omega_{R_1}), \quad x \in \Omega_{R_2},$$

where the tensorial kernel function $\mathbf{k}_{\mathbf{\Lambda}_{AP}}$ is defined to be

$$\mathbf{k}_{\mathbf{\Lambda}_{AP}}(x, y) = \sum_{n=0}^{\infty} \sum_{k=1}^{2n+1} (\mathbf{\Lambda}_{AP})^{\wedge}(n) u_{n,k}^{(1),R_2}(x) \otimes u_{n,k}^{(1),R_1}(y), \quad x \in \Omega_{R_2}, \quad y \in \Omega_{R_1},$$

and the symbol $\{(\mathbf{\Lambda}_{AP}(n))\}_{n=0,1,\dots}$ is given by

$$(\mathbf{\Lambda}_{AP})(n) = \left(\frac{R_2}{R_1}\right)^{n+1}, \quad n = 0, 1, \dots$$

If the scalar field U is of class $Pot(\Omega_R^{ext})$ the application of the Abel-Poisson operator Λ_{AP} to $U|_{\Omega_{R_1}}$, respectively of the tensorial Abel-Poisson operator $\mathbf{\Lambda}_{AP}$ to $f|_{\Omega_{R_1}} = (-\nabla U)|_{\Omega_{R_1}}$, makes physically only sense if $R_1, R_2 \geq R$, because otherwise the sphere Ω_{R_2} lies in Ω_R^{int} , i.e. in regions, where sources might be present.

For R_1 and R_2 related as above we can summarize our results in the spectral scheme given in Table 3.2. Similar schemes, in geodesy called Meissl schemes, have already been developed for the system of vector spherical harmonics $\{y_{n,k}^{(i)}\}$ in [50].

This spectral scheme and the considerations above give us the possibility to apply the multiscale methods for operator equations presented in Chapter 2, respectively, for regularization in the inverse case presented in Section 2.4. Formally, all the transformations under consideration are of the form

$$\Lambda h = k, \quad h \in \mathfrak{h}, \quad k \in \mathfrak{k}$$

where $\Lambda : \mathfrak{h} \rightarrow \mathfrak{k}$ is a compact, linear scalar, respectively tensor-operator and \mathfrak{h} and \mathfrak{k} are separable Hilbert spaces of (scalar or vector) functions. Table 3.3 summarizes the possible configurations for Λ , \mathfrak{h} and \mathfrak{k} . $\{\sigma_n, h_n, k_n\}$ symbolizes the singular system of the respective operator Λ in accordance to the nomenclature of Chapter 2.

$$\begin{array}{ccc}
\Omega_{R_1} \begin{array}{|c|} \hline U|_{\Omega_{R_1}} \\ \hline \{Y_{n,k}^{R_1}\} \\ \hline \end{array} & \xrightarrow{\frac{(2n+1)(n+1)}{R_1}} & \begin{array}{|c|} \hline (-\nabla U)|_{\Omega_{R_1}} \\ \hline \{u_{n,k}^{(1),R_1}\} \\ \hline \end{array} \\
\left(\frac{R_1}{R_2}\right)^n \downarrow & & \downarrow \left(\frac{R_1}{R_2}\right)^{n+1} \\
\Omega_{R_2} \begin{array}{|c|} \hline U|_{\Omega_{R_2}} \\ \hline \{Y_{n,k}^{R_2}\} \\ \hline \end{array} & \xrightarrow{\frac{(2n+1)(n+1)}{R_2}} & \begin{array}{|c|} \hline (-\nabla U)|_{\Omega_{R_2}} \\ \hline \{u_{n,k}^{(1),R_2}\} \\ \hline \end{array}
\end{array}$$

Table 3.2: Spectral scheme for the transformation of potentials of class $Pot(\Omega_R^{ext})$. Observe that a physically meaningful transformation is only given if $R_1, R_2 > R$.

$h \in \mathfrak{h}$	$k \in \mathfrak{k}$	Λ	\mathfrak{h}	\mathfrak{k}	$\{h_n, k_n, \sigma_n\}$
U	$-\nabla U$	$(-\nabla) _{Pot(\Omega_R^{ext})}$	$\mathcal{L}^2(\Omega_{R_1})$	$l_{\mathcal{U}}^{2,(1)}(\Omega_{R_1})$	$\left\{Y_{n,k}^{R_1}, u_{n,k}^{(1),R_1}, \frac{(n+1)(2n+1)}{R_1}\right\}$
U	U	Λ_{AP}	$\mathcal{L}^2(\Omega_{R_1})$	$\mathcal{L}^2(\Omega_{R_2})$	$\left\{Y_{n,k}^{R_1}, Y_{n,k}^{R_2}, \left(\frac{R_1}{R_2}\right)^n\right\}$
$-\nabla U$	$-\nabla U$	$\Lambda_{\mathbf{AP}}$	$l_{\mathcal{U}}^{2,(1)}(\Omega_{R_1})$	$l_{\mathcal{U}}^{2,(1)}(\Omega_{R_2})$	$\left\{u_{n,k}^{(1),R_1}, u_{n,k}^{(1),R_2}, \left(\frac{R_1}{R_2}\right)^{n+1}\right\}$

Table 3.3: Functional-analytic framework of the transformations presented in Table 3.2. The nomenclature is chosen in accordance to Chapter 2.

Equivalently to Definition 3.19 we can introduce the space of scalar potentials in the inner space of a sphere Ω_R , if we observe that for any given boundary function $F \in \mathcal{L}^2(\Omega_R)$, the corresponding Fourier series in inner harmonics is locally uniformly convergent on each subset of Ω_R^{int} with positive distance to the boundary (see e.g. [24]).

Definition 3.22

Let $\{Y_{n,k}^R\}_{\substack{n=0,1,\dots; \\ k=1,\dots,2n+1}}$ be a system of scalar spherical harmonics in $\mathcal{L}^2(\Omega_R)$ and let $\{H_{n,k}^{int}(R; \cdot)\}_{\substack{n=0,1,\dots; \\ k=1,\dots,2n+1}}$ be the system of inner harmonics with respect to Ω_R introduced in Definition 1.7. Then the space $Pot(\Omega_R^{int})$ is defined to be the space of all potentials $U : \overline{\Omega_R^{int}} \rightarrow \mathbb{R}$ of the form

$$U(x) = \sum_{n=0}^{\infty} \sum_{k=1}^{2n+1} U_R^\wedge(n, k) H_{n,k}^{int}(R; x), \quad x \in \overline{\Omega_R^{int}},$$

where the coefficients $U_R^\wedge(n, k)$ are given by

$$U_R^\wedge(n, k) = \int_{\Omega_R} U(x) Y_{n,k}^R(x) d\omega_R(x),$$

for $n = 0, 1, \dots; k = 1, \dots, 2n + 1$, and the coefficients satisfy

$$\sum_{n=0}^{\infty} \sum_{k=1}^n |U_R^\wedge(n, k)|^2 < \infty.$$

If we assume the vector field f to be source free in Ω_R^{int} , i.e. $\nabla \wedge f = 0, \nabla \cdot f = 0$ in Ω_R^{int} , then there exists a potential $U \in Pot(\Omega_R^{int})$ such that $f = \nabla U$ in Ω_R^{int} . The gradient field of the potential U of class $Pot(\Omega_R^{int})$ can be calculated, as before for the exterior case, using the decomposition of the gradient in terms of a normal and a tangential part (see Equation (1.2)). According to the definition of the $o^{(i)}$ -operators we obtain for $U \in Pot(\Omega_R^{int})$

$$\begin{aligned} f(x) &= (\nabla U)(x) \\ &= \sum_{n=0}^{\infty} \sum_{k=1}^{2n+1} U_R^\wedge(n, k) \left(\frac{|x|}{R} \right)^{n+1} \left(\frac{n}{|x|^2} o^{(1)} Y_{n,k} \left(\frac{x}{|x|} \right) + \frac{1}{|x|^2} o^{(2)} Y_{n,k} \left(\frac{x}{|x|} \right) \right), \\ &= \sum_{n=1}^{\infty} \sum_{k=1}^{2n+1} U_R^\wedge(n, k) \left(\frac{|x|}{R} \right)^{n+1} \frac{\sqrt{n(2n+1)}}{|x|} u_{n,k}^{(2),R}(x), \quad x \in \overline{\Omega_R^{int}}. \end{aligned}$$

Restricting f to Ω_R we especially get

$$f|_{\Omega_R} = \sum_{n=1}^{\infty} \sum_{k=1}^{2n+1} U_R^\wedge(n, k) \frac{\sqrt{n(2n+1)}}{R} u_{n,k}^{(2),R}$$

pointwise and in the sense of the $l^2(\Omega_R)$ -norm.

The previously defined scalar as well as the tensorial Abel-Poisson operator can be applied to a function of class $Pot(\Omega_R^{int})$ as well but it should be noted that the application of these operators physically only makes sense if $R_1 R_2 \leq R$ because otherwise the sphere Ω_{R_2} lies in regions where sources are present.

For R_1, R_2 fulfilling the property above we can summarize our results in the spectral scheme in Table 3.4 equivalently to the scheme given in Table 3.2.

As for the exterior case, we are now able to apply the multiscale methods for operator equations and the multiscale technique for regularization presented in Chapter 2. All the transformations can be written in operator notation as

$$\Lambda h = k, \quad h \in \mathfrak{h}, \quad k \in \mathfrak{k}$$

where $\Lambda : \mathfrak{h} \rightarrow \mathfrak{k}$ is a compact, linear scalar respectively tensor-operator and \mathfrak{h} and \mathfrak{k} are separable Hilbert spaces of (scalar or vector) functions. Table 3.5 gives the possible configurations for Λ , \mathfrak{h} and \mathfrak{k} for the interior case.

$$\begin{array}{ccc}
 \Omega_{R_1} \begin{array}{|c|} \hline U|_{\Omega_{R_1}} \\ \hline \{Y_{n,k}^{R_1}\} \\ \hline \end{array} & \xrightarrow{\frac{n(2n+1)}{R_1}} & \begin{array}{|c|} \hline (\nabla U)|_{\Omega_{R_1}} \\ \hline \{u_{n,k}^{(2),R_1}\} \\ \hline \end{array} \\
 \left(\frac{R_1}{R_2}\right)^n \downarrow & & \downarrow \left(\frac{R_1}{R_2}\right)^{n+1} \\
 \Omega_{R_2} \begin{array}{|c|} \hline U|_{\Omega_{R_2}} \\ \hline \{Y_{n,k}^{R_2}\} \\ \hline \end{array} & \xrightarrow{\frac{n(2n+1)}{R_2}} & \begin{array}{|c|} \hline (\nabla U)|_{\Omega_{R_2}} \\ \hline \{u_{n,k}^{(2),R_2}\} \\ \hline \end{array}
 \end{array}$$

Table 3.4: Spectral scheme for the transformation of potentials of class $Pot(\Omega_R^{int})$. Observe that a physically meaningful transformation is only given if $R_1, R_2 < R$.

$h \in \mathfrak{h}$	$k \in \mathfrak{k}$	Λ	\mathfrak{h}	\mathfrak{k}	$\{h_n, k_n, \sigma_n\}$
U	∇U	$\nabla _{Pot(\Omega_R^{int})}$	$\mathcal{L}^2(\Omega_{R_1})$	$l_{\mathcal{U}}^{2,(2)}(\Omega_{R_1})$	$\left\{Y_{n,k}^{R_1}, u_{n,k}^{(2),R_1}, \frac{(n+1)(2n+1)}{R_1}\right\}$
U	U	Λ_{AP}	$\mathcal{L}^2(\Omega_{R_1})$	$\mathcal{L}^2(\Omega_{R_2})$	$\left\{Y_{n,k}^{R_1}, Y_{n,k}^{R_2}, \left(\frac{R_1}{R_2}\right)^n\right\}$
∇U	∇U	$\mathbf{\Lambda}_{AP}$	$l_{\mathcal{U}}^{2,(2)}(\Omega_{R_1})$	$l_{\mathcal{U}}^{2,(2)}(\Omega_{R_2})$	$\left\{u_{n,k}^{(2),R_1}, u_{n,k}^{(2),R_2}, \left(\frac{R_1}{R_2}\right)^{n+1}\right\}$

Table 3.5: Functional-analytic framework of the transformations presented in Table 3.4. The nomenclature is chosen in accordance to Chapter 2.

3.3.1 An Application to a Multi-Satellite Constellation

The following section is concerned with a short overview of the advantages for magnetic field modelling of a multi-satellite constellation. We will show how a constellation of different satellites of CHAMP type on spherical orbits at different heights can be used to extract the sources lying between the orbital spheres. To simplify matters we will just have a look at a configuration of two satellites flying at two different altitudes R_1 and R_2 with $R_2 > R_1$.

Such a constellation may be given by a proposed satellite mission called SWARM, which consists of four satellites of the CHAMP type. In [40] the suggested constellation are two satellites at a height of $R_1 = 450 \text{ km}$ and two satellites at an altitude of $R_2 = 550 \text{ km}$. Two satellites at each altitude are needed to get a good method for correcting and preprocessing the magnetic field data on each sphere. For more information concerning the SWARM mission the reader is referred to [40] and to Section 4.4.5 later on in this thesis.

The method of transforming the respective fields from one sphere to another developed in the previous section enables us to extract the part of the magnetic field which is due to sources lying between the two spheres Ω_{R_1} and Ω_{R_2} . We will briefly present how this concept can be established. The functions representing magnetic field data on each sphere are denoted by $f_1 \in l^2(\Omega_{R_1})$ and $f_2 \in l^2(\Omega_{R_2})$.

1. Use the multiscale method developed in Section 3.2 to get that part of the magnetic field on each sphere which is induced by sources inside the orbital sphere. This results in fields $P_J^{(1)} f_1 \in l_{\mathcal{U}}^{2,(1)}(\Omega_{R_1})$ and $P_J^{(1)} f_2 \in l_{\mathcal{U}}^{2,(1)}(\Omega_{R_2})$ given by

$$\begin{aligned} P_J^{(1)} f_1 &= \varphi_J^{(1)} \star \varphi_J^{(1)} * f_1, \\ P_J^{(1)} f_2 &= \varphi_J^{(1)} \star \varphi_J^{(1)} * f_2, \end{aligned}$$

with $J \in \mathbb{Z}$ chosen suitably large. The scaling function $\varphi_J^{(i)}$ is here the vector scaling function defined in Definition 2.2 based on the system $\{u_{n,k}^{(i)}\}$ of vector spherical harmonics and the operators $P_J^{(1)}$, $J \in \mathbb{Z}$, are the projection operators defined in Definition 3.18.

2. Use the multiscale method based on vector scaling functions and wavelets for tensor-operator equations developed in Chapter 2 and the singular system for the tensorial Abel-Poisson operator to transform the field $P_J^{(1)} f_1$ from the sphere Ω_{R_1} to Ω_{R_2} . Since the corresponding singular value $\sigma_n = (R_1/R_2)^{n+1}$, $n \in \mathbb{N}_0$, is such that the problem is well-posed, no regularization has to be used and the multiscale method for tensor-operator equations developed in Section 2.2 can simply be applied. This results into a field $T_{J'} P_J^{(1)} f_1 \in l_{\mathcal{U}}^{2,(1)}(\Omega_{R_2})$ given by

$$T_{J'} P_J^{(1)} f_1 = {}^r \varphi_{J'} \star ({}^d \varphi_{J'} *_{l^2(\Omega_{R_1})} P_J^{(1)} f_1), \quad J \in \mathbb{Z},$$

where in this case the decomposition and the reconstruction vector scaling functions are given by

$$\begin{aligned} {}^d \varphi_{J'}(x, y) &= \sum_{n=0}^{\infty} \sum_{k=1}^{2n+1} (\varphi_{J'})^{\wedge}(n) u_{n,k}^{(1),R_1}(x) Y_{n,k}^{R_1}(y), \quad x \in \Omega_{R_1}, y \in \Omega_{R_1}, \\ {}^r \varphi_{J'}(x, y) &= \sum_{n=0}^{\infty} \sum_{k=1}^{2n+1} (\varphi_{J'})^{\wedge}(n) u_{n,k}^{(1),R_2}(x) Y_{n,k}^{R_1}(y), \quad x \in \Omega_{R_2}, y \in \Omega_{R_1}, \end{aligned}$$

and the symbols $\{(\varphi_{J'})^{\wedge}(n)\}_{n \in \mathbb{N}_0}$ satisfy

1. $\lim_{J' \rightarrow \infty} ((\varphi_{J'})^{\wedge}(n))^2 = \sigma_n = \left(\frac{R_1}{R_2}\right)^{n+1}, \quad n \in \mathbb{N}_0,$
2. $((\varphi_{J'-1})^{\wedge}(n))^2 \leq ((\varphi_{J'})^{\wedge}(n))^2, \quad J' \in \mathbb{Z}, n \in \mathbb{N}_0,$
3. $\lim_{J' \rightarrow -\infty} ((\varphi_{J'})^{\wedge}(n))^2 = 0, \quad n \in \mathbb{N}_0.$

As before $J' \in \mathbb{Z}$ should be chosen large enough (comparable to $J \in \mathbb{Z}$ from the first step). This upward continuation of the vector field $P_J^{(1)} f_1$ from the sphere Ω_{R_1} to the sphere Ω_{R_2} is based on the assumption that the region $\Omega_{R_1}^{ext}$ is source free. But this means that the sources lying between the two spheres Ω_{R_1} and Ω_{R_2} has no influence on the transformed field $T_{J'} P_J^{(1)} f_1 \in l_{\mathcal{U}}^{2,(1)}(\Omega_{R_2})$. The difference of the two fields $P_J^{(1)} f_2$ and $T_{J'} P_J^{(1)} f_1$ delivers us this special magnetic field which is induced by sources lying in the spherical shell $\Omega_{(R_1, R_2)}$.

3. Calculate the difference of the two fields $P_J^{(1)} f_2$ and $T_{J'} P_J^{(1)} f_1$ in $l_{\mathcal{U}}^{2,(1)}(\Omega_{R_2})$

$$f_{J,J'} = P_J^{(1)} f_2 - T_{J'} P_J^{(1)} f_1, \quad J, J' \in \mathbb{Z}.$$

This field now contains the magnetic field which is induced by sources lying in the spherical shell $\Omega_{(R_1, R_2)}$. Since, as for example in the case of the proposed SWARM constellation, this spherical shell is totally lying outside the spherical Earth and, hence, the sources which induce the magnetic field $f_{J,J'}$ are due to current systems in the shell. A multiscale approach for reconstructing an equivalent spherical current system from the magnetic field data will be presented in the following chapter and can be applied at this point to calculate an equivalent current system corresponding to the magnetic field data.

The above considerations show us that a constellation of two satellites at two different altitudes will improve the knowledge of the ionosphere. It will offer us the possibility to reconstruct the currents which are lying in between the two orbital spheres. Together with a possible reconstruction of the F region ionospheric current system which is present at a height of 110 km (the reconstruction of this current system from SWARM magnetic field data is simulated in Section 4.4.5), this technique yields a great improvement of the knowledge of the ionosphere in contrast to a single satellite constellation like the CHAMP mission. From the mathematical point of view a constellation of several satellites at different altitudes would be even better in order to resolve the resulting fields and by this the source fields of different layers of the ionosphere. But such a constellation of single satellites at different heights is not so advantageous for data preprocessing and correction. For more details about the advantages of the constellation of the proposed SWARM mission the reader is referred to [40].

3.4 An Application to CHAMP Magnetic Field Data

In this section we apply the previously presented multiscale approach for separating given spherical vector fields with respect to their sources to a set of CHAMP vector magnetic FGM data. At the end of the section we show how the approach can be used to improve the derivation of a crustal geomagnetic field model.

The magnetic field data set we use has been made available by Dr. Stefan Maus from the GFZ Potsdam. The data were sampled between June 2001 and December 2001. Standard methods of preprocessing and data selection have been applied which follow common criteria for main and crustal field modelling and which have been executed at the GFZ Potsdam. These steps are explained in detail in Appendix A.

In contrast to past satellite missions like MAGSAT, the orbit of the CHAMP satellite is almost spherical and we assume the spherical approximation to be valid. Consequently, after subtracting the low frequency contributions, we suppose the altitude variations to be negligible and assume the data to be given on a mean altitude. Actually this assumption has been used by other authors concerned with handling CHAMP magnetic field data (see e.g. [11] and [46]).

In order to apply the multiscale technique of Section 3.2 we need to discretize the appearing integrals by means of an appropriate integration rule. In our opinion, the method proposed in [15] is advantageous since the regular equiangular longitude-latitude grid reflects the real situation of higher density of data at the poles. Furthermore, the spherical integration rule proposed in [15] can be chosen to be exact up to a certain degree and the corresponding integration weights are given in closed form. Consequently, the next step in our approach of separating CHAMP magnetic

field data with respect to their sources is to average the scattered data onto the integration knots of our integration rule. This gridding procedure is a very important and sensitive step. Several techniques for averaging given disturbed spherical data to regular grids have been discussed in the literature (see [2]) and have been used in magnetic field analysis (e.g. [46] and [51] for satellite data and [1] for terrestrial data). Commonly used methods can roughly be divided into two categories, the distance method which is, for example, used for CHAMP data in [46] and the distribution method which has been applied to MAGSAT data in [51]. We are of the opinion that a combination of both methods is arguably the best choice.

For a given point x on the regular grid we search for all points lying within a certain spherical distance around x . Classical distance methods would weight all data points in this vicinity of x with respect to their distance to x . In contrast, our method is at first based on a robust iterative M-estimation to detect outliers in the distribution of the data in this very vicinity of x . This procedure of outlier detection is described in detail in Appendix B.

After sorting out outliers we average the remaining data using the distance weight function

$$(0.5 + 0.5 \cos(\pi d/D))^p, \quad p = 1, 2, 3, 4, \quad (3.49)$$

where d is the spherical distance of the data point to x on mean orbit height and D is the previously chosen search radius for the vicinity of x . The parameter p gives the strength of the weighting. For large p , sample values lying near to the point x are weighted much stronger than measurements lying far away, while for small p , the influence of those measurements is increasing. For a dense coverage of data a large value of p should be used while if the data are given more or less scattered, a small value of p is the better choice. A graphical illustration of the weight function can be seen in Figure 3.3. This sort of weight functions has already been used successfully by other groups working with CHAMP data (see [46]).

If the satellite data are averaged to a regular integration grid, the method of multiscale separation can be applied to the magnetic field. First of all we have a look at the pure data set obtained after the averaging procedure (see Figure 3.4). It is clearly visible that there are still contributions in the data which are not among the crustal field of the Earth but are induced by current systems crossing the orbit or flowing outside the orbit. These effects are especially visible in the tangential components in polar regions.

Next, we apply our method of separating the given vector field with respect to its sources, i.e. we apply the multiscale approach presented in the previous section to separate the magnetic field on satellite's height into the poloidal internally induced part contained in $l_{\mathcal{U}}^{2,(1)}$, the poloidal externally generated part belonging to $l_{\mathcal{U}}^{2,(2)}$ and the toroidal part contained in $l_{\mathcal{U}}^{2,(3)}$. The poloidal part of the magnetic field which is generated from sources inside the orbital sphere and which has been filtered out of

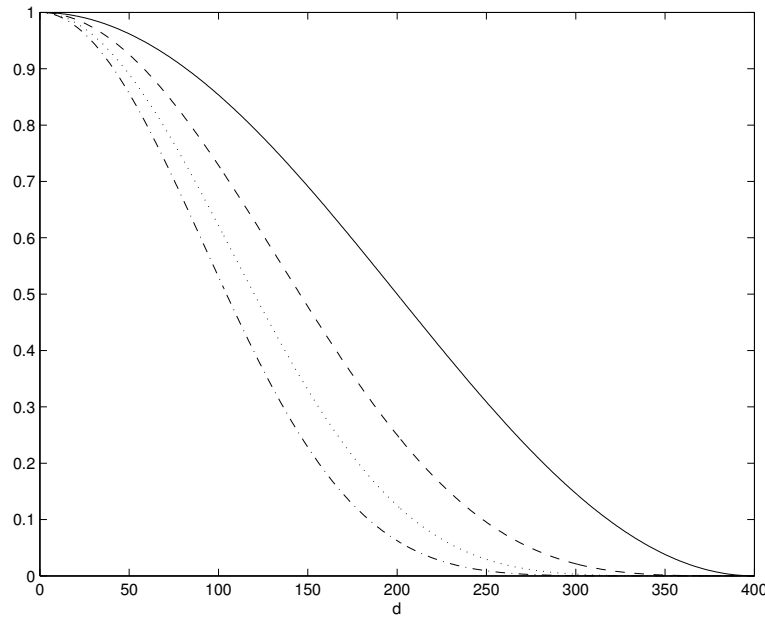


Figure 3.3: Distance weight function given in (3.49) for $p = 1$ (solid), $p = 2$ (dashed), $p = 3$ (dotted) and $p = 4$ (dash-dotted). The value of the search radius is $D = 400 \text{ km}$ in this case and d gives the spherical distance of the measurements to the point to be weighted on.

the CHAMP data set with a cubic polynomial vector scaling function at scale 5 can be found in Figure 3.5. The difference between the original data set and the wavelet approximation of the part resulting from inner sources can be seen in Figure 3.6. These contributions are containing the toroidal part of the magnetic field as well as the part which is induced by sources outside the satellite's orbit. It is obvious that they are not due to crustal field contributions. Even the structure of the source field which has induced these fields can be seen. In the radial component of the toroidal and the externally generated field (Figure 3.6(b)) a positive trend can be seen northward of the dipole equator while a negative trend is visible southwards of the equator. This field is the typical magnetic signature of a ring current outside the satellite's orbit which can be interpreted as that there are still contributions in the original data set coming from the magnetospheric ring current.

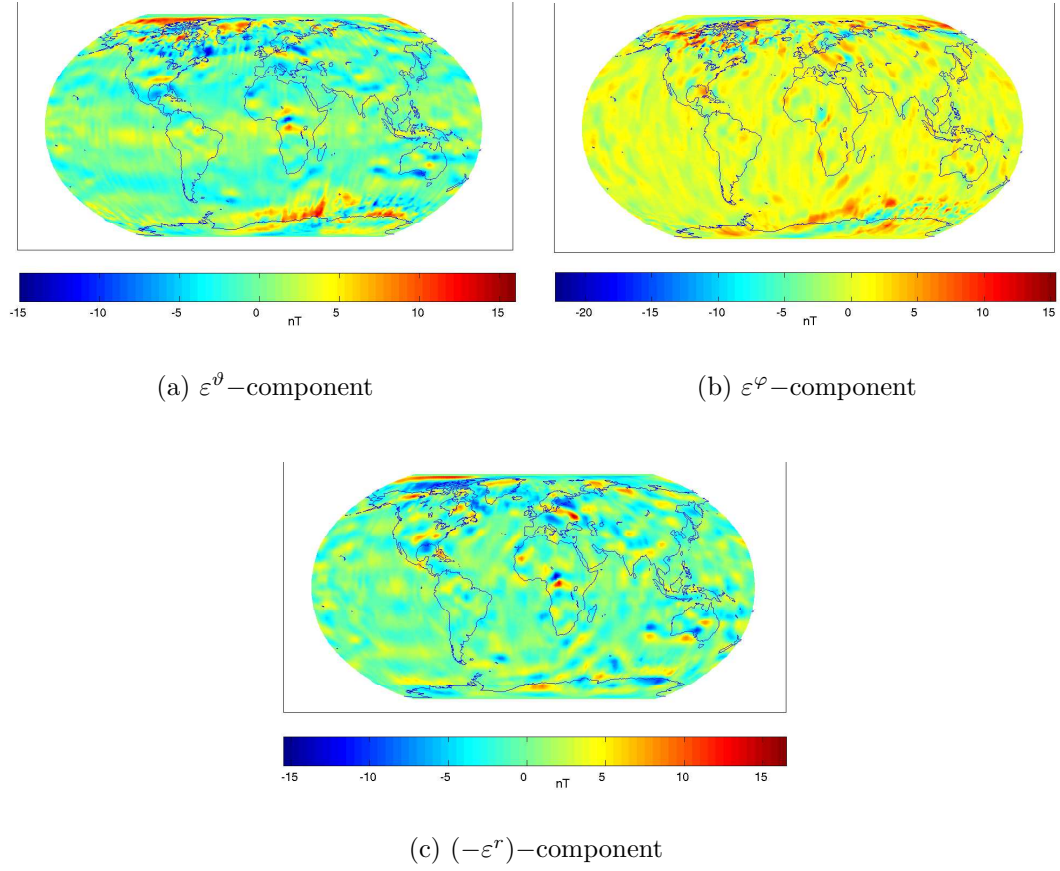


Figure 3.4: Original CHAMP data set averaged to a regular grid of 130×130 points.

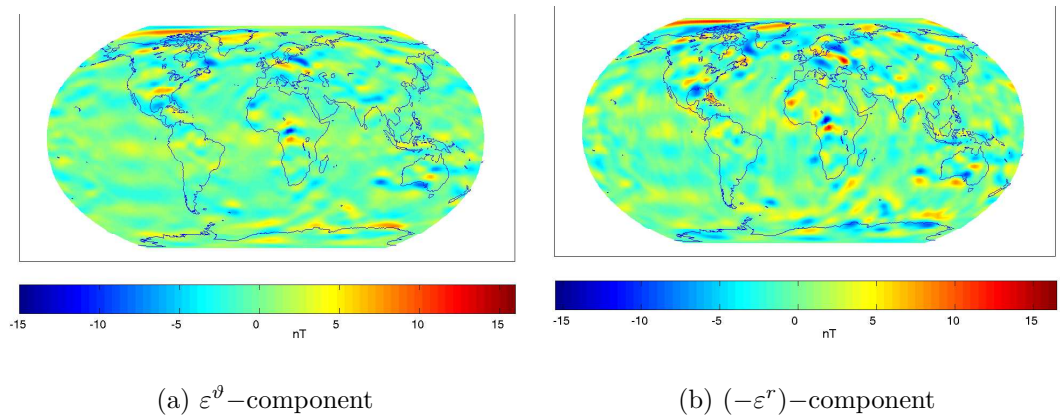


Figure 3.5: Magnetic field induced by sources lying inside the satellite's orbit. The field was obtained by convolution of the original data set given in Figure 3.4 with a cubic polynomial vector scaling function of type 1 at scale $J = 5$. It should be noted that it is also possible to reconstruct the ε^φ -component which is not plotted here for the sake of brevity.

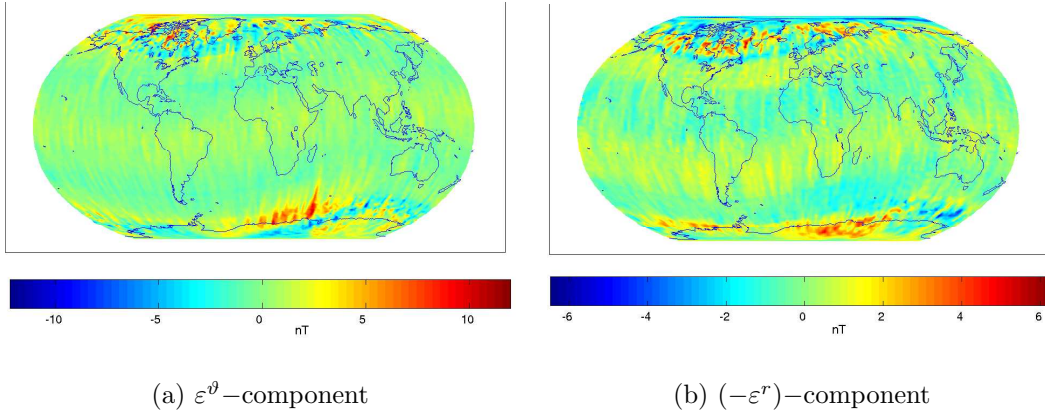


Figure 3.6: Toroidal and externally induced field of the CHAMP data set given in Figure 3.4. The field is the difference of the original data set and the magnetic field induced by sources lying inside the satellite's orbital sphere.

The separation of the magnetic field measured by CHAMP into the poloidal internally induced, the poloidal externally generated and the toroidal part can be used to improve main and crustal field modelling which are inner sources of the magnetic field corresponding to the satellite's orbit. This improvement will be demonstrated in the next section in the case of multiscale (i.e. local) crustal field modelling.

3.5 Improved Crustal Field Modelling

In this section we show, how the above developed separation of the magnetic field with respect to its sources and the application to CHAMP magnetic field data can be used to improve crustal field modelling.

The crustal magnetic field is that part of the Earth's magnetic field which is due to lithospheric magnetization. Appropriately low-flying satellites as the German geoscientific satellite CHAMP can measure and resolve these lithospheric contributions of the magnetic field. For modelling crustal field contributions from given satellite data we use a wavelet approach presented in [43]. It is essentially based on formulating the problem as an operator equation between two Hilbert spaces via certain integral equations and to use regularizing wavelets to get an inversion of the equation. The theory can easily be embedded in our general multiscale concept for regularizing of vectorial inverse problems presented in Section 2.4. At this point we just give the functionalanalytic framework in a comprehensive manner. Formally, all the integral equations under consideration are of the form

$$\Lambda h = k, \quad h \in \mathfrak{h}, \quad k \in \mathfrak{k},$$

where $\Lambda : \mathfrak{h} \rightarrow \mathfrak{k}$ is a compact operator and \mathfrak{h} and \mathfrak{k} are separable Hilbert spaces of (scalar or vector) functions. Elements of the Hilbert space \mathfrak{k} thereby correspond to the actual observables (i.e. the satellite measurements) and those in the Hilbert

space \mathfrak{h} are the quantities which are to be calculated from the former ones. Table 3.6 summarizes the possible configurations for Λ , \mathfrak{h} and \mathfrak{k} . $\{\sigma_n, h_n, k_n\}$ is the singular system of the operator Λ in accordance with the nomenclature of Chapter 2.

$h \in \mathfrak{h}$	$k \in \mathfrak{k}$	Λ	\mathfrak{h}	\mathfrak{k}	$\{h_n\}$	$\{k_n\}$	σ_n
U	$\partial_r U$	Λ_{Pot}	$\mathcal{L}^2(\Omega_{R_1})$	$\mathcal{L}^2(\Omega_{R_2})$	$Y_{n,k}^{R_1}$	$Y_{n,k}^{R_2}$	$\left(\frac{R_1}{R_2}\right)^n \frac{n+1}{R_2}$
$\partial_r U$	$\partial_r U$	Λ_{AP}	$\mathcal{L}^2(\Omega_{R_1})$	$\mathcal{L}^2(\Omega_{R_2})$	$Y_{n,k}^{R_1}$	$Y_{n,k}^{R_2}$	$\left(\frac{R_1}{R_2}\right)^n$
$\nabla^* U$	$\partial_r U$	λ_{∇^*}	$l_y^{2,(2)}(\Omega_{R_1})$	$\mathcal{L}^2(\Omega_{R_2})$	$y_{n,k}^{(2),R_1}$	$Y_{n,k}^{R_2}$	$\left(\frac{R_1}{R_2}\right)^n \frac{1}{R_2} \sqrt{\frac{n+1}{n}}$
U	$\nabla^* U$	λ_{Pot}	$\mathcal{L}^2(\Omega_{R_1})$	$l_y^{2,(2)}(\Omega_{R_2})$	$Y_{n,k}^{R_1}$	$y_{n,k}^{(2),R_2}$	$\left(\frac{R_1}{R_2}\right) \sqrt{n(n+1)}$
$\partial_r U$	$\nabla^* U$	λ_{∂_r}	$\mathcal{L}^2(\Omega_{R_1})$	$l_y^{2,(2)}(\Omega_{R_2})$	$Y_{n,k}^{R_1}$	$y_{n,k}^{(2),R_2}$	$\left(\frac{R_1}{R_2}\right) R_1 \sqrt{\frac{n}{n+1}}$

Table 3.6: Functionalanalytic framework of crustal field modelling. This table is due to [43].

The operators appearing in Table 3.6 can be described as follows. Λ_{Pot} is the operator connecting a harmonic function U on a sphere to the radial derivative of the same potential U on another sphere. Λ_{AP} is the Abel-Poisson operator connecting the restrictions to different spheres of a potential field U which has still been introduced in Definition 3.20. λ_{∇^*} denotes the operator connecting the surface gradient ∇^* of a certain potential function U to its radial derivative on another height. Finally, λ_{Pot} and λ_{∂_r} connect the potential field U respectively its radial derivative $\partial_r U$ at a certain height to its surface gradient at another height. For a mathematically correct definition of the above operators and the deduction of the corresponding singular systems the reader is referred to [43].

To show that the method of separating the magnetic field with respect to its sources is advantageous for crustal field modelling we regularize two different data sets. At first, we take the pure data set which has been made available by the GFZ Potsdam and which has already been described (see Figure 3.4). The data set is averaged to a regular equiangular longitude-latitude grid on mean orbit height and then a regularization by cubic polynomial regularizing scalar wavelets of the operator Λ_{AP} is applied to the radial projection of the magnetic field (geomagnetic Z-component, see Appendix A). Since we use scaling functions and wavelets which are spatially localizing trial functions to represent and to regularize the magnetic field this procedure of downward continuation can be applied locally. (For more information about local crustal field modelling see [43] or our results in [23] and [44].) Thus, we are able to regularize the crustal field only over arctic regions. This local reconstruction of the crustal field emphasizes the advantages of our method of separating the magnetic field with respect to its sources, since over the arctics the influence of outer sources

is stronger than in mid-latitude regions (see Section 3.4).

The regularization of the original data set is shown in Figure 3.7 where the $(-\varepsilon^r)$ -component of the lithospheric field at mean Earth's radius (6371.2 km) over the north pole is plotted. This reconstruction of the crustal field was obtained by using a CP regularization vector scaling function at scale $J = 6$.

In a second case we have taken the $(-\varepsilon^r)$ -component of the data set of Section 3.4 as our initial data set where the method of filtering out the externally induced and the toroidal magnetic field has previously been applied. This magnetic field corresponds to sources lying inside the satellite's orbital sphere (see Figure 3.5). The result of the regularization process can be seen in Figure 3.8. As before, the reconstruction of the crustal field was obtained by using a CP regularization vector scaling function at scale $J = 6$.

The difference of the two crustal field reconstructions is plotted in Figure 3.9. If the part of the field which is not coming from inner sources is not filtered out in advance, these parts of the measured magnetic field are treated as a crustal field contribution which vitiate and complicate crustal field determination and interpretation especially in polar regions.

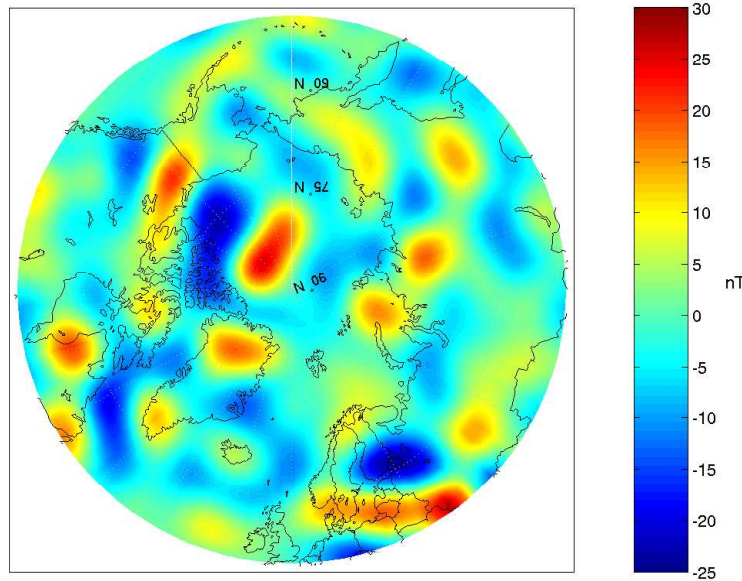


Figure 3.7: $(-\varepsilon^r)$ -component of the crustal field at mean Earth's surface (6371.2 km) over the north pole without applying the method of filtering out the externally induced and the toroidal magnetic field presented in the previous Sections. The result is obtained by multiscale regularization of the $(-\varepsilon^r)$ -component of the pure data magnetic field data set with a cubic polynomial regularizing scaling function at scale 6.

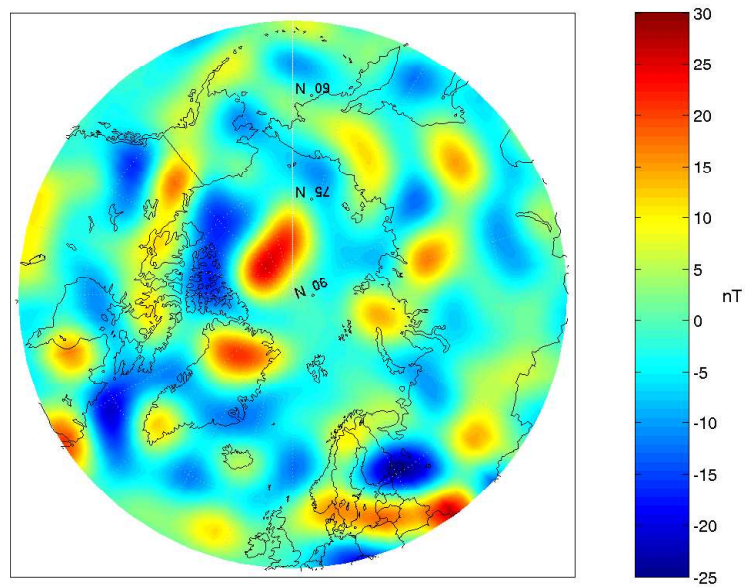


Figure 3.8: $(-\varepsilon^r)$ -component of the crustal field at mean Earth's surface (6371.2 km) over the north pole. The result is obtained by multiscale regularization of the $(-\varepsilon^r)$ -component of the magnetic field resulting from inner sources with a cubic polynomial regularizing scaling function at scale 6.

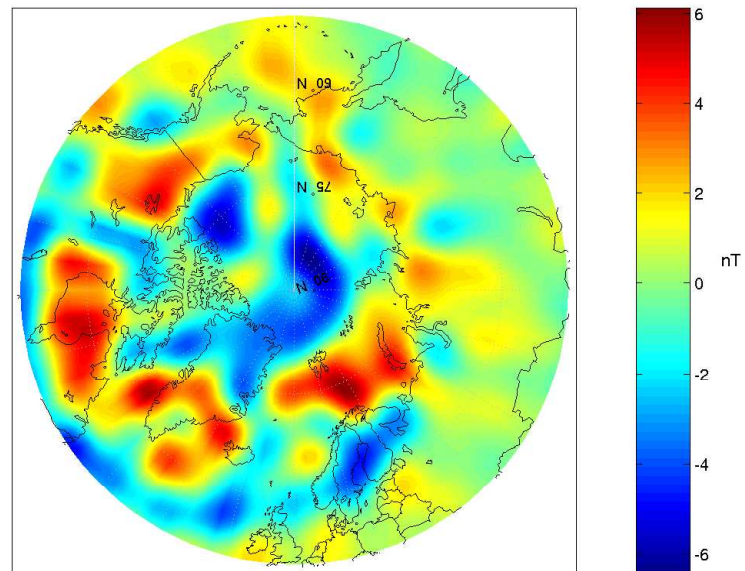


Figure 3.9: Difference in the $(-\varepsilon^r)$ -component between the crustal field obtained by the pure magnetic field data set (Figure 3.7) and the crustal field obtained by the magnetic field with sources only inside the satellite's orbit (Figure 3.8).

Chapter 4

Determination of Ionospheric Current Systems

In the following chapter we discuss the second essential topic of this thesis, the reconstruction of source terms corresponding to given resulting field measurements. The system of partial differential equations which describe the connection of the source field, g , and the resulting field, f , are, as in the previous chapter, the pre-Maxwell equations given by

$$\begin{aligned}\nabla \wedge f &= g, \\ \nabla \cdot f &= 0,\end{aligned}$$

in a certain domain $D \subset \mathbb{R}^3$. We assume the domain D to be a spherical shell, i.e. $D = \Omega_{(a,b)}$ and g ought to be vanishing outside $\Omega_{(a,b)}$. The system of partial differential equations is an elliptic problem which is solvable if the inhomogeneity g is known in $\Omega_{(a,b)}$ and boundary values for f are known on Ω_a and Ω_b . For modelling ionospheric current systems and the corresponding magnetic field this assumption, however, is unrealistic because neither the source system g is given anywhere nor the boundary values for f are given on both boundaries.

We are in the situation that magnetic field data are provided on a sphere $\Omega_c \subset \Omega_{(a,b)}$ with $c \in (a,b)$, i.e. lying completely in the ionosphere. To handle this situation the functionalanalytic framework presented in Chapter 2 turns out to be the appropriate one. If we assume the current system to be of spherical shape we can define an operator, called spherical Biot-Savart operator, which connects the source field g on the sphere Ω_{R_1} to the resulting field on another sphere Ω_{R_2} . This type of height integrated spherical current system is called equivalent current system in the geomagnetic literature (see e.g [6] or [37]), because the same magnetic field is induced by this system as by the real ionospheric current system. In a second step we will see that the orthonormal system $\{u_{n,k}^{(i)}\}$, which has already been used in the previous chapter, is an advantageous system to form the singular system of the corresponding operator. A major task of this chapter will be the calculation of the corresponding singular values of the Biot-Savart operator.

At this point we will see that the determination of the equivalent current system from given magnetic field data is an exponentially ill posed problem, i.e. suitable

regularization techniques have to be applied. Since the singular system of the corresponding operators are calculated we are able to apply the multiscale technique for regularization developed in Section 2.4.

At the end of the chapter we will present several numerical applications for reconstructing current systems from magnetic field measurements. The first two examples are simulations in order to verify the theoretical considerations and to clarify some physical problems. Then we apply our method to magnetic field data of two satellite missions, MAGSAT and CHAMP, which gives us an impression of the ionospheric current systems of the Earth. In this context we also apply our approach in a different coordinate system, given by the magnetic local time and by the quasi dipole latitude which is more useful for describing ionospheric current systems and the corresponding magnetic field. At the end we apply our approach to simulated SWARM magnetic field data in order to have a large amount of satellite's measurements in all local times available.

4.1 The Modelling of the Problem

In this first section we will introduce the problem and we will give some simplifications how the problem can be modelled to be uniquely solvable. First of all we are concerned with a problem of electromagnetism. Here, the full set of Maxwell's equations in a vacuum hold. They are given by

$$\nabla \wedge e(x, t) = -\partial_t b(x, t) \quad (4.1)$$

$$\nabla \cdot e(x, t) = \frac{1}{\varepsilon_0} \rho(x, t) \quad (4.2)$$

$$\nabla \wedge b(x, t) = \mu_0 (j(x, t) + \varepsilon_0 \partial_t e(x, t)) \quad (4.3)$$

$$\nabla \cdot b(x, t) = 0, \quad (4.4)$$

where x is in the ionosphere understood as a spherical shell $\Omega_{(a,b)}$, $a < b$ with a at approximately 110 km and b larger than 1000 km above the Earth's surface. ρ denotes the electric charge density, j the electric current density, e the electric field, b the magnetic field, μ_0 is the permeability of vacuum and ε_0 is the capacitivity of vacuum with $c^2 = 1/(\mu_0 \varepsilon_0)$ (see e.g. [35]).

As far as satellite measurements are concerned we are not able to solve the complete system of Maxwell's equations. Thus we discuss an approximation by dropping terms from the full system of equations that are suspected of being small. These simplifications are mainly due to [6] where a more physical justification can be found.

Suppose we are interested in fields whose typical length scale is L and whose typical time scale is T . Then a priori without any physical and mathematical laws to guide us we can conclude that

$$\begin{aligned} \nabla \cdot e &\approx E/L, & |\nabla \wedge b| &\approx B/L, \\ |\partial_t e| &\approx E/T, & |\partial_t b| &\approx B/T, \\ \nabla \wedge e &= E/L \end{aligned}$$

where E is the strength of the electric field and B is the magnitude of the magnetic field. Now (4.1) and (4.3) tell us that these various magnitudes are not independent. According to (4.3) $E/L \approx B/T$ and therefor $|\partial_t e| \approx LB/T^2$. Furthermore, it follows that

$$\frac{|\partial_t e|}{|\nabla \wedge b|} \approx \left(\frac{L}{T}\right)^2. \quad (4.5)$$

Hence, we see that if times scales are long compared to typical spatial scales the right hand side in (4.5) is small. It is apparently a good approximation, therefore, to drop $\varepsilon_0 \partial_t e$, which is called the displacement current, in (4.3). This simplification causes a partial decoupling of the system (4.1)–(4.4) into an electromagnetic and a magnetostatic part, called quasi static approach. The resulting system are called the *pre-Maxwell equations*. We are mainly interested in the magnetostatic part which reads as follows

$$\nabla \wedge b(x) = \mu_0 j(x), \quad (4.6)$$

$$\nabla \cdot b(x) = 0 \quad (4.7)$$

for $x \in \Omega_{(a,b)}$. In the nomenclature of Chapter 3 this means that μ_0 times the current density j is the source field for the magnetic field b , and b is divergence free, i.e. it has no scalar sources.

Since the magnetic field is of zero divergence in \mathbb{R}^3 it is solenoidal in $\Omega_{(a,b)}$ and the Mie representation can be applied. Hence, b can be represented as $b = \nabla \wedge LP_b + LQ_b$ in $\Omega_{(a,b)}$ where P_b and Q_b are the poloidal and toroidal Mie scalars of b . The source field of the magnetic field are the electric current densities. Following the arguments at the beginning of Chapter 3, the current density j is of zero divergence in \mathbb{R}^3 , too, and thus can be represented by the Mie representation $j = \nabla \wedge LP_j + LQ_j$ in $\Omega_{(a,b)}$ where P_j and Q_j are the Mie scalars of j . The Mie scalars of the source field and the resulting magnetic field are coupled via (see (3.5))

$$\mu_0 P_j = Q_b, \quad (4.8)$$

$$-\mu_0 Q_j = \Delta P_b, \quad (4.9)$$

in $\Omega_{(a,b)}$. This is from our point of view the fundamental system of equations to model ionospheric currents and their resulting field. The equations state that μ_0 times the poloidal scalar of the current density, P_j , is just the toroidal scalar of the magnetic field, Q_b . Furthermore, $-\mu_0$ times the toroidal scalar of the current density, Q_j , and the poloidal scalar of the resulting magnetic field, P_b , are coupled via a Poisson equation in $\Omega_{(a,b)}$. It reduces the problem of solving the vectorial system (4.6) – (4.7) to the problem of solving a scalar Poisson equation.

Using Theorem 1.26, the Mie representation of the magnetic field b and the current system j can, for each $x = r\xi$ with $r \neq 0$, be rewritten as

$$b = \xi \frac{\Delta^* P_b}{r} + \nabla^* \left(-\frac{\partial_r(r P_b)}{r} \right) + L^* Q_b$$

and

$$j = \xi \frac{\Delta^* P_j}{r} + \nabla^* \left(-\frac{\partial_r(r P_j)}{r} \right) + L^* Q_j.$$

But this provides us with a first very easy connection between the current system j and the induced magnetic field b . If we have a look at the radial projection of the current system j at a certain height r and if use (4.8) we arrive at

$$J_{rad}(r\xi) = \xi \cdot j(r\xi) = \frac{\Delta_\xi^* P_j(r\xi)}{r} = \frac{\Delta_\xi^* Q_b(r\xi)}{\mu_o r} \quad r > 0, \xi \in \Omega. \quad (4.10)$$

This means, that if we are able to represent the toroidal scalar Q_b of the magnetic field on a certain height in terms of radial basis functions and if we are furthermore able to apply the Beltrami operator to that radial basis function, then we are able to reconstruct the radial current density J_{rad} on that very height. Later on in Section 4.4 we will apply this method and see how (4.10) can be used in a multiscale framework. The above result has already been obtained in [51], where a reconstruction of the radial current density by means of scalar spherical harmonics has been performed. In [43] the same result has been used to get a reconstruction of the radial current density in terms of scaling functions and wavelets.

4.2 The Biot-Savart Operator

In the following section we introduce an approach of how the pre-Maxwell problem in spherical geometries can be modelled and modified to be uniquely solvable. We will present the general Biot-Savart operator which is based on Biot-Savart's law of electrodynamics (see e.g. [35]). In order to apply the operator when satellite measurement are concerned we will restrict it to spherical geometries. But at first the general definition.

Definition 4.1

Let $g : \mathbb{R}^3 \rightarrow \mathbb{R}^3$ be a divergence free, differentiable vector field. Then the *Biot-Savart operator* in \mathbb{R}^3 , $T : c^{(1)}(\mathbb{R}^3) \rightarrow c^{(2)}(\mathbb{R}^3)$, is defined by

$$f(x) = (Tg)(x) = \frac{1}{4\pi} \int_{\mathbb{R}^3} g(y) \wedge \nabla_y \frac{1}{|x-y|} dy, \quad x \in \mathbb{R}^3. \quad (4.11)$$

A simple calculation shows that

$$Tg(x) = \frac{\mu_0}{4\pi} \int_{\mathbb{R}^3} g(y) \wedge \frac{x-y}{|x-y|^3} dy, \quad x \in \mathbb{R}^3. \quad (4.12)$$

Equation (4.12) is equivalent to

$$f(x) = \nabla \wedge a(x), \quad x \in \mathbb{R}^3, \quad (4.13)$$

where

$$a(x) = \frac{1}{4\pi} \int_{\mathbb{R}^3} \frac{g(y)}{|x-y|} dy, \quad x \in \mathbb{R}^3. \quad (4.14)$$

The vector field a is called *vector potential* of g in \mathbb{R}^3 . The discussion of (3.7), (3.8), and (3.9) shows us that the sources of this field in the sense of Definition 3.1 are given by

$$\nabla \wedge f = g + \nabla(\nabla \cdot a), \quad \text{in } \mathbb{R}^3. \quad (4.15)$$

But the last term vanishes in \mathbb{R}^3 because of $\nabla \cdot a = 0$ which follows directly from (4.14) by partial integration and by g to be of zero divergence. Thus, g is the only source field of f , if f is given by (4.11).

The Biot-Savart operator solves the 'direct source problem' in \mathbb{R}^3 , i.e. the operator calculates the effects of a given vectorial source distribution. Its inverse operator T^{-1} , disregarding whether it exists, is unique or even continuous, would solve the 'inverse source problem', i.e. it would calculate the vectorial source system corresponding to a given field in \mathbb{R}^3 . As we have argued before, this operator is not suitable to cope with the present data situation. We neither know the resulting field nor the source distribution in the whole ionosphere, thus neither direct nor the inverse source problem can be solved.

To overcome this problem let us redefine the Biot-Savart operator in a slightly different manner adapted to spherical geometries.

Definition 4.2

Let $R_1, R_2 > 0, R_1 \neq R_2$, be given and let $g : \Omega_{R_1} \rightarrow \mathbb{R}^3$ be a vector field of class $l^2(\Omega_{R_1})$. Then the *spherical Biot Savart operator* from Ω_{R_1} to Ω_{R_2} , $T_{R_1, R_2} : l^2(\Omega_{R_1}) \rightarrow l^2(\Omega_{R_2})$, is defined by

$$f(x) = (T_{R_1, R_2} g)(x) = \frac{1}{4\pi} \int_{\Omega_{R_1}} g(y) \wedge \frac{x - y}{|x - y|^3} d\omega_{R_1}(y), \quad x \in \Omega_{R_2}. \quad (4.16)$$

Note that in contrast to Definition 4.1 of the Biot-Savart operator T in \mathbb{R}^3 we do not require g to be divergence free or surface divergence free here. For the spherical Biot-Savart operator we can immediately state the following lemma.

Lemma 4.3

The adjoint operator $T_{R_1, R_2}^* : l^2(\Omega_{R_2}) \rightarrow l^2(\Omega_{R_1})$ of T_{R_1, R_2} with respect to the l^2 -inner product is given by

$$T_{R_1, R_2}^* = T_{R_2, R_1}.$$

Proof:

For $f \in l^2(\Omega_{R_1})$, $g \in l^2(\Omega_{R_2})$ some easy calculations involving Fubini's Theorem

result in

$$\begin{aligned}
(T_{R_1, R_2} f, g)_{l^2(\Omega_{R_2})} &= \int_{\Omega_{R_2}} \left(\frac{1}{4\pi} \int_{\Omega_{R_1}} f(y) \wedge \frac{x-y}{|x-y|^3} d\omega_{R_1}(y) \right) \cdot g(x) d\omega_{R_2}(x) \\
&= \frac{1}{4\pi} \int_{\Omega_{R_2}} \int_{\Omega_{R_1}} \left(f(y) \wedge \frac{x-y}{|x-y|^3} \right) \cdot g(x) d\omega_{R_1}(y) d\omega_{R_2}(x) \\
&= \frac{1}{4\pi} \int_{\Omega_{R_1}} \int_{\Omega_{R_2}} \left(\frac{x-y}{|x-y|^3} \wedge g(x) \right) \cdot f(y) d\omega_{R_2}(x) d\omega_{R_1}(y) \\
&= \int_{\Omega_{R_1}} \left(\frac{1}{4\pi} \int_{\Omega_{R_2}} g(x) \wedge \frac{y-x}{|y-x|^3} d\omega_{R_2}(x) \right) \cdot f(y) d\omega_{R_1}(y) \\
&= (f, T_{R_2, R_1} g)_{l^2(\Omega_{R_1})}.
\end{aligned}$$

But this gives the desired result. \square

Furthermore, we are able to prove the following important properties of the operator T_{R_1, R_2} .

Lemma 4.4

The spherical Biot-Savart operator $T_{R_1, R_2} : l^2(\Omega_{R_1}) \rightarrow l^2(\Omega_{R_2})$ as defined in Definition 4.2 is linear, bounded and compact.

Proof:

The linearity of the operator is obvious. To prove the boundedness we note that the operator can be written as tensorial integral operator by

$$(T_{R_1, R_2} g)(x) = \int_{\Omega_{R_1}} \mathbf{k}_{R_1, R_2}(x, y) g(y) d\omega_{R_1}(y), \quad x \in \Omega_{R_2}$$

with

$$\mathbf{k}_{R_1, R_2}(x, y) = \frac{1}{4\pi} \begin{pmatrix} 0 & \frac{x_3 - y_3}{|x-y|^3} & -\frac{x_2 - y_2}{|x-y|^3} \\ -\frac{x_3 - y_3}{|x-y|^3} & 0 & \frac{x_1 - y_1}{|x-y|^3} \\ \frac{x_2 - y_2}{|x-y|^3} & -\frac{x_1 - y_1}{|x-y|^3} & 0 \end{pmatrix}, \quad x \in \Omega_{R_2}, y \in \Omega_{R_1}.$$

For fixed $x \in \Omega_{R_2}$ we have

$$\begin{aligned}
|(T_{R_1, R_2} g)(x)|^2 &= \left| \int_{\Omega_{R_1}} \mathbf{k}_{R_1, R_2}(x, y) g(y) d\omega_{R_1}(y) \right|^2 \\
&\leq \int_{\Omega_{R_1}} |\mathbf{k}_{R_1, R_2}(x, y)|^2 d\omega_{R_1}(y) \|g\|_{l^2(\Omega_{R_1})}^2.
\end{aligned} \tag{4.17}$$

Thus, we can conclude that

$$\|T_{R_1, R_2}\| = \sup_{g \in l^2(\Omega_{R_1})} \frac{\|T_{R_1, R_2} g\|_{l^2(\Omega_{R_2})}}{\|g\|_{l^2(\Omega_{R_1})}} \leq \|\mathbf{k}_{R_1, R_2}\|_{l^2(\Omega_{R_2} \times \Omega_{R_1})}$$

with

$$\begin{aligned}
\|\mathbf{k}_{R_1, R_2}\|_{\mathbf{l}^2(\Omega_{R_2} \times \Omega_{R_1})} &= \int_{\Omega_{R_1}} \int_{\Omega_{R_2}} \sum_{i,j=1}^3 (\mathbf{k}_{R_1, R_2}(x, y))_{ij}^2 d\omega_{R_2}(x) d\omega_{R_1}(y) \\
&= \frac{1}{8\pi^2} \int_{\Omega_{R_1}} \int_{\Omega_{R_2}} \frac{1}{|x - y|^4} d\omega_{R_2}(x) d\omega_{R_1}(y) \\
&\leq 2 \frac{R_1^2 R_2^2}{|R_2 - R_1|^4}.
\end{aligned}$$

This shows the boundedness of the operator T_{R_1, R_2} .

It remains to prove the compactness of the operator T_{R_1, R_2} , where we follow an idea due to [61]. Since the space $\mathbf{c}(\Omega_{R_2} \times \Omega_{R_1})$ is dense in $\mathbf{l}^2(\Omega_{R_2} \times \Omega_{R_1})$ we can find a sequence of tensor kernels $\{\mathbf{k}_n\}_{n=0,1,\dots} \subset \mathbf{c}(\Omega_{R_2} \times \Omega_{R_1})$ which converges against \mathbf{k}_{R_1, R_2} in the sense of the $\mathbf{l}^2(\Omega_{R_2} \times \Omega_{R_1})$ -norm. The integral operators corresponding to the integral kernels \mathbf{k}_n are denoted by T_n , $n = 0, 1, \dots$. By the compactness of $\Omega_{R_2} \times \Omega_{R_1}$ it follows that the kernels \mathbf{k}_n , $n = 0, 1, \dots$, are uniformly continuous and this implies that the image of the set

$$B = \{g \in l^2(\Omega_{R_1}) \mid \|g\|_{l^2(\Omega_{R_1})} \leq 1\}$$

under each operator T_n is equicontinuous (see [61]). By similar arguments as in Equation (4.17) the uniform boundedness of the set $T_n(B)$ can be shown for each $n \in \mathbb{N}_0$. Thus, we can conclude using the Theorem of Arzelà-Ascoli (see [61]) that the operators T_n are compact for all $n \in \mathbb{N}_0$. Involving Equation (4.17) we easily see that

$$\|T_{R_1, R_2} - T_n\| \leq \|\mathbf{k}_{R_1, R_2} - \mathbf{k}_n\|_{\mathbf{l}^2(\Omega_{R_2} \times \Omega_{R_1})} \quad (4.18)$$

which tends to zero as n tends to infinity. Since the space of all compact operators is a closed subspace, (4.18) shows the compactness of T_{R_1, R_2} . \square

If we extend the definition domain of the operator T of Definition 4.1 to the space of distributions, the field $T_{R_1, R_2}g(x)$, $x \in \Omega_{R_2}$, may formally be understood as the resulting field of the current distribution $g(y)\delta(r - R_1)$, $y = r\xi \in \mathbb{R}^3$, under the Biot-Savart operator T restricted to the sphere Ω_{R_2} . These considerations show us that (4.16) is equivalent to

$$T_{R_1, R_2}g(x) = \left(\nabla_{x'} \wedge \left(\frac{1}{4\pi} \int_{\Omega_{R_1}} \frac{g(y)}{|x' - y|} d\omega_{R_1}(y) \right) \right)_{x'=x}, \quad x \in \Omega_{R_2}. \quad (4.19)$$

The operator $P : l^2(\Omega_R) \rightarrow c^{(0)}(\mathbb{R}^3 \setminus \Omega_R)$, $R > 0$ given by

$$(Pg)(x) = \frac{1}{4\pi} \int_{\Omega_R} \frac{g(y)}{|x - y|} d\omega_R(y), \quad x \in \mathbb{R}^3 \setminus \Omega_R \quad (4.20)$$

is called *vector single layer operator* on $l^2(\Omega_R)$. The spherical vector field $f = Pg$ is called *single layer potential* of the layer function g on Ω_R .

The operator in (4.19) seems to be adequate for modelling the given data situation. It reflects the fact that we have only data on a single sphere from which we want to get as much information as possible. The spherical Biot-Savart operator solves the spherical 'direct source problem' from Ω_{R_1} to Ω_{R_2} , i.e. the operator calculates the vectorial effects on the sphere Ω_{R_2} of a given spherical source distribution on Ω_{R_1} . Its inverse operator T_{R_1, R_2}^{-1} , again disregarding any existence, uniqueness or continuity statements, solves the spherical 'inverse source problem', i.e. it calculates the vectorial source system on Ω_{R_1} corresponding to a given resulting field on Ω_{R_2} .

4.3 A Singular System of the Biot-Savart Operator

At this stage we have defined an operator to handle the 'direct source problem' and the 'inverse source problem' in spherical geometries. The aim of the following section is to calculate a singular system of this operator in order to apply the multiscale technique for operator equations and regularization developed in Chapter 2.

By the compactness of T_{R_1, R_2} we know that the operator has a countable singular system. In order to constitute a multiresolution analysis for operator equations in the sense of Chapter 2 we have to calculate the singular system denoted by $\{\sigma_{n'}, h_{n'}, k_{n'}\}$ of the operator $T_{R_1, R_2} : h = l^2(\Omega_{R_1}) \rightarrow \mathfrak{k} = l^2(\Omega_{R_2})$ explicitly. To find corresponding orthonormal systems in the Hilbert spaces \mathfrak{h} and \mathfrak{k} , respectively, is a very simple step. For the sake of clarity we recapitulate a result of Section 1.3.

Lemma 4.5

Let the system of vector spherical harmonics $\{u_{n,k}^{(i)}\}_{\substack{n=0_i, \dots; \\ k=1, \dots, 2n+1}}, i \in \{1, 2, 3\}$, be given as in Definition 1.17 and the system $\{y_{n,k}^{(i)}\}_{\substack{n=0_i, \dots; \\ k=1, \dots, 2n+1}}, i \in \{1, 2, 3\}$, as in Definition 1.15. Furthermore, let $R > 0$ be given. Then the system

$$u_{n,k}^{(i),R} = \frac{1}{R} u_{n,k}^{(i)}, \quad i \in \{1, 2, 3\}; n = 0_i, \dots; k = 1, \dots, 2n+1,$$

as well as the system

$$y_{n,k}^{(i),R} = \frac{1}{R} y_{n,k}^{(i)}, \quad i \in \{1, 2, 3\}; n = 0_i, \dots; k = 1, \dots, 2n+1, \quad (4.21)$$

forms an orthonormal system in $l^2(\Omega_R)$. Furthermore, both systems of spherical vector fields are closed and complete in $l^2(\Omega_R)$ with respect to $(\cdot, \cdot)_{l^2(\Omega_R)}$.

Which system of both is the adequate one for the orthonormal systems of the singular system of the operator T_{R_1, R_2} becomes clear in the next theorems which give a first step to derive the singular values of the operator.

Theorem 4.6

Let the system of vector spherical harmonics be given as in Definition 1.15.

Then we have for $R_2 < R_1$

$$T_{R_1, R_2} y_{n,k}^{(1), R_1} = -\frac{\sqrt{n(n+1)}}{2n+1} \left(\frac{R_2}{R_1}\right)^{n+1} y_{n,k}^{(3), R_2}, \quad (4.22)$$

$$T_{R_1, R_2} y_{n,k}^{(2), R_1} = \frac{n}{2n+1} \left(\frac{R_2}{R_1}\right)^{n+1} y_{n,k}^{(3), R_2}, \quad (4.23)$$

$$T_{R_1, R_2} y_{n,k}^{(3), R_1} = -\frac{n+1}{2n+1} \left(\frac{R_2}{R_1}\right)^n \left(\sqrt{\frac{n}{n+1}} y_{n,k}^{(1), R_2} + y_{n,k}^{(2), R_2} \right). \quad (4.24)$$

Proof:

For the proof of this theorem we use the representation (4.19) of the operator T_{R_1, R_2} . So let $r < R_1$ then we have by (1.10)

$$\frac{1}{|x-y|} = \sum_{m=0}^{\infty} \frac{r^m}{R_1^{m+1}} P_m(\xi \cdot \eta), \quad x = r\xi \in \Omega_{R_1}^{int}, y = R_1\eta \in \Omega_{R_1}. \quad (4.25)$$

Inserting this expansion into (4.20) gives for $x = r\xi, y = R_1\eta$

$$\begin{aligned} (P y_{n,k}^{(1), R_1})(x) &= \frac{1}{4\pi} \int_{\Omega_{R_1}} \sum_{m=0}^{\infty} \frac{r^m}{R_1^{m+1}} P_m(\xi \cdot \eta) \frac{1}{R_1} o_{\eta}^{(1)} Y_{n,k}(\eta) d\omega_{R_1}(\eta) \\ &= \frac{1}{4\pi} \sum_{m=0}^{\infty} \frac{r^m}{R_1^m} \int_{\Omega} o_{\eta}^{(1)} Y_{n,k}(\eta) P_m(\xi \cdot \eta) d\omega(\eta). \end{aligned}$$

Now, we can apply Theorem 1.15 and get

$$\begin{aligned} (P y_{n,k}^{(1), R_1})(x) &= \frac{1}{4\pi} \sum_{m=0}^{\infty} \left(\frac{r}{R_1}\right)^m \frac{1}{2n+1} \\ &\quad \left(((n+1)P_m^{\wedge}(n+1) + nP_m^{\wedge}(n-1)) o_{\xi}^{(1)} Y_{n,k}(\xi) \right. \\ &\quad \left. + (P_m^{\wedge}(n-1) - P_m^{\wedge}(n+1)) o_{\xi}^{(2)} Y_{n,k}(\xi) \right). \end{aligned}$$

Let us now observe that by Definition 1.4 we have that

$$P_m^{\wedge}(n) = \frac{4\pi}{2n+1} \delta_{m,n}, \quad m \in \mathbb{N}_0, n \in \mathbb{N}_0. \quad (4.26)$$

Thus, we get by using (1.21)

$$\begin{aligned} (P y_{n,k}^{(1), R_1})(x) &= \left(\frac{r}{R_1}\right)^{n+1} \frac{1}{(2n+1)(2n+3)} \left((n+1) o_{\xi}^{(1)} Y_{n,k}(\xi) - o_{\xi}^{(2)} Y_{n,k}(\xi) \right) \\ &\quad + \left(\frac{r}{R_1}\right)^{n-1} \frac{1}{(2n+1)(2n-1)} \left(n o_{\xi}^{(1)} Y_{n,k}(\xi) + o_{\xi}^{(2)} Y_{n,k}(\xi) \right) \\ &= \frac{1}{R_1^{n+1}} \frac{1}{(2n+1)(2n+3)} k_n^{(1)}(r^n Y_{n,k}(\xi)) \\ &\quad + \frac{1}{R_1^{n-1}} \frac{1}{(2n+1)(2n-1)} k_n^{(2)}(r^n Y_{n,k}(\xi)). \end{aligned} \quad (4.27)$$

Now, we can use Lemma 1.12 to obtain the curl in \mathbb{R}^3 of (4.27).

$$\begin{aligned}
\nabla_x \wedge (P y_{n,k}^{(1),R_1})(x) &= \frac{1}{R_1^{n+1}} \frac{1}{(2n+1)(2n+3)} \nabla_x \wedge k_n^{(1)}(r^n Y_{n,k}(\xi)) \\
&= -\frac{1}{R_1^{n+1}} \frac{2n+3}{(2n+1)(2n+3)} r^n k_n^{(3)} Y_{n,k}(\xi) \\
&= -\frac{1}{2n+1} \left(\frac{r}{R_1} \right)^{n+1} \frac{1}{r} o_\xi^{(3)} Y_{n,k}(\xi) \\
&= -\frac{(\mu_n^{(3)})^{1/2}}{2n+1} \left(\frac{r}{R_1} \right)^{n+1} y_{n,k}^{(3),r}(\xi). \tag{4.28}
\end{aligned}$$

Restricting (4.28) to the sphere Ω_{R_2} with $R_2 < R_1$ gives

$$T_{R_1, R_2} y_{n,k}^{(1),R_1}(\xi) = -\frac{(\mu_n^{(3)})^{1/2}}{2n+1} \left(\frac{R_2}{R_1} \right)^{n+1} y_{n,k}^{(3),R_2}(\xi).$$

This shows (4.22).

For Equation (4.23) we again use Equation (4.25) to get, for $x = r\xi, y = R_1\eta$ and $r < R_1$,

$$\begin{aligned}
(P y_{n,k}^{(2),R_1})(x) &= \frac{1}{4\pi} \int_{\Omega_{R_1}} \sum_{m=0}^{\infty} \frac{r^m}{R_1^{m+1}} P_m(\xi \cdot \eta) \frac{(\mu_n^{(2)})^{-1/2}}{R_1} o_\eta^{(2)} Y_{n,k}(\eta) d\omega_{R_1}(\eta) \\
&= \frac{1}{4\pi} \sum_{m=0}^{\infty} \frac{r^m}{R_1^m} (\mu_n^{(2)})^{-1/2} \int_{\Omega} o_\eta^{(2)} Y_{n,k}(\eta) P_m(\xi \cdot \eta) d\omega(\eta)
\end{aligned}$$

Applying Theorem 1.15 we find

$$\begin{aligned}
(P y_{n,k}^{(2),R_1})(x) &= \frac{1}{4\pi} \sum_{m=0}^{\infty} \frac{r^m}{R_1^m} \frac{(\mu_n^{(2)})^{-1/2}}{(2n+1)} \\
&\quad \left(n(n+1) (P_m^\wedge(n-1) - P_m^\wedge(n+1)) o_\xi^{(1)} Y_{n,k}(\xi) \right. \\
&\quad \left. + (nP_m^\wedge(n+1) + (n+1)P_m^\wedge(n-1)) o_\xi^{(2)} Y_{n,k}(\xi) \right)
\end{aligned}$$

Observing Equation (4.26) yields

$$\begin{aligned}
(P y_{n,k}^{(2),R_1})(x) &= \left(\frac{r}{R_1} \right)^{n+1} \frac{(\mu_n^{(2)})^{-1/2}}{(2n+1)(2n+3)} \left(-n(n+1) o_\xi^{(1)} Y_{n,k}(\xi) + n o_\xi^{(2)} Y_{n,k}(\xi) \right) \\
&\quad + \left(\frac{r}{R_1} \right)^{n-1} \frac{(\mu_n^{(2)})^{-1/2}}{(2n+1)(2n-1)} \left(n(n+1) o_\xi^{(1)} Y_{n,k}(\xi) + (n+1) o_\xi^{(2)} Y_{n,k}(\xi) \right).
\end{aligned}$$

Now, using Equation (1.21) we easily see that

$$\begin{aligned}
(P y_{n,k}^{(2),R_1})(x) &= \frac{-(\mu_n^{(2)})^{-1/2} n}{R_1^{n+1} (2n+1)(2n+3)} k_n^{(1)}(r^n Y_{n,k}(\xi)) \\
&\quad + \frac{(\mu_n^{(2)})^{-1/2} (n+1)}{R_1^{n-1} (2n+1)(2n-1)} k_n^{(2)}(r^n Y_{n,k}(\xi)). \tag{4.29}
\end{aligned}$$

Applying Lemma 1.12 to derive the curl in \mathbb{R}^3 of (4.29) and observing that $\mu_n^{(2)} = \mu_n^{(3)}$ gives

$$\begin{aligned}
\nabla_x \wedge (P y_{n,k}^{(2),R_1})(x) &= \frac{-n}{R_1^{n+1}} \frac{(\mu_n^{(2)})^{-1/2}}{(2n+1)(2n+3)} \nabla_x \wedge k_n^{(1)}(r^n Y_{n,k}(\xi)) \\
&= \frac{n}{R_1^{n+1}} \frac{(\mu_n^{(2)})^{-1/2}(2n+3)}{(2n+1)(2n+3)} r^n k_n^{(3)} Y_{n,k}(\xi) \\
&= \frac{n}{(2n+1)} \left(\frac{r}{R_1} \right)^{n+1} (\mu_n^{(3)})^{-1/2} \frac{1}{r} o_\xi^{(3)} Y_{n,k}(\xi) \\
&= \frac{n}{2n+1} \left(\frac{r}{R_1} \right)^{n+1} y_{n,k}^{(3),r}(\xi). \tag{4.30}
\end{aligned}$$

If we now restrict (4.30) to the sphere Ω_{R_2} with $R_2 < R_1$ we arrive at

$$T_{R_1,R_2} y_{n,k}^{(2),R_1}(\xi) = -\frac{-n}{2n+1} \left(\frac{R_2}{R_1} \right)^{n+1} y_{n,k}^{(3)}(\xi).$$

But this shows (4.23).

Proving (4.24) is on the one hand easier but on the other hand more difficult as the previous two ones. The first step is much easier than before. Again using (4.25), we get for $x = r\xi$, $y = R_1\eta$, $r < R_1$

$$\begin{aligned}
(P y_{n,k}^{(3),R_1})(x) &= \frac{1}{4\pi} \int_{\Omega} \sum_{m=0}^{\infty} \frac{r^m}{R_1^{m+1}} P_m(\xi \cdot \eta) \frac{1}{R_1} (\mu_n^{(3)})^{-1/2} o_\eta^{(3)} Y_{n,k}(\eta) d\omega_{R_1}(\eta) \\
&= \frac{1}{4\pi} \sum_{m=0}^{\infty} \frac{r^m}{R_1^m} (\mu_n^{(3)})^{-1/2} \int_{\Omega} o_\eta^{(3)} Y_{n,k}(\eta) P_m(\xi \cdot \eta) d\omega(\eta)
\end{aligned}$$

Applying Theorem 1.15 results in

$$(P y_{n,k}^{(3),R_1})(x) = \frac{1}{4\pi} \sum_{m=0}^{\infty} \frac{r^m}{R_1^m} \frac{(\mu_n^{(3)})^{-1/2}}{(2n+1)} P_m^\wedge(n) o_\xi^{(1)} Y_{n,k}(\xi). \tag{4.31}$$

By use of (4.26), we can simplify the sum in (4.31) to obtain

$$\begin{aligned}
(P y_{n,k}^{(3),R_1})(x) &= \left(\frac{r}{R_1} \right)^n \frac{(\mu_n^{(3)})^{-1/2}}{2n+1} o_\xi^{(3)} Y_{n,k}(\xi) \\
&= \left(\frac{1}{R_1} \right)^n \frac{(\mu_n^{(3)})^{-1/2}}{2n+1} k_n^{(3)}(r^n Y_{n,k}(\xi)). \tag{4.32}
\end{aligned}$$

Now we apply Lemma 1.12, respectively (1.20), to find the curl in \mathbb{R}^3 of (4.32)

$$\begin{aligned}\nabla_x \wedge (P y_{n,k}^{(3),R_1})(x) &= \left(\frac{1}{R_1}\right)^n \frac{(\mu_n^{(3)})^{-1/2}}{2n+1} \nabla_x \wedge k_n^{(3)}(r^n Y_{n,k}(\xi)) \\ &= \left(\frac{1}{R_1}\right)^n \frac{(\mu_n^{(3)})^{-1/2}}{(2n+1)} \left[o_\xi^{(1)} \left(\frac{1}{r} \Delta_\xi^* (r^n Y_{n,k}(\xi)) \right) \right. \\ &\quad \left. + o_\xi^{(2)} \left(-\frac{1}{r} \frac{\partial}{\partial r} (r^{n+1} Y_{n,k}(\xi)) \right) \right].\end{aligned}$$

Evaluating these terms and observing that $\mu_n^{(2)} = \mu_n^{(3)}$ yields

$$\begin{aligned}\nabla_x \wedge (P y_{n,k}^{(3),R_1})(x) &= -(\mu_n^{(2)})^{-1/2} \frac{n+1}{2n+1} \left(\frac{r}{R_1}\right)^n \frac{1}{r} \left(n o_\xi^{(1)} Y_{n,k}(\xi) + o_\xi^{(2)} Y_{n,k}(\xi) \right) \\ &= -\frac{n+1}{2n+1} \left(\frac{r}{R_1}\right)^n \left(\sqrt{\frac{n}{n+1}} y_{n,k}^{(1),r}(\xi) + y_{n,k}^{(2),r}(\xi) \right).\end{aligned}$$

Restricting this equation to the sphere Ω_{R_2} with $R_2 < R_1$ results in

$$T_{R_1,R_2} y_{n,k}^{(3),R_1}(\xi) = -\frac{n+1}{2n+1} \left(\frac{R_2}{R_1}\right)^n \left(\sqrt{\frac{n}{n+1}} y_{n,k}^{(1),R_2}(\xi) + y_{n,k}^{(2),R_2}(\xi) \right)$$

which is the desired result. \square

The above theorem for $R_1 < R_2$ is the first step to obtain the singular system of the operator T_{R_1,R_2} . In a second step we have to investigate the opposite case $R_2 > R_1$ since we know that $T_{R_1,R_2}^* = T_{R_2,R_1}$.

Theorem 4.7

Let the system of vector spherical harmonics be given as in Definition 1.15.

Then for $R_2 > R_1$ we have

$$T_{R_1,R_2} y_{n,k}^{(1),R_1} = -\frac{\sqrt{n(n+1)}}{2n+1} \left(\frac{R_1}{R_2}\right)^n y_{n,k}^{(3),R_2}, \quad (4.33)$$

$$T_{R_1,R_2} y_{n,k}^{(2),R_1} = -\frac{n+1}{2n+1} \left(\frac{R_1}{R_2}\right)^n y_{n,k}^{(3),R_2}, \quad (4.34)$$

$$T_{R_1,R_2} y_{n,k}^{(3),R_1} = -\frac{n}{2n+1} \left(\frac{R_1}{R_2}\right)^{n+1} \left(\sqrt{\frac{n+1}{n}} y_{n,k}^{(1),R_2} - y_{n,k}^{(2),R_2} \right). \quad (4.35)$$

Proof:

The proofs of (4.33)–(4.35) will be performed in a shorter way since they run similar to the proofs of (4.22)–(4.24). Only those steps which are different to the proof of Theorem 4.6 will be executed explicitly here.

So let $R_1 < r$, then (4.25) does not hold any more, but we can write

$$\frac{1}{|x-y|} = \frac{1}{|y-x|} = \sum_{m=0}^{\infty} \frac{R_1^m}{r^{m+1}} P_m(\xi \cdot \eta), \quad x = r\xi \in \Omega_{R_1}^{ext}, y = R_1\eta \in \Omega_{R_1}.$$

By similar calculations as for (4.22) we thus get

$$\begin{aligned}
(P y_{n,k}^{(1),R_1})(x) &= \left(\frac{R_1}{r}\right)^{n+2} \frac{1}{(2n+1)(2n+3)} \left((n+1)o_\xi^{(1)}Y_{n,k}(\xi) - o_\xi^{(2)}Y_{n,k}(\xi) \right) \\
&\quad + \left(\frac{R_1}{r}\right)^n \frac{1}{(2n+1)(2n-1)} \left(no_\xi^{(1)}Y_{n,k}(\xi) + o_\xi^{(2)}Y_{n,k}(\xi) \right) \\
&= -\frac{R_1^{n+2}}{(2n+1)(2n+3)} k_n^{(2)} \left(\frac{1}{r^{n+1}} Y_{n,k}(\xi) \right) \\
&\quad + \left(\frac{R_1}{r}\right)^n \frac{1}{(2n+1)(2n-1)} \left(no_\xi^{(1)}Y_{n,k}(\xi) + o_\xi^{(2)}Y_{n,k}(\xi) \right). \quad (4.36)
\end{aligned}$$

Applying the curl in \mathbb{R}^3 to (4.36) we see using Lemma 1.12 that the first term vanishes, i.e. we only have to evaluate

$$\begin{aligned}
\nabla_x \wedge (P y_{n,k}^{(1),R_1})(x) &= \frac{R_1^n}{(2n+1)(2n-1)} \nabla_x \wedge \left(\frac{1}{r^n} \left(no_\xi^{(1)}Y_{n,k}(\xi) + o_\xi^{(2)}Y_{n,k}(\xi) \right) \right), \\
&= \frac{R_1^n}{(2n+1)(2n-1)} \nabla_x \wedge \left(\xi \left[\frac{nY_{n,k}(\xi)}{r^n} \right] + \nabla_\xi^* \left[\frac{Y_{n,k}(\xi)}{r^n} \right] \right).
\end{aligned}$$

By means of Lemma 1.21 we can calculate the curl in \mathbb{R}^3 of this vector field in Helmholtz representation and obtain

$$\nabla_x \wedge (P y_{n,k}^{(1),R_1})(x) = -\frac{(\mu_n^{(3)})^{1/2}}{2n+1} \left(\frac{R_1}{r} \right)^n y_{n,k}^{(3),r}(\xi). \quad (4.37)$$

Restricting (4.37) to the sphere Ω_{R_2} with $R_2 > R_1$ gives

$$T_{R_1,R_2} y_{n,k}^{(1),R_1}(\xi) = -\frac{(\mu_n^{(3)})^{1/2}}{2n+1} \left(\frac{R_1}{R_2} \right)^n y_{n,k}^{(3),R_2}(\xi).$$

This shows (4.33).

To prove Equation (4.34) similar calculations as for (4.23) and (4.33) have to be performed. As an intermediate result we get for $r > R_1$

$$\begin{aligned}
(P y_{n,k}^{(2),R_1})(x) &= \frac{n(\mu_n^{(2)})^{-1/2} R_1^{n+2}}{(2n+1)(2n+3)} k_n^{(2)} \left(\frac{1}{r^{n+1}} Y_{n,k}(\xi) \right) \\
&\quad + \left(\frac{R_1}{r}\right)^n \frac{(\mu_n^{(2)})^{-1/2} (n+1)}{(2n+1)(2n-1)} \left(no_\xi^{(1)}Y_{n,k}(\xi) + o_\xi^{(2)}Y_{n,k}(\xi) \right).
\end{aligned}$$

Applying the curl in \mathbb{R}^3 and using equivalent arguments as for the application of the curl in \mathbb{R}^3 to $P y_{n,k}^{(1),R_1}$ yields

$$\nabla_x \wedge (P y_{n,k}^{(2),R_1})(x) = -\frac{n+1}{2n+1} \left(\frac{R_1}{r} \right)^n y_{n,k}^{(3),r}(\xi). \quad (4.38)$$

Restricting this equation to Ω_{R_2} with $R_2 > R_1$ gives the desired result

$$T_{R_1, R_2} y_{n,k}^{(2), R_1}(\xi) = -\frac{n+1}{2n+1} \left(\frac{R_1}{R_2}\right)^n y_{n,k}^{(3), R_2}(\xi).$$

The final part of the proof now shows Equation (4.35). By some easy computations similar to those for the proof of (4.24) we achieve

$$(P y_{n,k}^{(3), R_1})(x) = \left(\frac{R_2}{r}\right)^{n+1} \frac{(\mu_n^{(3)})^{-1/2}}{2n+1} o_\xi^{(3)} Y_{n,k}(\xi). \quad (4.39)$$

Involving Lemma 1.12, respectively (1.20), we get the curl in \mathbb{R}^3 of (4.39) by

$$\begin{aligned} \nabla_x \wedge (P y_{n,k}^{(3), R_1})(x) &= -\frac{n(\mu_n^{(3)})^{-1/2}}{2n+1} \left(\frac{R_1}{r}\right)^{n+1} \frac{1}{r} \left((n+1)o_\xi^{(1)} Y_{n,k}(\xi) - o_\xi^{(2)} Y_{n,k}(\xi)\right) \\ &= -\frac{n}{2n+1} \left(\frac{R_1}{r}\right)^{n+1} \left(\frac{n+1}{\sqrt{n(n+1)}} y_{n,k}^{(1), r}(\xi) - y_{n,k}^{(2), r}(\xi)\right) \end{aligned} \quad (4.40)$$

Restricting (4.40) to the sphere Ω_{R_2} with $R_2 > R_1$ yields

$$T_{R_1, R_2} y_{n,k}^{(3), R_1}(\xi) = -\frac{n}{2n+1} \left(\frac{R_1}{R_2}\right)^{n+1} \left(\sqrt{\frac{n+1}{n}} y_{n,k}^{(1), R_2}(\xi) - y_{n,k}^{(2), R_2}(\xi)\right).$$

This gives (4.35) and finishes the proof of Theorem 4.7. \square

Using the representation of the system $\{u_{n,k}^{(i)}\}$ in terms of the system $\{y_{n,k}^{(i)}\}$ (see Lemma 1.17) we immediately get the following result which reveals the system $\{u_{n,k}^{(i)}\}$ to be the orthonormal systems suitable for dealing with the spherical Biot-Savart operator T_{R_1, R_2} .

Corollary 4.8

Let the system of vector spherical harmonics be given as in Lemma 1.17.

Then we have for $R_2 < R_1$

$$T_{R_1, R_2} u_{n,k}^{(1), R_1} = -\sqrt{\frac{n}{2n+1}} \left(\frac{R_2}{R_1}\right)^{n+1} u_{n,k}^{(3), R_2}, \quad (4.41)$$

$$T_{R_1, R_2} u_{n,k}^{(2), R_1} = 0, \quad (4.42)$$

$$T_{R_1, R_2} u_{n,k}^{(3), R_1} = -\sqrt{\frac{n+1}{2n+1}} \left(\frac{R_2}{R_1}\right)^n u_{n,k}^{(2), R_2}, \quad (4.43)$$

while for $R_2 > R_1$

$$T_{R_1, R_2} u_{n,k}^{(1), R_1} = 0, \quad (4.44)$$

$$T_{R_1, R_2} u_{n,k}^{(2), R_1} = -\sqrt{\frac{n+1}{2n+1}} \left(\frac{R_1}{R_2}\right)^n u_{n,k}^{(3), R_2}, \quad (4.45)$$

$$T_{R_1, R_2} u_{n,k}^{(3), R_1} = -\sqrt{\frac{n}{2n+1}} \left(\frac{R_1}{R_2}\right)^{n+1} u_{n,k}^{(1), R_2}, \quad (4.46)$$

This corollary points out the essential advantage of the system $\{u_{n,k}^{(i)}\}$ of vector spherical harmonics when we deal with the operator T_{R_1,R_2} . It allows us to write the operator equation in the sense of Chapter 2 in a concise form.

Physically interpreted Corollary 4.8 connects the components of a spherical current system to the corresponding magnetic field at a different height. In other words the corollary states that current systems of class $l_{\mathcal{U}}^{2,(2)}(\Omega_{R_1})$ induce no magnetic field inside the sphere where they are present and current systems of class $l_{\mathcal{U}}^{2,(1)}(\Omega_{R_1})$ produce no magnetic field outside the sphere Ω_{R_1} . This is a generalized mathematical form of a result presented in [27] which says that spherical poloidal currents produce no magnetic field inside the sphere where they are present.

Observing that $T_{R_1,R_2}^* = T_{R_2,R_1}$ and combining the two previous corollaries we get the following result.

Corollary 4.9

Let the system of vector spherical harmonics be given as in Lemma 1.17.

Then we have for $R_2 < R_1$

$$T_{R_1,R_2}^* T_{R_1,R_2} u_{n,k}^{(1),R_1} = \frac{n}{2n+1} \left(\frac{R_2}{R_1} \right)^{2n+2} u_{n,k}^{(1),R_1}, \quad (4.47)$$

$$T_{R_1,R_2}^* T_{R_1,R_2} u_{n,k}^{(2),R_1} = 0, \quad (4.48)$$

$$T_{R_1,R_2}^* T_{R_1,R_2} u_{n,k}^{(3),R_1} = \frac{n+1}{2n+1} \left(\frac{R_2}{R_1} \right)^{2n} u_{n,k}^{(3),R_1}, \quad (4.49)$$

and for $R_2 > R_1$

$$T_{R_1,R_2}^* T_{R_1,R_2} u_{n,k}^{(1),R_1} = 0, \quad (4.50)$$

$$T_{R_1,R_2}^* T_{R_1,R_2} u_{n,k}^{(2),R_1} = \frac{n+1}{2n+1} \left(\frac{R_1}{R_2} \right)^{2n} u_{n,k}^{(2),R_1}, \quad (4.51)$$

$$T_{R_1,R_2}^* T_{R_1,R_2} u_{n,k}^{(3),R_1} = \frac{n}{2n+1} \left(\frac{R_1}{R_2} \right)^{2n+2} u_{n,k}^{(3),R_1}, \quad (4.52)$$

Since we deal with the situation that resulting field measurements are given on a sphere which is above the source field, we are mainly interested in the last three equations of Corollary 4.9 and in Equations (4.44 - 4.46) of Corollary 4.8.

Equations (4.41 - 4.43) and Equations (4.44 - 4.46) now establish the starting point to apply the multiscale methods for tensor-operator equations and the multiscale regularization techniques for vectorial inverse problems which we have developed in Chapter 2. The singular system of the Biot-Savart operator $T_{R_1,R_2} : \mathfrak{h} \rightarrow \mathfrak{k}$, for $R_2 < R_1$, is given in Table 4.1 and, for $R_1 < R_2$, in Table 4.2.

\mathfrak{h}	\mathfrak{k}	$\{h_n\}$	$\{k_n\}$	σ_n
$l_{\mathcal{U}}^{2,(1)}(\Omega_{R_1})$	$l_{\mathcal{U}}^{2,(3)}(\Omega_{R_2})$	$u_{n,k}^{(1),R_1}$	$-u_{n,k}^{(3),R_2}$	$\sqrt{\frac{n}{2n+1}} \left(\frac{R_2}{R_1}\right)^{n+1}$
$l_{\mathcal{U}}^{2,(3)}(\Omega_{R_1})$	$l_{\mathcal{U}}^{2,(2)}(\Omega_{R_2})$	$u_{n,k}^{(3),R_1}$	$-u_{n,k}^{(2),R_2}$	$\sqrt{\frac{n+1}{2n+1}} \left(\frac{R_2}{R_1}\right)^n$

Table 4.1: Singular system of the spherical Biot-Savart operator $T_{R_1,R_2} : \mathfrak{h} \rightarrow \mathfrak{k}$ for the case $R_2 < R_1$.

\mathfrak{h}	\mathfrak{k}	$\{h_n\}$	$\{k_n\}$	σ_n
$l_{\mathcal{U}}^{2,(2)}(\Omega_{R_1})$	$l_{\mathcal{U}}^{2,(3)}(\Omega_{R_2})$	$u_{n,k}^{(2),R_1}$	$-u_{n,k}^{(3),R_2}$	$\sqrt{\frac{n+1}{2n+1}} \left(\frac{R_1}{R_2}\right)^n$
$l_{\mathcal{U}}^{2,(3)}(\Omega_{R_1})$	$l_{\mathcal{U}}^{2,(1)}(\Omega_{R_2})$	$u_{n,k}^{(3),R_1}$	$-u_{n,k}^{(1),R_2}$	$\sqrt{\frac{n}{2n+1}} \left(\frac{R_1}{R_2}\right)^{n+1}$

Table 4.2: Singular system of the spherical Biot-Savart operator $T_{R_1,R_2} : \mathfrak{h} \rightarrow \mathfrak{k}$ for the case $R_2 > R_1$.

In the unified functionalanalytic framework as developed in Chapter 2 these equations are of the form

$$\Lambda h = k, \quad h \in \mathfrak{h}, k \in \mathfrak{k},$$

where $\Lambda : \mathfrak{h} \rightarrow \mathfrak{k}$ is a compact operator and \mathfrak{h} and \mathfrak{k} are separable Hilbert spaces of square-integrable vector functions. The singular system of Λ is, for $n' \in \mathbb{N}_0$, given by $\{\sigma_{n'}, h_{n'}, k_{n'}\}$.

Remembering Definition 2.4 of a well-posed problem, i.e. existence, uniqueness and continuity of the inverse, we realize that the problem of calculating $h \in \mathfrak{h}$ with

$$\Lambda h = k \tag{4.53}$$

for given $k \in \mathfrak{k}$ is ill-posed since the first and the third property of a well-posed problem are violated. At first, for arbitrary functions $k \in \mathfrak{k}$, k is not necessary in the range of Λ which violates the first property (note that we have to assume observational errors or noise in any practical application which may cause that $k \notin \mathcal{R}(\Lambda) \oplus \mathcal{R}(\Lambda)^\perp$ such that even the generalized inverse, Λ^+ , cannot be applied). At this point a first regularization step has to be applied. Second, if we have a look at the generalized solution of (4.53), i.e. the Moore-Penrose inverse which is given by

$$\Lambda^+ k = \sum_{n' \in \mathbb{N}} \sigma_{n'}^{-1}(k, k_{n'})_{\mathfrak{k}} h_{n'} \tag{4.54}$$

for $k \in \mathcal{R}(\Lambda) \oplus \mathcal{R}(\Lambda)^\perp$, the singular system of Λ indicates the type of violation of the third property of a well-posed problem. The right hand side of (4.54) is not

necessarily convergent. Thus, it is obvious that the singular values of the Biot-Savart operator given in Table 4.1 and Table 4.2 constitute an exponentially ill posed problem. In order to force convergence we have to replace (4.54) by a filtered version of this expansion. This has been done in Section 2.4 in a general multiscale framework for regularization of vectorial inverse problems.

4.4 Simulations and Numerical Applications

In the following section we will give different applications of our previously presented multiscale approach for reconstructing current systems from given magnetic field data. At first, we will apply our methods to two simulations, where we are able to calculate the magnetic field corresponding to the simulated current configuration explicitly. After these simulated examples we apply our method to real satellite magnetic field data. To demonstrate the applicability of our approach, we use data of three different satellite missions, the MAGSAT mission (1979-1980), the CHAMP mission (2000-2005) and the proposed SWARM mission, where simulated data are available.

4.4.1 A Simulation of a Ring Current System

As a first application of our method of reconstructing current systems from given magnetic field data we simulate a spherical ring current which can be seen in Figure 4.1. The current system is supposed to exist on a sphere with radius $R_1 = 100 \text{ km}$ and is assumed to be purely tangential where the north-component j_ϑ is vanishing and the east component j_φ is given by

$$j_\varphi(\varphi, \vartheta) = \begin{cases} \left(1 - \frac{|\vartheta - \pi/2|}{\pi/18}\right)^2 \left(1 + 2\frac{|\vartheta - \pi/2|}{\pi/18}\right), & \vartheta \in [\pi/2 - \pi/18, \pi/2 + \pi/18] \\ 0, & \text{else,} \end{cases}$$

for $\varphi \in [0, 2\pi)$. The corresponding magnetic field is calculated at a height of $R_2 = 400 \text{ km}$ in order to simulate satellite configurations. The field is computed using Biot-Savart's law given by

$$b(x) = \frac{\mu_0}{4\pi} \int_{\Omega_{100}} \frac{j(y) \wedge (x - y)}{|x - y|^3} d\omega_{100}(y), \quad x \in \Omega_{400}, \quad (4.55)$$

using suitable rules for numerical integration, where $\mu_0 = 4\pi \cdot 10^{-7} \text{ N/A}^2$ is the magnetic permeability of the vacuum. The resulting magnetic field can be seen in Figure 4.1.

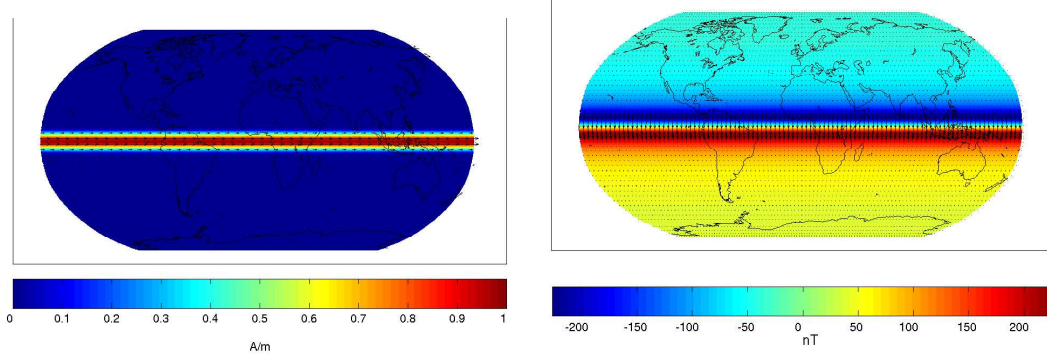


Figure 4.1: Left: Simulated configuration of a spherical ring current at radius $R_1 = 100 \text{ km}$. Color indicates the absolute value of the current at a height of $R_2 = 400 \text{ km}$. Right: Calculated induced magnetic field b of the simulated ring current system. Arrows indicate tangential components while colour indicates the negative radial component.

Since the simulated current system is purely toroidal and we are in the case of $R_2 > R_1$, only Equation (4.46) plays a role. i.e. we have to regularize

$$T_{R_1, R_2} : \mathfrak{h} \rightarrow \mathfrak{k},$$

where T_{R_1, R_2} is the spherical Biot-Savart operator given in Definition 4.2 and

$$\begin{aligned} \mathfrak{h} &= l_{\mathcal{U}}^{2,(3)}(\Omega_{R_1}), & \{h_{n'}\} &= \{-u_{n,k}^{(3),R_1}\}_{\substack{n=1,\dots; \\ k=1,\dots,2n+1}}, \\ \mathfrak{k} &= l_{\mathcal{U}}^{2,(1)}(\Omega_{R_2}), & \{k_{n'}\} &= \{u_{n,k}^{(1),R_2}\}_{\substack{n=1,\dots; \\ k=1,\dots,2n+1}}, \\ \sigma_{n'} &= \sqrt{\frac{n}{2n+1}} \left(\frac{R_1}{R_2}\right)^{n+1}, & n' &\in \mathbb{N}. \end{aligned}$$

This leads to decomposition regularization vector scaling functions $\{^d\varphi_J\}$, $J \in \mathbb{Z}$, (see Definition 2.28) given by

$$^d\varphi_J(x, y) = \sum_{n=1}^{\infty} \sum_{k=1}^{\infty} (\varphi_J)^{\wedge}(n) u_{n,k}^{(1),R_2}(x) Y_{n,k}^{R_2}(y), \quad x \in \Omega_{R_2}, y \in \Omega_{R_2},$$

and reconstruction regularization vector scaling functions $\{^r\varphi_J\}$, $J \in \mathbb{Z}$, of the form

$$^r\varphi_J(x, y) = - \sum_{n=1}^{\infty} \sum_{k=1}^{\infty} (\varphi_J)^{\wedge}(n) u_{n,k}^{(3),R_1}(x) Y_{n,k}^{R_2}(y), \quad x \in \Omega_{R_1}, y \in \Omega_{R_2},$$

where the symbol $\{(\varphi_J)^{\wedge}(n)\}_{n=1,2,\dots}$ satisfies

1. $\lim_{J \rightarrow \infty} ((\varphi_J)^{\wedge}(n))^2 = \sigma_n^{-1}, \quad n \in \mathbb{N},$
2. $((\varphi_J)^{\wedge}(n))^2 \geq ((\varphi_{J-1})^{\wedge}(n))^2, \quad J \in \mathbb{Z}, n \in \mathbb{N},$

$$3. \lim_{J \rightarrow -\infty} ((\varphi_J)^\wedge(n))^2 = 0, \quad n \in \mathbb{N}.$$

The result of our reconstruction with a regularization vector cubic polynomial scaling function at scale $J = 8$ can be seen in Figure 4.2. In Figure 4.3 we have plotted the absolute value of the ε^φ -component (geomagnetic Y-component) of the reconstructed current system along the zero meridian for different scales. It is clearly visible that the reconstruction of the current system is improved by increasing the scale. But this procedure can only be continued up to a certain scale. After this maximal scale the problem will be over-regularized, i.e. the regularization error is still reduced but the error occurring from noisy data will increase (see (2.12)). (Note that in the case of simulations we do not have any noise but since we use approximate integration rules to evaluate the appearing convolution integrals we produce errors which behave like noise.)

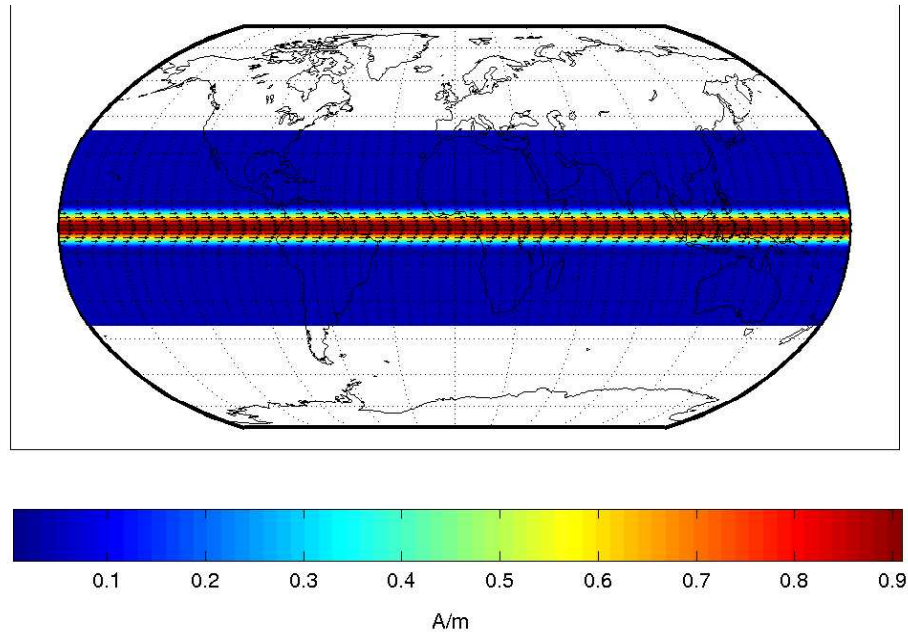


Figure 4.2: Reconstruction of the simulated ring current system with a regularization cubic polynomial scaling function at scale $J = 8$. Note that the area of reconstruction is just the coloured area in order to minimize computational effort.

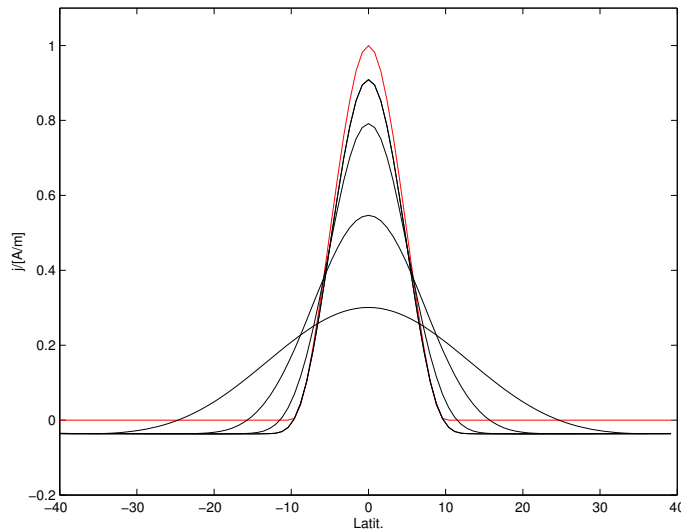


Figure 4.3: Absolute value of the ε^φ -component (geomagnetic Y-component) of the reconstructed current system along the zero meridian for scales $J = 4$, $J = 5$, $J = 6$ and $J = 8$. The red line shows the original simulated current system.

4.4.2 A Simulation of a Local Current System (Cowling Channel)

As a second example we have simulated a geophysically more relevant current system. We approximated the current configuration of a Cowling channel.

A Cowling channel is a confined ionospheric area with an enlarged conductance (up to 17 times higher than the conductance of the surrounding area), leading to horizontal ionospheric currents with magnitudes that are enhanced compared to the background. The channel usually has a larger extent in the direction of the current flow ('channel direction') than perpendicular to it. At the edges of the cowling channel direction, radial currents are present to feed or diverge the enlarged horizontal currents, respectively. For a detailed description of a cowling channel and the geophysical background the reader is referred to [36] and [37]. We simulate the current configuration of such a Cowling channel by three line currents flowing radially from infinity onto the Earth up to a height of $R_1 = 100 \text{ km}$, then flowing parallel to the Earth for about 10° and then diverging radially to infinity again. A sketch of the current system can be seen in Figure 4.4. A similar model has been used in [1] and [4] to simulate a Cowling channel in a different context.

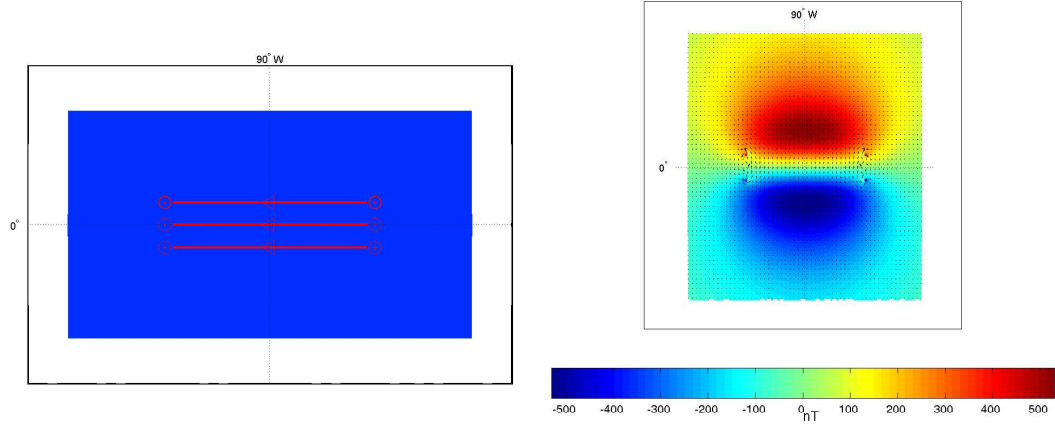


Figure 4.4: Left: Simulated current configuration of a Cowling Channel. The current strength of one line current is 1 A . Crosses indicate currents flowing onto the Earth, whereas dots indicate radially diverging currents. The height of the horizontal current system is $R_1 = 100\text{ km}$. Right: Induced magnetic field at a height of $R_2 = 400\text{ km}$. Color indicates negative radial component, whereas arrows indicate horizontal components.

The corresponding induced magnetic field is calculated at a height of $R_2 = 400\text{ km}$ to simulate satellite like configurations using Biot-Savart's law (4.55), where the simple configuration of the current system has the great advantage of being able to calculate the integral in (4.55) explicitly. The induced magnetic field can be seen in Figure 4.4.

Since we are now in the case of horizontal as well as radial currents, the induced magnetic field consists of a poloidal and a toroidal part. To reconstruct poloidal currents from the toroidal magnetic field the following method is used, which has already been described in [7] and applied to CHAMP magnetic field measurements in [43] and [47].

Reconstruction of Radial Current Densities

As we have seen in (4.10) the connection between toroidal magnetic field scalar Q_b and the radial current density J_{rad} at the same height is given by

$$J_{rad}(r\xi) = \xi \cdot j(r\xi) = \frac{\Delta_\xi^* P_j(r\xi)}{r} = \frac{\Delta_\xi^* Q_b(r\xi)}{\mu_0 r} \quad r > 0, \xi \in \Omega. \quad (4.56)$$

Using the vector scaling function of type 3, $\varphi_J^{(3)}$, defined in Section 3.2 with a suitable chosen maximum scale J we are able to approximate the toroidal part, q_b , of the magnetic field b on Ω_r . Thus we have

$$q_b(r \cdot) \simeq \varphi_J^{(3)} \star \left(\varphi_J^{(3)} * b \right) = \sum_{J'=0}^J \psi_{J'}^{(3)} \star \left(\psi_{J'}^{(3)} * b \right),$$

in the sense of the $l^2(\Omega)$ -norm, where the functions $\psi_J^{(3)}$ are the vector wavelets of type 3 introduced in Section 3.2. Observing the fact, that $p_b = L^*Q_b$ we immediately get an approximation of the toroidal scalar, Q_b , by

$$Q_b(r \cdot) \simeq \Phi_J * \left(\varphi_J^{(3)} * b \right) = \sum_{J'=0}^J \Psi_{J'} * \left(\psi_{J'}^{(3)} * b \right), \quad (4.57)$$

in the sense of the $\mathcal{L}^2(\Omega)$ -norm, where the kernels Φ_J and Ψ_J are, for $\xi, \eta \in \Omega$, given by

$$\begin{aligned} \Phi_J(\xi, \eta) &= \sum_{(n,k) \in \mathcal{N}^{(3)}} \frac{1}{\sqrt{n(n+1)}} \left(\varphi_J^{(3)} \right)^\wedge(n) Y_{n,k}(\eta) Y_{n,k}(\xi), \\ \Psi_J(\xi, \eta) &= \sum_{(n,k) \in \mathcal{N}^{(3)}} \frac{1}{\sqrt{n(n+1)}} \left(\psi_J^{(3)} \right)^\wedge(n) Y_{n,k}(\eta) Y_{n,k}(\xi) \end{aligned}$$

and $(\varphi_J^{(3)})^\wedge(n)$ and $(\psi_J^{(3)})^\wedge(n)$ are the symbols of the vector scaling function $\varphi_J^{(3)}$ of type 3 and the vector wavelet $\psi_J^{(3)}$ of type 3, respectively, used in (4.57). Using the fact that $\varphi_J^{(3)}(\eta, \xi) = L_\xi^* \Phi_J(\eta, \xi)$ and $\psi_J^{(3)}(\eta, \xi) = L_\xi^* \Psi_J(\eta, \xi)$ for $\xi, \eta \in \Omega$ and observing (4.56) we end up with an approximation of the radial current density J_{rad} on Ω_r given by

$$J_{rad}(r\xi) \simeq \frac{1}{r\mu_0} \left(\tilde{\Phi}_J * \left(\varphi_J^{(3)} * b \right) \right) (\xi) \quad (4.58)$$

$$= \frac{1}{r\mu_0} \sum_{J'=0}^J \left(\tilde{\Psi}_{J'} * \left(\psi_{J'}^{(3)} * b \right) \right) (\xi) \quad \text{for } \xi \in \Omega, \quad (4.59)$$

where the scalar valued kernels $\tilde{\Phi}_J$ and $\tilde{\Psi}_J$ are, for $\xi, \eta \in \Omega$, given by

$$\begin{aligned} \tilde{\Phi}_J(\xi, \eta) &= \Delta_\xi^* \Phi_J(\eta, \xi) \\ &= \sum_{(n,k) \in \mathcal{N}^{(3)}} -\sqrt{n(n+1)} \left(\varphi_J^{(3)} \right)^\wedge(n) Y_{n,k}(\eta) Y_{n,k}(\xi), \\ \tilde{\Psi}_J(\xi, \eta) &= \Delta_\xi^* \Psi_J(\eta, \xi) \\ &= \sum_{(n,k) \in \mathcal{N}^{(3)}} -\sqrt{n(n+1)} \left(\psi_J^{(3)} \right)^\wedge(n) Y_{n,k}(\eta) Y_{n,k}(\xi). \end{aligned}$$

Expression (4.58) connects the toroidal part of the magnetic field on a certain height to the radial current density at that very height in terms of radial basis functions. This equation yields the possibility to compute the radial current density J_{rad} from given magnetic field data on a certain height numerically in a multiscale framework. The equation is just a different expression for the well known fact that the toroidal magnetic field at a certain altitude is solely due to the radial currents crossing the sphere at that height.

In Figure 4.5, Figure 4.6 and Figure 4.7 three reconstructions of the radial current density at satellite's height (400 km) of the simulated Cowling channel can be seen. In the low scale reconstruction, radial currents densities are detected but they are not clearly resolved. The three line currents which are flowing towards the Earth on the right side and away on the left side are reconstructed as one current system. If we now increase the scale, then it can be seen that there is a second high frequent structure embedded in the two current systems crossing the satellite's sphere. If we increase the scale of the reconstruction scaling functions another time the real structure of the current system becomes visible, i.e. the three line currents are resolved. To approximate such a detailed structure is almost impossible using scalar or vector spherical harmonics.

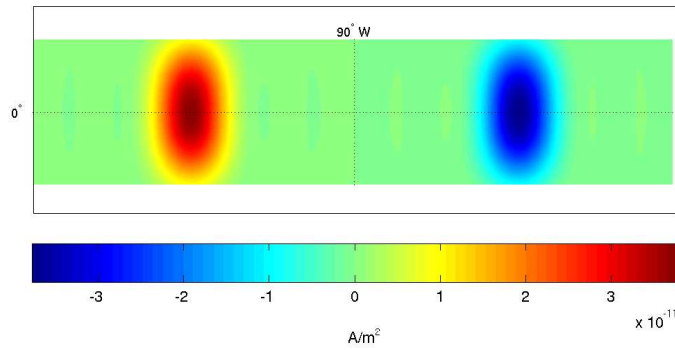


Figure 4.5: Radial current density at a height of 400 km of the simulated Cowling channel obtained by a cubic polynomial scaling function given in (4.58) at scale $J = 8$. Radial currents are detected but the exact shape of the current system can not be resolved at this scale.

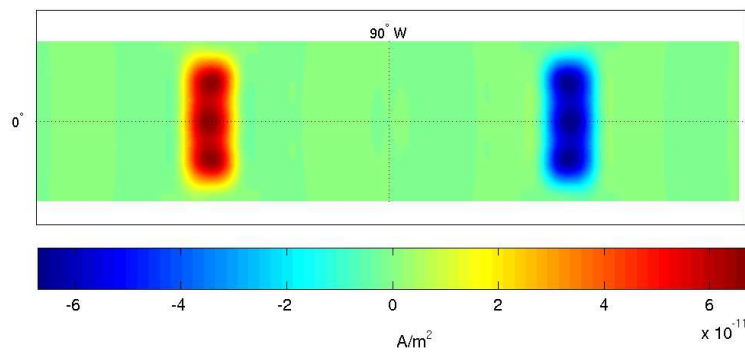


Figure 4.6: Radial current density at a height of 400 km of the simulated Cowling channel obtained by a cubic polynomial scaling function given in (4.58) at scale $J = 9$. The high frequent structure of the current system can be anticipated.

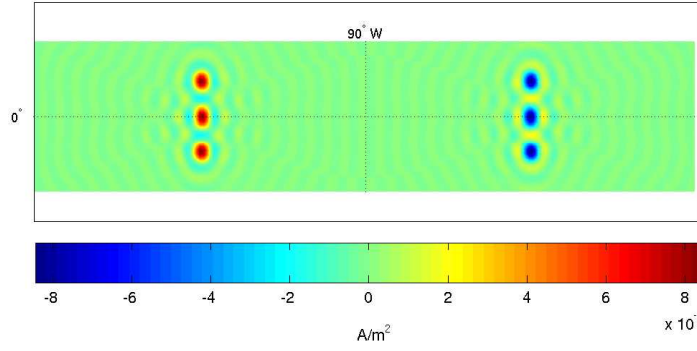


Figure 4.7: Radial current density at a height of 400 km of the simulated Cowling channel obtained by a cubic polynomial scaling function given in (4.58) at scale $J = 11$. The complete structure of the current system, i.e. the three line currents are resolved.

Reconstruction of Toroidal Currents

In the following paragraph we apply our method developed in Section 4.2 to reconstruct the horizontal toroidal part of the current system from the simulated magnetic field data. Since the current system that we reconstruct is below the (simulated) satellite's orbit we are in the case of $R_2 > R_1$ and the Hilbert space framework states as follows. We have to regularize

$$T_{R_1, R_2} : \mathfrak{h} \rightarrow \mathfrak{k},$$

where T_{R_1, R_2} is the spherical Biot-Savart operator given in Definition 4.2 and

$$\begin{aligned} \mathfrak{h} &= l_{\mathcal{U}}^{2,(3)}(\Omega_{R_1}), & \{h_{n'}\} &= \{-u_{n,k}^{(3),R_1}\}_{k=1,\dots,2n+1}^{n=1,\dots;}, \\ \mathfrak{k} &= l_{\mathcal{U}}^{2,(1)}(\Omega_{R_2}), & \{k_{n'}\} &= \{u_{n,k}^{(1),R_2}\}_{k=1,\dots,2n+1}^{n=1,\dots;}, \\ \sigma_{n'} &= \sqrt{\frac{n}{2n+1}} \left(\frac{R_1}{R_2}\right)^{n+1}, & n' &\in \mathbb{N}. \end{aligned}$$

The corresponding reconstruction and decomposition regularization scaling functions are given as in the previous section.

The final result, a reconstruction of the current system at a height of 100 km with a regularization vector cubic polynomial scaling function at scale $J = 7$ can be seen in Figure 4.8. In the right of Figure 4.9 the $-\varepsilon^\varphi$ -component (geomagnetic negative Y-component) of the reconstructed current system along the 90° -meridian for different scales is plotted. As in the previous example of the simulated ring current, it is clearly visible that the reconstruction is improved from one scale to the next one. The left of Figure 4.9 shows a zoomed-in version of the reconstructed current system of Figure 4.8 including the original simulated current system.

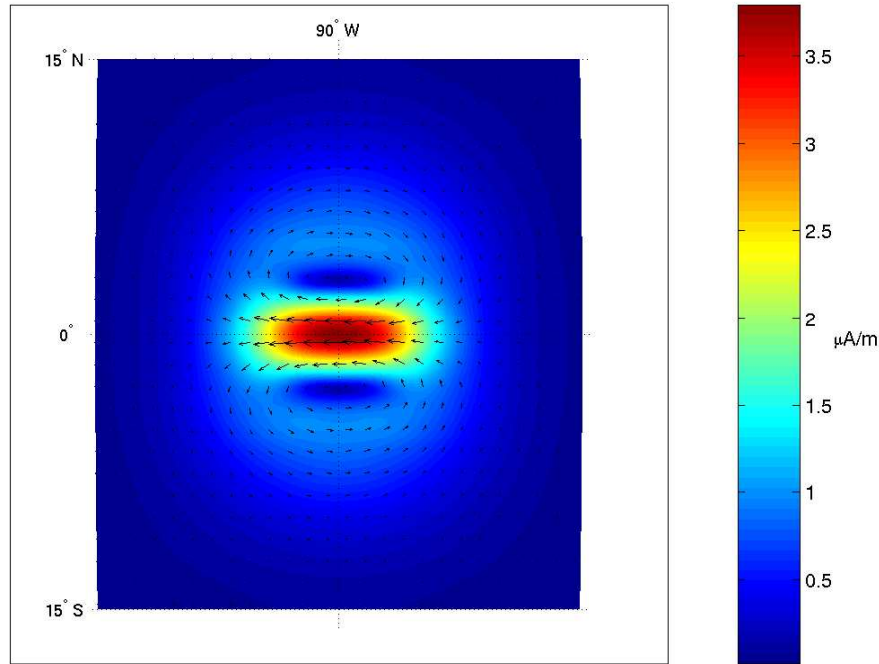


Figure 4.8: Reconstruction of the horizontal current system of the simulated Cowling channel obtained with a regularization vector cubic polynomial scaling function at scale $J = 7$.

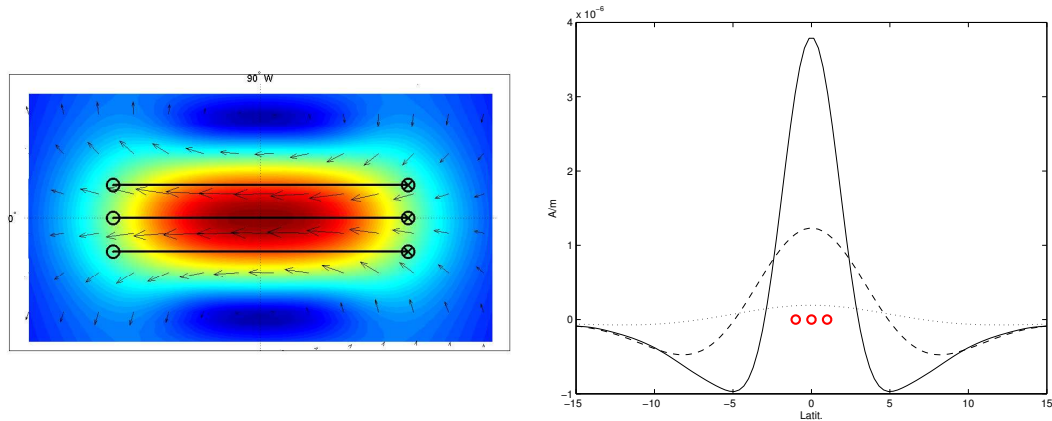


Figure 4.9: Left: Zoom in into Figure 4.8 with original simulated current system. Right: Absolute value of the $-\varepsilon^\varphi$ -component of the reconstructed current system along the 90° -meridian for scales $J = 5$, $J = 6$ and $J = 7$. The red circles give the position of the original simulated current system.

As the reader can see the reconstruction of the horizontal part of the current system is qualitatively very good, i.e. the reconstruction reflects the shape of the simulated current system and it is at the right position. But on the other hand the magnitude

of the reconstruction absolutely fails to approximate the strength of the original current system. This can be explained as follows. The horizontal current system which we have simulated in this case consists of three line currents. If we characterize these current systems in the sense of the $l^2(\Omega_{R_1})$ Hilbert space we find out that their norm is *zero* because the current system is defined on a set of measure zero. This formally means that we are not able to reconstruct the current system from the magnetic field data because our theory developed in Chapter 2 is based on the regularization of a compact operator between two Hilbert spaces. But this means that we have to reconstruct the zero function in the Hilbert space of functions which represents the current systems (i.e. in $l^2(\Omega)$).

What we see in Figure 4.8 and Figure 4.8 is clearly not an approximation of the zero function, but it is a current system which induces the same magnetic field on the satellite's orbit as the simulated line currents system. This reconstructed current system is called *equivalent current system* in the geophysical literature (see [1], [4], [36] and [37]).

Our theory developed in Section 4.2 and Section 4.3 is geophysically based on the reconstruction of these equivalent current systems. As we have already stated in Section 4.1 we are not able to reconstruct the complete three-dimensional current system from the magnetic field information on just a single sphere. The best thing we can do is to reconstruct the poloidal part of the current system on satellite's height from the toroidal part of the magnetic field measurements (see Figure 4.7) and to reconstruct an equivalent toroidal current system below the satellite's altitude from the poloidal part of the magnetic field measurements (see Figure 4.8). This toroidal current system is a height integrated current system representing all toroidal currents existing below the satellite's orbit. Thus, the height of this equivalent current is best chosen to be the height, where the main toroidal currents exist (in this example 100 km and in most geophysical applications 110 km (see e.g. [1], [4] or [37])).

4.4.3 An Application to MAGSAT Magnetic Field Data

In the following section we apply our previously tested algorithms for reconstructing ionospheric current systems to real satellite data. At first we will apply our multiscale technique of reconstructing radial current densities on satellite's height due to (4.58). In [51] a similar technique, in terms of spherical harmonics, is applied to MAGSAT data and in [43] radial current densities have been reconstructed from given MAGSAT magnetic field data by means of wavelet techniques. The radial current distributions are due to ionospheric F region currents and their radial compensation currents. In a second step we apply the method presented in Section 4.2 and Section 4.3 to reconstruct a horizontal equivalent current system at an altitude of $R_1 = 110\text{ km}$ from the given satellite's magnetic field data.

The data sets used in this application are similar to those in [51]. They have been made available to us by Nils Olsen, the author of [51], who has also done the whole preprocessing and averaging process. MAGSAT was a low flying satellite with a

Sun synchronous orbit, thus the satellite was measuring the magnetic field only at dawn and dusk local times. Neglecting the variations in altitude of the satellite, one month of data (centered at March 21, 1980) are averaged onto the equiangular longitude-latitude grid at mean altitude R_2 which has already been used in the previous sections for numerical integration (see [15]). As stated before, the averaging process was done by Nils Olsen using his method which is presented in [51]. The dusk and dawn data are treated separately such that two separate data sets are obtained. Prior to the averaging process a geomagnetic main field model (GSFC(12/83) up to degree and order 12) has been subtracted from the measurements in order to avoid any effects due to neglected altitude variations. For a detailed description of the data preprocessing and handling the reader is again referred to [51].

The radial current distribution at a fixed height and the corresponding magnetic field can be connected in a multiscale framework by Equation (4.58). As in the previous application we calculate the radial current density by means of a vector cubic polynomial scaling functions of degree $J = 6$ from the evening data set. Figure 4.10 shows the reconstruction of the radial current density J_{rad} .

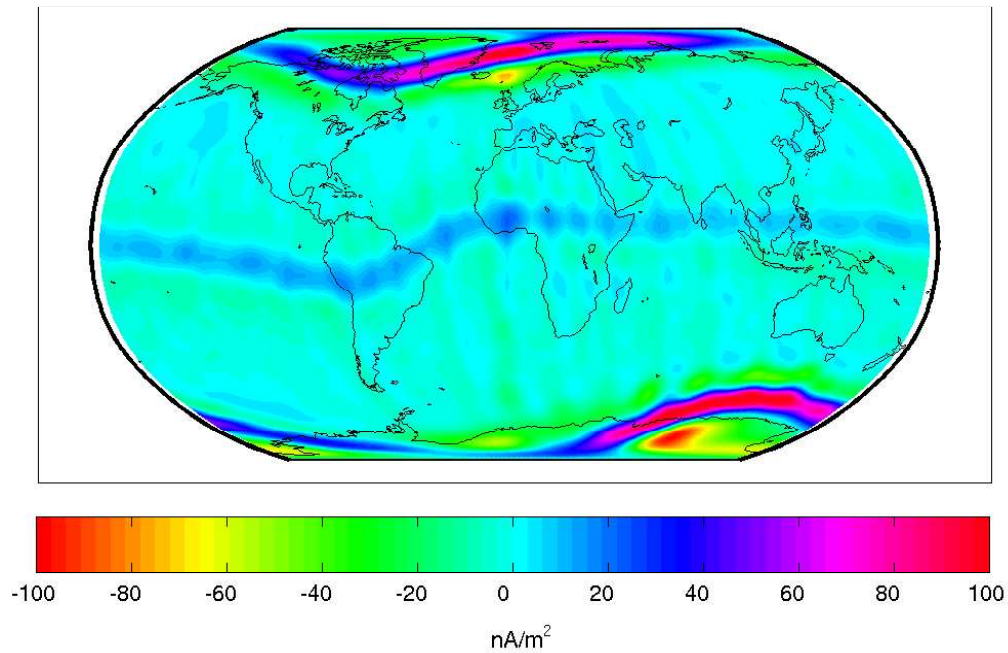


Figure 4.10: Radial current distribution during evening local time calculated in accordance with Equation (4.58) using a vector cubic polynomial scaling function expansion at scale $J = 6$.

The largest radial current densities are present in polar regions. At the magnetic geomagnetic equator comparatively weak upward currents are detected. These current distributions are due to vertical compensation currents of the equatorial electrojet which is a typical ionospheric F region current system built up by a Cowling channels which has been discussed in the previous section. The signatures follow the

geomagnetic equator which is expected from theoretical considerations concerning a Cowling channel (see [37]). The reader should observe that the current system will never be present as we see it in Figure 4.10. What we see is the behavior of a small part of the equatorial electrojet's radial compensation currents during the course of a day. This is because ionospheric current systems can not be described in an Earth fixed coordinate system. Ionospheric currents are Sun fixed systems since the conductance of the ionosphere is varying with the influence of the Sun and not with respect to geographical longitude and latitude. A better coordinate system to describe these effects is given by the magnetic local time and the quasi dipole latitude which is presented in Section 4.4.5. Since MAGSAT with its Sun synchronous orbit is measuring the magnetic time only in two fixed magnetic local times, it is not possible to get a real good image of the ionospheric current systems from this data. Moreover, we get an impression of a small strip of the total current system while moving over the Earth within a day.

In a second step we apply the method presented in Section 4.2 to the MAGSAT data set. In order to get just the magnetic field which is due to horizontal ionospheric current systems we subtract the evening and the morning data set. As we have seen before, at evening local time, ionospheric current systems are present while we can assume that in the morning data the influence of those currents systems is comparatively small. Since we reconstruct the toroidal part of the ionospheric current system from the poloidal part of the magnetic field measurements and since we are in the case of $R_2 > R_1$, only Equation (4.44) of Corollary 4.8 plays a role in our regularization step. i.e. we have to regularize

$$T_{R_1, R_2} : \mathfrak{h} \rightarrow \mathfrak{k},$$

where T_{R_1, R_2} is the spherical Biot-Savart operator given in Definition 4.2 and

$$\begin{aligned} \mathfrak{h} &= l_{\mathcal{U}}^{2,(3)}(\Omega_{R_1}), & \{h_{n'}\} &= \{-u_{n,k}^{(3),R_1}\}_{k=1,\dots,2n+1}^{n=1,\dots;}, \\ \mathfrak{k} &= l_{\mathcal{U}}^{2,(1)}(\Omega_{R_2}), & \{k_{n'}\} &= \{u_{n,k}^{(1),R_2}\}_{k=1,\dots,2n+1}^{n=1,\dots;}, \\ \sigma_{n'} &= \sqrt{\frac{n}{2n+1}} \left(\frac{R_1}{R_2}\right)^{n+1}, & n' &\in \mathbb{N}. \end{aligned}$$

The corresponding decomposition and reconstruction regularization vector scaling functions are then given as in the previous sections.

The result of our reconstruction with a regularization vector cubic polynomial scaling function at scale $J = 6$ can be found in Figure 4.11. The strong influence of the ring currents around the poles can be seen. But also the current system of the equatorial electrojet can clearly be seen. The strange current systems at the zero meridian in the middle of the figure is not a real current system but it is more or less due to errors in the averaging process, since, as already stated at the reconstruction of the radial current densities from given MAGSAT data, we are just able to reconstruct a small time band of the ionospheric current system smeared out over

the Earth. Thus, any averaging error or a gap in the data coverage will produce an artificial current system which is not physically motivated and which is not present in reality.

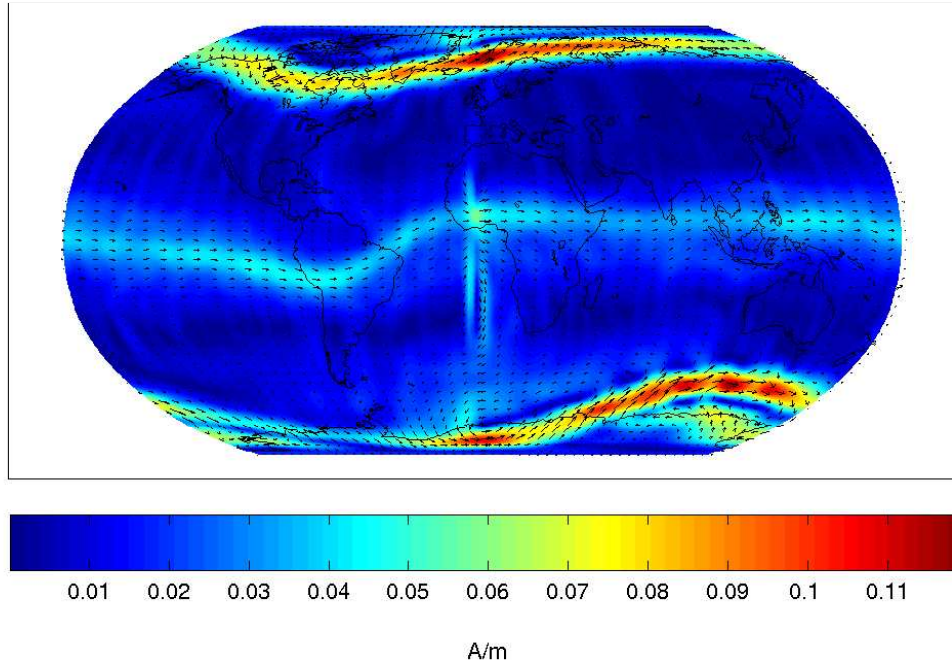


Figure 4.11: Equivalent horizontal current distribution during evening local time at a height of 110 km calculated from MAGSAT magnetic field measurements using a regularization vector cubic polynomial scaling function expansion at scale $J = 6$.

In order to show the possibilities of regional calculations, Figure 4.12 presents a reconstruction of the horizontal current distribution during evening local time along the magnetic equator at a height of 110 km . The result is obtained using regularization vector cubic polynomial scaling functions at scale $J = 6$. The data window was chosen slightly larger than the reconstruction area in the case of a local reconstruction in order to suppress Gibbs phenomena at the boundary of the visualization area.

Figure 4.13 shows the course of the equatorial electrojet during a day. In this figure the area where the absolute value of the ε^φ -component (geomagnetic Y-component) of the current system is larger than 90% of its maximum on the corresponding meridian is coloured red.

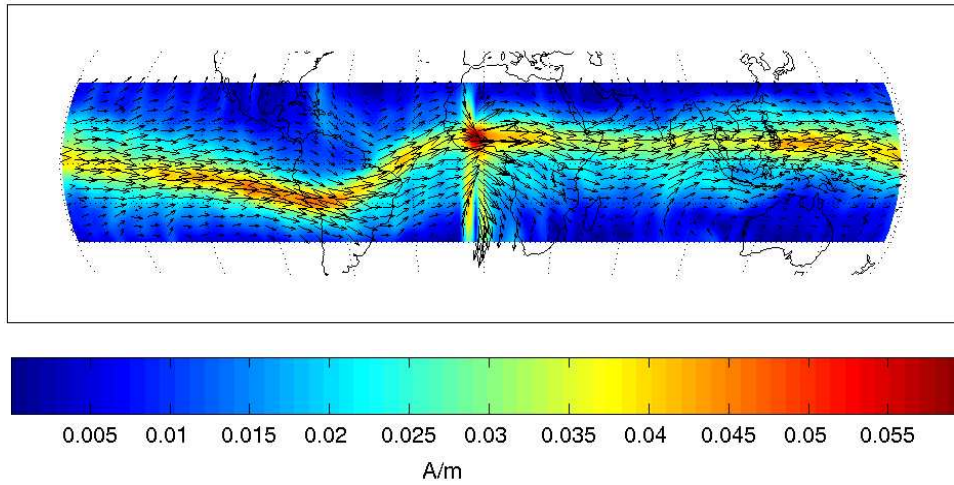


Figure 4.12: Local reconstruction of the equivalent horizontal current distribution during evening local time at a height of 110 km calculated using a regularization vector cubic polynomial scaling function expansion at scale $J = 6$.

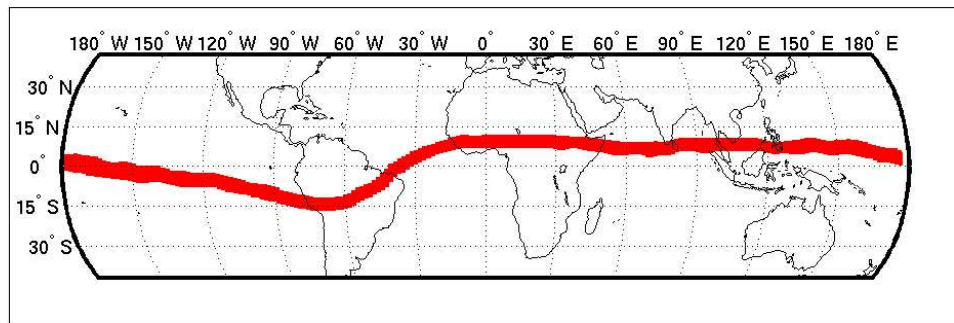


Figure 4.13: Course of the equatorial electrojet during a day. Red area indicates $|j \cdot \varepsilon^\varphi|$ to be larger than 90% of the maximum along the corresponding meridian.

4.4.4 An Application to CHAMP Magnetic Field Data

The next step in testing our methods for reconstructing ionospheric current systems from given magnetic field data is the application to data measured by the CHAMP satellite. In contrast to the MAGSAT mission CHAMP is covering all local times within approximately four months. As we have already stated before, the Earth fixed coordinate system (lat, lon) is not the appropriate one to describe ionospheric currents and their corresponding magnetic effects, because these systems are varying with respect to the position of the Sun and not with respect to the Earth. Thus, we will change the parametrization of the sphere to a new coordinate system given by the magnetic local time (MLT) substituting the longitude and the quasi dipole latitude (QDlat) instead of the latitude. This new coordinate system will be explained in more detail during the course of the section.

We will apply in this section both, our method of reconstructing radial current densities on satellite's height due to (4.58) and the approach of reconstructing a horizontal equivalent current system from given CHAMP satellite's magnetic field data presented in Section 4.2 and Section 4.3 in this new coordinate system.

Reconstruction of Current Systems in Magnetic Local Time

The morphology of the geomagnetic variations produced by ionospheric currents can only weakly be represented in a coordinate system which is Earth fixed. This is because the magnetic field induced by currents is not linked to geographical longitude and latitude as, for example, is the lithospheric field. It is rather fixed to the position of the Sun and the distance of the observer (in this case the satellite) to the geomagnetic equator. Thus, in order to describe these phenomena we have to change the reference system from an Earth fixed frame to a Sun fixed frame. A coordinate system which is commonly used in geophysics in this context is the Magnetic Local Time (MLT) and Quasi Dipole Latitude (QDlat). The magnetic local time thereby denotes the relative position of the observer with respect to the magnetic field and the Sun and the quasi dipole latitude represents the relative position of the observer with respect to the geomagnetic equator. In Figure 4.14 a single day (9. September 2001) of the position of CHAMP measurements can be seen in the geographical coordinate system (lat,lon) and the Sun fixed reference frame (QDlat, MLT). For more information concerning the description of geomagnetic coordinate system the reader is referred to [56] or [58] and the reference therein.

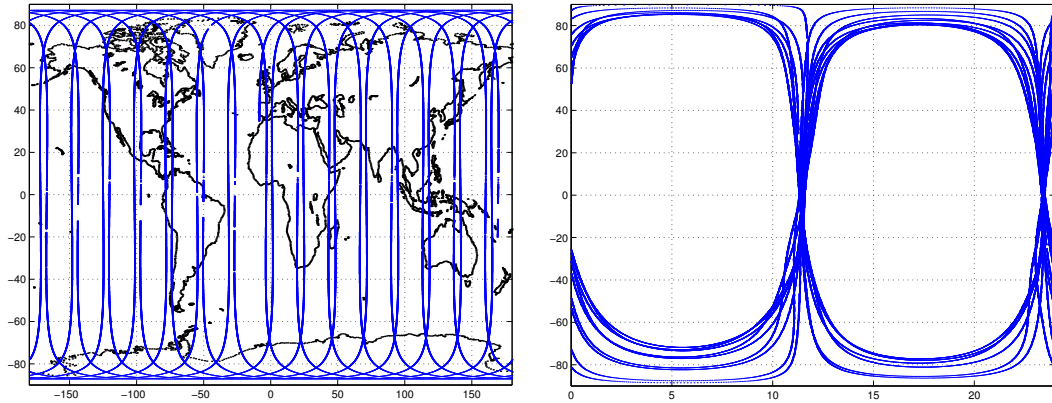


Figure 4.14: Left: Position of one day (20.09.2001) of CHAMP measurements in the Earth fixed geographic coordinate system (lat, lon). Right: The same day in the Sun fixed coordinate system (QDlat, MLT).

To show that our method is also able to handle data in this coordinate system we take just three days of CHAMP data (10., 16. and 17. September 2001) which were available at the internet page http://www.dsri.dk/multimagsatellites/types/equatorial_electrojet.html. In these days CHAMP was at 12.30 and

00.30 local time. The advantage of these data sets is the explicitly given main field, crustal field and magnetospheric ring current correction such that these complicated steps can be avoided. We transform the data to the (MLT, QDlat) coordinate system by use of an algorithm made available by the GFZ Potsdam and implemented by Nils Olsen from the DSRI Copenhagen. Then, we average the data to an equiangular integration grid (in the coordinate system (MLT, QDlat)) using the algorithm presented in Section 3.4. The reference system (MLT, QDlat), with values $QDlat \in [-90, 90]$ and $MLT \in [0, 24]$ is thereby just seen as another coordinate system parameterizing the unit sphere where the magnetic local time is seen as a linear transformation of the longitude with $MLT = 12$ representing the zero meridian.

We apply the method presented in Section 4.2 to the CHAMP data set in the Sun fixed reference frame (MLT, QDlat) in order to reconstruct the toroidal part of the equivalent ionospheric current system from the poloidal part of the magnetic field measurements. Since we are in the case of $R_2 > R_1$, only Equation (4.44) of Corollary 4.8 plays a role in our regularization step. The functionalanalytic framework is given as follows. We have to regularize

$$T_{R_1, R_2} : \mathfrak{h} \rightarrow \mathfrak{k},$$

where T_{R_1, R_2} is the spherical Biot-Savart operator given in Definition 4.2 and

$$\begin{aligned} \mathfrak{h} &= l_{\mathcal{U}}^{2, (3)}(\Omega_{R_1}), & \{h_{n'}\} &= \{-u_{n,k}^{(3), R_1}\}_{\substack{n=1, \dots; \\ k=1, \dots, 2n+1}}, \\ \mathfrak{k} &= l_{\mathcal{U}}^{2, (1)}(\Omega_{R_2}), & \{k_{n'}\} &= \{u_{n,k}^{(1), R_2}\}_{\substack{n=1, \dots; \\ k=1, \dots, 2n+1}}, \\ \sigma_{n'} &= \sqrt{\frac{n}{2n+1}} \left(\frac{R_1}{R_2}\right)^{n+1}, & n' &\in \mathbb{N}. \end{aligned}$$

The corresponding decomposition and reconstruction regularization vector scaling functions are then given as in the previous sections.

The result of our reconstruction with a regularization vector cubic polynomial scaling function at scale $J = 3$ can be seen in Figure 4.15. The maximal strength of the detected equivalent ionospheric current system is approximately 10 mA/m . According to [12] and [39] the amplitude of the solar quiet mid latitude ionospheric current systems is $10 - 36 \text{ mA/m}$. This shows that the detected current system is in the lower band width of the real ionospheric current systems. Since the scale of reconstruction is very low it can be assumed that the real strength of the current system is higher than the reconstructed amplitude.

With respect to the given amount of data (3 days of CHAMP magnetic field measurements) the reconstructed current system shown in Figure 4.15 is a good result. It demonstrates that the used trial functions, i.e. regularization vector scaling functions and wavelets, are a good choice for handling the problem. As already mentioned in [37] the main disadvantage of spherical harmonics is that the reconstructed current system on the day-side of the Earth will appear on the night-side as well because of symmetry arguments. This problem does not appear if scaling functions

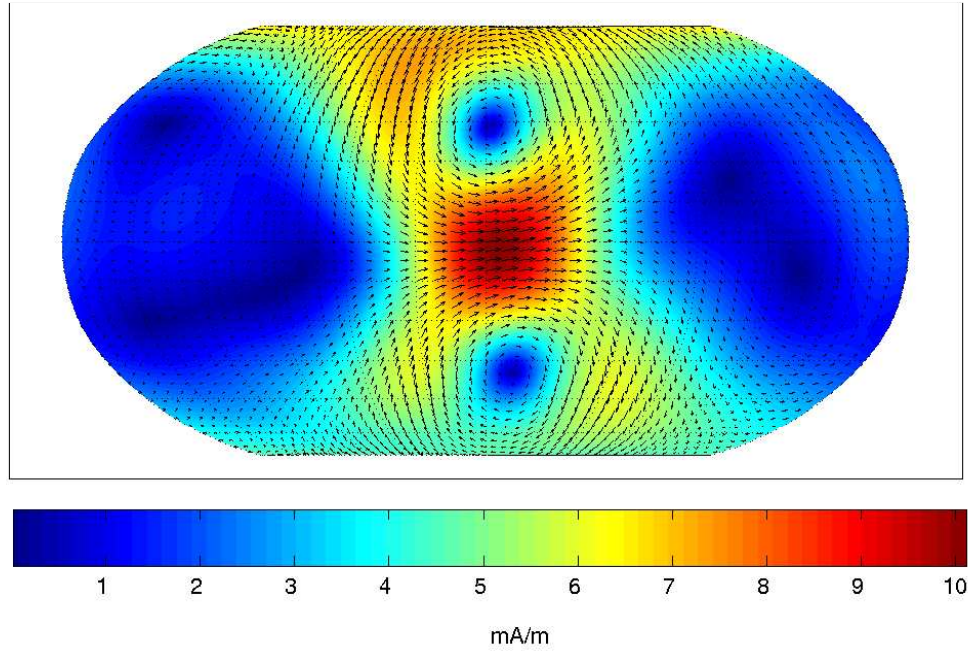


Figure 4.15: Equivalent horizontal current distribution in the Sun fixed coordinate system (QDlat, MLT) at a height of 110 km calculated using a regularization vector cubic polynomial scaling function expansion at scale $J = 3$.

and wavelets are used. These kernel functions do not fulfill an exact frequency localization property which is not needed for the reconstruction of the current system anyway, but they provide the possibility of space localizing reconstruction and this property is much more important for the reconstruction of a ionospheric current distribution from given magnetic field measurements.

In order to demonstrate the regional applicability of the presented multiscale techniques for reconstructing ionospheric current systems from CHAMP magnetic field data we present two local applications in the following.

At first we reconstruct the radial current density at satellite's height from the data in the Sun fixed reference frame (QDlat, MLT). The radial current distribution at a fixed height and the corresponding magnetic field at the same height are connected in a multiscale framework by Equation (4.58). As in the previous applications to MAGSAT data and to the simulated Cowling channel we calculate the radial current density by means of a vector cubic polynomial scaling functions of degree $J = 6$ from the data set. Figure 4.16 shows a local reconstruction of the radial current density J_{rad} over the north pole. The obtained radial current distribution is in correspondence with the models of these current systems of polar regions discussed in [34] and [53].

In a second local application we calculate the toroidal part of the equivalent ionospheric current system at a height of 110 km from the poloidal part of the CHAMP magnetic field measurements. The local reconstruction is performed in a region

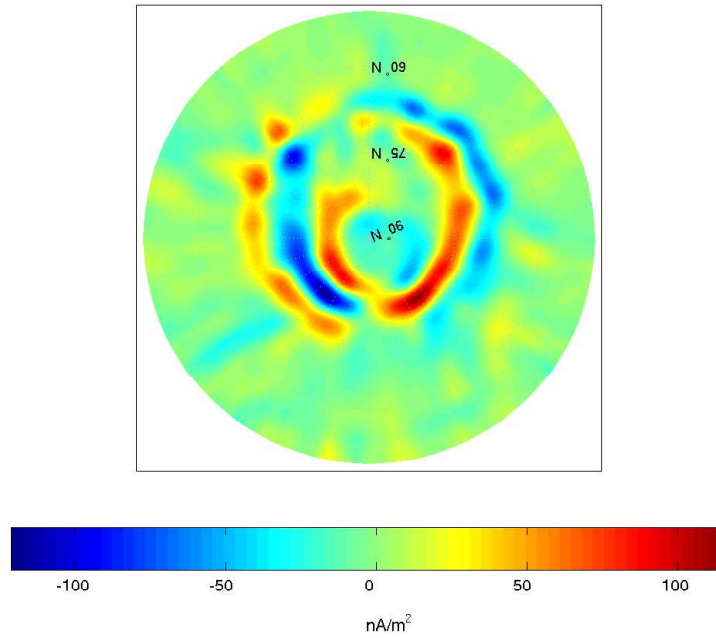


Figure 4.16: Radial current distribution in the coordinate system (MLT, QDlat) calculated using Equation (4.58) with a vector cubic polynomial scaling function expansion at scale $J = 6$ over the geomagnetic north pole.

given by $QDlat \in [-30, 30]$ and $MLT \in [08.00, 16.00]$, i.e. in an area where strong ionospheric current systems like the equatorial electrojet are present. For this reconstruction we took data of several months between September 2001 and June 2002 in order to get a good coverage of measurements in the region of interest. Main field, crustal field and magnetospheric ring current corrections have been executed as described in Appendix A. Furthermore, several data selection steps have been applied in order to filter out tracks with particular high residuals. For further information concerning data selection and preprocessing see Appendix A.

The functionalanalytic framework is given as before. The reconstruction of the equivalent ionospheric current system with a regularization vector cubic polynomial scaling function at scale $J = 5$ can be seen in Figure 4.17. The maximal reconstructed strength of the current system is approximately 25 mA/m which is a more realistic value than the amplitude of the reconstruction in Figure 4.15 which is due to the increased scale. The structure of the reconstructed ionospheric current system in Figure 4.17 is not like the reader might expect in equatorial regions, which can be explained by gaps in the data coverage and by the presence of disturbed data due to temporally fast changing field aligned currents or other effects.

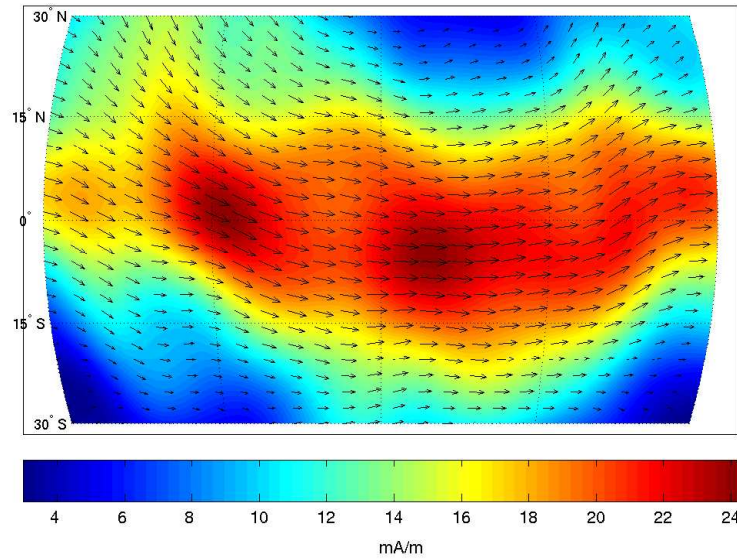


Figure 4.17: Local reconstruction ($QDlat \in [-30, 30]$, $MLT \in [08.00, 16.00]$) of the equivalent ionospheric current distribution at a height of 110 km calculated using a regularization vector cubic polynomial scaling function expansion at scale $J = 5$.

4.4.5 An Application to SWARM Magnetic Field Data

In the following section we give an example how the multiscale method of reconstructing current systems from magnetic field data can be used in connection with the proposed satellite mission SWARM, and how the constellation of this satellite mission can be used to improve the knowledge of ionospheric current systems.

SWARM is a satellite mission proposed by a consortium of 27 institutes and universities under the leadership of the Danish Space Research Institute (DSRI Copenhagen). It is designed to study the dynamics of the Earth's magnetic field and its interactions with the system Earth. The concept consists of a constellation of four satellites of the CHAMP type in two different polar orbits between 400 km and 550 km altitude. The proposed configuration over a period of 5 years is illustrated in Figure 4.18.

To simulate the SWARM mission and to emphasize its advantages a simulator (based on the comprehensive model of the near-Earth magnetic field described in [58]) has been implemented at the GFZ Potsdam and the data have been made available at the DSRI Copenhagen. For more information concerning SWARM and the EndToEnd simulation of the SWARM mission the reader is referred to [40] and to the internet page <http://www.dsri.dk/swarm/>.

Reconstruction in Magnetic Local Time

To show that our method is also able to handle a big amount of data in the Sun fixed coordinate system (MLT, $QDlat$) we take 60 days of data between January 2000 and April 2000 of one of the low flying SWARM satellite's. Since the satellite is flying a quasi circular orbit with nearly no polar gap, the rotation of the plane

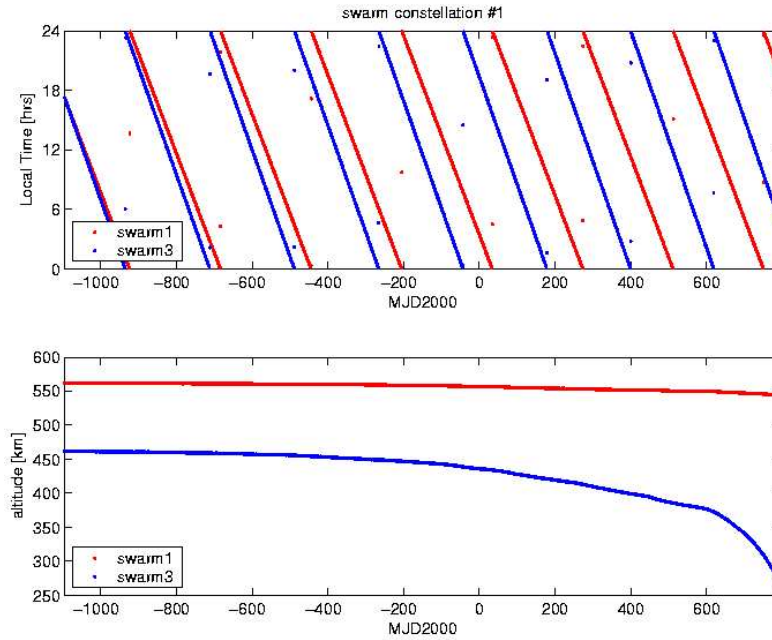


Figure 4.18: Constellation of the simulation of the proposed SWARM satellite mission. The simulated period of the mission is 1997 - 2002. In the upper figure the local time behavior of the four satellites can be seen. In the lower figure the altitude of respectively two satellites during the course of the mission is illustrated.

where the satellite is flying in with respect to the Sun is very slow. Thus, the period of 4 months is necessary to get data within all magnetic local times which can be seen in the upper part of Figure 4.18.

As before the data are transformed to the (MLT, QDlat) coordinate system and averaged to an equiangular integration grid (in the coordinate system (MLT, QDlat)) using the algorithm presented in Section 3.4.

The ionospheric current system which has been used to simulate SWARM magnetic field data is a purely toroidal, horizontal current system at a height of 110 km (see [58]). Thus, in order to apply our method developed in Section 4.2 to reconstruct the current system corresponding to the simulated magnetic field data we are in the following functionalanalytic situation. We have to regularize

$$T_{R_1, R_2} : \mathfrak{h} \rightarrow \mathfrak{k},$$

where T_{R_1, R_2} is the spherical Biot-Savart operator given in Definition 4.2 and

$$\begin{aligned} \mathfrak{h} &= l_{\mathcal{U}}^{2,(3)}(\Omega_{R_1}), & \{h_{n'}\} &= \{-u_{n,k}^{(3),R_1}\}_{k=1,\dots,2n+1}^{n=1,\dots;}, \\ \mathfrak{k} &= l_{\mathcal{U}}^{2,(1)}(\Omega_{R_2}), & \{k_{n'}\} &= \{u_{n,k}^{(1),R_2}\}_{k=1,\dots,2n+1}^{n=1,\dots;}, \\ \sigma_{n'} &= \sqrt{\frac{n}{2n+1}} \left(\frac{R_1}{R_2}\right)^{n+1}, & n' &\in \mathbb{N}. \end{aligned}$$

The corresponding reconstruction and decomposition regularization scaling functions are given as in the previous sections.

A reconstructed equivalent ionospheric current system at a height of 110 km obtained with a regularization cubic polynomial vector scaling function at scale $J = 5$ can be found in Figure 4.19. The main contours of the ionospheric current system are reconstructed. In order to reconstruct finer details of the current system a higher resolution of the simulated satellite tracks (at the moment $1\text{ sample/min} \simeq 440\text{ km}$ sample distance) would be necessary.

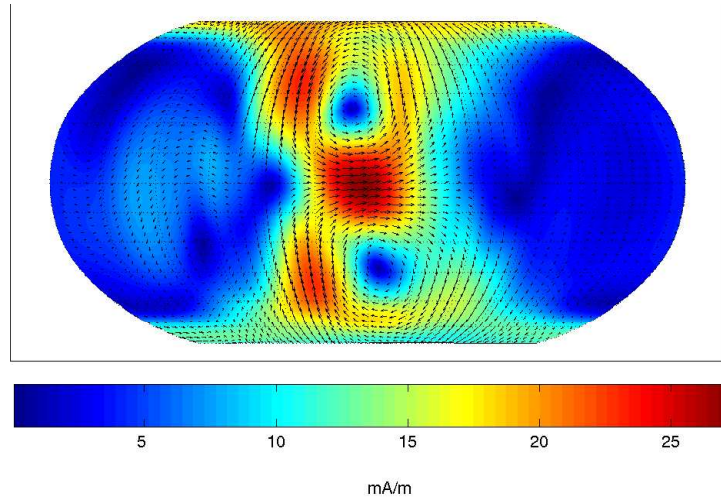


Figure 4.19: Equivalent horizontal current distribution in the Sun fixed coordinate system (QDlat, MLT) at a height of 110 km calculated using a regularization vector cubic polynomial scaling function expansion at scale $J = 5$.

The maximal strength of the detected equivalent ionospheric current system is more than 25 mA/m . As already mentioned before, according to [12] and [39] the amplitude of the solar quiet current system is $10 - 36\text{ mA/m}$.

Determination of the Current Function

In the following paragraph we show that our multiscale approach for reconstructing ionospheric current systems from magnetic field data can even be used to determine the current function of the corresponding current system. But at first we have to define the term current function.

Definition 4.10

Let the spherical vector field $f \in l^2(\Omega)$ be surface divergence free, i.e. there exists a scalar field $F \in \mathcal{L}^2(\Omega)$ with

$$f = L^*F \quad \text{on } \Omega.$$

Then the function F is called a *current function* of the vector field f .

In other words, the current function F is the Helmholtz scalar of type 3 of the vector field f (see Corollary 1.20). Note that the current function as defined in Definition 4.10 is only unique up to a constant. In order to force uniqueness of the definition we have to demand that the integral of F over the unit sphere (Ω) is vanishing, i.e. $\int_{\Omega} F(\xi) d\omega(\xi) = 0$.

Using the regularization vector scaling function which we have introduced in Section 2.4 with a suitable chosen maximum scale J we are able to approximate the toroidal part q_j of the equivalent current system j on Ω_{R_1} . Thus, we have for b being of class $l^2(\Omega_{R_2})$

$$q_j \simeq {}^r\varphi_J \star ({}^d\varphi_J * b) \quad \text{on } \Omega_{R_1},$$

where the decomposition regularization vector scaling functions, $\{{}^d\varphi_J\}$, $J \in \mathbb{Z}$, and the reconstruction regularization vector scaling functions, $\{{}^r\varphi_J\}$, $J \in \mathbb{Z}$, are given by

$$\begin{aligned} {}^d\varphi_J(x, y) &= \sum_{n=1}^{\infty} \sum_{k=1}^{\infty} (\varphi_J)^{\wedge}(n) u_{n,k}^{(1), R_2}(x) Y_{n,k}^{R_2}(y), \quad x \in \Omega_{R_2}, y \in \Omega_{R_2}, \\ {}^r\varphi_J(x, y) &= - \sum_{n=1}^{\infty} \sum_{k=1}^{\infty} (\varphi_J)^{\wedge}(n) u_{n,k}^{(3), R_1}(x) Y_{n,k}^{R_2}(y), \quad x \in \Omega_{R_1}, y \in \Omega_{R_2}, \end{aligned}$$

and the symbol $\{(\varphi_J)^{\wedge}(n)\}_{n=1,2,\dots}$ establishes a multiresolution regularization, i.e. it satisfies the essential property of the generator of a regularization

$$\lim_{J \rightarrow \infty} ((\varphi_J)^{\wedge}(n))^2 = \sigma_n^{-1} = \frac{2n+1}{n} \left(\frac{R_2}{R_1} \right)^{n+1}, \quad n \in \mathbb{N}.$$

Observing the fact, that $q_j = L^*Q_j$ on Ω_{R_1} and using the relation

$$u_{n,k}^{(3), R_1} = \frac{1}{\sqrt{n(n+1)}} L^* Y_{n,k}^{R_1} \quad \text{on } \Omega_{R_1},$$

we immediately get an approximation of the toroidal scalar Q_j by

$$Q_j \simeq \Phi_J * ({}^d\varphi_J * b) \quad \text{on } \Omega_{R_1}, \quad (4.60)$$

where the scalar kernels Φ_J is, for $\xi, \eta \in \Omega$, given by

$$\Phi_J(\xi, \eta) = \sum_{n=1}^{\infty} \sum_{k=1}^n \frac{1}{\sqrt{n(n+1)}} (\varphi_J)^{\wedge}(n) Y_{n,k}^{R_1}(\eta) Y_{n,k}^{R_2}(\xi), \quad (4.61)$$

and $\{(\varphi_J)^{\wedge}(n)\}$ is the symbol of the regularization vector scaling function ${}^r\varphi_J$, resp. ${}^d\varphi_J$ presented above.

Equation (4.60) connects the magnetic field on a certain sphere Ω_{R_2} to the current function Q_j of the equivalent current system j on Ω_{R_1} in terms of radial basis functions. In the general functionalanalytic framework of Chapter 2 the connection

between current function and corresponding magnetic field is given in Table 4.3. As can be seen from the singular values the problem is still of ill-posed nature such that the multiscale regularization technique of Section 2.4 has to be applied.

\mathcal{H}	\mathfrak{E}	$\{h_n\}$	$\{k_n\}$	σ_n
$\mathcal{L}^2(\Omega_{R_1})$	$l_{\mathcal{U}}^{2,(1)}(\Omega_{R_2})$	$Y_{n,k}^{R_1}$	$-u_{n,k}^{(1),R_2}$	$\sqrt{\frac{1}{(n+1)(2n+1)}} \left(\frac{R_1}{R_2}\right)^{n+1}$

Table 4.3: Singular system of the operator, $T : \mathcal{H} \rightarrow \mathfrak{E}$, connecting the current function on a sphere Ω_{R_1} , given in \mathcal{H} , with the corresponding induced magnetic field on a sphere Ω_{R_2} contained in \mathfrak{E} .

In Figure 4.20 we have plotted equipotential lines of the current function of the equivalent current system shown in Figure 4.20.

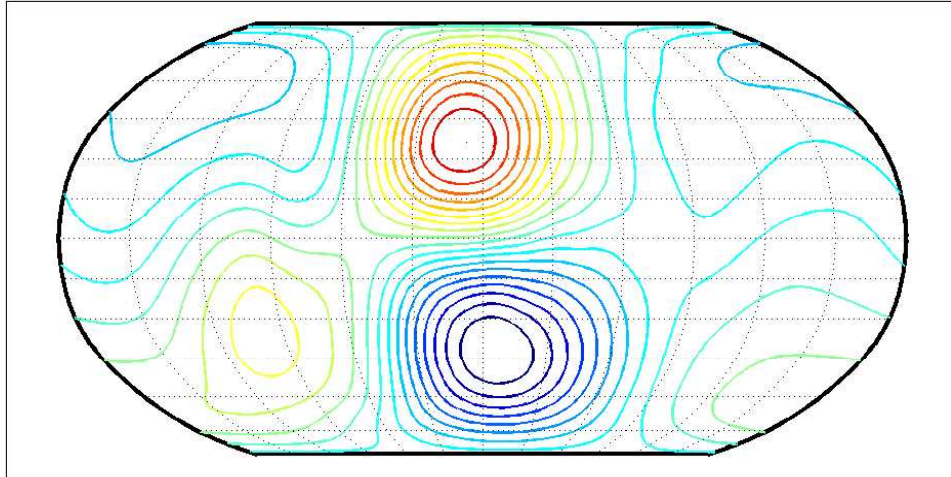


Figure 4.20: Equipotential lines of the current function of the equivalent horizontal current distribution in the Sun fixed coordinate system (QDlat, MLT) calculated using a regularization scalar cubic polynomial scaling function Φ_J defined in Equation (4.61) at scale $J = 5$. Red indicates the maximum strength of the current function while blue indicates the minimum.

Summary and Outlook

During the course of this thesis a comprehensive framework for the connection of ionospheric current systems and the corresponding magnetic field has been developed. A general Hilbert space approach to vector wavelet techniques was introduced in Chapter 2 including multiscale regularization of ill-posed vectorial problems in Section 2.4. From this general principle concrete examples were deduced, i.e. the multiscale decomposition of the identity operator with respect to a special system of vector spherical harmonics in Chapter 3 and the multiscale regularization of the Biot-Savart operator in Chapter 4.

In Chapter 2 we presented a general Hilbert space approach for operator equations with known singular system in a multiscale framework. At first we introduced the scalar case since the necessary notation and the multiscale principle can be explained very well in this case. Then we generalized our concept to the vectorial case and we compared the canonical tensorial approach with the bilinear vectorial approach. Furthermore, we showed that the two techniques are equivalent. In the concept of multiresolution analysis for operator equations the multiscale regularization technique for ill-posed problems can be included which has been done in Section 2.4.

Chapter 3 was concerned with the multiscale decomposition of magnetic field measurements with respect to a special system of vector spherical harmonics. First of all the separation of a spherical vector field with respect to its sources was introduced in a Fourier concept, i.e. the Hilbert space $l^2(\Omega)$ was decomposed by the system of vector spherical harmonics $\{u_{n,k}^{(i)}\}$ into three subspaces. The subspace $l_{\mathcal{U}}^{2,(1)}$ contains that part of the vector field which is induced by sources inside the sphere Ω , the space $l_{\mathcal{U}}^{2,(2)}$ contains the part which is due to sources outside the sphere Ω , and $l_{\mathcal{U}}^{2,(3)}$ contains the toroidal part of the vector field which is induced by the radial projection of the source fields crossing Ω . In the course of Chapter 3 this concept of decomposing a spherical vector field was transferred to the multiscale case. Vector scaling functions and wavelets were introduced which retain the property of separating a vector field with respect to its sources. The main advantage of those kernel functions is the possibility of space localizing decomposition, i.e. they deliver the possibility to decompose a vector field with respect to its sources just by having only regional or even local information. As an application of this multiscale technique a CHAMP magnetic field data set was decomposed and it was shown that, although common techniques for correcting effects of outer sources have been applied, there

are still contributions of outer sources present in the data. These interferences can be corrected by using the presented technique. Furthermore, it was shown that multiscale crustal field determination as presented in [43] can be improved by previously applying the technique of filtering out effects of outer sources introduced in this chapter.

In Chapter 4 the multiscale approach for regularization of vectorial inverse problems developed in Section 2.4 was applied to the problem of reconstructing source terms, i.e. ionospheric current systems, from given magnetic field measurements. To model the problem such that unique solvability is achieved, the concept of a height integrated ionosphere was introduced. The current system and the corresponding magnetic field were connected via the spherical Biot-Savart operator. In order to apply the multiscale techniques of Section 2.4 the singular system of this operator was calculated. Thereby the system of vector spherical harmonics $\{u_{n,k}^{(i)}\}$ plays a decisive role. The central mathematical results of this chapter are the proofs of Theorem 4.6 and Theorem 4.7 which give in connection with Corollary 4.8 and Corollary 4.9 the singular values of the spherical Biot-Savart operator.

To demonstrate the applicability of the approach, the technique was applied to two simulated current systems. The corresponding magnetic field data were simulated using explicit representations or approximate integration rules and then the current system was reconstructed from this data using the multiscale regularization techniques. To demonstrate the advantages of regularization scaling functions and wavelets in contrast to vector spherical harmonics, a space localizing current system was simulated and reconstructed which is not possible with a vector spherical harmonic approach.

Since an essential task of this thesis is the application to satellite data we tested our approach with magnetic field data of three different satellite missions. At first, we calculated current systems from given MAGSAT magnetic field data. The reconstructed current systems gave us a first impression of the shape of the real ionospheric current systems but since MAGSAT was only flying in a small local time band (dawn-dusk orbit), this impression has to be interpreted very carefully. Nevertheless, we were able to calculate the course of the equatorial electrojet over the Earth during a whole day from the MAGSAT data.

In a second satellite application we reconstructed a ionospheric current system corresponding to given CHAMP magnetic field data. For a realistic image of the ionosphere an Earth fixed reference frame is the wrong coordinate system. Thus, we transformed CHAMP magnetic field data to a Sun fixed reference frame given by the magnetic local time (MLT) and the quasi dipole latitude (QDlat). Our calculations could easily be implemented in this new coordinate system. The results achieved in this application gave us a first detailed impression of the real shape of the solar quiet current system in the lower ionosphere. Since only regional magnetic field measurements in this Sun fixed coordinate system were available the advantageous applicability of scaling functions and wavelets could clearly be demonstrated in this context.

In order to apply the multiscale regularization techniques to a global data set in magnetic local time and quasi dipole latitude we used the simulated measurements of the proposed SWARM satellite mission. The achieved result agrees with the model of the ionospheric current system which has been used to simulate SWARM magnetic field data. This demonstrates the applicability of our technique to future satellite missions.

A future task of developing the theory as presented in this thesis, especially as regards Chapter 4, is the generalization to non-spherical geometries. While in the whole thesis we were concerned with problems of multiscale regularization and decomposition in spherical geometries, we will now briefly introduce an approach in non-spherical geometries such that in practical applications it is no longer necessary to consider additional assumptions concerning the geometry of the satellite's orbit. For the sake of brevity we assume that we are interested in the toroidal part of the equivalent spherical current distribution contained in the subspace $l_{\mathcal{U}}^{2,(3)}(\Omega_{R_1})$ and we assume that the magnetic field measurements are taken in $\Omega_{R_1}^{ext}$, the exterior space of Ω_{R_1} . In order to formulate the problem in non-spherical nomenclature we have to use the generalized version of the Biot-Savart operator as defined in Definition 4.1. Let $R_1 > 0$ be given and let $g : \Omega_{R_1} \rightarrow \mathbb{R}^3$ be a vector field of class $l^2(\Omega_{R_1})$. Then the operator $T : l^2(\Omega_{R_1}) \rightarrow c^{(\infty)}(\Omega_{R_1}^{ext})$ is given by

$$f(x) = (Tg)(x) = \frac{1}{4\pi} \int_{\Omega_{R_1}} g(y) \wedge \frac{x-y}{|x-y|^3} d\omega_{R_1}(y), \quad x \in \Omega_{R_1}^{ext}. \quad (4.62)$$

As we have seen in Section 4.2 this definition is equivalent to

$$Tg(x) = \left(\nabla_{x'} \wedge \left(\frac{1}{4\pi} \int_{\Omega_{R_1}} \frac{g(y)}{|x'-y|} d\omega_{R_1}(y) \right) \right)_{x'=x}, \quad x \in \Omega_{R_1}^{ext}. \quad (4.63)$$

The measurements performed by the satellite give us the possibility to derive, from a specific vectorial function g representing the magnetic field, N discrete samples $g(x_l)$ at positions $\{x_1, \dots, x_N\} \subset \Omega_{R_1}^{ext}$. The problem can now be formulated as follows:

Find a function $f \in l_{\mathcal{U}}^{2,(3)}(\Omega_{R_1})$ such that

$$(Tf)(x_l) = g(x_l), \quad l = 1, \dots, N.$$

In order to get an approximation of f we take a scaling function approximation of the function f in $l_{\mathcal{U}}^{2,(3)}(\Omega_{R_1})$, i.e. we substitute f by

$$P_J(f)(x) = \sum_{k=1}^{N_J} a_k \varphi_J^{(3)}(x, y_k), \quad x \in \Omega_{R_1},$$

with $a_i \in \mathbb{R}$, $\{y_1, \dots, y_{N_J}\} \subset \Omega_{R_1}$ and J, N_J sufficiently large. The points $\{y_k\}_{k=1, \dots, N_J}$ are called the model points on the sphere Ω_{R_1} . These points can be taken, for example, to be the integration knots of a certain spherical integration rule. The function

$\varphi_J^{(3)}$ is the spherical scaling function of type 3 defined in Definition 2.2.

The values a_k can be obtained by solving a linear system given by

$$\sum_{k=1}^{N_J} a_k (T \varphi_J^{(3)}(\cdot, y_k))(x_l) = g(x_l), \quad l = 1, \dots, N.$$

The remaining problem is the evaluation of the matrix elements for establishing the linear system, i.e. we have to evaluate for $k = 1, \dots, N_J$

$$(T \varphi_J^{(3)}(\cdot, y_k))(x), \quad x \in \Omega_{R_1}^{ext}.$$

This can be done in accordance to the proof of Theorem 4.7 and Corollary 4.8 and results in

$$\begin{aligned} (T \varphi_J^{(3)}(\cdot, y_k))(x) &= \sum_{n=1}^{\infty} \sum_{k=1}^{2n+1} (\varphi_J^{(3)})^{\wedge}(n) (T u_{n,k}^{(3), R_1})(x) Y_{n,k}^{R_1}(y_k) \\ &= - \sum_{n=1}^{\infty} \sum_{k=1}^{2n+1} (\varphi_J^{(3)})^{\wedge}(n) \sqrt{\frac{n}{2n+1}} \left(\frac{R_1}{r} \right)^{n+1} u_{n,k}^{(1), r}(x) Y_{n,k}^{R_1}(y_k) \end{aligned}$$

with $r = |x| > 0$, $x \in \Omega_{R_1}^{ext}$.

For evaluating the product kernel function connecting the magnetic field and the corresponding current system, fast multipole methods are available. They have been introduced for the scalar case in [30] and [48]. Another possibility of reducing the computational effort of solving the linear system is the application of domain decomposition methods, which have been developed in [31] and [32].

It should be noted that, in general, $N > N_J$ such that the system of linear equations is overdetermined. A possible method to restrict the degree of overdetermination is to choose a subset out of the vast amount of observational data. This subset should ensure global coverage and uniform distribution as well as preferably good condition of the linear system. For strategies of choosing such a subset the reader is referred to [17] and [43].

This non-spherical approach for reconstruction ionospheric current systems from given magnetic field data can easily be applied to the case where ground based measurements of the magnetic field are available. A similar approach using explicitly given, space localizing radial basis functions, called elementary currents, has been applied in [1] to ground based magnetic field measurements. For the calculation of the matrix elements Equation (4.43) instead of Equation (4.46) has to be taken into consideration.

Appendix A

CHAMP Magnetic Data Preprocessing

In this appendix we present some brief information concerning the geophysical nomenclature and the magnetic data preprocessing for CHAMP FGM data.

In Chapter 1 we have introduced spherical coordinates. The standard parametrization used for geophysical data is such that $-180^\circ \leq \varphi < 180^\circ$, $-90^\circ \leq \vartheta \leq 90^\circ$, where $\vartheta = -90^\circ$ is the south pole and $\vartheta = 90^\circ$ is the north pole. $\varphi = 0$ is identified with the Greenwich meridian. If the corresponding unit vectors are given by $\hat{\varepsilon}^r$, $\hat{\varepsilon}^\vartheta$ and $\hat{\varepsilon}^\varphi$ then they can be identified with the components of the geomagnetic coordinates by the scheme given in Table A.1.

Local Coordinates	Geomagnetic Coordinates	Name of the Geom. Coord.
$\hat{\varepsilon}^\vartheta$	X	north component
$\hat{\varepsilon}^\varphi$	Y	east component
$-\hat{\varepsilon}^r$	Z	downward component

Table A.1: Relation between local spherical and geomagnetic coordinates.

The downward component is sometimes also called vertical component and the geomagnetic north and east components are referred to as the horizontal components.

In Chapter 1 the system of spherical harmonics has been introduced in a coordinate free form without giving any numerical realization. Every orthonormal system in $\mathcal{L}^2(\Omega)$ has been called a system of spherical harmonics which indicates that there are infinitely many of them. Here we will give one special example of a system of spherical harmonics which is frequently used in geomagnetic applications. It is the system of Schmidt semi-normalized spherical harmonics in terms of Legendre

functions. The system is given in polar coordinates by

$$\begin{aligned}\tilde{Y}_{n,k}(\xi) &= c_{n,k} P_n^{|k|}(t) \cos(k\varphi), \quad k = -n, \dots, 0, \\ \tilde{Y}_{n,k}(\xi) &= c_{n,k} P_n^{|k|}(t) \sin(k\varphi), \quad k = 1, \dots, n,\end{aligned}$$

where the normalization factors $c_{n,k}$ are given by

$$c_{n,k} = \sqrt{\frac{2(n-|k|)!}{(n+|k|)!}},$$

and P_n^k denotes the associated Legendre Functions of degree n and order k given by

$$P_n^k(t) = (1-t^2)^{k/2} \left(\frac{d}{dt} \right)^k P_n(t), \quad t \in [-1, 1],$$

$k = 1, \dots, n$. The tilde is just to point out that in this example of a system of spherical harmonics the second index k is not running as usual from 1 to $2n+1$ but from $-n$ to n .

Next we present a realization of the geomagnetic potential U in terms of the special system of spherical harmonics presented above. It is given by

$$\begin{aligned}U &= R \left\{ \sum_{n=1}^{N_{MF}} \sum_{k=0}^n (g_n^k \cos(k\varphi) + h_n^k \sin(k\varphi)) \left(\frac{R}{r} \right)^{n+1} \bar{P}_n^k(\cos(\vartheta)) \right. \\ &+ \sum_{n=1}^{N_{SV}} \sum_{k=0}^n (\dot{g}_n^k \cos(k\varphi) + \dot{h}_n^k \sin(k\varphi)) \left(\frac{R}{r} \right)^{n+1} (t - t_0) \bar{P}_n^k(\cos(\vartheta)) \\ &+ \sum_{n=1}^2 \sum_{k=0}^n (q_n^k \cos(k\varphi) + s_n^k \sin(k\varphi)) \left(\frac{r}{R} \right)^{n+1} \bar{P}_n^k(\cos(\vartheta)) \\ &\left. + Dst \left[\frac{r}{R} + Q_1 \left(\frac{R}{r} \right)^2 \right] [\tilde{q}_1^0 \bar{P}_1^0(\cos(\vartheta)) + (\tilde{q}_1^1 \cos(\varphi) + \tilde{s}_1^1 \sin(\varphi)) \bar{P}_1^1(\cos(\vartheta))] \right\},\end{aligned}\tag{A.1}$$

where $\bar{P}_n^k = c_{n,k} P_n^k$. $R = 6371.2 \text{ km}$ is the mean radius of the Earth, (r, ϑ, φ) are geocentric coordinates and the quantities (g_n^k, h_n^k) and (q_n^k, s_n^k) are the so-called Gauss coefficients (special realizations of the Fourier coefficients with respect to the system $\tilde{Y}_{n,k}$) describing sources internal to the satellite's orbit (up to degree $N_{MF} = 13$ for main field correction) and external to the orbit (up to degree 2), respectively. $(\dot{g}_n^k, \dot{h}_n^k)$ describe the linear secular variation (calculated to degree $n_{SV} = 13$ around the model epoch t_0 which is chosen to be $t_0 = 2001$ for the model CO2 (see [54])). The coefficients \tilde{q}_1^0 , \tilde{q}_1^1 and \tilde{s}_1^1 account for the variability of contributions from the magnetospheric ring current (parameterized by the Dst index) plus their internal, induced counterpart (considered to be coupled by the factor $Q_1 = 0.27$ a value found by [38]). The Dst index is an hourly measured value reflecting the strength of the magnetospheric ring current. It can be download from the World Data Center of Geomagnetism, Kyoto, (<http://swdcdb.kugi.kyoto-u.ac.jp>). As already stated in

[54] and [57], especially the magnetospheric ring current correction is a very critical point. There are often unmodelled external field contributions left in the data which we have already seen in Section 3.4. To overcome these problems the author of [52] proposes to use another index than Dst , called RC , to characterize the Magnetospheric ring current. An even better approach would be a better parametrization of the ring current, in particular to model its local time dependence (as for example suggested in [60]).

To finish this chapter we shortly present the standard correction and preprocessing steps which have been applied to the CHAMP magnetic field data set being made available by the GFZ Potsdam.

For the lower latitudes, which are latitudes of 60° below and above the geomagnetic equator, night time data are selected between 22:00 and 06:00 local time. The period between 19:00 to 22:00 local time has been excluded to avoid disturbance of night time F region currents which have been shown to be existent for CHAMP data in [41]. For polar latitudes a 5% subset of data were selected with particular low residuals. All the data were selected in times with a global index of geomagnetic activity $Kp \leq 2$. Main field, including secular variations, external field and magnetospheric ring current contributions are subtracted using a model given by the gradient field of a harmonic potential U as presented in Equation (A.1). After these standard corrections the magnetospheric signal remaining in the data is still of the order of the strength of the crustal field signal. These external contributions are removed by fitting and subtracting track by track an external field including the corresponding induced internal fields. This is done up to a spherical harmonic degree of $n = 2$. For a justification of this method and for more information the reader is referred to [46] and [57].

Appendix B

M-Estimation for Outlier Detection

In the following we explain in a very comprehensive manner how we use a statistical method to detect outliers in the satellite magnetic field data set in a certain vicinity of the point we want to average the data to. The method we use is strongly related to M-estimation, a robust statistical method for estimating parameters. For more information about robust estimation and the standard nomenclature of M-estimation the reader is referred to [33].

Let x_1, x_2, \dots, x_n be a random sample (measurements) that arises from a distribution with density $F(x - m)$ where m is a location parameter and F is assumed to be continuous. The maximum likelihood estimator \hat{m} is the maximum of the likelihood function or, for simplicity, of the logarithm of the likelihood function which is given by

$$\ln L(m) = \sum_{i=1}^n \ln F(x_i - m) = - \sum_{i=1}^n \rho(x_i - m),$$

where $\rho(x) = -\ln F(x)$. ρ is called the *objective function* of the estimation. Thus, maximizing $\ln F(x)$ is equivalent to minimizing

$$K(m) = \sum_{i=1}^n \rho(x_i - m) \tag{B.1}$$

and this is equivalent to solving the equation $K'(m) = 0$ or

$$\sum_{i=1}^n \psi(x_i - m) = 0, \tag{B.2}$$

where we have set $\psi(x) = \rho'(x)$. The function ψ is called the *influence function* of the M-estimation. In principle, Equation (B.1) can be seen as the starting point of the M-estimation. The function ρ can be chosen arbitrarily, fulfilling the properties of being symmetric, positive-definite and with a unique minimum at zero. But there is still a little problem concerning the estimator resulting from (B.2). If we multiply the measurements x_1, \dots, x_n by a constant, the original estimator is not necessarily

multiplied by the same constant. In order to overcome this inconsistency we have to define a scale invariant M-estimator \hat{m} given by the solution of

$$\sum_{i=1}^n \psi \left(\frac{x_i - \hat{m}}{s} \right) = 0, \quad (\text{B.3})$$

where s is a robust estimate of the scale such as, for example,

$$s = \frac{\text{median}(|x_i - \text{median}(x_i)|)}{0.645}.$$

To find the solution of (B.3) we use an iterative method, called weighted least squares which is for an arbitrary starting point $m^{(0)}$ given by

$$m^{(l+1)} = \frac{\sum_{i=1}^n w_i x_i}{\sum_{i=1}^n w_i}, \quad \text{with } w_i = w \left(\frac{x_i - m^{(l)}}{s} \right), \quad i = 1, \dots, n, \quad (\text{B.4})$$

$l = 1, 2, \dots$, where we have set $w(x) = \psi(x)/x$. The function w is called the *weight function* of the M-estimation. Convergence of the above iteration can be proven if the ρ -function is chosen to be convex (see e.g. [33]).

The most typical classroom example of the above described process is the \mathcal{L}^2 -M-estimator given by

$$\rho(x) = \frac{x^2}{2}, \quad \psi(x) = x, \quad w(x) = 1, \quad x \in \mathbb{R}. \quad (\text{B.5})$$

The iteration (B.4) is becoming stationary after just one iteration step and results in the mean value \bar{x} of the samples $\{x_i\}$. A graphical illustration of the corresponding function can be seen in Figure B.1.

A more complicated but frequently used example is Huber's M-estimation given by

$$\rho(x) = \begin{cases} x^2/2, \\ c(|x| - c/2), \end{cases} \quad \psi(x) = \begin{cases} x, \\ c \operatorname{sgn}(x), \end{cases} \quad w(x) = \begin{cases} 1, & |x| \leq c, \\ c/|x|, & |x| > c. \end{cases} \quad (\text{B.6})$$

An illustration of Huber's functions can be found in Figure B.2. Huber's functions are chosen such that all measurements in a certain band around 0 are weighted with 1 and all the other samples are weighted as small as possible such that convexity of the ρ -function is still guaranteed. As stated before, convexity of the ρ -function is needed to prove convergence of the iteration scheme (B.4) (for details see [33]).

The M-estimation functions we use in our approach for detecting outliers are given by

$$\rho(x) = \begin{cases} x^2/2, \\ c^2/2, \end{cases} \quad \psi(x) = \begin{cases} x, \\ 0, \end{cases} \quad w(x) = \begin{cases} 1, & |x| \leq c, \\ 0, & |x| > c. \end{cases} \quad (\text{B.7})$$

These functions can be called modified Huber's functions. As we can see in Figure B.3 the corresponding ρ -function is no more convex. This means that convergence in (B.4) can no longer be guaranteed but if the threshold c is taken not too small and, at the same time, the starting point of the iteration $m^{(0)}$ is chosen appropriately (e.g. the median of the data samples), convergence in (B.4) can be assumed.

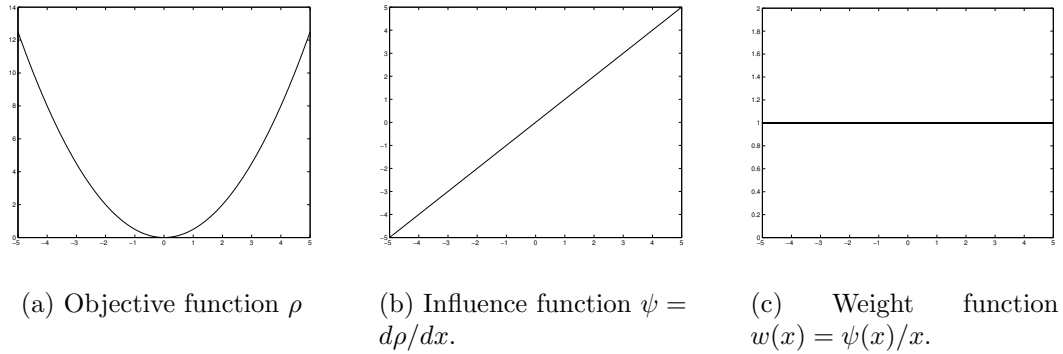
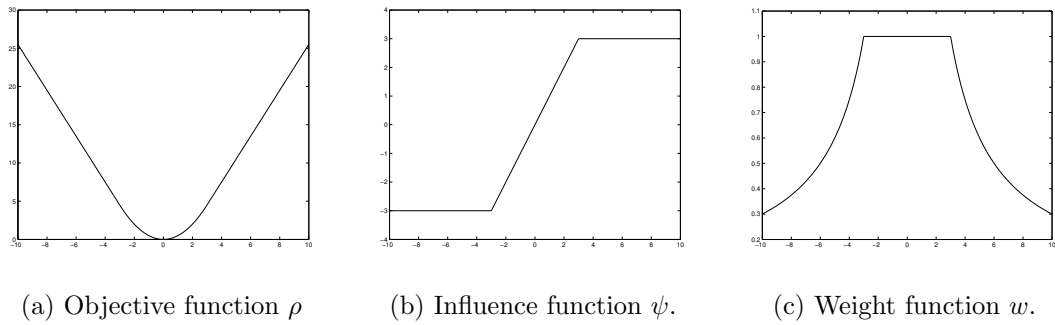
Figure B.1: Corresponding functions for \mathcal{L}^2 -M-estimation.

Figure B.2: Corresponding functions for Huber's M-estimation.

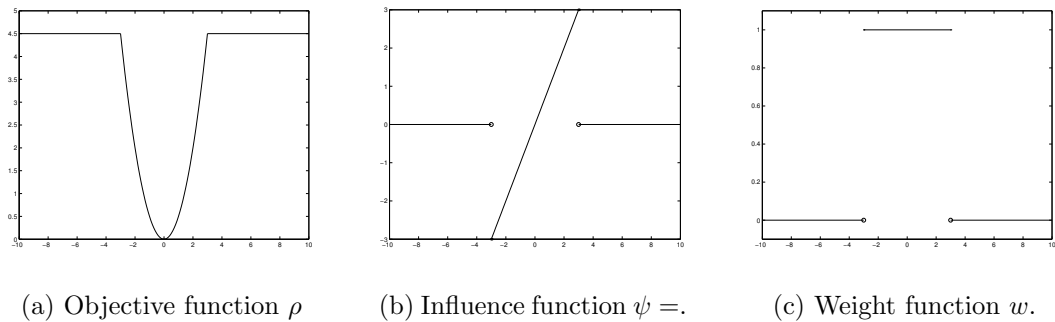


Figure B.3: Corresponding functions for modified Huber's M-estimation.

The aim of using such an M-estimation for averaging CHAMP magnetic field data is the detection of outliers. We do not use the estimated weighted mean value of the iteration (B.4) as our final value for the point for further considerations but we use the M-estimation to detect outliers in the data set in the vicinity of x . This means that only those data which are weighted by 1 in the last iteration step of (B.4) are taken and those which are weighted by 0 are neglected. Practical reasons for outliers may be considered to be measuring errors due to performance of the instruments or, in polar regions, the magnetic signature of temporally fast changing field aligned currents. Finally, our methods for outlier detection in a given data set x_1, \dots, x_n results in the following algorithm.

Algorithm B.1

SET

$$m^{(0)} = \frac{1}{n} \sum_{i=1}^n x_i, \quad s = \text{median} \left\{ \left| \frac{x_i - m^{(0)}}{0.6745} \right|, i = 1, \dots, n \right\}$$

WHILE $\left| \frac{m^{(l+1)}}{m^{(l)}} - 1 \right| > \varepsilon$

SET

$$w_i = \text{WEIGHTFKT} \left(\frac{x_i - m^{(l)}}{s} \right), \quad i = 1, \dots, n$$

SET

$$m^{(l+1)} = \frac{\sum_{i=1}^n w_i x_i}{\sum_{i=1}^n w_i}$$

END

FOR $i = 1$ to n

IF $(w_i = 0)$: x_i is outlier

END

where WEIGHTFKT is the modified Huber's weight function.

Bibliography

- [1] O. Amm. Ionospheric elementary current systems in spherical coordinates and their application. *J. Geomag. Geoelectr.*, 49:947–955, 1997.
- [2] O. Amm. *Direkte Bestimmung flächenhafter Verteilungen ionosphärischer elektrodynamischer Parameter aus Bodenmessungen: Theorie und Anwendungen in sphärischen Koordinaten*. PhD thesis, Naturwissenschaftliche Fakultät, Technische Universität Braunschweig, 1998.
- [3] O. Amm. The elementary current method for calculating ionospheric current systems from multi-satellite and ground magnetometer data. *J. Geophys. Res.*, 2000.
- [4] O. Amm and A. Viljanen. Ionospheric disturbance magnetic field continuation from the ground to the ionosphere using spherical elementary current systems. *Earth Planets Space*, 1999.
- [5] G.E. Backus. Poloidal and toroidal fields in geomagnetic field modeling. *Rev. Geophys.*, 24:75–109, 1986.
- [6] G.E. Backus, R. Parker, and C. Constable. *Foundations of Geomagnetism*. Cambridge University Press, Cambridge, 1996.
- [7] M. Bayer. *Geomagnetic Field Modelling from Satellite Data by First and Second Generation Vector Wavelets*. PhD thesis, Geomathematics Group, Department of Mathematics, University of Kaiserslautern, 2000.
- [8] M. Bayer, S. Beth, and W. Freedden. Geophysical field modelling by multiresolution analysis. *Acta Geod. Geoph. Hung.*, 33(2-4):289–319, 1998.
- [9] M. Bayer, W. Freedden, and T. Maier. A vector wavelet approach to iono- and magnetospheric geomagnetic satellite data. *J. Atmos. Sol.-Terr. Phy.*, 63:581–597, 2001.
- [10] S. Beth. *Multiscale Approximation by Vector Radial Basis Functions on the Sphere*. PhD thesis, Geomathematics Group, Department of Mathematics, University of Kaiserslautern. Shaker, Aachen, 2000.
- [11] J. Cain, Z. Wang, C. Kluth, and D.R. Schmitz. Derivation of a geomagnetic model to n=63. *Geophys. J. Int.*, 97:432–441, 1989.

- [12] W.H. Cambell. *Quit Daily Geomagnetic Fields*. Birkhäuser Verlag, 1989.
- [13] P.J. Davis. *Interpolation and Approximation*. Dover Publications Inc., New York, 1975.
- [14] P. Deuffhard. On algorithms for the summation of certain special functions. *Computing*, 17:37–48, 1976.
- [15] J.R. Driscoll and D.M. Healy. Computing Fourier transforms and convolutions on the 2-sphere. *Adv. Appl. Math.*, 15:202–250, 1994.
- [16] A.R. Edmonds. *Angular Momentum in Quantum Mechanics*. Princeton University Press, 1957.
- [17] M. Fengler. *Multiscale Modelling of the Earth's Gravitational Potential from Discrete Noisy CHAMP-Ephemerides*. Diploma Thesis, Geomathematics Group, Department of Mathematics, University of Kaiserslautern, 2001.
- [18] W. Freeden. The uncertainty principle and its role in physical geodesy. In W. Freeden, editor, *Progress in Geodetic Science*, pages 225–236, Aachen, 1998. Shaker.
- [19] W. Freeden. *Multiscale Modelling of Spaceborne Geodata*. B.G. Teubner, Stuttgart, Leipzig, 1999.
- [20] W. Freeden, T. Gervens, and M. Schreiner. *Constructive Approximation on the Sphere (With Applications to Geomathematics)*. Oxford Science Publications, Clarendon, 1998.
- [21] W. Freeden, O. Glockner, and R. Litzenberger. A general Hilbert space approach to wavelets and its application in geopotential determination. *Numer. Func. Anal. and Optimiz.*, 20:853–879, 1999.
- [22] W. Freeden and T. Maier. Spectral and multiscale signal-to-noise thresholding of spherical vector fields. *Computational Geosciences*, 7(3):215–250, 2003.
- [23] W. Freeden, T. Maier, and C. Mayer. Multiscale crustal field determination from CHAMP vector magnetic data. *Geophys. Res. Lett.*, 2002 (submitted).
- [24] W. Freeden and C. Mayer. Wavelets generated by layer potentials. *Appl. Comp. Harm. Anal.*, 14:195–237, 2003.
- [25] W. Freeden and F. Schneider. Regularization wavelets and multiresolution. *Inverse Problems*, 14:225–243, 1998.
- [26] W. Freeden and U. Windheuser. Spherical wavelet transform and its discretization. *Adv. Comput. Math.*, 5:51–94, 1996.
- [27] N. Fukushima. Generalized theorem for no ground magnetic effect of vertical currents connected with pedersen currents in the uniform-conductivity ionosphere. *Rep. Ionos. Space Res. Jpn.*, 30:35–40, 1976.

- [28] C. F. Gauss. Allgemeine Theorie des Erdmagnetismus. Resultate aus den Beobachtungen des magnetischen Vereins im Jahre 1838 (English translation: General theory of terrestrial magnetism). In R. Taylor, editor, *Scientific Memoirs Selected from the Transactions of Foreign Academies of Science and Learned Societies and from Foreign Journals*, volume 2, pages 184–251, 1841.
- [29] G. Gerlich. Magnetfeldbeschreibung mit verallgemeinerten poloidalen und toroidalen skalaren. *Z. Naturforsch.*, 8:1167–1172, 1972.
- [30] O. Glockner. *On Numerical Aspects of Gravitational Field Modelling from SST and SGG by Harmonic Splines and Wavelets*. PhD thesis, Geomathematics Group, Department of Mathematics, University of Kaiserslautern. Shaker, Aachen, 2002.
- [31] M. Gutting. *Multiscale Gravitational Field Modeling from Oblique Derivatives*. Diploma Thesis, Geomathematics Group, Department of Mathematics, University of Kaiserslautern, 2002.
- [32] K. Hesse. *Domain Decomposition Methods for Multiscale Geopotential Determination from SST and SGG*. PhD thesis, Geomathematics Group, Department of Mathematics, University of Kaiserslautern. Shaker, Aachen, 2003.
- [33] R.V. Hogg. An introduction to robust estimation. In G.N. Launer and R.L. Wilkinson, editors, *Robustness in Statistics*, pages 1–17, San Diego, California, 1979. Academic.
- [34] T. Iijima and T.A. Potemra. Large-scale characteristics of field-aligned currents associated with substorms. *J. Geophys. Res.*, 83:599–615, 1978.
- [35] J.D. Jackson. *Classical Electrodynamics*. John Wileys and Sons, 1975.
- [36] W. Kertz. *Einführung in die Geophysik 1*. B.I. Hochschultaschenbücher, Mannheim, Wien, Zürich, 1969.
- [37] W. Kertz. *Einführung in die Geophysik 2*. B.I. Hochschultaschenbücher, Mannheim, Wien, Zürich, 1969.
- [38] R.A. Langel and R.H. Estes. Large-scale, near-Earth magnetic fields from external sources and the corresponding induced internal field. *J. Geophys. Res.*, 90:2487–2494, 1985.
- [39] R.A. Langel, M. Purucker, and M. Rajaram. The equatorial electrojet and associated currents as seen in MAGSAT data. *J. Atmos. Sol.-Terr. Phy.*, 55(3):1233–1269, 1992.
- [40] E. Friis-Christensen (lead proposer). Proposal for Earth Explorer Opportunity Mission: SWARM, a Constellation to Study the Dynamics of the Earth’s Magnetic Field and its Interactions with the Earth System. Technical report, A Consortium of 27 Institutes and Universities under leadership of Danish Space Research Institute, Copenhagen, 2002.

- [41] H. Lühr. Night-Time Ionospheric Currents. In P. Schwintzer C. Reigber, H. Lühr, editor, *First CHAMP Mission Results for Gravity, Magnetic and Atmospheric Studies*, pages 328–338, Berlin, Heidelberg, New York, 2003. Springer.
- [42] T. Maier. *Multiscale Analysis of the Geomagnetic Field*. Diploma Thesis, Computational Material Science Group, Department of Physics and Geomathematics Groups, Department of Mathematics, University of Kaiserslautern, 1999.
- [43] T. Maier. *Multiscale Geomagnetic Field Modelling from Satellite Data: Theoretical Aspects and Numerical Application*. PhD thesis, Geomathematics Group, Department of Mathematics, University of Kaiserslautern, 2003.
- [44] T. Maier and C. Mayer. Multiscale Downward Continuation of CHAMP FGM-Data for Crustal Field Modelling. In P. Schwintzer C. Reigber, H. Lühr, editor, *First CHAMP Mission Results for Gravity, Magnetic and Atmospheric Studies*, pages 288–295, Berlin, Heidelberg, New York, 2003. Springer.
- [45] E. Martensen. *Potentialtheorie*. Teubner, 1968.
- [46] S. Maus, M. Rother, R. Holme, H. Lühr, N. Olsen, and V. Haak. First champ satellite magnetic data resolve uncertainty about strength of the lithospheric magnetic field. *Geophys. Res. Lett.*, 29(14):47/1–47/4, 2002.
- [47] C. Mayer and T. Maier. Multiscale Determination of Radial Current Distribution from CHAMP FGM-Data. In P. Schwintzer C. Reigber, H. Lühr, editor, *First CHAMP Mission Results for Gravity, Magnetic and Atmospheric Studies*, pages 339–346, Berlin, Heidelberg, New York, 2003. Springer.
- [48] D. Michel. *On the Combination of Harmonic Splines and Fast Multipole Methods for CHAMP Data Modelling*. Diploma Thesis, Geomathematics Group, Department of Mathematics, University of Kaiserslautern, 2001.
- [49] V. Michel. *A Multiscale Approximation for Operator Equations in Separable Hilbert Spaces – Case Study: Reconstruction and Description of the Earth’s Interior*. Habilitation, Geomathematics Group, Department of Mathematics, University of Kaiserslautern, 2002.
- [50] H. Nutz. *A Unified Setup of Gravitational Field Observables*. PhD thesis, Geomathematics Group, Department of Mathematics, University of Kaiserslautern. Shaker, Aachen, 2002.
- [51] N. Olsen. Ionospheric f region currents at middle and low latitudes estimated from Magsat data. *J. Geophys. Res.*, A, 3:4563–4576, 1997.
- [52] N. Olsen. A model of the geomagnetic field and its secular variation for epoch 2000 estimated from Ørsted data. *Geophys. J. Int.*, 4:453–462, 2002.

- [53] N. Olsen and U. Engles. Computation of magnetic fields within source regions of ionospheric and magnetospheric currents. *J. Atmos. Sol.-Terr. Phy.*, 60:1585–1592, 1998.
- [54] R. Holme and N. Olsen and M. Rother and H. Lühr. CO2 - A CHAMP Magnetic Field Model. In P. Schwintzer C. Reigber, H. Lühr, editor, *First CHAMP Mission Results for Gravity, Magnetic and Atmospheric Studies*, pages 220–225, Berlin, Heidelberg, New York, 2003. Springer.
- [55] C. Reigber, H. Lühr, and P. Schwintzer. *First CHAMP Mission Results for Gravity, Magnetic and Atmospheric Studies*. Springer, Berlin, Heidelberg, New York, 2003.
- [56] A.D. Richmond. Ionspheric electrodynamics using magnetic apex coordinates. *J. Geomag. Geoelec.*, 47:191–212, 1995.
- [57] S. Maus and K. Hemant and M. Rother and H. Lühr. Mapping the Lithospheric Magnetic Field from CHAMP Scalar and Vector Magnetic Data. In P. Schwintzer C. Reigber, H. Lühr, editor, *First CHAMP Mission Results for Gravity, Magnetic and Atmospheric Studies*, pages 269–274, Berlin, Heidelberg, New York, 2003. Springer.
- [58] T.J. Sabaka, N. Olsen, and R.A. Langel. A Comprehensive Model of the Near-Earth Magnetic Field: Phase 3. *NASA/TM-2000-209894*, 2000.
- [59] B.J. Schmitt. The poloidal-toroidal representation of solenoidal fields in spherical domains. *Analysis*, (15):257–277, 1995.
- [60] J. Schwarte, H. Lühr, and R. Holme. Improved Parametrization of External Magnetic Fields from CHAMP Measurements. In P. Schwintzer C. Reigber, H. Lühr, editor, *First CHAMP Mission Results for Gravity, Magnetic and Atmospheric Studies*, pages 239–244, Berlin, Heidelberg, New York, 2003. Springer.
- [61] H. Triebel. *Höhere Analysis*. VEB Deutscher Verlag der Wissenschaft, Berlin, 1972.

Wissenschaftlicher Werdegang

23. Feb. 1976	Geboren in Trier
1982 - 1986	Grundschule St. Nikolaus Konz
1986 - 1995	Gymnasium Konz
1995	Abitur
1996 - 2001	Studium der Mathematik mit Nebenfach Physik an der Universität Kaiserslautern Diplom in Mathematik am 12. Juni 2001 (Note 1.0)
1999 - 2000	Auslandsstudium an der ETH Zürich (Jahrestipendium des DAAD)
Jul. 2001 - Sep. 2001	Wissenschaftlicher Mitarbeiter der AG Geomathematik, Universität Kaiserslautern
Okt. 2001 - Sep. 2002	Stipendiat im Graduiertenkolleg "Mathematik und Praxis", Universität Kaiserslautern
seit Sep. 2002	Wissenschaftlicher Mitarbeiter der AG Geomathematik, Universität Kaiserslautern

Scientific Career

Feb. 23. 1976	Born in Trier
1982 - 1986	Elementary School St. Nikolaus Konz
1986 - 1995	Gymnasium Konz
1995	Abitur
1996 - 2001	Studies in Mathematics with minor subject Physics at the University of Kaiserslautern German Diplom in Mathematics, June 12. 2001 (grade 1.0)
1999 - 2000	Studies at the ETH Zürich (one year scholarship of the DAAD)
Jul. 2001 - Sep. 2001	Research associate at the Geomathematics Group, University of Kaiserslautern
Okt. 2001 - Sep. 2002	Scholarship holder in the Graduiertenkolleg "Mathematics and Practice", University of Kaiserslautern
seit Sep. 2002	Research associate at the Geomathematics Group, University of Kaiserslautern

Eidesstattliche Erklärung

Hiermit erkläre ich an Eides statt, dass ich die vorliegende Arbeit selbst und nur unter Verwendung der in der Arbeit genannten Hilfen und Literatur angefertigt habe.

Kaiserslautern, 03. Juli 2003

Carsten Mayer